2006

Tribological Aspects of Journal Bearings Focusing on the Stribeck Curve

Xiaobin Lu
Louisiana State University and Agricultural and Mechanical College, xlu1@lsu.edu

TRIBOLOGICAL ASPECTS OF JOURNAL BEARINGS FOCUSING ON THE STRIBECK CURVE

A Dissertation
Submitted to the Graduate Faculty of the
Louisiana State University and
Agricultural and Mechanical College
In Partial Fulfillment of the
requirements for the degree of
Doctor of Philosophy

in

The Department of Mechanical Engineering

by
Xiaobin Lu
B.S., Zhengzhou Textile Institute, China, 1997
M.S., Univeristy of Petroleum, China, 2000
December, 2006

To whom I love

Yihui Zeng

ACKNOWLEGEMENTS

This work is carried out under the direction of Professor Michael M. Khonsari. I have been enjoying his great advices and thoughtful insights during the time of research. What I have learned is far beyond those words written in the dissertation. If the work fortunately contributes a little to tribology of journal bearings, half of the credit goes to him.

I am sincerely thankful to my committee members: Dr. Ram, Dr. Pang, Dr. Wang and Dr. Monroe for their valuable time in evaluating this work.

The authors gratefully acknowledge the support of Louisiana Board of Regents through an industrial-ties grant with Caterpillar Inc. The instrument used in this research was purchased through the grant. The authors also acknowledge the constant support and encouragement of their colleagues and members of the Center for Rotating Machinery (CeRoM) at Louisiana State University.

My parents and grandparents support me mentally through any pain in the past, current and future.

TABLE OF CONTENTS

ABSTRACT

The dissertation focuses on the frictional characteristics of journal bearings as represented by the Stribeck curve. The behavior of lift-off speed and the factors that affect it are explored. An equation is proposed for predicting the lift-off speed. The comparison between the experimental results of oil- and grease-lubricated journal bearings with a mixed elastohydrodynamic lubrication model for line contacts is indicative of good agreement in the mixed lubrication regime. Efforts are made to modify the surface profile of bushing by putting dimples on its surface. Experimental results show that with proper dimensions of dimples, the friction performance of journal bearings can be improved, particularly for light oils. The friction hysteresis of oil and grease-lubricated journal bearings undergoing oscillatory motion are investigated under different load, with or without oil, oil type, oil inlet temperature, oscillating frequency, and bushing material. A dynamic friction model for infinitely long journal bearing is also developed that demonstrates the existence of hysteresis loop. Finally, a thermal analysis of oscillatory journal bearings is carried out by finite element method using ANSYS. Simulations are found to be in good agreement with experimental measurement of temperature at four locations along the circumference.

CHAPTER 1 ON THE LIFT-OFF SPEED IN JOURNAL BEARINGS

1.1. Introduction

The celebrated work of Stribeck [1] trailed the work of Hirn [2] in 1846 who reported the results of experiments with a journal bearing and found that the coefficient of friction was directly proportional to speed. His work was published in 1854. In dedicating his book to Hirn, Thurston [3] reported that the coefficient of friction passed through a minimum which is now recognized as the transition point from mixed to hydrodynamic lubrication. About half of a century after Hirn, Stribeck (1902) carried out systematic experiments to show the existence of the minimum point proposed by Thurston and provided a clear view of the characteristic curve of the coefficient of friction versus speed. In recognition of his contribution, this curve is universally referred to as "the Stribeck curve" (Dowson, [4]).

After Stribeck's original contribution, many researchers endeavored to broaden our insight into the understanding of the physical meaning and its implication on the different lubrication regimes. In some sense, especially after the speed parameter was extended to the Sommerfeld number ([5], [6]), the Stribeck curve acquired a much greater breadth as its applicability extended to a far greater number of tribological components than merely journal bearings. For example, the concept has been applied to ball bearings [7], seals ([8], [9]), wet clutches [10], piston pumps [11], hip joints [12], and even fiber-capstan [13].

It has been long recognized that the coefficient of friction is influenced by many parameters such as the material properties, the surface finish, the viscosity of the oil, and the operating conditions such as the speed and the pressure on the bearing. As early as 1922, Wilson [14] compiled a comprehensive review of forerunners' research on the

clearance ratio, bearing material, and the oil and its arrangements. The McKee brothers [15] in 1932 employed three different oils in bronze and babbitt bearings to show that the coefficient of friction depends on the viscosity in the boundary or mixed lubrication regime. Their conclusion was supported by Bridgeman's experiments [16] in which four different oils were used in babbitt and mild steel bearings. In 1941, Burwell [17] conducted a series of experiments on surfaces with a wide range of surface roughness, and showed that the critical speed was influenced by the surface finish. Later, in 1959, Ocvirk [18] analyzed the clearance's effect based on the short-bearing approximation. While these researchers illustrated the shift of the Stribeck curve under various conditions, none attempted to predict the transition point—the point that marks the watershed of the mixed and the hydrodynamic lubrication. This problem was tackled by Vogelpohl [19] in 1958 who was probably the first researcher to have succeeded in developing an empirical equation to calculate the lift-off speed.

In the current paper, we present the results of a series of experiments that are conducted to explore the behavior of the lift-off speed. We study the influence of oil inlet temperature, the oil type and the load. Comparison with Vogelpohl's equation is also presented.

1.2. Experimental

Figure 1.1 shows the schematic of the apparatus (Lewis LRI-8H) used for measuring the coefficient of friction of journal bearings.

The Shaft is tapered at one end and is centered in the rear supporting base. It is driven by an electronic motor with a maximum speed of 3300 rpm. The desired load is applied using a dead weight located on the right hanger device via a lever. The lever scale is 1:10, so that one Newton on the hanger is equivalent to 10 Newton on the

bearing. The left hanger works to balance the self-weight of the level bar and the right one. The lubrication system is capable of supplying heated oil flow at the rate of 10 *l*/min. It consists of an oil pump, a reservoir, a temperature controller, an oil filter, tubes and valves. The oil temperature floats within ±0.5 ^{0}C of the targeted temperature. The supply pressure is 3.45×10^4 Pa (5 psi). The friction force is transformed into compression or tension of a linkage bar and sensed by a load cell, and the signal is transferred to the computer system for recording and processing. The coefficient of friction, the speed, and

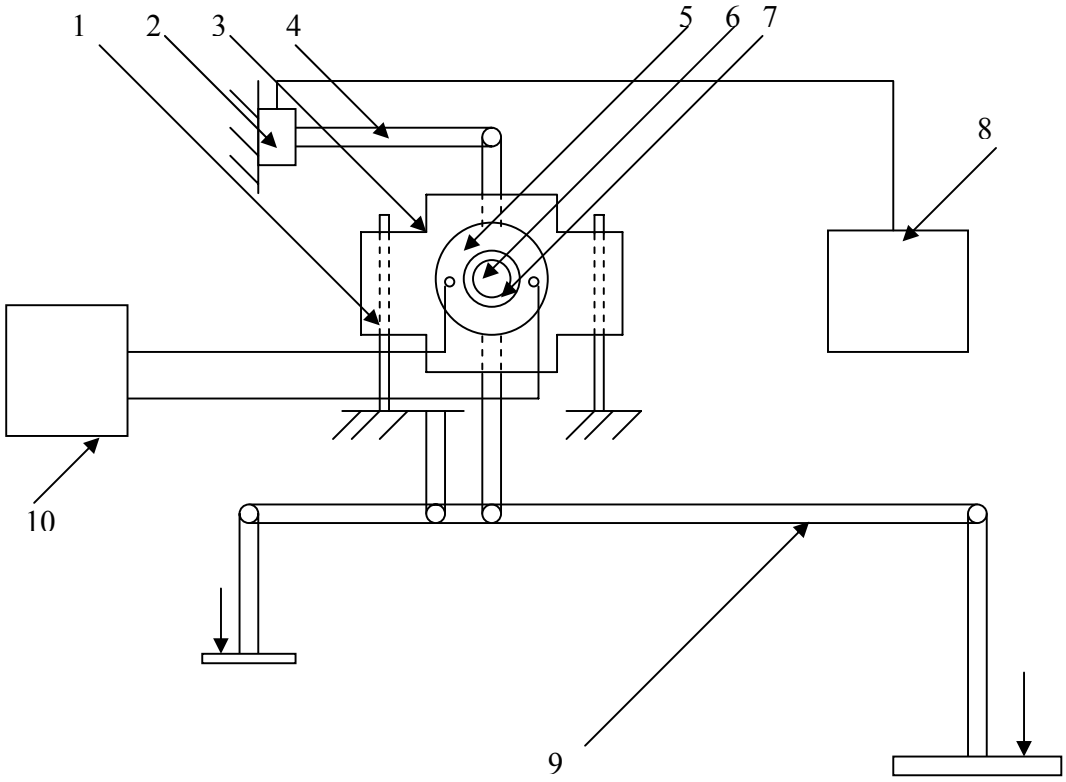

Figure 1.1 - Schematic of the friction apparatus (not to scale)

1-Guiding poles, 2-Load cell, 3-Base, 4-Linkage bar, 5-Housing, 6-Shaft, 7-Lip seal, 8-Computer system, 9-Load applying device, 10-Lubrication system

the load are processed by software and displayed on the computer screen. The time interval of data reading is adjustable and is independent of the duration of the test. In the current study, the minimum time interval is 20 seconds.

The shaft is made up of hardened AISI 1020 steel. Its material properties are given in Table 1.1.

Table 1.1- Shaft dimension and material properties

Material	Diameter mm	Poisson's ratio	Young's Modulus GPa	Hardness Brinell
AISI 1020 steel	24.54	0.29	200	163

The bushing is made up of SAE 660 alloy bronze. It is a high-quality smooth machine finish material and highly resistant to impact, wear and corrosion. Its chemical composition, mechanical properties, and surface finish parameters are given in Tables 1.2-1.4, respectively.

Table 1.2- Bushing material composition

Copper	Tin	Lead	Zinc
83%	7%	7%	7%

Table 1.3- Bushing mechanical properties

Tensile MPa	Yield MPa	Elongation % in 50.8 mm	Brinnell No. @500KG Load
303	165	16% min	72

Table 1.4- Surface finish (CLA) and dimensions

Shaft roughness µm	Bushing roughness µm	Shaft Diameter mm	Bushing ID mm	Length mm
0.05	0.2	24.54	24.71	25.4

Two types of oils (SAE30 and SAE5W30) whose properties are shown in Table 1.5 are used. The applied loads are: 222N (50 lb), 445 N (100 lb), 543 N (122 lb), 667 N (150 lb), and 890 N (200 lb). The range of speeds tested is between 2 rpm to 500 rpm.

Table 1.5- Oil properties

Oil Type	Viscosity (cSt)		Specific Gravity at 15^0C	Viscosity Index
	40 ^{0}C	100 ^{0}C		
SAE 30	93	10.8	0.890	100
SAE 5W30	65	10.4	0.875	147

1.2.1 Experiment Procedure

Before any measurement is taken, the system is balanced so that the coefficient of friction is nil when the shaft is in static position. The lubrication supply system is turned on to allow lubricant to enter in the bearing for 2 hours at the running speed of 100 rpm. Air bubbles, if any, are eliminated through a branch return path. At each speed, the history of the coefficient of friction is monitored. The friction coefficient oscillates periodically around a relatively constant value. The rms value of the history is taken as the coefficient of friction for that speed. By observation, 4 minutes are regarded as a reasonable testing period for each velocity point.

1.2.2. Experiment Results

1.2.2.1 Effect of Inlet Oil Temperature

The oil viscosity can have a pronounced effect on the Stribeck curve. Experimentally this can be easily demonstrated by varying the inlet oil temperature. As shown in Figure 1.2, while the profile remains the same, the speed at which the coefficient of friction is the minimum is shifted by varying the oil temperature. The higher the inlet oil temperature, the greater is the transition speed.

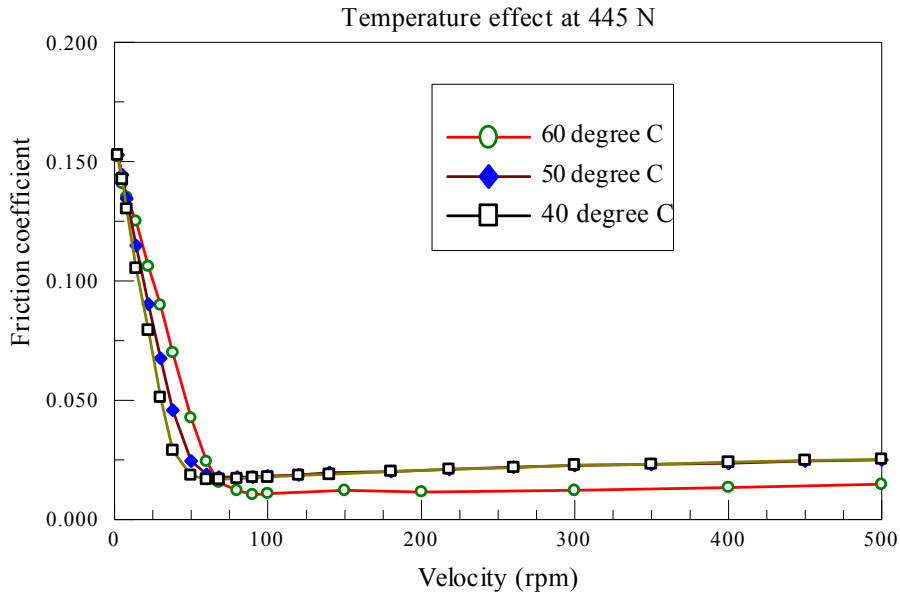

Figure 1.2 - Effect of inlet oil temperature on the friction coefficient
(Oil: SAE 30, Load: 445N)

It should be pointed out that the minimum speed in all tests is 2 rpm. Therefore, there is a gap between zero and the first data point obtained. Due to this limitation, the boundary lubrication regime is not clearly captured. For measurements involving very low speeds, the reader may refer to the work of Forrester [20] and Lovell et al. [21]. In mixed lubrication regime, it can be seen that with rising inlet oil temperature, the friction coefficient increases. When the oil temperature is higher, the viscosity decreases. Less viscosity translates to more metal-to-metal contact to support the same load, which can result in the asperity contact dominating the coefficient of friction.

After the lift-off, hydrodynamic action dominates and the friction coefficient is directly related to the viscosity. Therefore, higher temperature oil yields a lower friction coefficient.

1.2.2.2 Effect of Load

Figure 1.3 shows the results for the coefficient of friction as a function of speed for different loads ranging from 222 N to 890 N. The oil type is SAE 30, and the inlet temperature is 40^0 C.

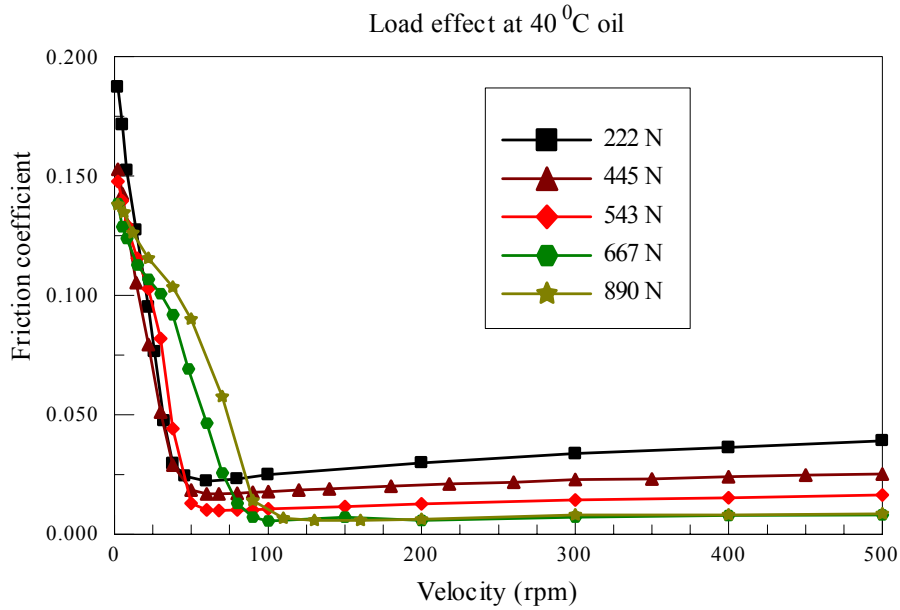

Figure 1.3 Variation of coefficient of friction with speed under different load.
(Oil: SAE 30, Inlet temperature: 40^0 C)

The error associated with the friction coefficient measurement with each load is tabulated in Table 1.6. With this friction apparatus, increasing load results in a smaller error. Thus, this test rig is best suited for higher loads where the experimental error is considerably lower.

Table 1.6- Friction error for different load

Load	**222 N (50 lb)**	**445 N (100 lb)**	**543N (122lb)**	**667 N (150 lb)**	**890 N (200 lb)**
Error (±)	0.0333	0.0229	0.0136	0.0111	0.0083

When lift-off occurs, the speed N_T satisfies the definition of the Sommerfeld number:

$$S = \frac{\mu \times \frac{N_T}{60}}{P_L}\left(\frac{Rs}{C}\right)^2 \qquad (1.1)$$

So that

$$N_T = \frac{S \times P_L}{\mu}\left(\frac{C}{Rs}\right)^2 \times 60 \qquad (1.2)$$

Using equation (1.2), the lift-off speed N_T can be calculated. The lift-off speed is directly proportional to the projected load, $P_L = \frac{W}{DL}$, hence to the bearing load. This fact is reflected by the results of the experiments shown in Figure 1.3. In mixed lubrication regime, a light load creates a smaller coefficient of friction than the heavy load. Mixed lubrication is a lubrication state in which the load is supported by both fluid pressure and asperities (Spikes [22] and [23]). When load is higher, more metal-to-metal asperity contact occurs, which causes the friction coefficient to increase.

On the other hand, the opposite is true in the full-film lubrication regime. In this regime, a high load translates into a higher eccentricity ratio ε and a thinner film. Therefore, the friction coefficient is lower. These trends are consistent with the experimental findings of Stribeck's [24] and Vogelpohl's [19].

Solutions of full Reynolds equation also reveal the same information. According to [25], in a bearing whose length is equal to the shaft diameter (L/D =1), the coefficient of friction varies from f (C/R) = 53.4294 at ε =0.05 to f (C/R) =0.6896 for ε =0.95.

1.2.2.3 Effect of Load with another Oil

Figure 1.4 demonstrates the results from oil SAE 5W30 with an inlet temperature of 40^0 C and different loads.

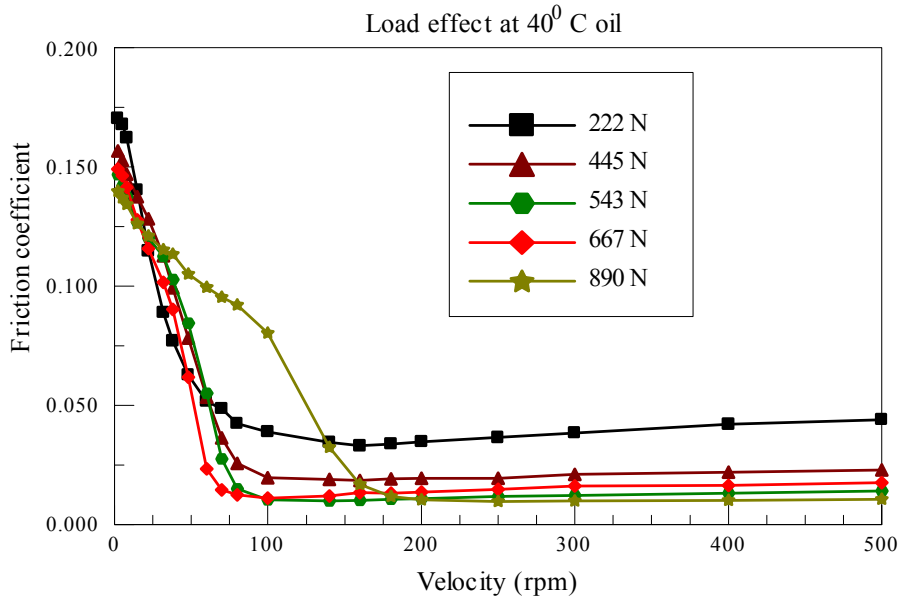

Figure 1.4 Effect of Load on the friction coefficient
(Oil: SAE 5W30, Load: 445N)

The results with SAE 5W30 (a multi-grade oil) are similar to those of SAE30 oil. Referring to Table 1.5, the viscosity of SAE 5W30 oil (65 cSt) is smaller than that of SAE 30 oil (93 cSt). Compared with Fig. 1.3, it can be seen that the decrease of the oil viscosity shifts the lift-off speed to the right. This shift can be derived from equation (1.2).

1.2.2.4 Comparison of Theoretical Prediction and Experiment Results

In order to avoid metal-to-metal contact between journal and bearing, a minimum oil film thickness is required. The minimum film thickness corresponds to the lift-off speed. In other words, the operation speed must be equal to or greater than the lift-off speed to ensure that the bearing runs in fully lubricated regime. Hence, the determination of the minimum film thickness becomes essential.

On the basis of Tarasov's examination of surface roughness reading to actual surface profile [26], Ocvirk [18] hypothesized that for journal bearings with ground

surface finish, the minimum film thickness is 9 times of the combination of two surface roughnesses in rms. Dawson defined a so-called "D" ratio whose reversal is now known as the lambda ratio "Λ" (see Dowson [4]). Martin [27] described two ways to predict the minimum film thickness. One uses the work of Davis [28], Rubert [29] and Ocvirk [30] which is based on the surface finish criterion. The other considers the oil film temperature effect at high speed operation from white-metal wiping criterion. Hamrock & Dowson [31] mark the transition between lubrication regimes using the definition of Λ ratio. Cann et al. [32] and Masen [33] examined the relationship of Λ to the minimum film thickness considering heavily loaded elastohydrodynamic contacts and non-Newtonian effects. Nevertheless, it is generally agreed that for full-film lubrication, Λ should be greater than 3 in journal bearings (Spikes [22]).

In the present article, the transition point is taken to be $\Lambda = 3$. We now apply two approaches to estimate lift-off speed corresponding to the experimental results. Vogelpohl's empirical equation for predicting the lift-off speed reads:

$$N_T = \frac{W}{C_T \mu V} \qquad (1.3)$$

where W is the bearing load in pound; μ is viscosity in microreyn; C_T denotes a factor related to the oil flow and such geometric quantities as clearance and minimum oil thickness; C_T =1/4 for most applications; V is defined as bearing volume $= \left(\pi LD^2\right)/4$ in $inch^3$.

Alternatively, the minimum film thickness equation can be directly obtained from the numerical solution to the Reynolds equation (Khonsari & Booser [25]). Fitting an equation to cover high eccentricity values range for different *L/D* ratios results in the following equation for an iso-viscous Newtonian lubricant:

$$\frac{h_{min}}{C} = 4.678(L/D)^{1.044} S \qquad (1.4)$$

Solving for the Sommerfeld number yields:

$$S = \frac{h_{min}}{4.678C(L/D)^{1.044}} \qquad (1.5)$$

The minimum film thickness h_{min} can be calculated by the definition of Λ:

$$h_{min} = \Lambda \times \left(R_a{}^2 + R_b{}^2\right)^{1/2} \qquad (1.6)$$

It is assumed that $\Lambda = 3$. For Gaussian distribution of the summits, R_a and R_b are 1.25 times of the average roughness.

After h_{min} is determined, equation (1.6) is employed to obtain S. Combining with equation (1.1), the lift-off speed can be determined by

$$N_T = \frac{60P_L\Lambda\left(R_a{}^2 + R_b{}^2\right)^{1/2}}{4.678C\left(\frac{L}{D}\right)^{1.044}\mu\left(\frac{Rs}{C}\right)^2} \qquad (1.7)$$

Assuming that the viscosity-temperature relation obey the Walther equation [25]

$$\log\log(\nu + 0.7) = A - B\log T \qquad (1.8)$$

where A and B are constants for any given oil. The viscosity at 50^0C and 60^0C can be estimated from known charts [26].

The lift-off speed for SAE30 oil from equations and experiments are tabulated in Table 1.7. The experimental data for 543 N, 667 N, 890 N loads with 50^0C and 60^0C inlet oil temperature are not available. So the prediction of the lift-off speed for those cases is left blank.

It can be seen from the table that the calculated lift-off speed from two approaches are comparable.

Table 1.7- Prediction of the lift-off speed and comparison to experiment

Load (N)	**Lift-off speed (rpm) Vogelpohl (eq. 1.2)**			**Lift-off speed (rpm) Equation (1.7)**			**Lift-off speed (rpm) Experiment**		
	40^0C	50^0C	60^0C	40^0C	50^0C	60^0C	40^0C	50^0C	60^0C
445	46	68	99	49	73	106	55	68	90
543	56	---	---	60	---	---	68	---	---
667	69	---	---	74	---	---	95	---	---
890	92	---	---	98	---	---	115	---	---

1.3. Discussion

It is noticed that when the load is relatively small, its effect on the shift of the lift-off speed does not obey the rule that they are directly proportional. For instance, the lift-off speed is around the same (46 rpm) for both 222 N and 445N loads (Figure 1.2). To examine this phenomenon, an additional test of 98 N load is performed.

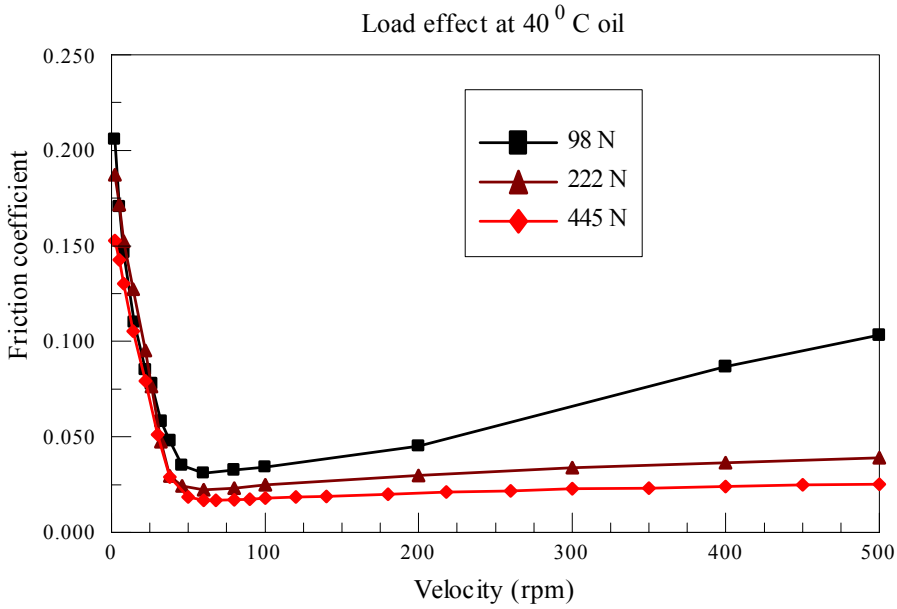

Figure 1.5 Load effect with SAE30 oil

In Figure 1.5, the lift-off speeds of these three loads almost overlap. Similar trends also exist in Vogelpohl's and Stribeck's experiments. According to equation (1.2), when the load is nil, the required lift-off speed is very small. Nevertheless, at a near zero velocity like 2 rpm, a continuous oil film cannot be developed [14]. The authors' deduction is that no matter how small the load is, the shaft speed must be big enough to establish a continuous oil film. Quantitative analysis is beyond the scope of this paper.

In Figure 1.4, when the load is 890 N, the Stribeck curve presents some curvature in mixed lubrication regime. One cannot find this curvature in other reported results. SAE 5W30 is a multigrade oil and uses polymeric additives to improve its viscosity index (VI-improver) and this phenomenon is more pronounced in its tests. Equation (1.7) is derived based on iso-viscous solution of Reynolds' equation. The experimental results of SAE5W30 oil do not fit equation (1.7) well.

1.4. Conclusions

The shift of the Stribeck curve is examined in terms of varying load, oil temperature, and oil type. Increasing oil temperature and load shifts the lift-off speed to the right. In mixed or boundary lubrication regime, a higher temperature creates a greater friction coefficient, while in the full-film lubrication regime, the opposite is true. A higher load causes a smaller friction coefficient in the full-film lubrication regime. It is also shown that an equation derived based on the numerical solution of the finite Reynolds equation can effectively predict the lift off speed.

1.5. Nomenclature

A	constant in viscosity-temperature relation
B	constant in viscosity-temperature relation
C	radial clearance, m

C_T	factor related to the oil flow and geometric quantities
D	shaft diameter, m
f	coefficient of friction
h_{min}	minimum film thickness, m
L	bearing length, m
N_T	lift-off speed, rpm
P_L	projected load, N
R_a	rms of the shaft surface roughness, μm
R_b	rms of the bearing surface roughness, μm
Rs	shaft radius, m
S	Sommerfeld number
T	temperature, ^0C
V	bearing volume, m^3
W	load, N
μ	dynamic viscosity, Pa.s
ν	kinematic viscosity, cSt
Λ	film thickness parameter

CHAPTER 2 THE STRIBECK CURVE: EXPERIMENTAL RESULTS AND THEORETICAL PREDICTION

2.1. Introduction

Stribeck [1] is credited for carrying out the first systematic experiments unfolding a clear view of the characteristic curve of the coefficient of friction versus speed. In recognition of his contribution, this curve is universally referred to as "the Stribeck curve" [4], as shown in Fig 2.1. The Stribeck curve has also been proven to be useful for identifying boundary, mixed, elastohydrodynamic and hydrodynamic lubrication regimes. After the speed parameter was extended to the Sommerfeld number [5, 6, 40], this single curve incorporated all the main characteristics of bearings and gained a much greater breadth.

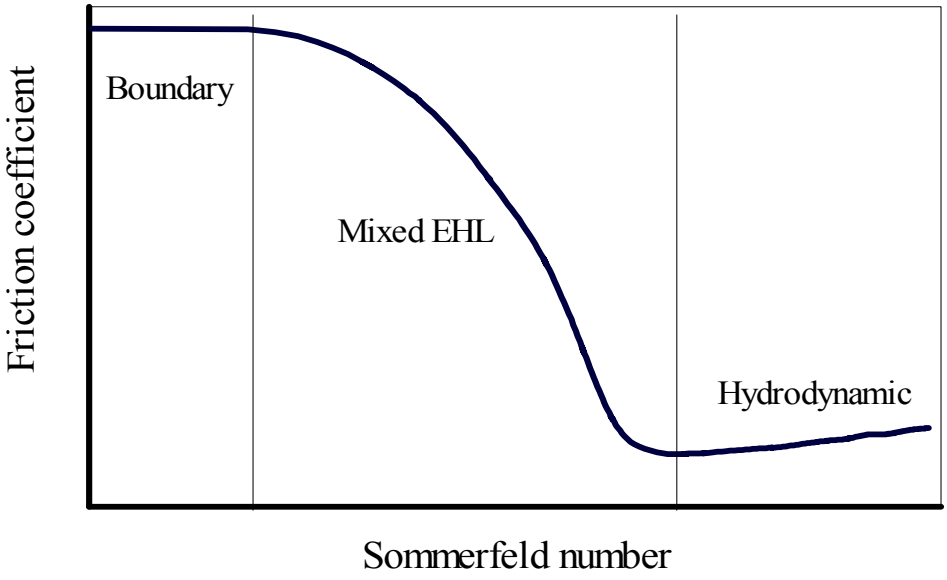

Figure 2.1 – The Stribeck curve

Works on the Stribeck curve fall into two categories: one is experimental examination of its variation by altering the material property, the surface finish, the

viscosity of the oil, and the operating condition; the other is theoretical exploration of its behavior which parallels the development of the modeling of mixed lubrication.

The term “mixed friction” first appeared in the literature early in the 1930s [41]. It evolved into “mixed or quasi-hydrodynamic lubrication” in 1966 [42]. Mixed lubrication commonly defines a lubrication state in which both fluid film and asperity contact exist to support the applied load. However, a thorough understanding of this lubrication state still remains rudimentary. Its progress heavily relies on the breakthrough of knowledge in two areas: an integrative knowledge of fluid film and boundary lubrication, and a sufficient recognition of the stochastic property of rough surface interaction. The year 1966 witnessed a major stride on the statistical analysis of rough surface contact by Greenwood and Williamson [43]. Meanwhile, elastohydrodynamic lubrication attracted the focus of a number of researchers’ attention. These preliminaries paved the way to probing into the depth of mixed lubrication.

The modeling of mixed lubrication is bifurcated into pursuing a full solution of pressure distribution and film thickness of rough surfaces, researched by Cheng [44] and Chang [45]; and modeling the load sharing between hydrodynamic pressure and asperity contact pressure of rough surfaces, pioneered by Johnson [46] and Tallian [47]. The concept of load sharing is relatively straightforward, hence it gains popularity.

Circa 1926, Karelitz [48] was probably the first researcher who formulated the load sharing relationship $P = P_H + P_C$. Thereafter, Fuller [49], Lenning [50], Tsao [51], Soda [52, 53] and Yamaguchi [54] continued to apply this basic concept to improve on the modeling of mixed lubrication regime. More recently, Gelinck [55, 56] proposed a mixed elastohydrodynamic lubrication model by taking advantage of the Moes’ central film thickness equation and Greenwood’s asperity contact pressure expression, including

Johnson's concept of applying a scaling factor γ to hydrodynamic component. This model successfully predicted the trend of the Stribeck curve.

In the present paper, we present the Stribeck curves of a series of experiments under various oil inlet temperatures and loads. The results are compared with the simulations of the Stribeck curves using the approach presented in [55, 56]. The theoretical verifications presented in this paper pertain to mixed lubrication and EHL regimes where the Bair-Winer model is adopted to describe the shear stress of the lubricant. The theoretical analysis, therefore, provide a simple, but realistic model, for prediction of the bearing behavior before lift off occurs. Simplicity in the treatment of friction is often required in precision control industry for development of rapid friction compensation algorithms; see Olsson [57]. More complicated mixed-lubrication models have been developed by Wang [58, 59] and Liu [60].

2.2. Theoretical

2.2.1 Friction Expression

The total normal load F_T is shared by the hydrodynamic lifting force F_H and the asperity interacting force F_C. Consequently,

$$F_T = F_H + F_C \qquad (2.1)$$

Applying Johnson's concept of scaling factors [47], Eq. (2.1) can be rewritten as

$$F_T = \frac{F_T}{\gamma_1} + \frac{F_T}{\gamma_2} \qquad (2.2)$$

where γ_1 and γ_2 are the scaling factors for hydrodynamic part and asperity contact part respectively, which can be simplified as:

$$1 = \frac{1}{\gamma_1} + \frac{1}{\gamma_2} \qquad (2.3)$$

Similarly, the total friction force is the sum of two components

$$F_f = F_{f,H} + F_{f,C} \tag{2.4}$$

where $F_{f,H}$ is the hydrodynamic friction force given by the following expression

$$F_{f,H} = \iint_{A_H} \tau_H dA_H \tag{2.5}$$

where τ_H represents the shear stress and A_H is the contact area of the fluid.

The expression for $F_{f,H}$ is derived based on the Bair-Winer model [61]. The equivalent viscosity η^* for this model is [62]:

$$\eta^* = \eta \frac{1}{\lambda}\left(1 - e^{-\lambda}\right) \tag{2.6}$$

where

$$\lambda = \frac{\eta|\dot{\gamma}|}{\tau_L} \tag{2.7}$$

The limiting shear stress τ_L varies in accordance to pressure described by

$$\tau_L = \tau_{L0} + \beta_0 p_m \tag{2.8}$$

where τ_{L0} is the limiting shear stress at ambient pressure, β_0 is the slope of the limiting shear stress-pressure relation, and p_m is the mean pressure of Hertzian contact.

The traction force per unit length F_l is determined by integrating the shear stress

$$F_l = \int \tau dx = \int \eta^* \dot{\gamma} dx \tag{2.9}$$

The separation of two rough surfaces is assumed to be constant and equal to the central film thickness h_c. By incorporating Eqs. (2.6) and (2.7) into Eq. (2.9), F_l reads:

$$F_l = \pm\tau_L\left(1 - e^{-\frac{\eta\left(\pm\frac{u}{h_c}\right)}{\tau_L}}\right)\cdot 2a \qquad (2.10)$$

where a is the half width of Hertzian contact. Taking the "+" sign, the hydrodynamic friction force $F_{f,H}$ is represented as

$$F_{f,H} = \tau_L\left(1 - e^{-\frac{\eta\left(\frac{u}{h_c}\right)}{\tau_L}}\right)\cdot 2aB \qquad (2.11)$$

with B the bearing length and u the shaft velocity. It is assumed that the oil viscosity η obeys the Roelands' formula [32]:

$$\eta = \eta_0\left(\frac{\eta_\infty}{\eta_0}\right)^{\left[1-\left(1+\frac{p_m}{c_p}\right)^Z\right]} \qquad (2.12)$$

where η_0 is the oil viscosity at inlet temperature. Its value can be found in reference [26]. η_∞ is 6.315×10^{-5} Pa·s. c_p is equal to 1.962×10^8 Pa. The Roelands' pressure-viscosity index Z can be estimated from the lubricant's viscosity (in centipoises) at 40^0 C and 100^0 by using the following equation [63]:

$$Z = \left[7.81\left(H_{40} - H_{100}\right)\right]^{1.5}\left(F_{40}\right) \qquad (2.13)$$

where

$$H_{40} = \log\left(\log\left(\mu_{40}\right) + 1.200\right)$$
$$H_{100} = \log\left(\log\left(\mu_{100}\right) + 1.200\right)$$
$$F_{40} = 0.885 - 0.864H_{40}$$

The parameter $F_{f,C}$ represents the asperity interacting friction force given by

$$F_{f,C} = \sum_{i=1}^{N} \iint_{A_{C_i}} \tau_{C_i} dA_{C_i} \tag{2.14}$$

where τ_{C_i} denotes the shear stress, N represents the number of asperities, and A_{C_i} is the area of asperities in contact.

For a single asperity, the coefficient of friction f_{C_i} is:

$$f_{C_i} = \frac{\tau_{C_i}}{p_{C_i}} \tag{2.15}$$

Assuming that f_{C_i} is constant for all asperities, we arrive at the following relationship for the friction force.

$$F_{f,C} = \sum_{i=1}^{N} \iint_{A_{C_i}} f_{C_i} p_{C_i} dA_{C_i} = f_C \sum_{i=1}^{N} \iint_{A_{C_i}} p_{C_i} dA_{C_i} = f_C F_C \tag{2.16}$$

where f_C is determined from experiments.

Hence, the coefficient of friction can be obtained from

$$f = \frac{F_f}{F_T} = \frac{F_{f,H} + f_c F_c}{F_T} \tag{2.17}$$

2.2.2 Elastohydrodynamic Component

Employing Moes' equation [64], the central film thickness reads:

$$H_c = \left[\left(H_{RI}^{\frac{7}{3}} + H_{EI}^{\frac{7}{3}} \right)^{\frac{3}{7}s} + \left(H_{RP}^{-\frac{7}{2}} + H_{EP}^{-\frac{7}{2}} \right)^{-\frac{2}{7}s} \right]^{s^{-1}} \tag{2.18}$$

where

$$s = \frac{1}{5}\left(7 + 8e^{\left(-2\frac{H_{EI}}{H_{RI}} \right)} \right)$$

with the following group of dimensionless parameters:

$$H_{RI} = 3M^{-1}$$

$$H_{EI} = 2.621M^{-\frac{1}{5}}$$

$$H_{RP} = 1.287L^{\frac{2}{3}}$$

$$H_{EP} = 1.311M^{-\frac{1}{8}}L^{\frac{3}{4}}$$

$$H_c = h_c' U_\Sigma^{-\frac{1}{2}}, h_c' = \frac{h_c}{R}$$

$$M = WU_\Sigma^{-\frac{1}{2}}, L = GU_\Sigma^{\frac{1}{4}}$$

$$W = \frac{F_T}{E'RB},\ U_\Sigma = \frac{\eta_0 u}{E'R},\ G = \alpha E'$$

Applying Johnson's concept of scaling factors, and substituting $\frac{E'}{\gamma_1}$ for E', $\frac{F_T}{\gamma_1}$ for F_T into these equations, it can be shown that

$$h_c' U_\Sigma^{-\frac{1}{2}} = \left[(\gamma_1)^{\frac{s}{2}} \left(H_{RI}^{\frac{7}{3}} + (\gamma_1)^{-\frac{14}{15}} H_{EI}^{\frac{7}{3}} \right)^{\frac{3}{7}s} + (\gamma_1)^{-\frac{s}{2}} \left(H_{RP}^{-\frac{7}{2}} + H_{EP}^{-\frac{7}{2}} \right)^{-\frac{2}{7}s} \right]^{s^{-1}} (\gamma_1)^{\frac{1}{2}} \qquad (2.19)$$

where

$$s = \frac{1}{5}\left(7 + 8e^{\left(-2\gamma_1^{-\frac{2}{5}} \cdot \frac{H_{EI}}{H_{RI}} \right)} \right)$$

2.2.3 Asperity Contact Component

Greenwood and Williams' model is adopted to calculate the interacting pressure of asperities [43]. The appropriate expression is:

$$p(x) = \frac{2}{3} n\beta\sigma_s \sqrt{\frac{\sigma_s}{\beta}} E' F_{3/2}\left(\frac{h(x)}{\sigma_s} \right) \qquad (2.20)$$

where

$$F_{3/2}\left(\frac{h(x)}{\sigma_s}\right)=\frac{1}{\sqrt{2\pi}}\int_{\frac{h(x)}{\sigma_s}}^{\infty}\left(s-\frac{h(x)}{\sigma_s}\right)^{\frac{3}{2}}e^{-\frac{1}{2}s^2}ds$$

The distance between the mean plane through the summits and the mean plane through the surface heights is d_d. Because the latter is taken as the reference plane for the hydrodynamic component in the current calculation, d_d is subtracted by the separation of rough surfaces $h(x)$. According to Whitehouse and Archard [65], d_d is approximately $1.15\sigma_s$. Therefore the central contact pressure of an asperity can be expressed as:

$$p_c=\frac{2}{3}n\beta\sigma_s\sqrt{\frac{\sigma_s}{\beta}}E'F_{3/2}\left(\frac{h_c-d_d}{\sigma_s}\right) \tag{2.21}$$

Gelinck [55] fitted the following expression to the central contact pressure:

$$p_c=p_h\left[1+\left(a_1 n'^{a_2}\sigma_s'^{a_3}W^{a_2-a_3}\right)^{a_4}\right]^{\frac{1}{a_4}} \tag{2.22}$$

where $a_1 = 1.558$, $a_2 = 0.0337$, $a_3 = -0.442$, $a_4 = -1.70$, and p_h represents the maximum Hertzian pressure of line contact:

$$p_h=\sqrt{\frac{F_T E'}{2\pi B R'}}$$

Combining Eqs. (2.21) and (2.22), we arrive at the following equation:

$$\frac{2}{3}n\beta\sigma_s\sqrt{\frac{\sigma_s}{\beta}}E'F_{3/2}\left(\frac{h_c-d_d}{\sigma_s}\right)=p_h\left[1+\left(a_1 n'^{a_2}\sigma_s'^{a_3}W^{a_2-a_3}\right)^{a_4}\right]^{\frac{1}{a_4}} \tag{2.23}$$

Substituting $\frac{E'}{\gamma_2}$ for E', $\frac{F_T}{\gamma_2}$ for F_T, and $n\gamma_2$ for n into it, and making it dimensionless, yields:

$$\frac{2}{3}n'\sigma_s'\sqrt{\sigma_s'}F_T'F_{3/2}\left(\frac{h_c'-d_d'}{\sigma_s'}\right)=\left[1+\left(a_1 n'^{a_2}\sigma_s'^{a_3}W^{a_2-a_3}\gamma_2{}^{a_2}\right)^{a_4}\right]^{\frac{1}{a_4}}\frac{1}{\gamma_2} \qquad (2.24)$$

with the following group of dimensionless parameters:

$$n' = nR\sqrt{\beta R}$$

$$\sigma_s' = \frac{\sigma_s}{R}$$

$$F_T' = \sqrt{\frac{2\pi B R' E'}{F_T}}$$

$$d_d' = \frac{d_d}{R}$$

Combining Eqs. (2.3), (2.19), and (2.24) provides the appropriate equations for evaluating the unknown parameters γ_1, γ_2, h_c. Substituting γ_2 into Eq. (2.2), h_c into Eq. (2.11), together with Eqs. (2.16) and (2.17), enables one to determine the coefficient of friction.

2.3. Experimental

Lewis LRI-8H tribometer is used for measuring the coefficient of friction of journal bearings. Its detail has been described in §1.2, Chapter 1.

2.3.1 Bearing Properties and Operating Conditions

The shaft is made up of hardened AISI 1020 steel. The bushing is composed of SAE 660 alloy bronze. It is a high-quality smooth machine finish material and highly resistant to impact, wear and corrosion. Their characteristics are tabulated in Table 2.1. The properties of SAE30 oil are referred to Table 1.5. The applied loads are: 667 N (150 lb), 890 N (200 lb), 1112 N (250 lb). The range of speeds tested is between 2rpm to 500rpm.

Table 2.1- Bearing characteristics

Length (mm)	Shaft Diameter (mm)	Bushing Inner Diameter (mm)	Young's Modulus (GPa)		Poisson's Ratio		Surface Roughness R_a (μm)	
			shaft	bushing	shaft	bushing	shaft	bushing
25.4	24.54	24.71	209	100	0.29	0.33	0.05	0.2

2.3.2 Experimental Procedure

The same experimental procedure as in §1.2.1, Chapter 1 is followed.

2.4. Numerical Simulations

Three unknown parameters γ_1, γ_2 and h_c are included in three nonlinear Eqs. (2.3), (2.19) and (2.24). Using Eq. (2.3), γ_1 is expressed in terms of γ_2 and substituted into Eq. (2.19). The parameter h_c is on the left side of Eq. (2.19) and can be substituted into Eq. (2.24). Therefore, three equations are condensed into one nonlinear equation. The bisection scheme is employed to solve it. An initial guess is made for γ_2. In the boundary or mixed lubrication regime, asperity contact friction plays a major role so that γ_2 is taken as 1.0001. The speed range is divided into 1000 points.

2.5. Results and Discussion

Additional input parameters used in the simulations are provided in Table 2.2.

Table 2.2- Input parameters of simulation

Parameter	Value
n	2.5×10^{10} m^{-2}
β	10×10^{-6} m
σ_s	0.2×10^{-6} m
E'	1.50×10^{11} Pa
η_0	0.0815 Pa·s
β_0	0.047
τ_{L0}	2.5×10^{6} Pa

2.5.1 Effect of Inlet Oil Temperature

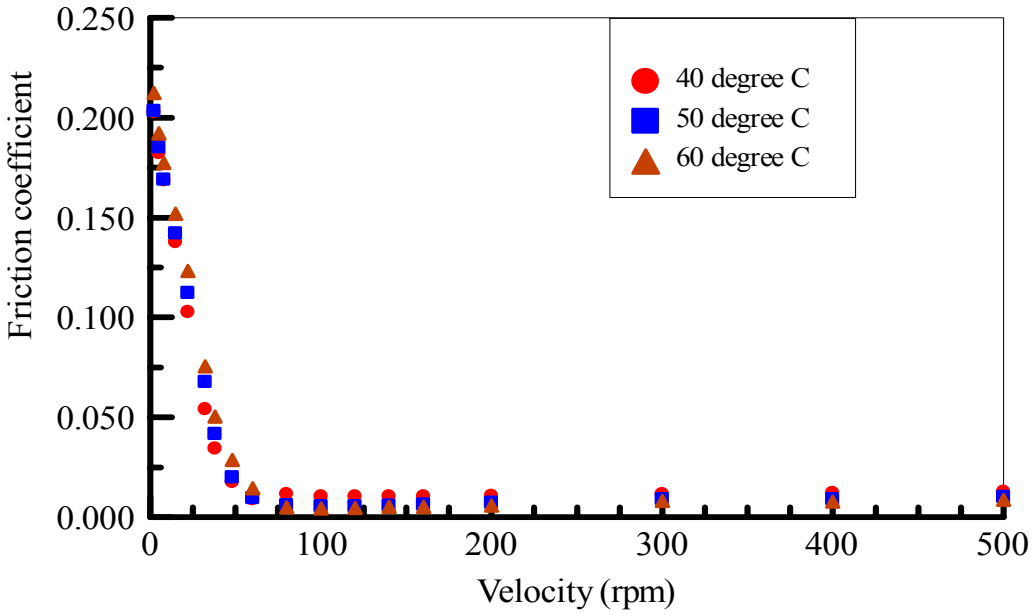

Figure 2.2 - Effect of inlet oil temperature on the friction coefficient plotted as a function of velocity, experiment

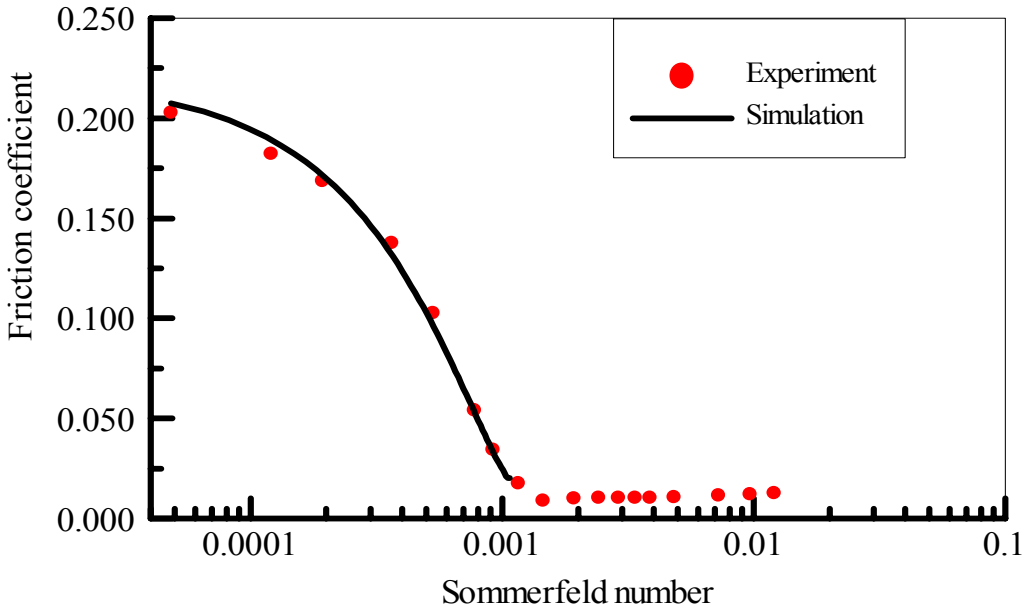

Figure 2.3 - The friction coefficient as a function of the Sommerfeld number (Oil temperature: 40 ^{0}C)

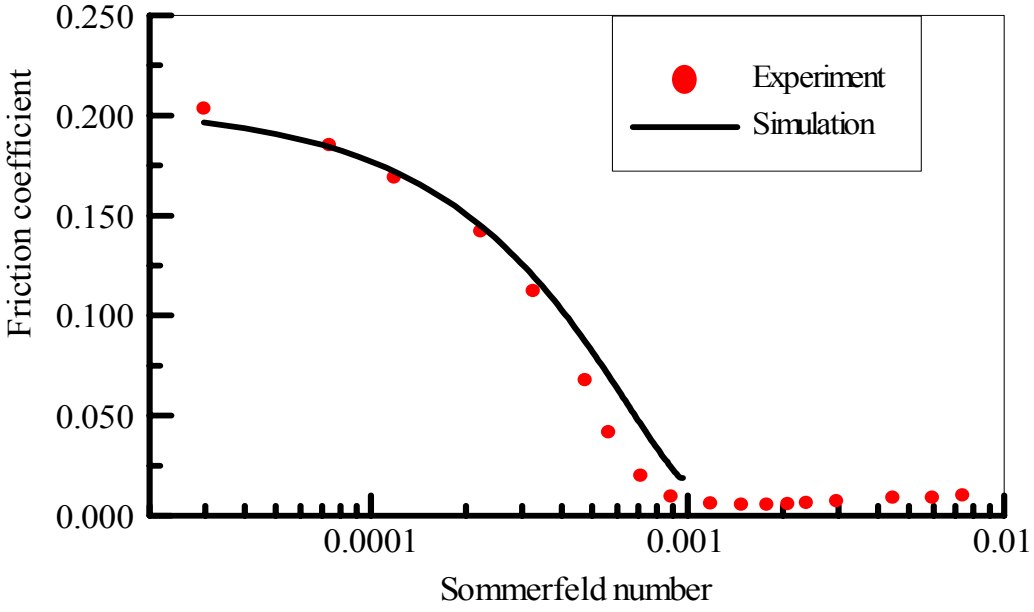

Figure 2.4 - The friction coefficient as a function of the Sommerfeld number (Oil temperature: 50 ^{0}C)

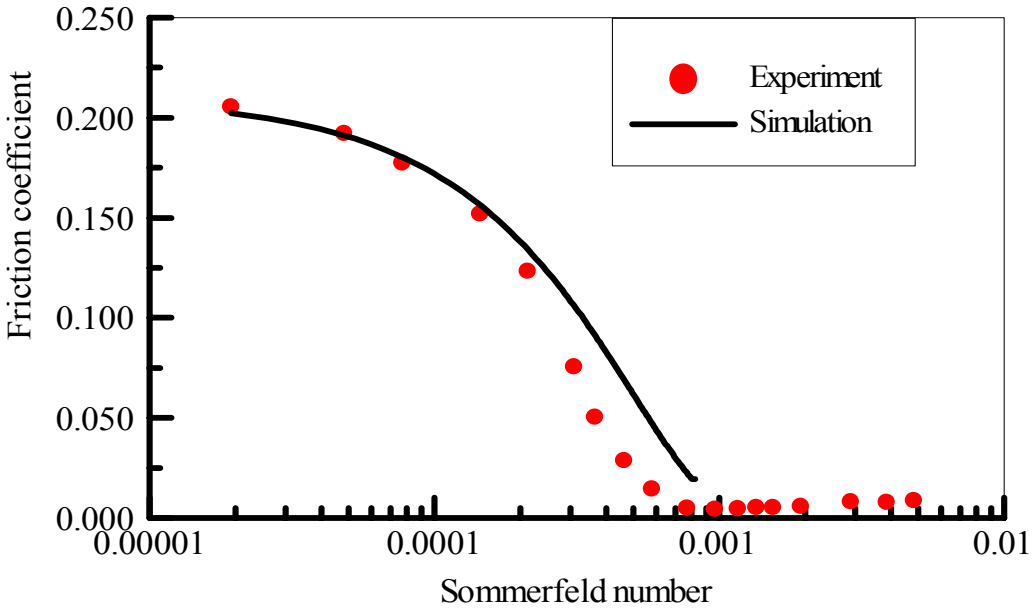

Figure 2.5 - The friction coefficient as a function of the Sommerfeld number (Oil temperature: 60 ^{0}C)

The effect of oil viscosity on the Stribeck curve can be demonstrated by varying the inlet oil temperature, as shown in Figs. 2.2-2.5. 667 N load is applied.

Fig. 2.2 shows the experimental results of the inlet oil temperature effect on the Stribeck curve. In the mixed lubrication regime, the oil temperature is higher and, as a result, the viscosity decreases. Less viscosity translates to a greater extent of metal-to-metal contact to support the same load, which translates into the asperity contact dominating the coefficient of friction. In hydrodynamic lubrication regime, the coefficient of friction is reduced as the oil viscosity decreases with increasing inlet temperature.

Figs. 2.3-2.5 compare simulation and experiment under various inlet oil temperature conditions. To demonstrate the agreement between simulation and experiment in boundary and mixed lubrication regimes, the coefficient of friction is plotted versus a logarithm abscissa of the Sommerfeld number. They illustrate that the simulation captures the inlet oil temperature effect on the Stribeck curve in boundary and mixed lubrication regimes.

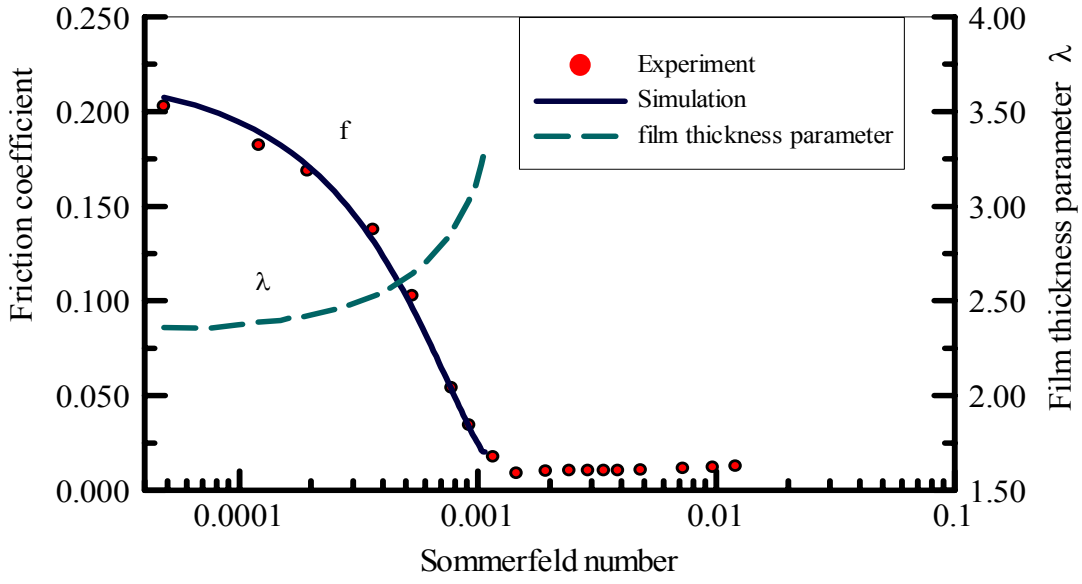

Figure 2.6 - The film thickness parameter as a function of the Sommerfeld number, 667 N load, 40 ^{0}C oil

Fig. 2.6 examines the variation of the film thickness parameter λ ($\lambda = h_c/\sigma_s$) with the Sommerfeld number. λ = 3.3 at the lift-off speed, which is close to the widely accepted value λ=3.

2.5.2 Effect of Load

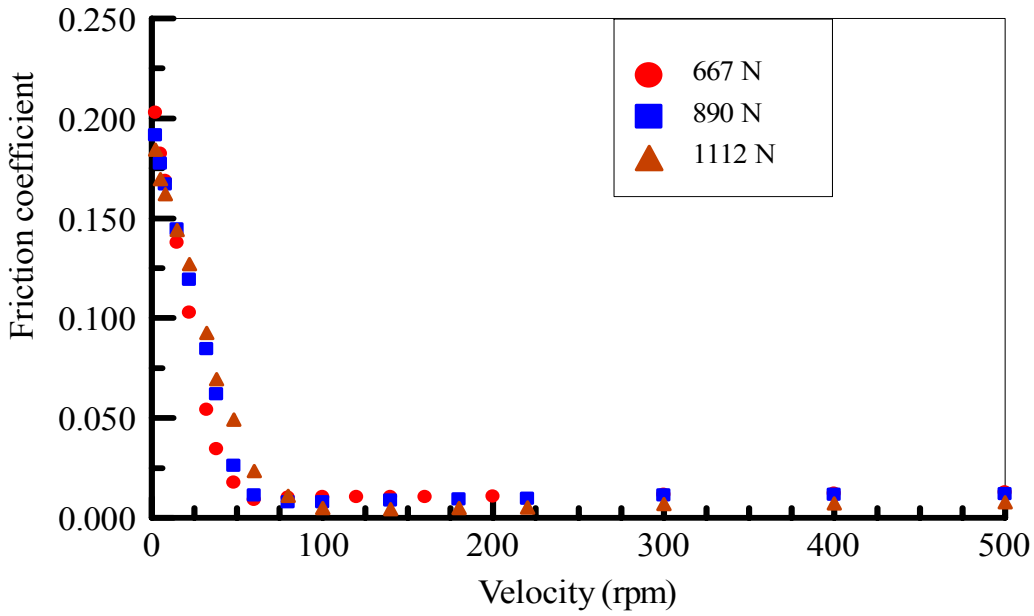

Figure 2.7 - Effect of load on the friction coefficient plotted as a function of velocity, experiment, 40 ^{0}C oil

Figures 2.7-2.8 shows the results for the coefficient of friction as a function of Sommerfeld number for different loads ranging from 667 N to 1112 N. The oil inlet temperature is 40 ^{0}C. In the mixed lubrication regime, simulations successfully predict that a light load creates a smaller coefficient of friction than does the heavy load. The experimental results exhibit the same trend. The model is based on the load sharing concept. When the imposed load is heavy, more metal-to-metal asperity contact occurs, which creates a greater asperity friction and causes the coefficient of friction to increase.

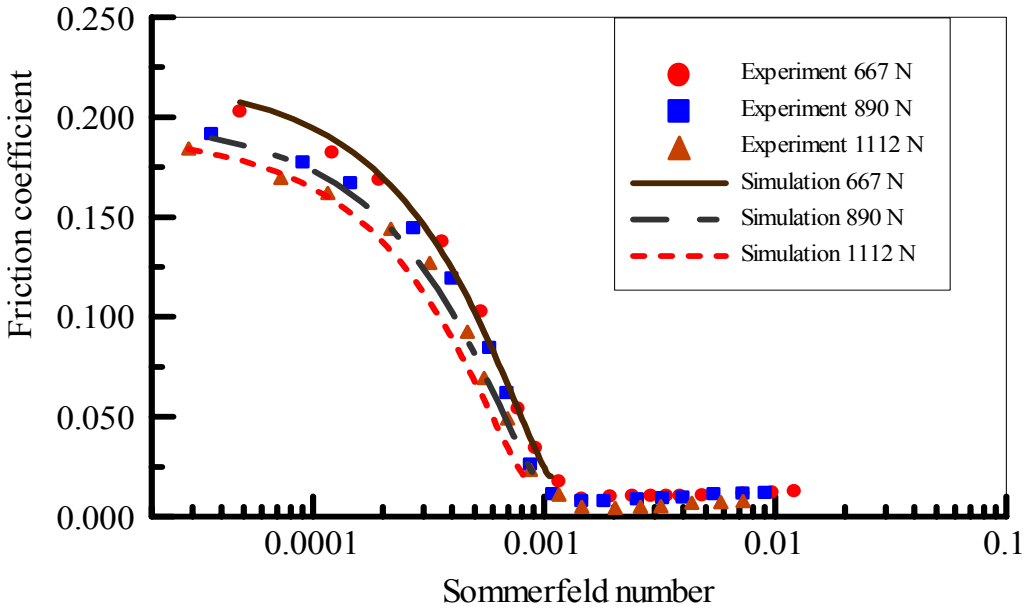

Figure 2.8 - Effect of load on the friction coefficient as a function of the Sommerfeld number

In hydrodynamic regime, a higher load translates into a higher eccentricity ratio ε, and a thinner film. Therefore, the friction coefficient is lower, as shown in the experiments. Solutions of the full Reynolds equation also reveal the same information [25]. According to [25], in a bearing whose length is equal to the shaft diameter (L/D =1), the coefficient of friction varies from f (C/R) = 53.4294 at ε =0.05 to f (C/R) =0.6896 at ε =0.95.

Since the simulation results presented in this paper are limited to the mixed lubrication regime, all the curves are truncated after reaching the minimum friction coefficient. In this regime, the simulations and the experimental results are in good agreement.

It is worthwhile to note that when the oil inlet temperature or the load is higher, the discrepancy between simulation and experiment become greater. Increasing the oil

temperature or the load tends to magnify the influence of thermal effect on the performance of bearings. Additional factors that may affect the results include thermal expansion and starvation effects.

2.6. Conclusions

The behavior of Stribeck curve is examined both theoretically and experimentally. Employing the load sharing concept, a mixed elastohydrodynamic model using the Bair-Winer constitutive equation is proposed. This model is based on the line contact formulation and incorporates surface roughness, the pressure-viscosity, and the temperature-viscosity effects. In the mixed lubrication regime, a higher lubricant temperature creates a larger friction coefficient, while in the full-film lubrication regime, the opposite is true. The model effectively predicts the friction behavior in the mixed lubrication regime.

2.7. Nomenclature

a	half width of Hertzian contact $= \sqrt{8F_T R' / \pi E' B}$, m
A	contact area, m^2
B	bearing length, m
C	radial clearance, m
c_p	constant, 1.962×10^8 Pa
d_d	distance between mean line of asperities and mean line of surface, m
E	modulus of elasticity for shaft, Pa
E_b	modulus of elasticity for bushing, Pa
E'	equivalent modulus of elasticity, $= 2/\left(\left(1-\nu^2\right)/E + \left(1-\nu_b^2\right)/E_b\right)$, Pa
$F_{f,C}$	friction force from asperity interaction, N

$F_{f,H}$ hydrodynamic friction force, N

f coefficient of friction

h film thickness, m

n density of asperities, $1/m^2$

N_T shaft velocity, revolution per second

p pressure, Pa

p_h maximum Hertzian pressure, Pa

p_m mean Hertzian pressure $= F_T/2aB$, Pa

P, F load, N

P_L projected load, $= P/(2RB)$, Pa

R shaft radius, m

R_b bushing radius, m

R' equivalent radius, $= RR_b/(R_b - R)$, m

S Sommerfeld number, $= \eta N_T (R/C)^2 / P_L$

u effective velocity, m/s

Z pressure-viscosity index

α pressure-viscosity coefficient, 1/Pa

β average radius of asperities, m

β_0 slope of the limiting shear stress-pressure relation, 0.047

γ scaling factor

$\dot{\gamma}$ shear strain rate, 1/s

λ film thickness parameter

η dynamic viscosity, Pa·s

η_0 dynamic viscosity at zero pressure and 40^0 C temperature, Pa·s

η_∞ constant, 6.315×10^{-5} Pa·s

μ kinematic viscosity, m^2/s

ν Poisson's ratio for shaft

ν_b Poisson's ratio for bushing

σ_s standard deviation of asperities, m

τ shear stress, Pa

τ_L limiting shear stress, Pa

τ_{L0} limiting shear stress at ambient pressure, Pa

Subscripts

c central

C, 2 Asperity component

f friction

H, 1 Hydrodynamic component

T total or normal

CHAPTER 3 AN EXPERIMENTAL INVESIGATION OF GREASE-LUBRICATED JOURNAL BEARINGS

3.1. Introduction

Grease is widely used in journal bearings that are tasked to function under relatively low to moderate speeds but heavily loaded operating conditions. Compared to conventional oils, grease offers some advantages in terms of enhanced stability, reduced maintenance requirements, and considerably lower leakage rate. While in typical applications the contact is starved of bulk grease, the base oil is released from bulk grease outside the contact either by hydrodynamic pressure or by soap structure shrinking. This grease replenishment mechanism will serve to maintain a lubricating film in the contact track [66-71]. This mechanism allows for a longer service life [72]. Moreover, experience shows that in boundary or mixed lubrication regime, a grease-lubricated journal bearing performs better than an oil-lubricated one [73-75]. Another advantage is that the dimensions of a greased-lubricated bearing are smaller than that of an oil-lubricated bearing with the identical load capacity [76], and there is no need for an elaborate oil supply system.

Despite its extensive use, the underlying lubrication mechanism of grease is still poorly understood [77, 78]. The paucity of available literature stems from the complexity of behavior of grease and its non-Newtonian response to shear.

One of the early attempts at understanding the general nature of grease lubrication is the experimental studies reported by Westcott [79] who tested a number of greases under a variety of conditions and was published in 1913. Westcott presented results for the history of the coefficient of friction versus time and temperature. His experiments showed that grease was suitable as a general lubricant. Cohn [80] measured the film

pressure in grease lubrication. Chakrabarti [81] concluded that lithium greases could be treated as a Bingham plastic. In his article, the friction torque was empirically expressed in terms of the yield stress, the plastic viscosity, the speed, the load, and the clearance. Unfortunately the relationship between the friction coefficient and those factors was not clarified. Bradford's work [73] on a cast bronze half-bearing made further advancement. He plotted the friction coefficient versus the so-called Hersey number. But the lubrication regime was restricted to hydrodynamic part. A pressure-velocity limitation chart was established by Glaeser [82] from design point of view. With some additive like PTFE, the performance of grease-lubricated journal bearing was improved [83] and facilitated the application of grease to spiral-groove bearings [84].

Theoretical studies on the behavior of grease began with calculation of pressure distribution by Lawrence [85]. Milne [86] analyzed the performance of a simple slider bearing with complete core formation. Wada [87-90] and Hayashi [91] devoted considerable attention to grease lubrication of journal bearings. They introduced a "nonlinear factor" into the Reynolds equation to characterize the behavior of a pseudo-plastic type grease. Tichy [92] presented a modified Reynolds equation for Bingham plastic. More recently, papers dealing with the EHL aspects [93-95] and grease-lubricated bearings with consideration of thermal effect [96] have been published.

A review of the open literature reveals that the transition of the regimes of grease lubrication in bearings has not been studied. Given that many grease lubricated bearings operate in oscillatory or intermittent fashion, it is essential to examine the transition of grease lubrication. In the current paper, a series of experimental results is presented to emphasize the transition and describe the friction characteristic of grease-lubricated journal bearings. Also presented in this paper are the prediction results of a mixed

elastohydrodynamic lubrication model for line contacts to estimate the coefficient of friction in mixed lubrication regime.

3.2. Experimental

Lewis LRI-8H tribometer is used for measuring the coefficient of friction of journal bearings. Its detailed description is available in §1.2, Chapter 1. Briefly, the machine is capable of measuring the friction coefficient under varying operating conditions such as load, speed, and temperature. Load is applied through a level mechanism. The friction force is sensed by a measuring cell and data are continuously recorded into a computer via an automated data acquisition system.

The measuring error of the friction coefficient is based on the accuracy of the load cell. For a given load cell, the amount of the friction force error is fixed. A 44 N load cell is used in experiments reported in this paper. With increasing load, the error of the friction coefficient becomes smaller as shown in Table 3.1.

Table 3.1 - Error of the friction coefficient associated with load

Load (N)	667	890	1112
Error (±)	0.0023	0.0017	0.0014

3.2.1 Bearing Properties

The shaft is made of hardened AISI 1020 steel with 0.29 Poisson's ratio, 200 GPa elastic modulus. The shaft diameter is 24.54 mm. Its surface roughness is 0.05 μm (R_a). Bronze and steel bushings are employed in tests. Their properties and dimensions are listed in Table 3.2.

Two different greases are chosen as the lubricants: Moly#5 and ALG#1. Table 3.3 summarizes their properties.

Table 3.2 - Bushing dimensions, surface finish (R_a) and material properties

Material	Young's modulus (GPa)	Inner diameter mm	Outer diameter mm	Length mm	Surface roughness μm
SAE 660 alloy bronze	100	24.71	33.66	25.4	0.20
Steel	200	25.4	34.04	25.4	0.32

Table 3.3 - Grease properties

	NLGI Grade	Thickener type	Dropping point (^{0}C)	Base oil viscosity (cSt) @ 40 ^{0}C
Moly#5	1	Lithium complex	260	357
ALG#1	1	Calcium sulfonate	260	150

Table 3.4 shows the combination of load and grease tested. The range of the tested speed is from 2 rpm to 500 rpm.

Table 3.4 - Experiment cases

Bushing	Grease	Load (N)
Steel	Moly#5	667
		890
		1112
	ALG#1	667
		890
		1112
Bronze	Moly#5	667
		890
		1112
	ALG#1	667
		890
		1112

3.2.2. Experimental Procedure

Before recording measurement data, the system is balanced so that the coefficient of friction is nil when the shaft is at static position. The system is run-in for two hours at the running speed of 100 rpm and the load of 667 N. A computerized data acquisition system allows monitoring the history of the coefficient of friction at each running speed. The friction coefficient tends to oscillate periodically around a relatively constant value. The rms value of the history is taken as the coefficient of friction for that speed. By observation, a testing period of four minutes is regarded to be a reasonable testing period for each velocity. After each test is completed, the system is given enough time, typically two hours, to cool down before conducting the next test.

3.2.3. Experimental Results and Discussion

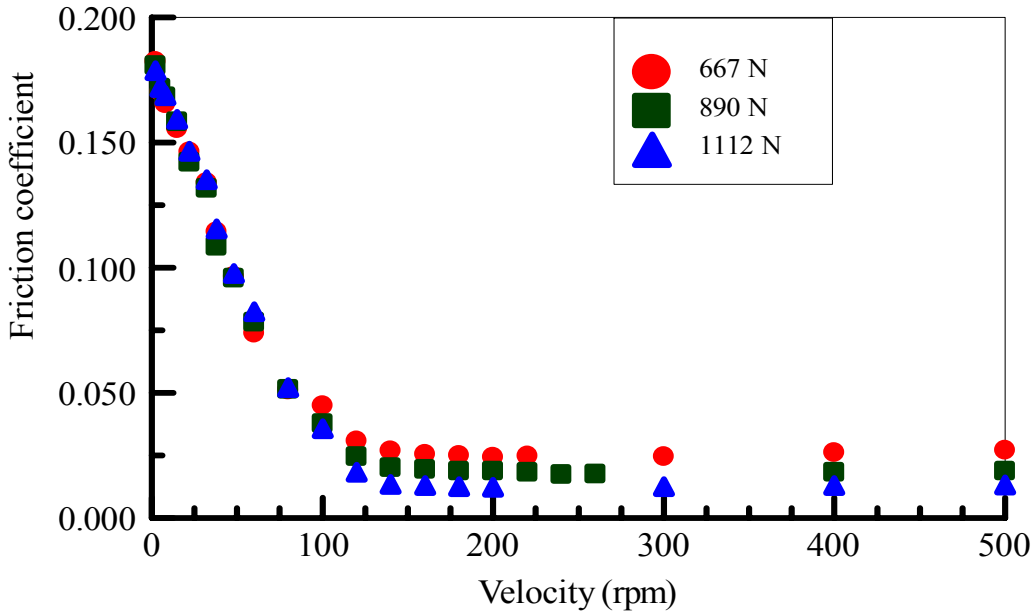

Figure 3.1 - The friction coefficient as a function of velocity (Moly#5 grease, steel bushing)

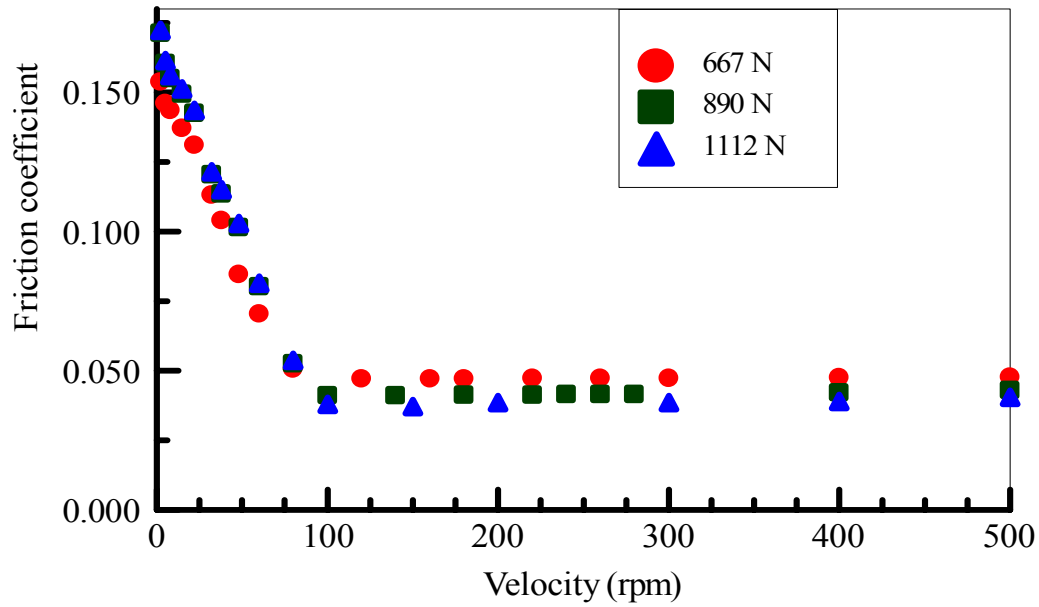

Figure 3.2 - The friction coefficient as a function of velocity (ALG#1 grease, steel bushing)

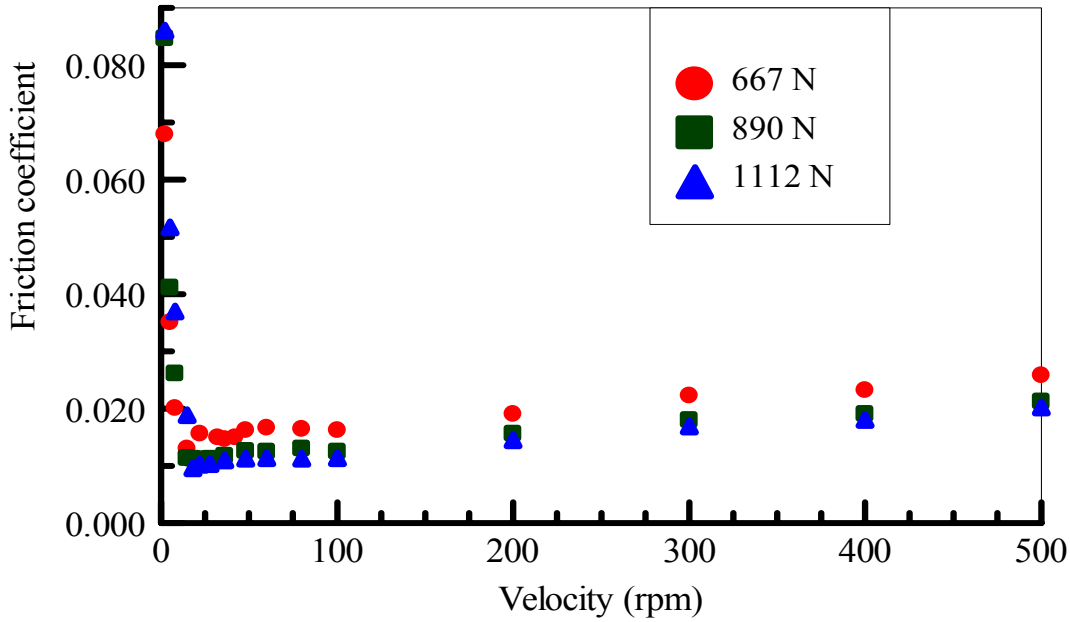

Figure 3.3 - The friction coefficient as a function of velocity (Moly#5 grease, bronze bushing)

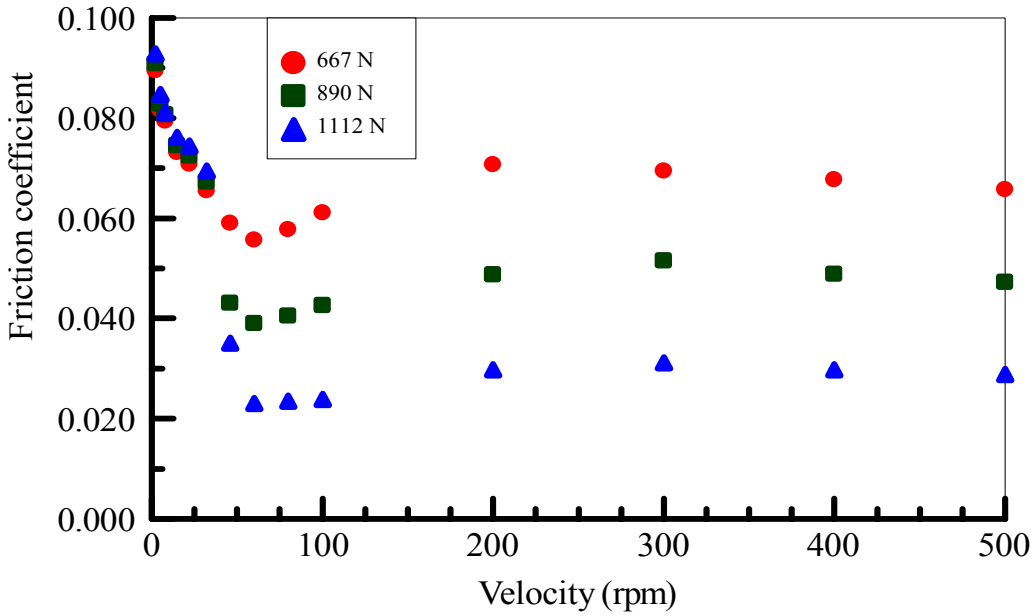

Figure 3.4 - The friction coefficient as a function of velocity (ALG#1 grease, bronze bushing)

Figures 3.1-3.4 display the experimental results of twelve cases, also summarized in Table 3.4. The results reveal that in each case there exists a distinct minimum friction coefficient point which marks the transition between mixed lubrication and hydrodynamic lubrication. In the hydrodynamic regime, increasing the load tends to reduce the friction coefficient. This trend remains the same for oil lubricated bearings as well [97]. A heavier load translates to a bigger eccentricity and a thinner film thickness, which produces a smaller friction coefficient. Numerical solutions of Reynolds equation for a finite oil-lubricated journal bearing also reveal the same information. According to [25], in a bearing whose length is equal to the shaft diameter (B/D =1), the value of f (C/R) varies from 53.4294 at ε =0.05 to 0.6896 for ε =0.95, where f is the coefficient of friction; C is the radial clearance; and R is the radius of the journal.

In the hydrodynamic lubrication regime, the friction coefficient drops almost linearly with increasing load at a specific velocity. The load is increased by 222 N evenly

from 667 N, to 890 N, to 1112 N. For example, at the speed of 300 rpm, the friction coefficient decreases respectively by 0.0068 and 0.0053 in Fig. 3.1; by 0.0057 and 0.0030 in Fig. 3.2; by 0.0043 and 0.0011 in Fig. 3.3; by 0.0180 and 0.0204 in Fig. 3.4. The variation of the friction coefficient reflects a change in the lubricant film thickness. With increasing load, the film thickness becomes thinner. The load effect on the film thickness becomes more distinctive in the case of less viscous lubricant (ALG#1 grease) and more elastic and a bushing of smoother surface finish (bronze), as shown in Fig. 3.4.

In boundary or mixed lubrication regime, a higher load produces a greater friction coefficient. Mixed lubrication is a lubrication state in which the load is supported by both fluid pressure and asperities. When the load becomes greater, more metal-to-metal asperity contact occurs and brings about a rise in the friction coefficient.

To probe further into the frictional characteristics of grease, it is useful to borrow the concept of dimensionless Sommerfeld number from the well-established principles of hydrodynamic lubrication theory. Let us introduce a "grease-Sommerfeld number" defined as:

$$S = \frac{\eta_{BO} \times N_s}{P_L}\left(\frac{R}{C}\right)^2 \qquad (3.1)$$

where η_{BO} is the viscosity of the grease base oil; N_s is the shaft velocity (rev/s); P_L is the projected load $P_L = \frac{W}{2RB}$; R is the shaft radius; C is the radial clearance $C = \frac{R_b - R}{2}$. Applying this definition to the cases of steel bushing and Moly#5 grease (the base oil viscosity: 357 cSt), the coefficient of friction is plotted against the grease-Sommerfeld number as in Fig. 3.5, where the base oil viscosity is used in calculating the

Sommerfeld number. This figure reveals a shape similar to the friction characteristic of oil-lubricated journal bearings.

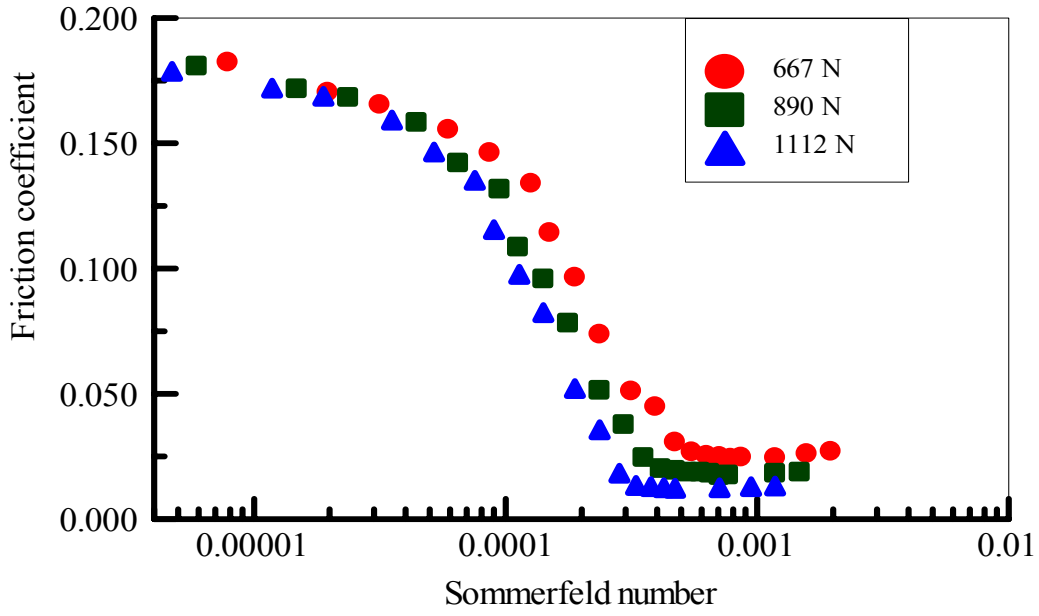

Figure 3.5 - The friction coefficient as a function of Sommerfeld number (Moly#5 grease, steel bushing)

3.2.4. Comparison with Oil Lubrication

Since the frictional characteristic of the grease lubricated bearings exhibits a similar trend to the Stribeck curve for oil, it is natural to compare their characteristics. SAE40 oil is chosen to make the comparison, for its viscosity at 40^0C is 150 cSt which is identical to that of the base oil of ALG#1 grease. The results are shown in Figs. 3.6-3.8.

Clearly, in the boundary or mixed lubrication regimes, the friction coefficient with grease is lower than that of oil. Horth [74] added various percentage of soap into the base oil to formulate different greases and obtained the same conclusion. The viscosities of the base oils are 150 cSt for ALG#1 grease and 357 cSt for Moly#5 grease. At low speeds

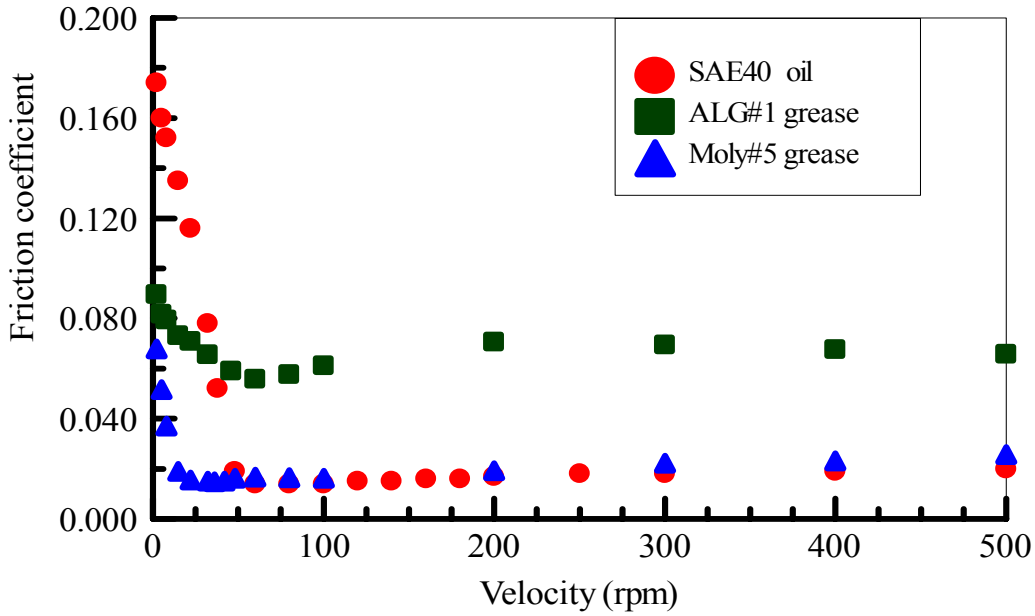

Figure 3.6 - Comparison of two greases with SAE40 oil lubrication (667 N load, bronze bushing)

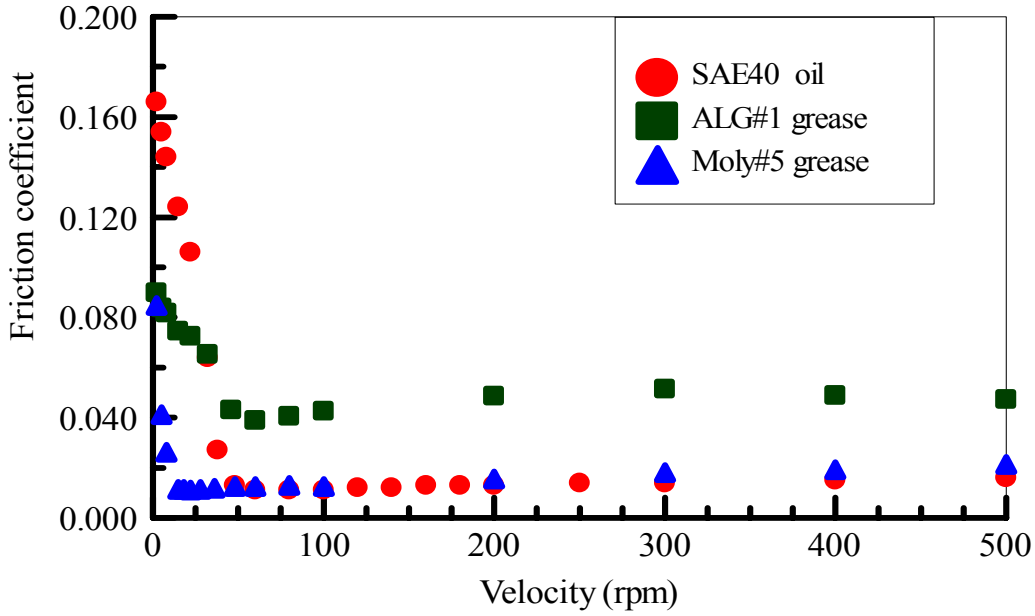

Figure 3.7 - Comparison of two greases with SAE40 oil lubrication (890 N load, bronze bushing)

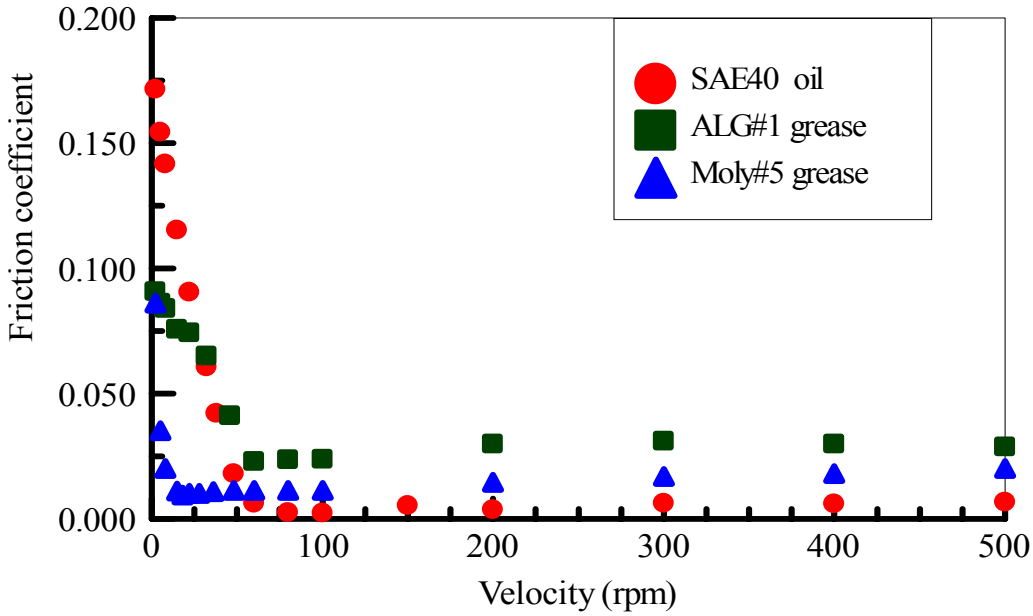

Figure 3.8 - Comparison of two greases with SAE40 oil lubrication (1112 N load, bronze bushing)

when boundary lubrication prevails, the thickener of grease enters the contact and forms a deposited film which reduces asperity interaction [98]. Therefore, the friction coefficient associated with oil is higher than that of grease. This explanation also holds in that the friction coefficient with Moly#5 grease is smaller than that with ALG#1 grease because of the higher viscosity of its base oil. Furthermore, the transition point of lubrication regimes from mixed one to hydrodynamic one shifts to the left with a more viscous lubricant, which implies that a higher viscosity lubricant can result in lift-off at a lower speed.

In the hydrodynamic lubrication regime, the bearing surfaces are separated by a relatively thick film and friction is caused by the shear stress of the lubricant. In this regime, the friction of grease is greater than that of oil due to its higher viscosity.

3.2.5 Theoretical Predictions

A mixed elastohydrodynamic lubrication model for line contacts is presented in §2.2, Chapter 2. While the procedure is developed for oil lubricated bearings, it can provide insight into the frictional characteristics of grease lubrication. The critical procedure in calculating the coefficient of friction is to determine the thickness of the lubricant film. For grease lubrication, although the role of thickener should not be ignored [98], the properties of the base oil are assumed to be the key factors in predicting the film thickness [99, 100].

The asperity-film load sharing concept is employed into a mixed elastohydrodynamic lubrication model to determine the friction coefficient. As shown in §2.2, Chapter 2, the mixed elastohydrodynamic lubrication model is described by three equations:

$$1 = \frac{1}{\gamma_1} + \frac{1}{\gamma_2} \tag{3.2}$$

$$h_c' U_\Sigma^{-\frac{1}{2}} = \left[(\gamma_1)^{\frac{s}{2}} \left(H_{RI}^{\frac{7}{3}} + (\gamma_1)^{-\frac{14}{15}} H_{EI}^{\frac{7}{3}} \right)^{\frac{3}{7}s} + (\gamma_1)^{-\frac{s}{2}} \left(H_{RP}^{-\frac{7}{2}} + H_{EP}^{-\frac{7}{2}} \right)^{-\frac{2}{7}s} \right]^{s^{-1}} (\gamma_1)^{\frac{1}{2}} \tag{3.3}$$

$$\frac{2}{3} n' \sigma_s' \sqrt{\sigma_s'} F_T' F_{3/2} \left(\frac{h_c' - d_d'}{\sigma_s'} \right) = \left[1 + \left(a_1 n'^{a_2} \sigma_s'^{a_3} W^{a_2 - a_3} \gamma_2^{a_2} \right)^{a_4} \right]^{\frac{1}{a_4}} \frac{1}{\gamma_2} \tag{3.4}$$

Numerical solution of Eqs. (3.2)-(3.4) gives the Johnson's scaling factor [47] γ_1 and γ_2 associate with the hydrodynamic lifting force and asperity contact force, respectively. This information in conjunction with an appropriate lubricant constitutive equation allows one to predict the coefficient of friction in the mixed lubrication regime. See §2.2,

Chapter 2 for the details of formulation and numerical solution technique. The data used in the simulations are summarized in Table 3.5.

Table 3.5- Input parameters of simulations

Parameter	Value
n	1.25×10^{10} m^{-2}
β	10×10^{-6} m
σ_s	0.4×10^{-6} m
E'	2.28×10^{11} Pa
η_0	0.0815 Pa·s
β_0	0.047
τ_{L0}	2.5×10^{6} Pa

The simulation results along with experimental measurements for the steel bushing are shown in Figs. 3.9-3.11. They reveal good estimation of the friction coefficient in mixed lubrication regime. As the velocity increases, the film thickness becomes greater, providing greater separation between the shaft and bushing surfaces. This is reflected by the variation of film thickness parameter λ $(=h_c/\sigma_s)$ in Fig. 3.9.

Since the simulation results presented in this paper are limited to the mixed lubrication regime, all the curves are truncated after reaching the minimum friction coefficient. In this regime, the simulations and the experimental results are in good agreement. It is worthwhile to note that when the load is higher, the discrepancy between the simulations and the experimental results become greater. Increasing the load tends to magnify the influence of thermal effect on the performance of bearings, which is not considered in this paper. An additional factor neglected in the analysis that may affect the results is thermal expansion.

3.3. Conclusions

Experiments reveal that there is distinctive regime transition in grease lubrication,

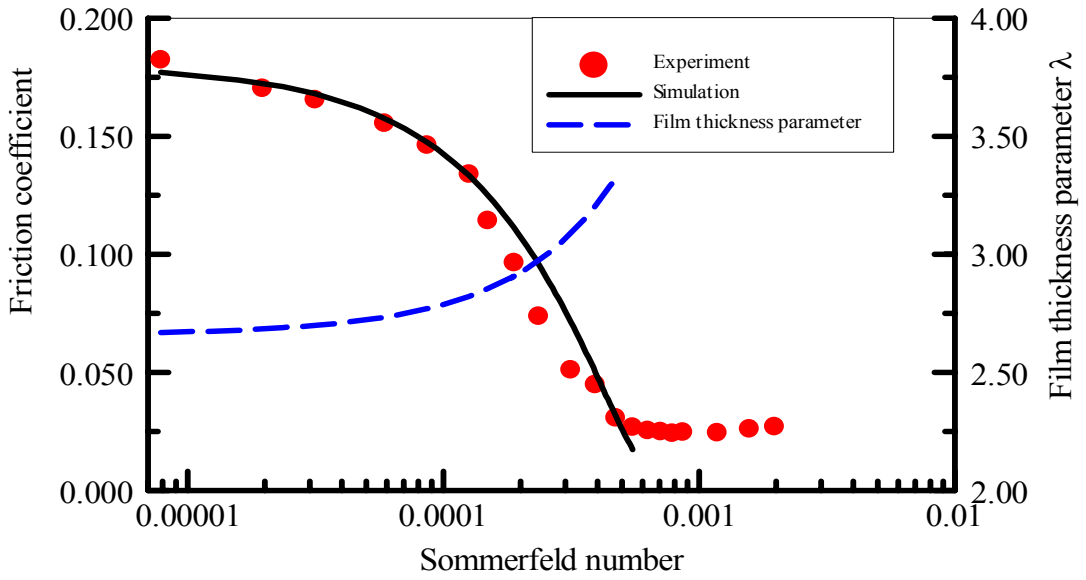

Figure 3.9 - Comparison of simulation and experiment (667 N load, Moly#5 grease, steel bushing)

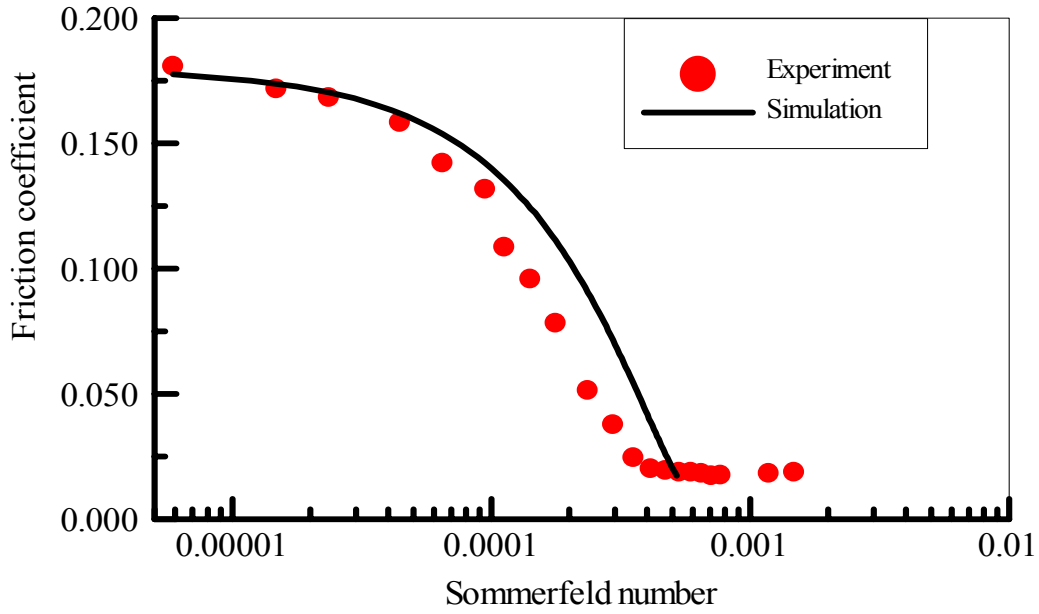

Figure 3.10 - Comparison of simulation and experiment (890 N load, Moly#5 grease, steel bushing)

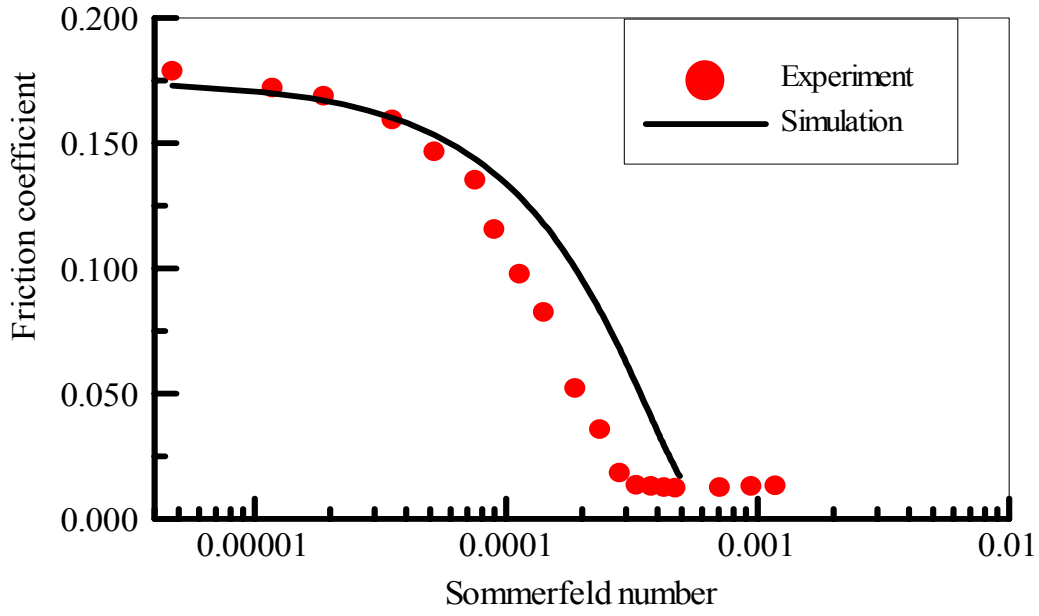

Figure 3.11 - Comparison of simulation and experiment (1112 N load, Moly#5 grease, steel bushing)

akin to that of an oil-lubricated bearing. Grease is the preferred lubricant for heavily-loaded bearings operating in boundary or mixed lubrication regime, where it offers many advantages including smaller friction coefficient than oil. A mixed elastohydrodynamic lubrication model for line contact with consideration of starvation utilizing the viscosity of the base oil in grease is presented. The simulation shows good agreement with experimental results in mixed lubrication regime. Experiments also reveal that in the hydrodynamic lubrication regime, grease presents similar lubricating characteristics as oil. The friction coefficient is reduced by a higher load in this regime. When the base oil viscosity of grease is the same as that of oil, the friction of grease is greater than that of oil due to the existence of thickener.

3.4. Nomenclature

B	bearing length, m
C	radial clearance, m

$d_d^{'}$ dimensionless distance between mean line of asperities and mean line of surface

$E^{'}$ equivalent modulus of elasticity, $= 2/\left(\left(1-\nu^2\right)/E + \left(1-\nu_b^2\right)/E_b\right)$, Pa

$F_T^{'}$ dimensionless load

f coefficient of friction

$h_c^{'}$ dimensionless film thickness

N_s shaft velocity, rev/s

n density of asperities

$n^{'}$ dimensionless density of asperities

P load, N

P_L projected load, $= P/(2RB)$, Pa

R shaft radius, m

R_b bushing radius, m

S Sommerfeld number, $= \eta N_T (R/C)^2 / P_L$

U_Σ velocity number

W dimensionless load

α pressure-viscosity coefficient, 1/ Pa

β average radius of asperities, m

β_0 slope of the limiting shear stress-pressure relation, 0.047

γ scaling factor

λ film thickness parameter, h_c / σ_s

η_{BO} dynamic viscosity of the base oil, Pa.s

σ_s standard deviation of asperities, m

$\sigma_s^{'}$ dimensionless standard deviation of asperities

τ_{L0} limiting shear stress at ambient pressure, Pa

CHAPTER 4 AN EXPERIMENTAL INVESTIGATION OF DIMPLE EFFECT ON THE STRIBECK CURVE OF JOURNAL BEARINGS

4.1. Introduction

According to the hydrodynamic lubrication theory, two ideally flat, parallel surfaces, with one sliding against the other, in the presence of an isothermal, Newtonian fluid will not generate hydrodynamic pressure to support an external load. However, in 1946 and 1947, Fogg [101] and Shaw & Mass [102] reported experimental results that revealed the existence of load carrying capacity in parallel thrust bearings. Later in 1961, Denny [3] substantiated the generation of fluid pressure in parallel surfaces in a seal-like configuration. Ever since publication of these reports, researchers have attempted to explain this load-generation phenomenon by attributing it to thermal effect [101, 102, 104], roughness [105], macro-roughness [106, 107], micro-irregularities [108-1010], waviness and corning [111] and non-Newtonian effect [112]. Further, to take advantage of this phenomenon, with the recognition that the surface profile plays an important role in creating the hydrodynamic pressure, researchers have made numerous attempts to modify the shape of the mating surfaces to facilitate and optimize the generation of the hydrodynamic pressure.

The recognition that the surface profile plays an important role in creating the hydrodynamic pressure has led the researchers to actively seek techniques to modify the shape of the mating surfaces in order to facilitate and optimize the generation of the hydrodynamic pressure. The principle of enhancing performance via improved surface pattern has been applied in seal industry to minimize friction and leakage [113-119]; in computers to improve hard drive reading [120-122]; in thrust bearings to enhance load carrying capacity [123-126]; and in automotive industry to reduce friction of piston rings

[127-129]. Theoretical studies have also been reported that suggest how to optimize the parameters of patterned surface [130-132]. However, a review of articles in the open literature reveals that this principle has not been thoroughly examined in journal bearings.

In this paper, we focus our attention to the friction performance of journal bearings with dimpled bushing. General techniques available for implementing a desired patterned profile on the surface include: machining [106], photo etching [109-110, 120], reactive iron etching [124], micro-blasting [125], and laser-texturing [116-119, 123, 126-131, 133, 134]. In the current research, experiments were performed on journal bearings whose bushings inner surfaces were dimpled by machining and chemical etching techniques. Results are provided with different dimple sizes, shapes and depths. Their effects on the Stribeck curve are investigated.

4.2. Experimental

Lewis LRI-8H tribometer is used for measuring the coefficient of friction of journal bearings. Its detailed description is available in [97]. Briefly, the machine is capable of measuring the friction coefficient under varying operating conditions such as load, speed, and oil inlet temperature. Load is applied through a level mechanism. The friction force is sensed by a measuring cell and data are continuously recorded into a computer via an automated data acquisition system.

4.2.1. Bearings

The shaft is made of hardened AISI 1020 steel with 0.29 Poisson's ratio, 200 GPa elastic modulus. The shaft diameter is 24.54 mm. The bushing material is SAE660 alloy bronze with 0.33 Poisson's ratio, 100 GPa elastic modulus. The bushing has an inner diameter 24.71 mm and an outer diameter 33.66 mm. The bearing length is 25.4 mm.

The dimpled bushings are prepared using two methods: machining and chemical etching. For machining, carbide ball shape burs are used as the indenters. For chemical etching, two steps are followed: imprinting pattern and etching. The designed pattern is printed on press-and-peel PCB transfer film. Then the film is attached to the inner surface of the bushing. They are put on a hot plate for 8 minutes, with temperature set to medium (368 ^{0}C). The film is then firmly pressed against the bushing inner surface. After that, immediately, the bushing and the film are dipped into iced water and cooled down for one minute. Next, the film is peeled off, having the dimple pattern formed on the bushing inner diameter. The outer surface and the end section are then sealed with bees wax and the bushing is immersed into a solution of 30% percent $FeCl_3$ and 70% percent distilled water by weight. $FeCl_3$ is dissolved in 50 ^{0}C water. The dimple depth is controlled by the etching time. In the current study, it reaches 0.130 mm after one hour. When the etching process is finished, the wax is cleaned out mechanically, while the PCB film coating is washed away using acetone.

The specifications of bushings tested in the current paper are tabulated in Table 4.1 and 4.2. Those dimple shapes are illustrated by Fig. 4.1. The actual bushings are shown in Fig. 4.2. There are two etched 4mm diameter circular dimpled bushings. Dimples are distributed around the entire circumference of the inner surface (360^0) on one bushing and half of the circumference (180^0) on the other.

The area ratio (the ratio of dimple area to bushing inner surface area) is set to 20% [30, 31]. For 2 mm diameter circular dimpled bushing, there are 8×16=128 dimples; for 4 mm diameter circular dimpled bushing, there are 4×8=32 dimples for 360^0 etched and 4×4=16 ones for 180^0 etched; for elliptical dimpled bushing, there are also 4×8=32 dimples.

Table 4.1- Machined bushings

Bushing	Dimple diameter (mm)	Dimple depth (mm)	Bur diameter (mm)
Conventional	0	0	0
Machined 1	2	0.165	6.223
Machined 2	4	0.448	9.373

Table 4.2- Etched bushings

Bushing	Dimple shape	Dimple depth (mm)	Etching time (hour)
Etched 1	4 mm diameter circle, 360^0	0.130	1.0
Etched 2	4 mm diameter circle, 180^0	0.130	1.0
Etched 3	4mm:1mm ellipse, 360^0	1.040	8.0

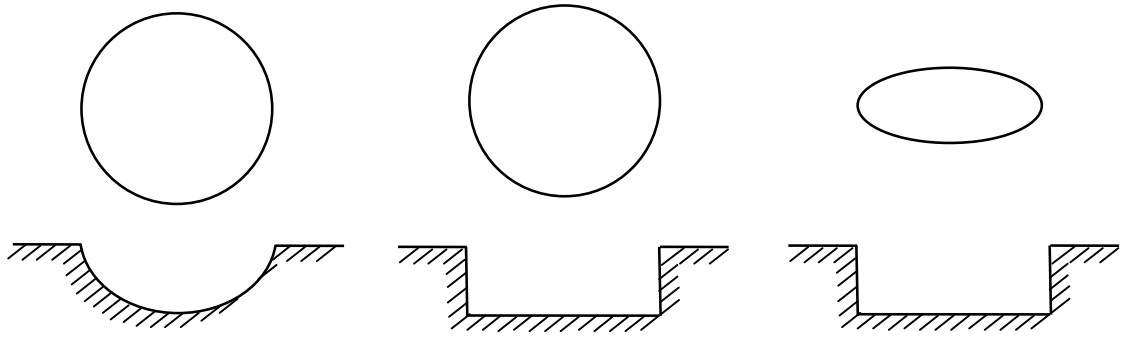

(a) machined dimple 1 & 2 (b) etched dimple 1 & 2 (c) etched dimple 3

Figure 4.1 - dimple illustration

Castrol SAE30 oil and Exxon Teresstic GT32 oil are applied as the lubricants with properties shown in Table 4.3.

(a) machined dimpled bushings (b) etched dimpled bushings

Figure 4.2 - dimpled bushings

Table 4.3- Oil properties

	Viscosity (cSt)		Specific Gravity at 15^0C
	40^0C	100^0C	
Castrol SAE30	93	10.8	0.890
Teresstic GT32	31.3	5.25	0.877

4.2.2. Experiment Procedure

The bearing is run-in for 12 hours with 445 N load and a running speed of 300 rpm. The rms value of the friction coefficient history is taken as the coefficient of friction for that speed. By observation, 4 minutes are regarded as a reasonable testing period for each velocity point. Additional details of the experimental procedure are given in [97].

4.2.3. Experimental Results and Discussion

4.2.3.1. SAE30 Oil as Lubricant

4.2.3.1.1. Comparison of Machined Dimpled Bushings

The machined 2 mm and 4 mm diameter circular dimpled bushings are tested first to examine the dimple size and depth effect on the friction performance of journal bearings. They are compared with the conventional journal bearing. SAE30 oil is used as lubricant, with 40 ^{0}C oil inlet temperature. The results are displayed in Figs. 4.3-4.5.

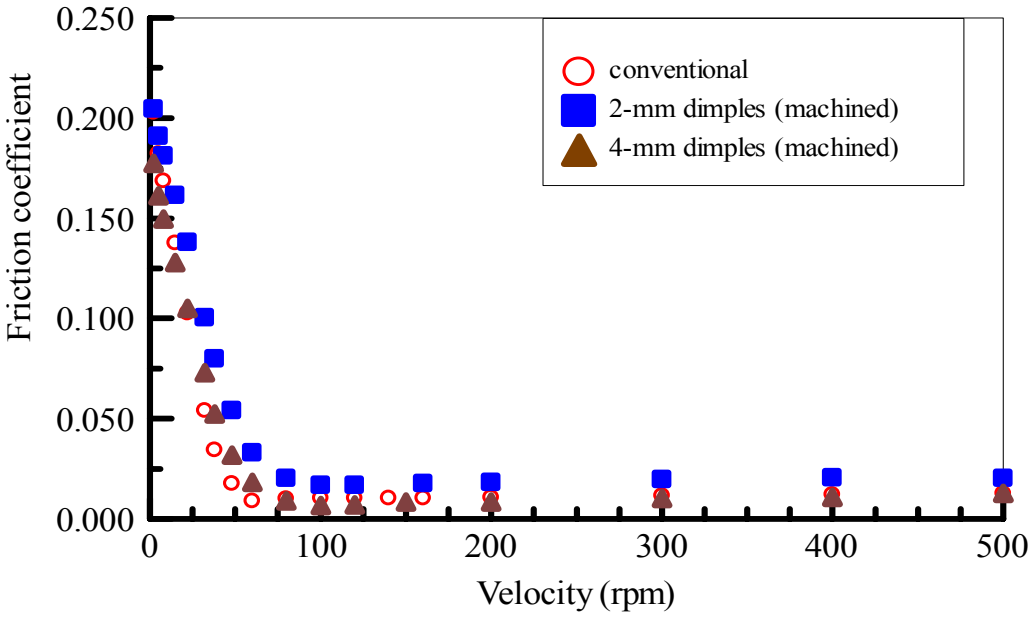

Figure 4.3 - friction coefficient as a function of velocity (667 N load, SAE30 oil)

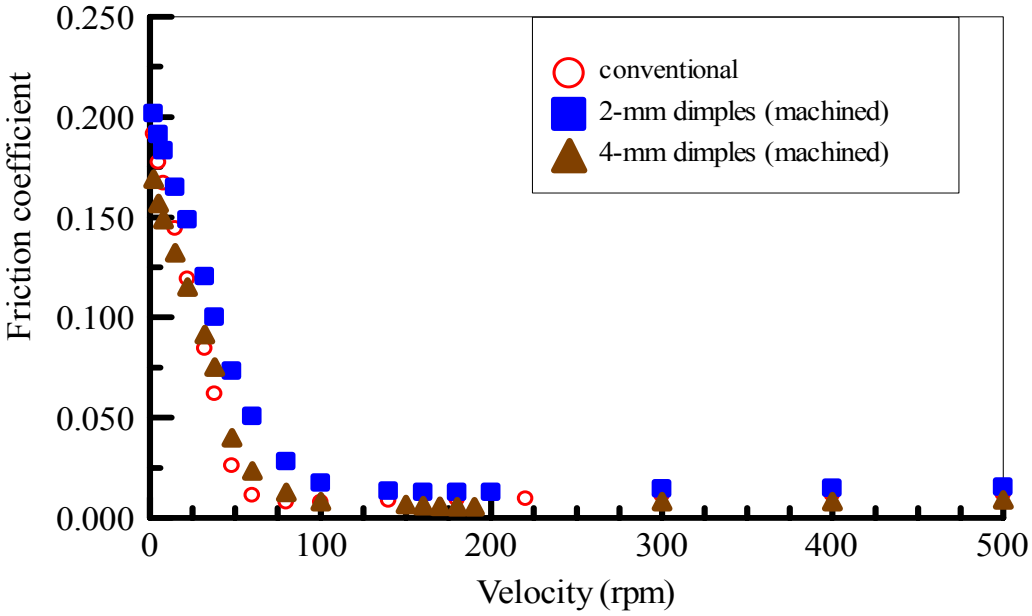

Figure 4.4 - friction coefficient as a function of velocity (890 N load, SAE30 oil)

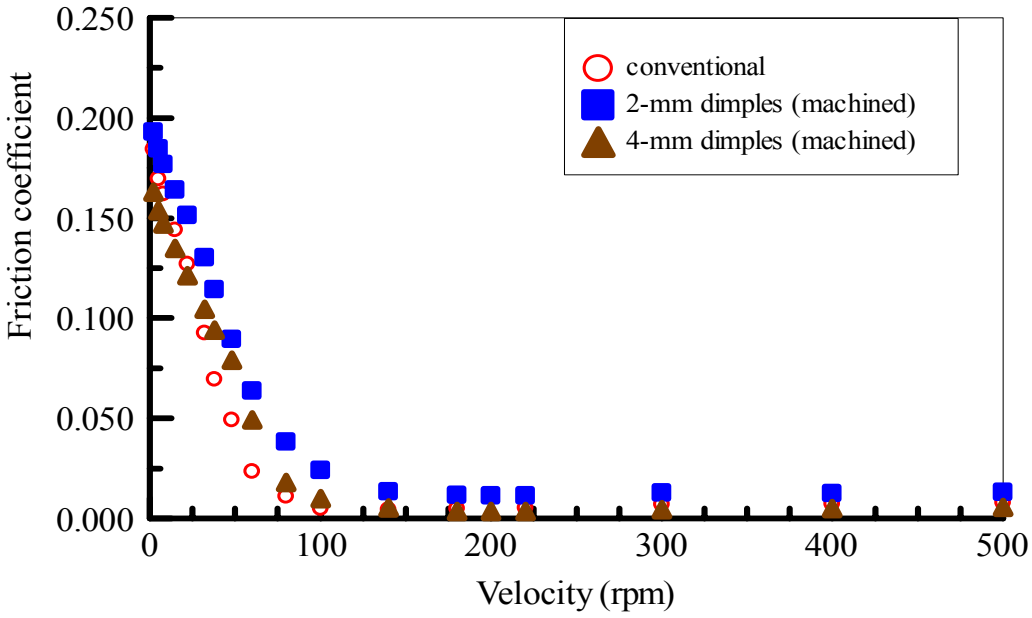

Figure 4.5 - friction coefficient as a function of velocity (1112 N load, SAE30 oil)

The friction characteristic of dimpled bearings is consistent with that of conventional journal bearings detailed in [97]. With increasing speed, the friction coefficient drops in the mixed lubrication regime before the lift-off and rises after the lift-off, as the hydrodynamic regime prevails. The lift-off speed point distinguishes between the mixed lubrication and the hydrodynamic lubrication. In the mixed lubrication regime, the friction is dominated by asperity contact. With increasing speed, the separation gap (film thickness) between surfaces becomes greater, and the friction coefficient drops. In the hydrodynamic lubrication regime, the friction force can be predicted by examining the fluid shearing. With increasing speed, the shear rate increases and so does the fluid shear stress. As a result, the friction force becomes lager [25].

The friction coefficient of machined dimpled bushing of 2-mm diameter and circular in shape is higher than that of the conventional and the corresponding 4-mm diameter dimpled bushings throughout the mixed and the hydrodynamic regimes. Due to the

presence of dimples, the actual contact surface area of the bushing becomes smaller leading to an increase of the actual contact pressure. If the dimpled bushing of 2-mm diameter and circular in shape fail to generate extra hydrodynamic pressure to compensate the increment of contact pressure [125], the friction coefficient will become higher.

A bushing with 4-mm circular-shaped dimples has a greater potential than that with 2-mm circular-shaped dimples to improve friction performance. It has a higher friction value than that of conventional bushing in the mixed lubrication regime. For instance, f =0.0729 (dimpled bushing) compared to f =0.0542 (conventional bushing) at the speed of 32 rpm with 667 N load. In hydrodynamic regime, on the other hand, a lower friction value than the conventional bushing in hydrodynamic lubrication regime is obtained. For instance, f =0.0044 (dimpled bushing) compared to f =0.0070 (conventional bushing) at the speed of 300 rpm with 1112 N load. This implies that extra hydrodynamic pressure is developed in the dimpled areas.

4.2.3.1.2. Comparison of Machined and Etched Dimpled Bushings

The friction results of etched dimpled bushing of 4-mm diameter and circular in shape (360^0, 0.130 mm depth) are shown in Figs. 4.6-4.8. The lubricant is SAE30 oil and inlet temperature is 40 ^{0}C.

In the mixed lubrication regime, the friction coefficient of etched dimpled bushing of 4-mm diameter and circular in shape is higher than that of the conventional bushing. For instance, f =0.1060 (dimpled bushing) compared to f = 0.0542 (conventional bushing) at the speed of 32 rpm with 667 N load. In the hydrodynamic lubrication regime, on the

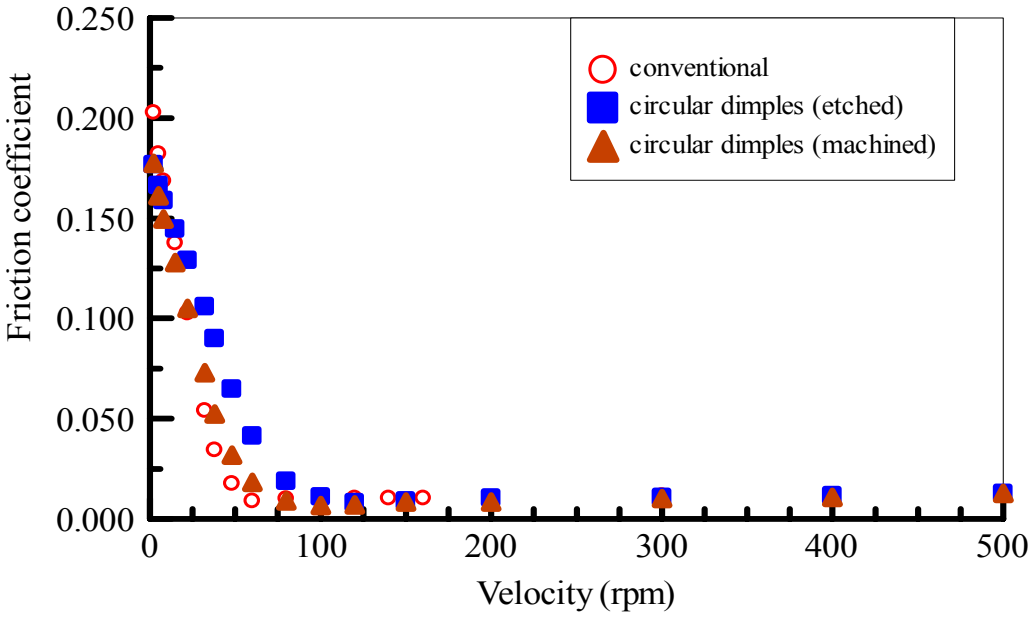

Figure 4.6 - friction coefficient as a function of velocity (667 N load, SAE30 oil)

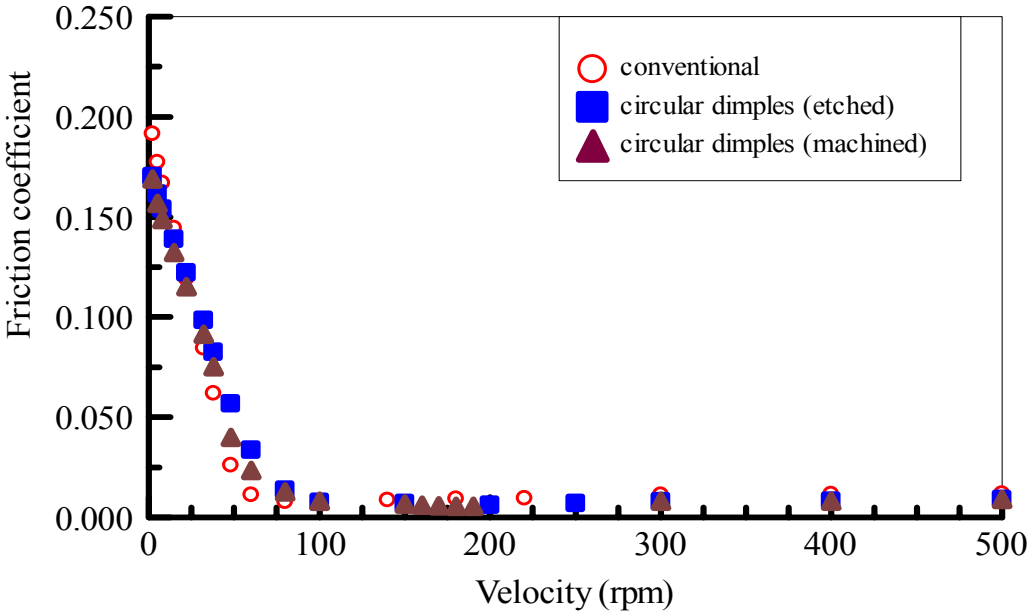

Figure 4.7 - friction coefficient as a function of velocity (890 N load, SAE30 oil)

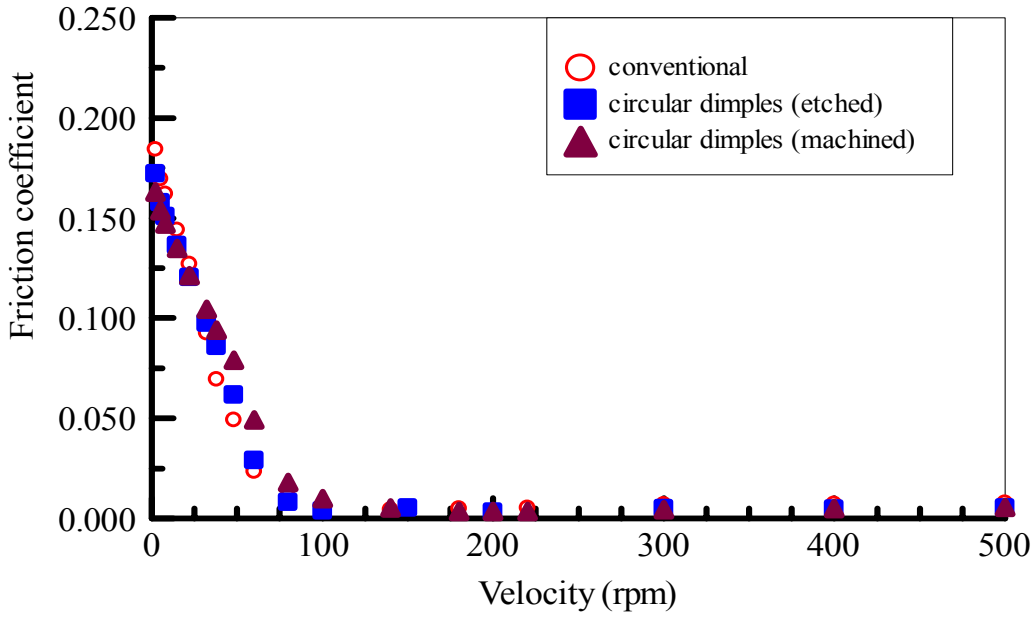

Figure 4.8 - friction coefficient as a function of velocity (1112 N load, SAE30 oil)

other hand, this trend reverses. For instance, f =0.0091 (dimpled bushing) compared to 0.0104 (conventional bushing) at the speed of 150 rpm with 667 N load. This is similar to the effect of the machined dimpled bushing of 4-mm diameter and circular in shape. However, the results show that the friction drops more with machined dimpled bushing (0.448 mm depth) in hydrodynamic lubrication regime. The machined dimples have a partial-spherical shape (See Fig. 4.1(a)) with 0.448 mm depth while the etched dimples have a square shape (See Fig. 4.1(b)) with 0.130 mm depth. The shape and the depth of machined dimples facilitate the generation of hydrodynamic pressure to lift-off the shaft.

4.2.3.2. GT32 Oil

The friction performance of dimpled bushings can be better distinguished with a lighter oil. For this purpose, GT32 (31.3 cSt at 40 ^{0}C) is chosen for further comparison. The speed range is extended from 2~500 rpm to 2~1500 rpm. The oil inlet temperature is maintained at 40 ^{0}C.

4.2.3.2.1. Comparison of Machined and Etched Dimpled Bushings

The results of machined and etched dimpled bushings (360^0) of 4-mm diameter and circular in shape and conventional bushing are shown in Figs. 4.9-4.11. Both machined and etched dimpled bushings create a smaller friction coefficient throughout mixed and hydrodynamic lubrication regimes. The friction performance of dimpled bushings is close in mixed lubrication regime. However, the machined dimpled bushing performs the best in hydrodynamic lubrication regime. For instance, the friction coefficient is 0.1953 (conventional bushing), 0.1388 (etched bushing) and 0.1325 (machined bushing) at the speed of 32 rpm with 667 N load; 0.0229 (conventional bushing), 0.0128 (etched bushing) and 0.0088 (machined bushing) at the speed of 300 rpm with 667 N load.

It is noted that the in mixed lubrication regime, the friction coefficient of machined and etched dimpled bushings is higher than that of conventional bushing for SAE30 oil, while the opposite is true for GT32 oil. This can be attributed to the so-called secondary lubrication effect in dimple surface [123, 124, 133, 135-136]. The oil retained in the dimples works as a secondary lubricant source which permeates to the interspace of asperities and causes a reduction in the friction. GT32 oil has a much smaller viscosity (31.3 cSt at 40 ^{0}C) than SAE30 oil (93 cSt at 40 ^{0}C). Therefore, it is easier for GT32 oil to flow into asperities interspaces and reduce the friction. The friction difference with these two oils suggests that the secondary lubrication effect can be the dominant factor for dimpled bearings in mixed lubrication regime.

4.2.3.2.2. Comparison of Conventional and Etched Elliptical Dimpled Bushings

In order to further explore the effect of dimple shape, a series of elliptical shape dimples were etched into the bushing, as shown in Fig. 4.12. The semi-major axis of the ellipse is

4 mm and the semi-minor axis of the ellipse is 1 mm. The dimple depth is 1.040 mm. The experimental results are exhibited in Figs. 4.13-4.15.

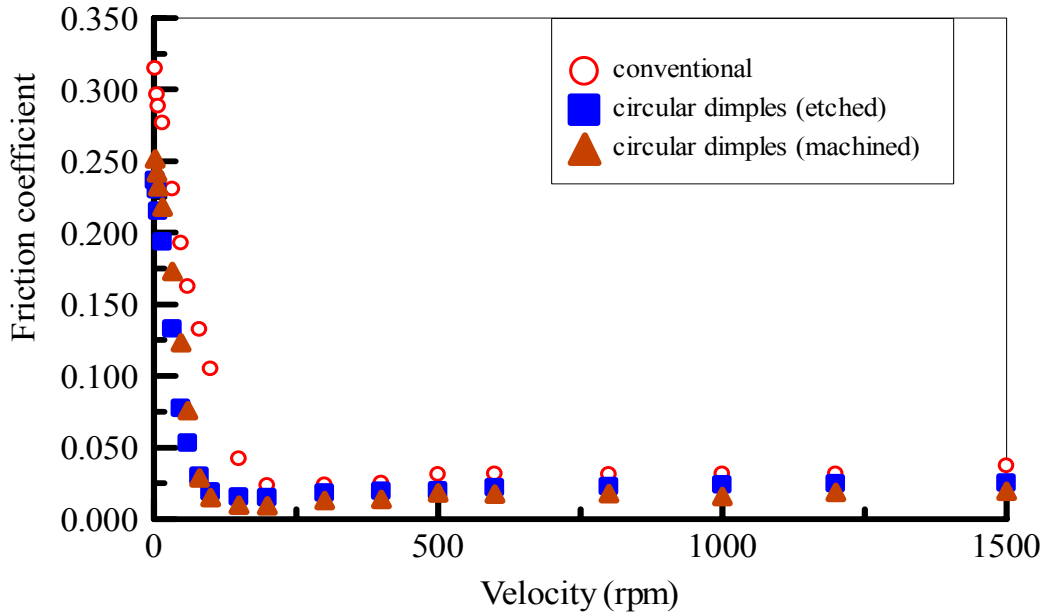

Figure 4.9 - friction coefficient as a function of velocity (445 N load, GT32 oil)

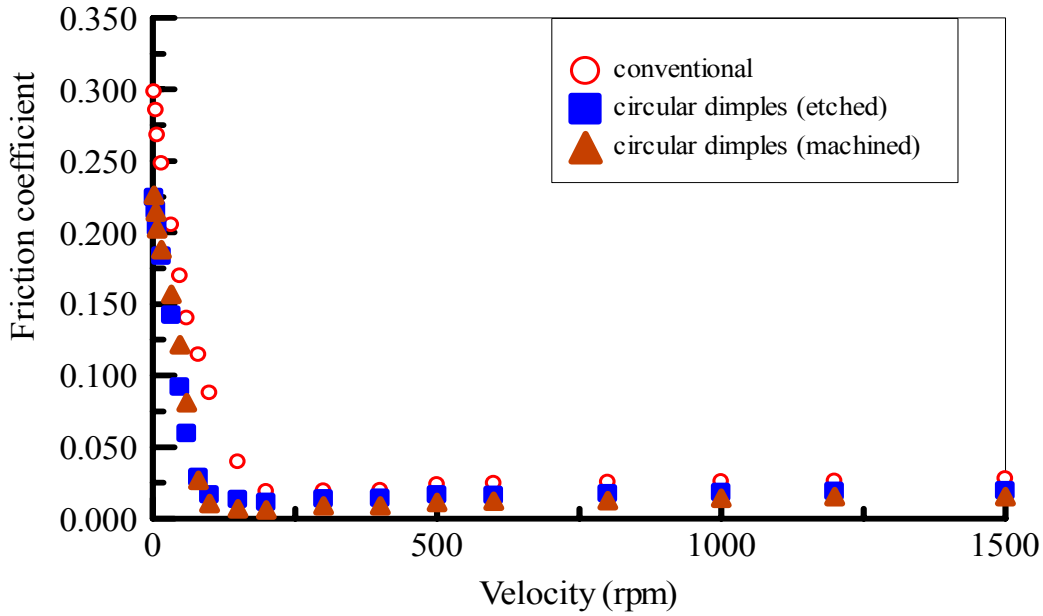

Figure 4.10 - friction coefficient as a function of velocity (560 N load, GT32 oil)

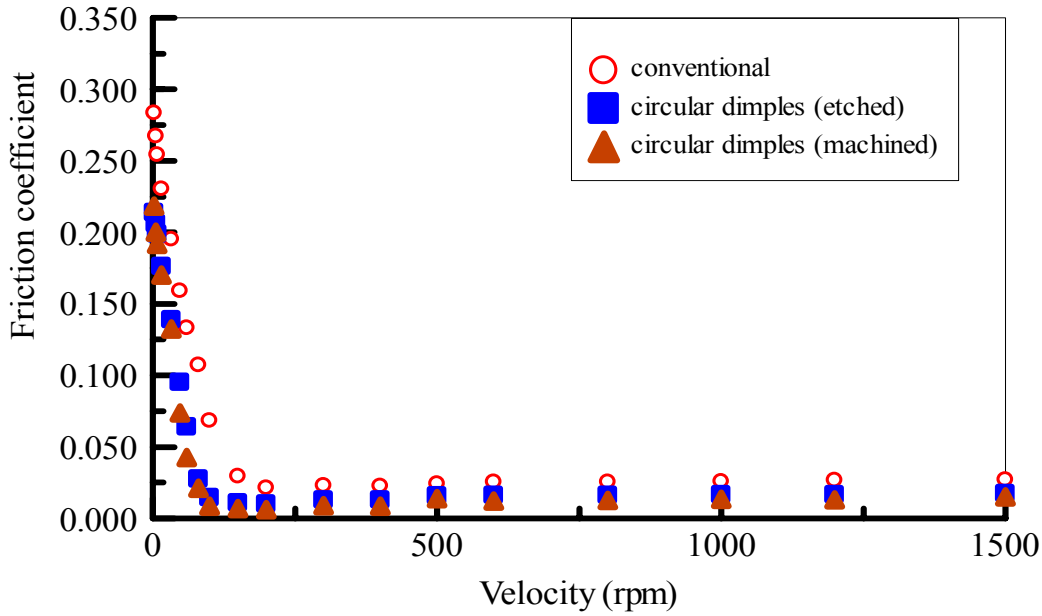

Figure 4.11 - friction coefficient as a function of velocity (667 N load, GT32 oil)

In mixed lubrication regime, when the load is high, the friction coefficient with elliptical dimpled bushing is greater. This implies a deeper dimple does not necessarily generate hydrodynamic pressure more or facilitate the secondary lubrication effect.

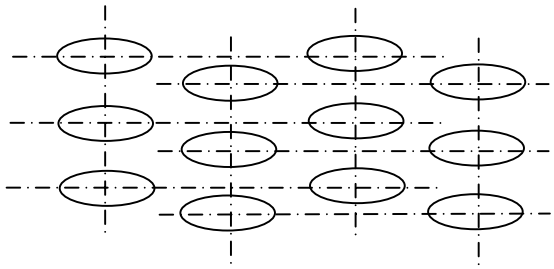

Figure 4.12 - dimple arrangement for elliptical dimpled bushing

4.2.4 Discussion

4.2.4.1. Pressure Distribution in Dimple Area

A generally accepted pressure distribution in each dimple area [124] is illustrated by Fig. 4.16. It has a negative pressure (ambient pressure as the reference) within the

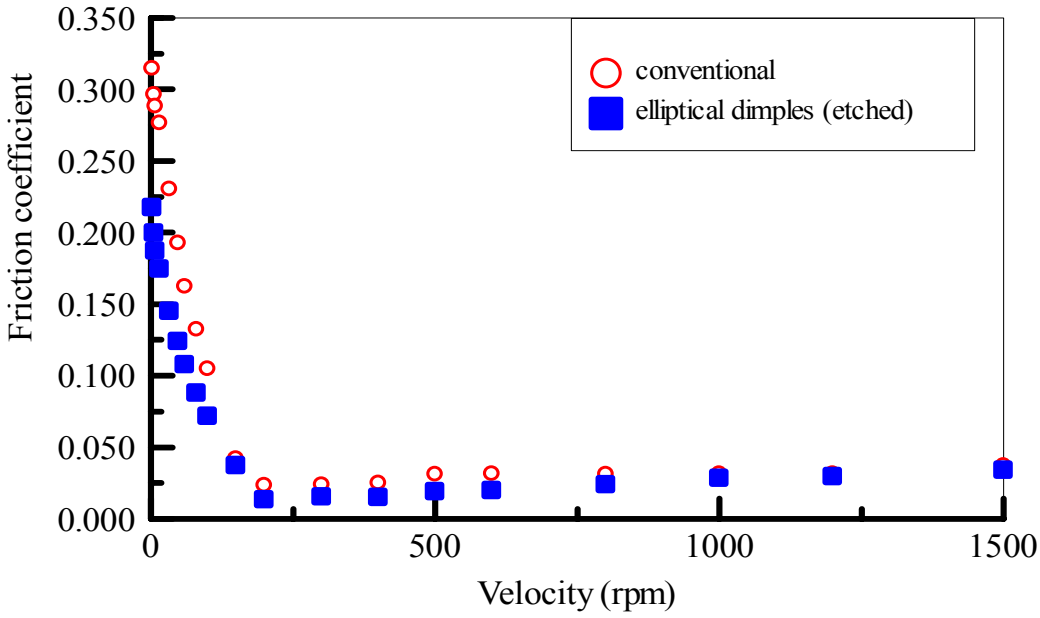

Figure 4.13 - friction coefficient as a function of velocity (445 N load, GT32 oil)

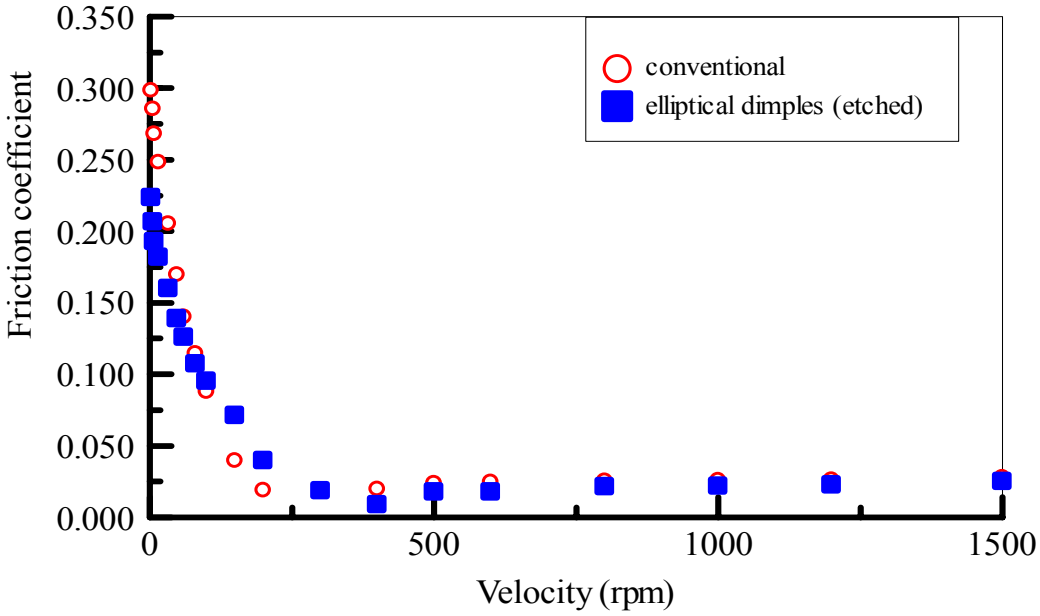

Figure 4.14 - friction coefficient as a function of velocity (560 N load, GT32 oil)

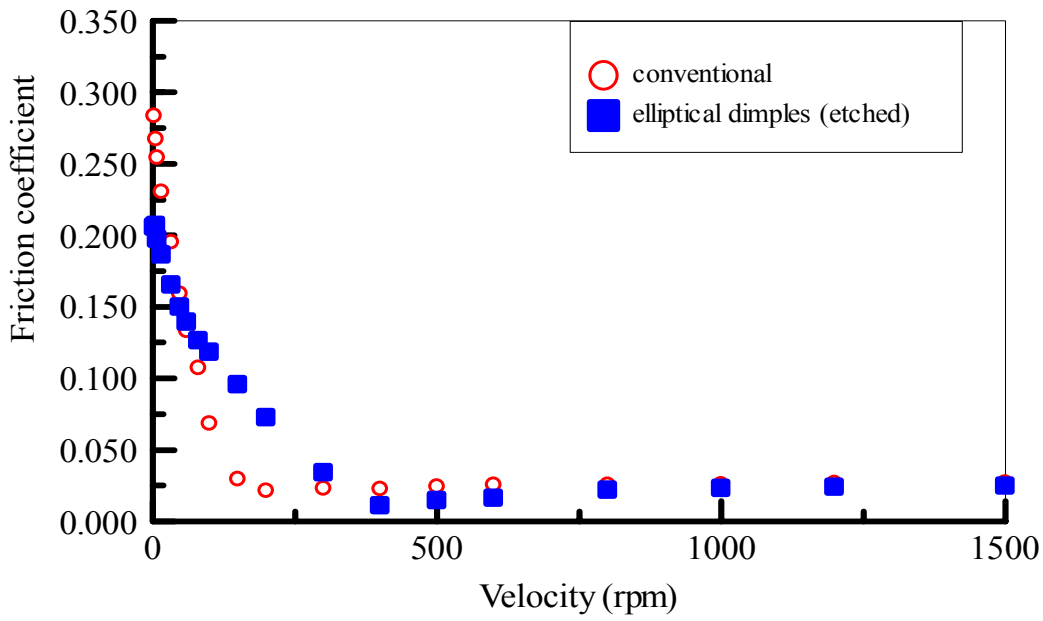

Figure 4.15 - friction coefficient as a function of velocity (667 N load, GT32 oil)

divergent region and a positive pressure within the convergent region. Without cavitation, the negative pressure and the positive pressure will cancel out. However, due to release of gas entrained in oil, the negative pressure cannot be lower than vapor pressure or saturation pressure. In most cases the saturation pressure is nearly ambient due to long time exposure to air. It is argued that this asymmetric pressure distribution results in additional load carrying capacity [123, 124, 130, 137]. In hydrodynamic lubrication regime, a greater hydrodynamic pressure creates a thicker film thickness, thus resulting in a smaller shearing stress and a lower friction coefficient.

4.2.4.2. Comparison of Half and Full Etched Dimpled Bearings

In hydrodynamic lubrication, the bushing circumference is divided into active and inactive loading sections. The inactive section (± 90^{o} from the load line) contributes a little to the load carrying capacity. This principle has been recognized for a long time [2].

In the current study, the results of the full-area (360^0) etched-dimpled bushing and half-area (180^0) etched-dimpled bushing are compared in Figs.4.17-4.22.

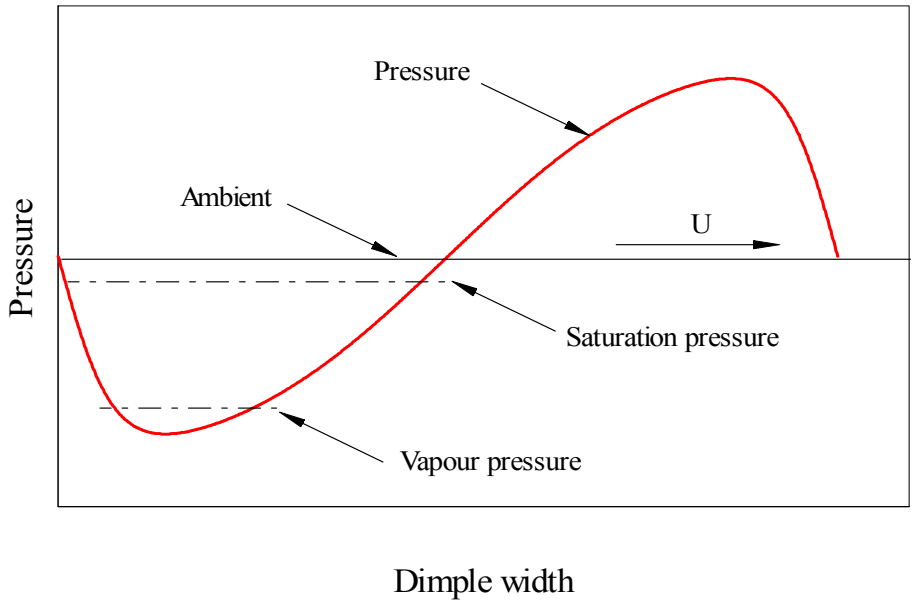

Figure 4.16 - Pressure distribution in dimple along flow direction

The results show that the friction coefficients of full- and half- area etched-dimpled bushing are almost overlapped in hydrodynamic lubrication regime, which suggests that for the full-area dimpled bushing, the inactive area does not contribute to the load carrying capacity. However, in mixed lubrication regimes, the full-area etched-dimpled bushing performs better than the half-area etched one because of the existence of secondary lubrication effect.

4.3. Conclusions

A series of experiments is conducted to examine the dimple effect on the Stribeck curve of journal bearing. Load, oil type, dimple size, depth and shape are varied to explore their influence on the friction characteristics. It is found that:

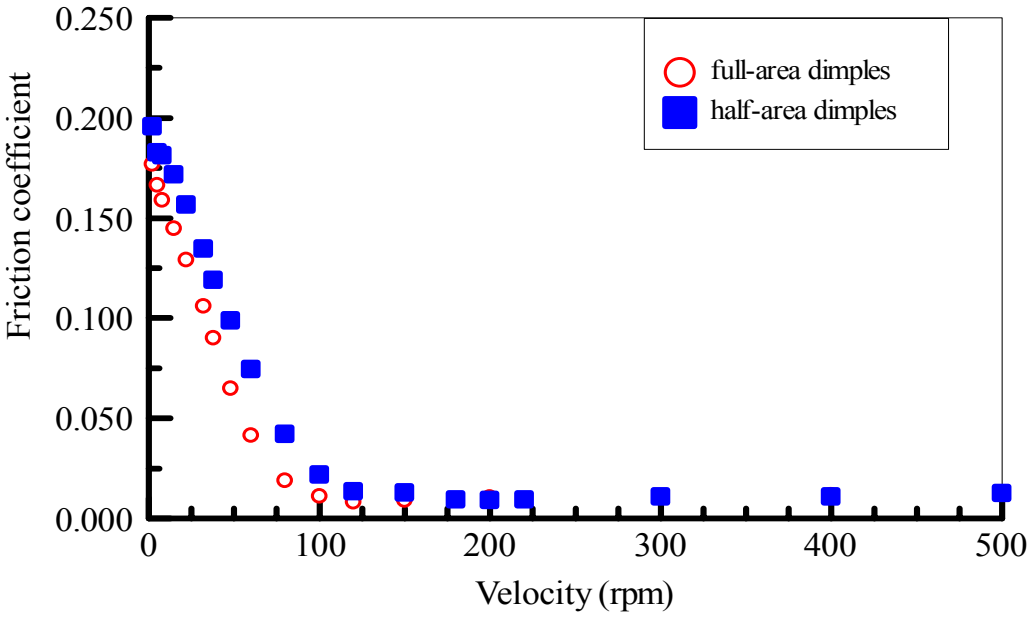

Figure 4.17 - friction coefficient as a function of velocity (667 N load, SAE30 oil)

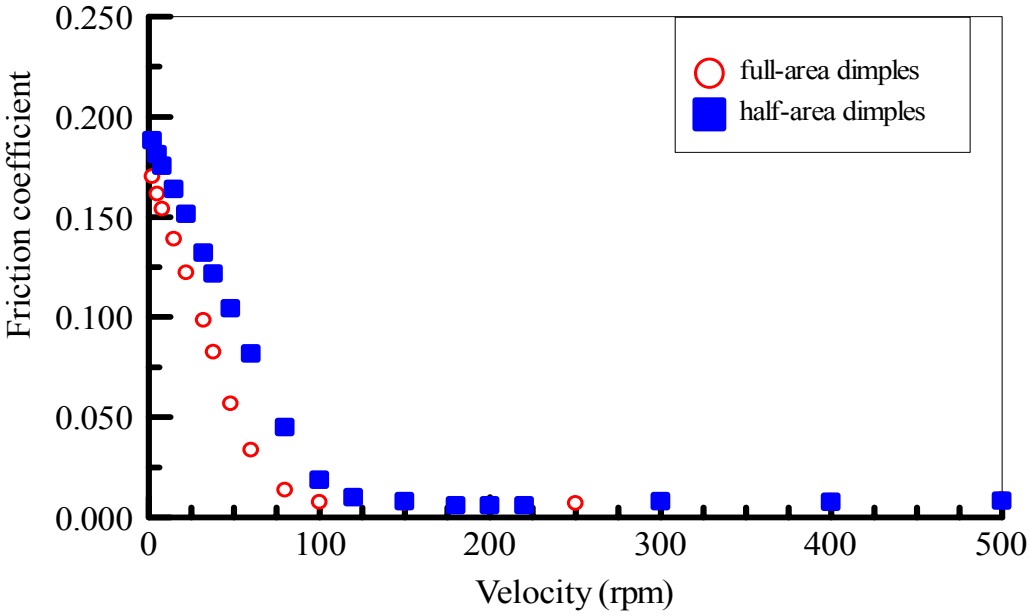

Figure 4.18 - friction coefficient as a function of velocity (890 N load, SAE30 oil)

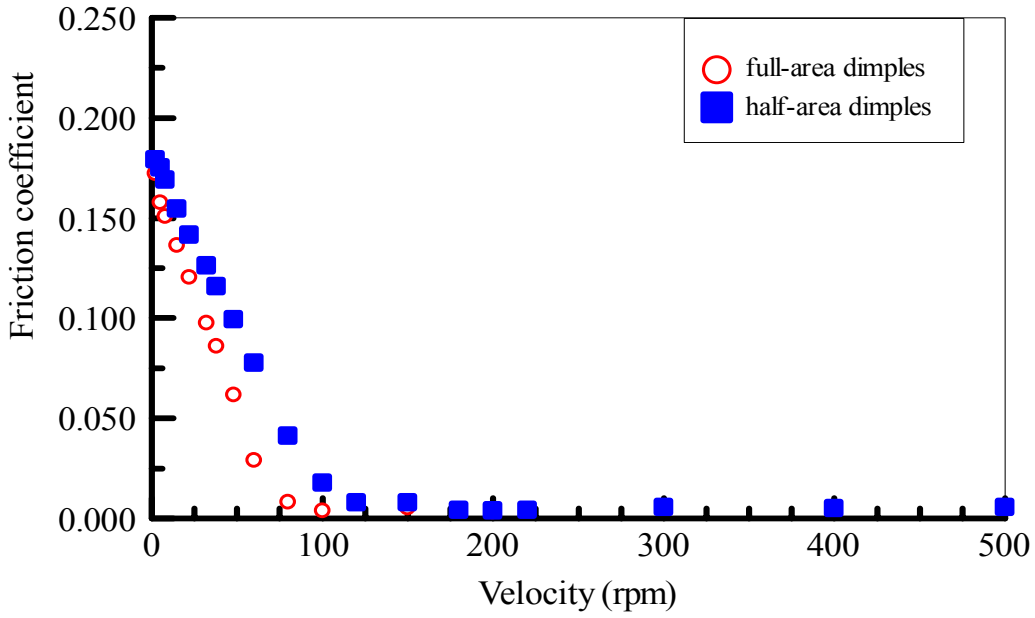

Figure 4.19 - friction coefficient as a function of velocity (1112 N load, SAE30 oil)

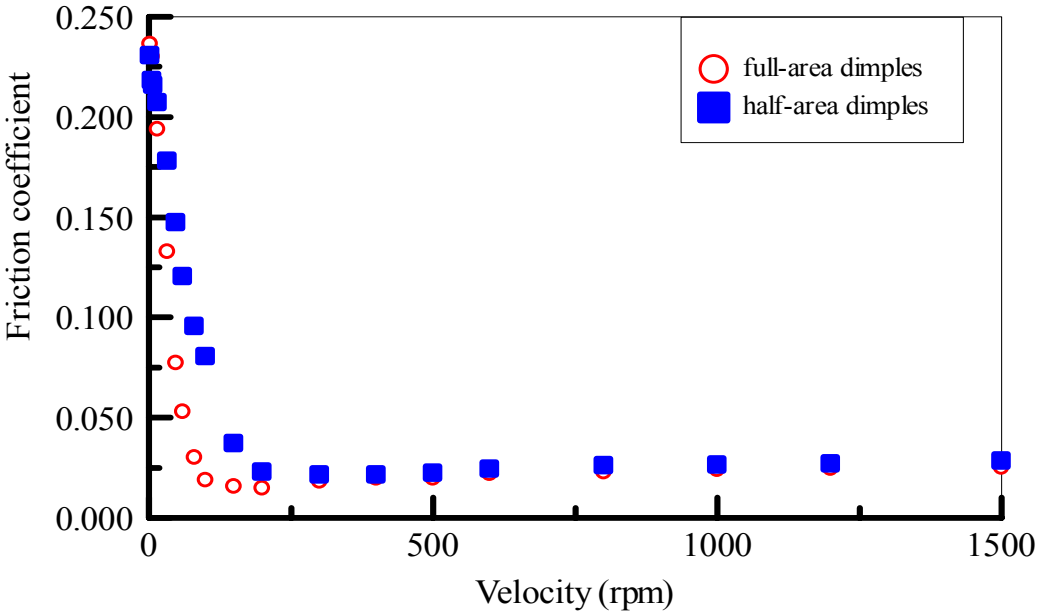

Figure 4.20 - friction coefficient as a function of velocity (445 N load, GT32 oil)

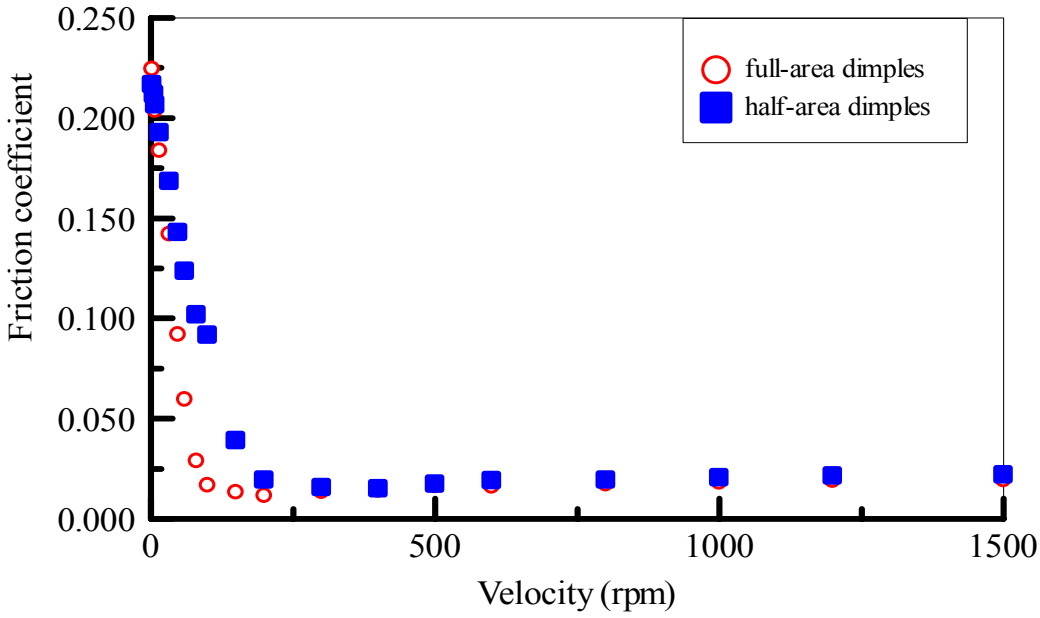

Figure 4.21 - friction coefficient as a function of velocity (560 N load, GT32 oil)

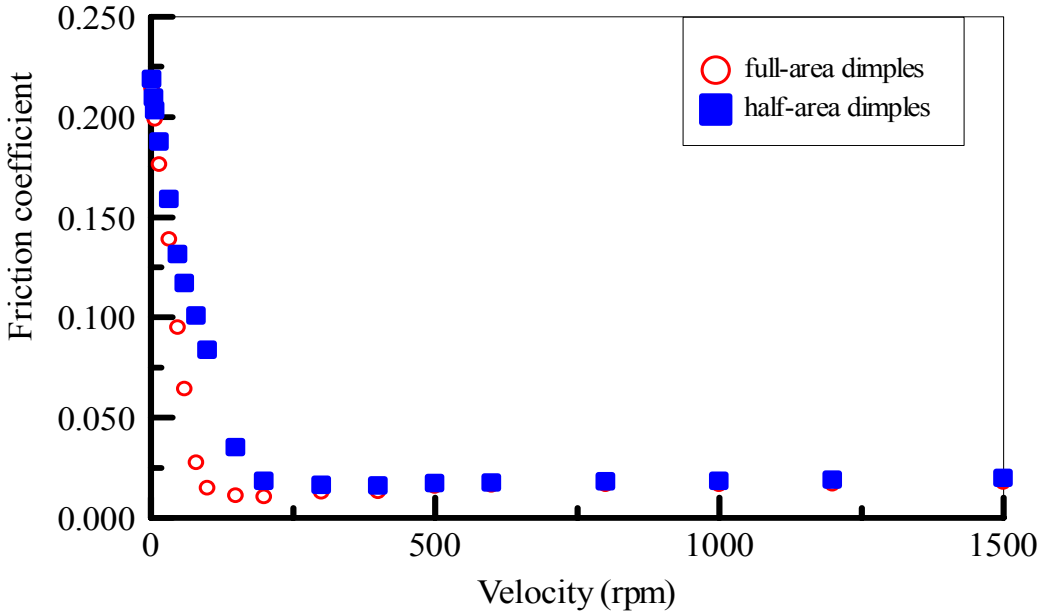

Figure 4.22 - friction coefficient as a function of velocity (667 N load, GT32 oil)

- The typical friction characteristic of a dimpled journal bearing is similar in trend to that of a conventional bearing, as prescribed by the Stribeck curve.

- Proper dimple size, shape and depth are essential to improve the friction performance. It becomes more pronounced if an oil with lower viscosity is utilized.
- In mixed lubrication regime, the secondary lubrication effect is dominant for dimpled journal bearings. Improper size of dimple will be deleterious to the friction reduction.
- In hydrodynamic lubrication regime, the asymmetric pressure distribution in the dimple area generates extra hydrodynamic pressure to separate the surfaces, resulting in a lower friction coefficient.
- In mixed lubrication regime, the full-area etched bushing (dimpled over the entire circumference, 360^o) performs better than the half-area (dimpled over the active zone, $180^{o)}$ bushing due to secondary lubrication effect; in hydrodynamic lubrication regime, their performance is nearly the same.

4.4. Nomenclature

f friction coefficient

CHAPTER 5 AN EXPERIMENTAL STUDY OF OIL LUBRICATED JOURNAL BEARINGS UNDERGOING OSCILLATORY MOTION

5.1. Introduction

Journal bearings have broad range of applications in industry. Most journal bearings are designed to rotate uni-directionally and operate with a relatively thick film of fluid that separates the journal and the bushing so that the hydrodynamic lubrication regime prevails. There are volumes of archival publications devoted to this subject, many of which deal with performance analyses, experimental investigations, and design aspects. Nevertheless, there are applications where the journal does not rotate uni-directionally, rather it is designed to oscillate periodically at a specified frequency and amplitude. Correspondingly, the state of lubrication undergoes a transition from boundary, to mixed, and to hydrodynamic regimes. This shift of regime considerably complicates the analysis of bearing performance.

A distinctive behavior of oscillating bearings is the evolution of friction hysteresis which is a retardation phenomenon of the friction coefficient when the velocity changes direction while traversing through the zero speed, manifesting itself in the form of a friction hysteresis.

Research dealing with friction hysteresis originated with stick-slip phenomenon. Sampson [138] is probably the first researcher who witnessed this behavior experimentally. Bell [139-141] recorded the friction force and the velocity history in machine tool slideway and reported hysteresis loop behavior. Thereafter, researchers [142-150] continued their efforts on studies devoted to the understanding of hysteresis phenomenon. Among the noteworthy publications relevant to the present paper are the work of Polycarpou [151-153], Hess [154, 155] and Harnoy [156-160] who carried out a

series of experiments and presented distinct feature for the friction hysteresis of oil-lubricated oscillatory journal bearings. However, the lubrication mechanism and the affecting factors of the hysteresis behavior remain largely unexplored.

In the current paper, the friction performance of oil-lubricated oscillatory journal bearings is investigated. The effects of load, with or without oil, oil type, oil inlet temperature, oscillating frequency, and bushing type are examined. The cause and the variation of the friction hysteresis loop are analyzed qualitatively.

5.2. Experimental

The apparatus employed in this research is LRI-8H—a versatile journal bearing friction tester manufactured by Lewis. A detailed description of the apparatus is described in [57]. Briefly, the machine is capable of measuring the friction coefficient under varying operating conditions such as load and oscillating frequency. Load is applied through a level mechanism. The friction force is read by a measuring cell and data are continuously recorded into a computer via an automated data acquisition system. The coefficient of friction, the oscillating frequency, and the load are processed by software, displayed on computer screen, and recorded for future analysis. The interval for recording data is adjustable and is independent of the duration of the test. Two types of sampling frequencies are adopted. One is for recording the global history of the coefficient of friction. The other is for recording the local history of the coefficient of friction in one oscillation cycle. In the current study, a minimum of 20 seconds for the global history and a 0.0185 second for the local history are taken.

5.2.1 Bearing Properties

The shaft is made up of hardened AISI 1020 steel. Its diameter is 24.54 mm. Bronze and steel bushings are used in tests. The inner diameters are 24.71 mm and 25.4 mm,

respectively. Their length is 25.4 mm. SAE30 oil and SAE40 oil are applied as the lubricants with properties shown in Table 5.1.

Table 5.1- Oil properties

	Viscosity (cSt)		Specific Gravity at 15^0C
	40^0C	100^0C	
SAE30	93	10.8	0.890
SAE40	134	13.7	0.895

The applied loads are: 222 N (50 lb), 450 N (100 lb), 667 N (150 lb), and 890 N (200 lb). The measuring error of the friction coefficient is based on the accuracy of the load cell. A 44 N load cell is used in experiments. For a given load cell, the amount of the friction force error is fixed. With increasing loads, the error of the friction coefficient becomes smaller. It is tabulated in Table 5.2.

Table 5.2- Error of the friction coefficient associated with load

Load (N)	222	450	667	890
Error (±)	0.0069	0.0034	0.0023	0.0017

5.2.2 Experiment Procedure

Before any measurement is taken, the system is balanced so that the coefficient of friction is nil when the shaft is in its static position. The system is run-in for one hour with 1.0 Hz oscillating frequency and 445 N load. When each test is complete, the system is given enough time, typically 2 hours, to cool down. For each test, the global history of the coefficient of friction is monitored. The friction coefficient tends to oscillate periodically around a relatively constant value. By observation, this state is normally reached in 4 minutes. The total measuring time for each test is 8 minutes. Starting from the moment of 4 minutes, the local history loop of the coefficient of friction in one oscillation cycle is extracted for processing.

5.2.3 Development of Oscillatory Motion

The oscillatory motion of the shaft is generated by a four-bar linkage device. The derivation of the oscillating speed can be referred to [161]. The result is displayed in Fig. 5.1.

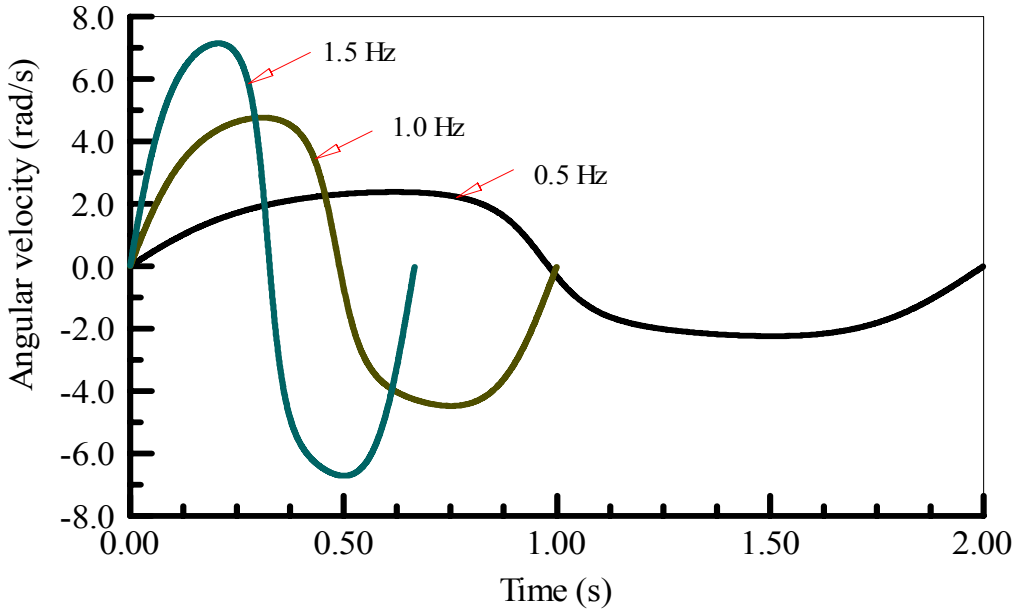

Figure 5.1 - the angular velocity of the shaft with different oscillating frequencies

5.2.4 Results and Discussion

The repeatability of the coefficient of friction in several oscillation cycles is demonstrated in Fig. 5.2. As the discrepancy between cycles is small, in the analysis that follows, only one cycle for a given test will be shown.

In what follows, the coefficient of friction is plotted against the shaft velocity (rpm). The measured friction registers negative when the velocity is reversed. In the vicinity of zero velocity, the coefficient of friction experiences a steep change due to the static-kinetic traverse. It should be pointed out that coefficient of friction may not be a closed loop, for one cannot expect that the coefficient of friction to remain exactly the same

when returning to the starting point in each cycle due to plastic deformation at asperity level and material damping, etc.

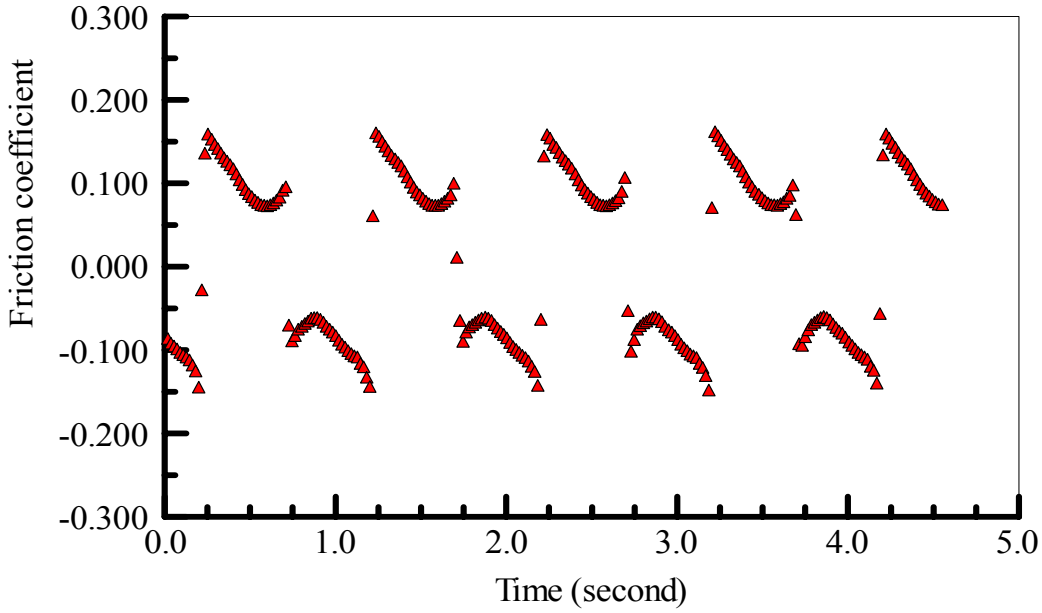

Figure 5.2 - the local history of the friction coefficient, 445 N load, 1.0 Hz oscillating frequency, bronze bushing, SAE30 oil

5.2.4.1 Load Effect

Figs. 5.3-5.8 show the variation of the local history of the friction coefficient with different loads for 0.5 Hz, 1.0 Hz, and 1.5 Hz oscillating frequencies, respectively. The arrow shows the velocity history during one oscillation cycle (222 N load). The detailed discussion of different load, frequency, inlet temperature and bushing type are presented in §5.2.4.6.3. Bronze bushing is used. The oil inlet temperature is 40^0C.

Load and oscillating frequency are two critical factors in determining the loop "bandwidth". By "bandwidth", we mean that the difference of the friction coefficient at the same speed, i.e. the extent of the friction hysteresis. In Figs. 5.3-5.8, a higher load lowers the friction level and "squeezes" the hysteresis loop. During the oscillatory

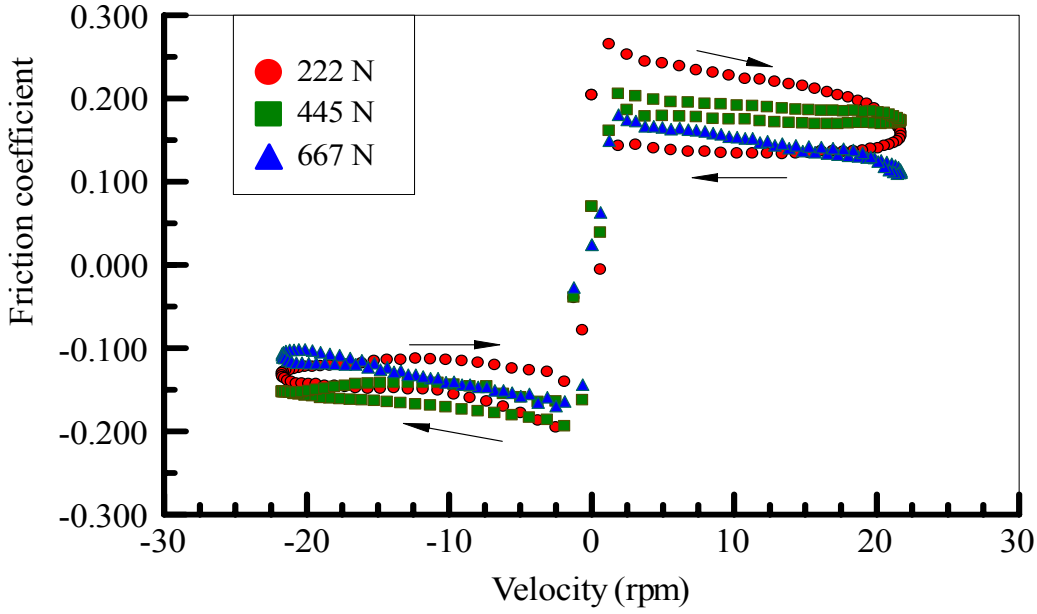

Figure 5.3 - Friction coefficient versus velocity (bronze bushing, 0.5 Hz oscillating frequency, SAE30 oil)

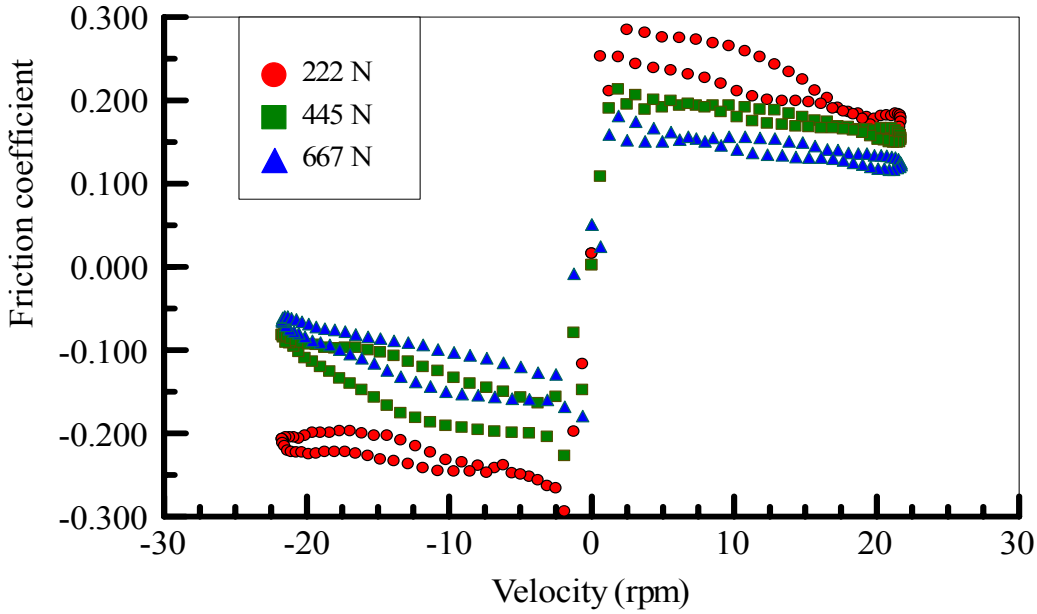

Figure 5.4 - Friction coefficient versus velocity (bronze bushing, 0.5 Hz oscillating frequency, SAE40 oil)

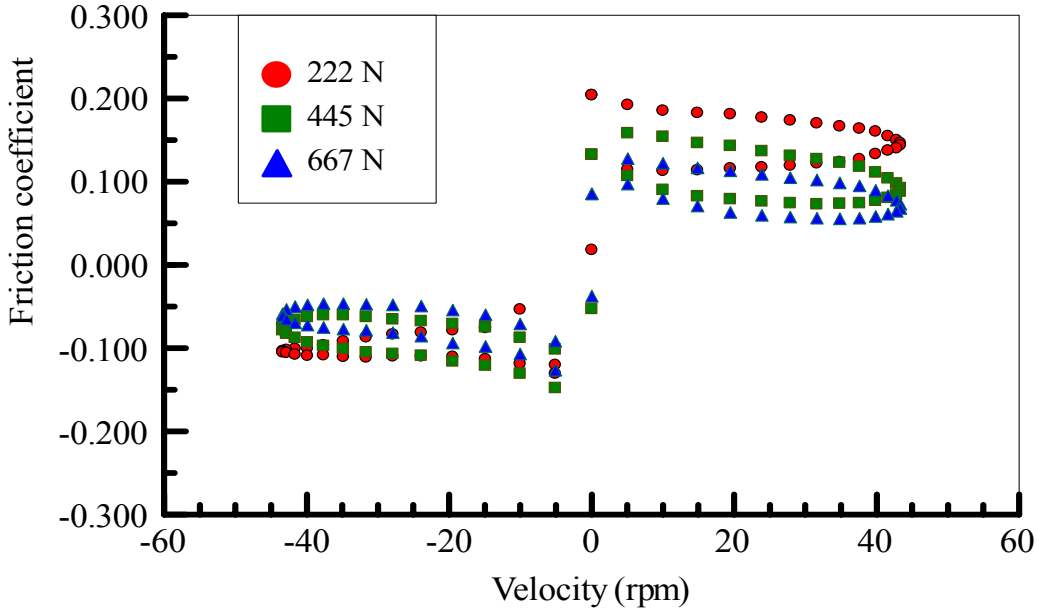

Figure 5.5 - Friction coefficient versus velocity (bronze bushing, 1.0 Hz oscillating frequency, SAE30 oil)

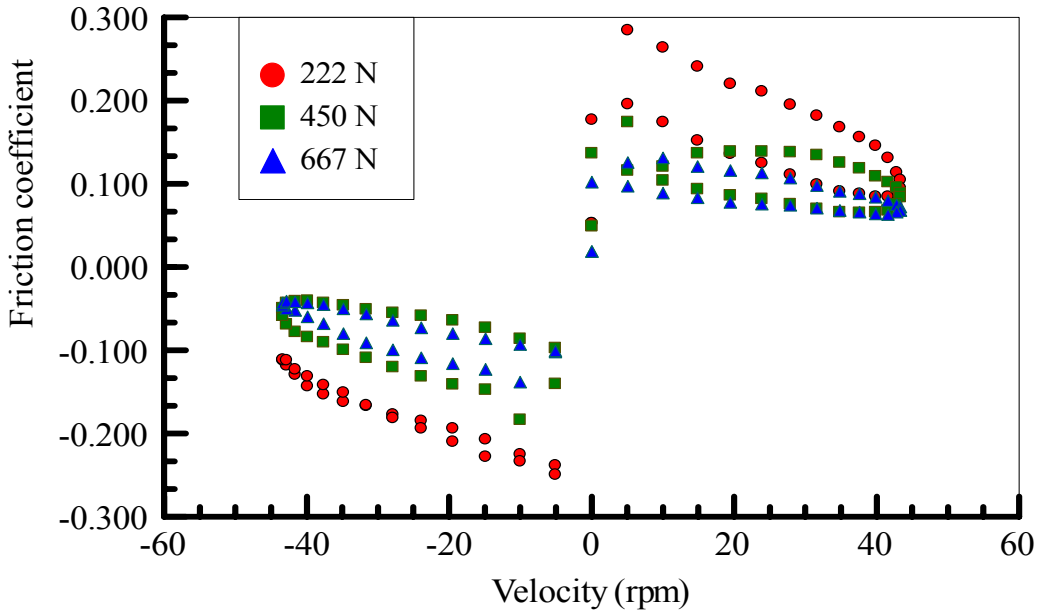

Figure 5.6 - Friction coefficient versus velocity (bronze bushing, 1.0 Hz oscillating frequency, SAE40 oil)

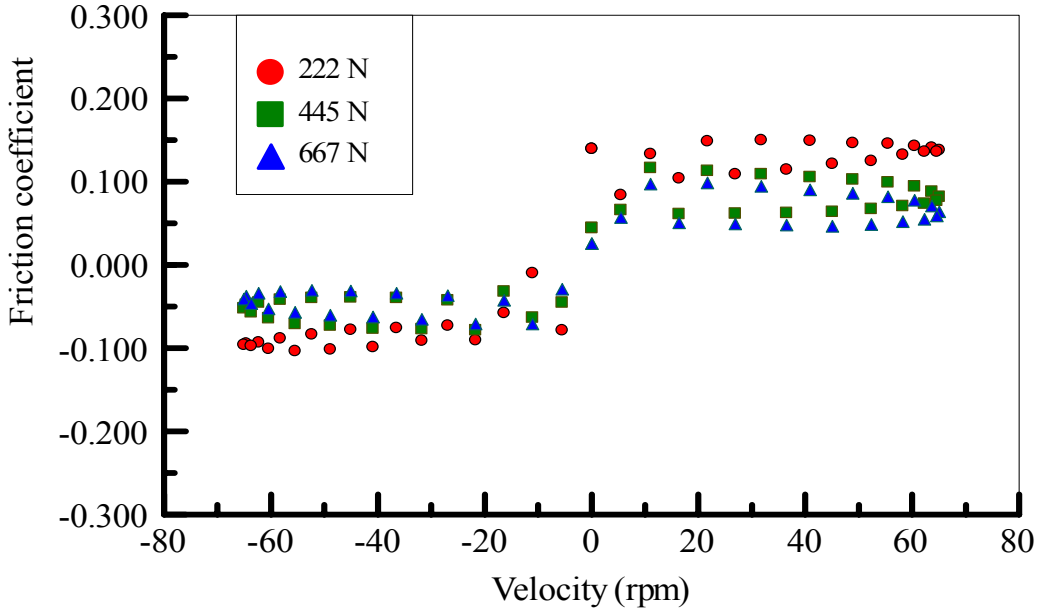

Figure 5.7 - Friction coefficient versus velocity (bronze bushing, 1.5 Hz oscillating frequency, SAE30 oil)

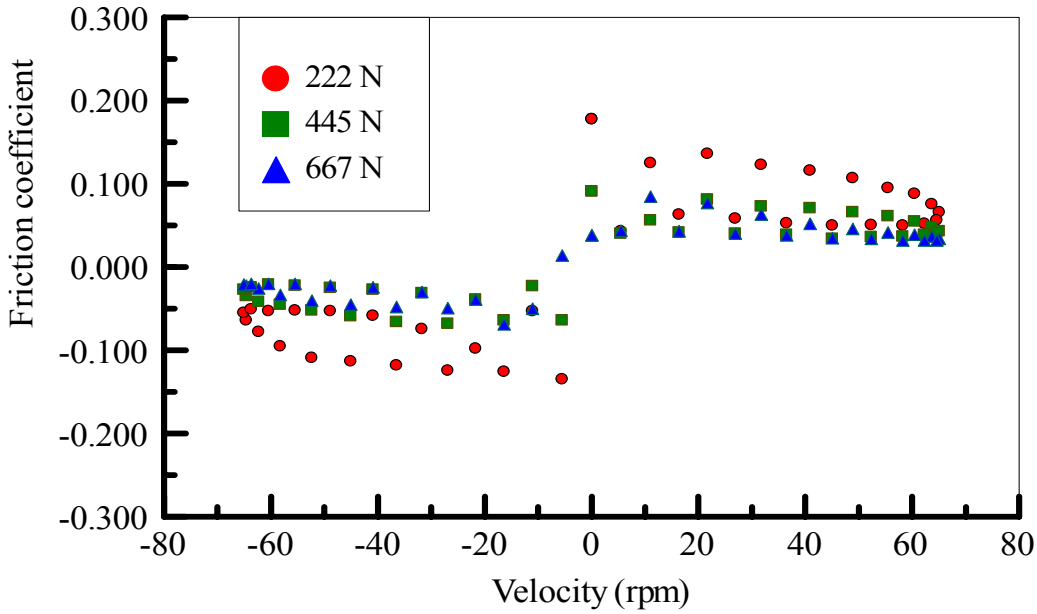

Figure 5.8 - Friction coefficient versus velocity (bronze bushing, 1.5 Hz oscillating frequency, SAE40 oil)

motion, the oil flow is wedged into the contact track by the journal rotation and oscillates with it. Different from typical journal bearings that operate under a constant, uni-directional motion, in our tests the shaft always accelerates/decelerates during cycles. When the load on the shaft is higher, the inertia of the shaft is greater, and the interaction of shaft and oil becomes stronger. As a result, the retardation effect of the friction coefficient is reduced. The shaft induces more oil into contact region to separate shaft and bushing asperities. The friction hysteresis loop becomes narrower and the friction level gets lower.

Under 667 N load and 0.5 Hz oscillating frequency for SAE30 oil, the hysteresis loop almost vanishes. A flatter or narrower hysteresis loop implies that the friction difference between increasing velocity and decreasing velocity is smaller. In precision control industry, such as robotic positioning, the control engineer requires a suitable friction model to compensate the effects of friction [162-168]. When the area within the loop vanishes, the friction is easier to model. In addition, a flatter friction curve suggests more stable friction performance.

5.2.4.2 Oil Inlet Temperature Effect

Figs. 5.9-5.14 demonstrate the oil inlet temperature effect on the local history of the friction coefficient for 0.5 Hz, 1.0 Hz, and 1.5 Hz frequencies, respectively. The oil inlet temperatures are 40^0C, 50^0C, and 60^0C. 445 N load is imposed on the bronze bushing.

To identify the lubrication regime which the tested journal bearing undergoes, the Stribeck curve for a uni-directional rotation motion is characterized in Figs. 15 and 16. The applied load is 445 N. The speed ranges from 2 to 500 rpm. The oil inlet temperature changes from 40^0C, 50^0C, to 60^0C.

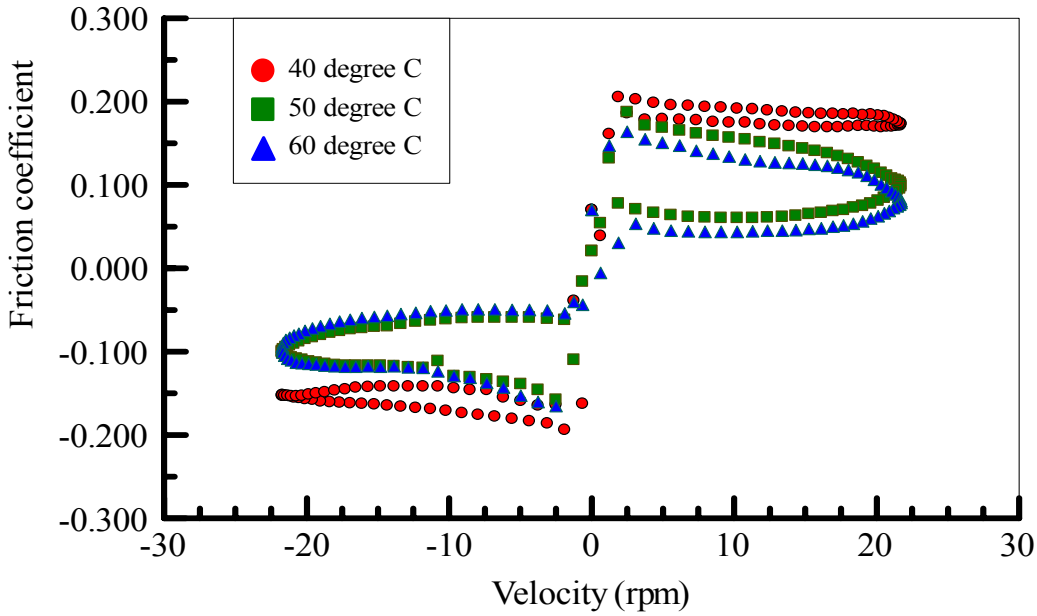

Figure 5.9 - Friction coefficient versus velocity (bronze bushing, 0.5 Hz oscillating frequency, SAE30 oil)

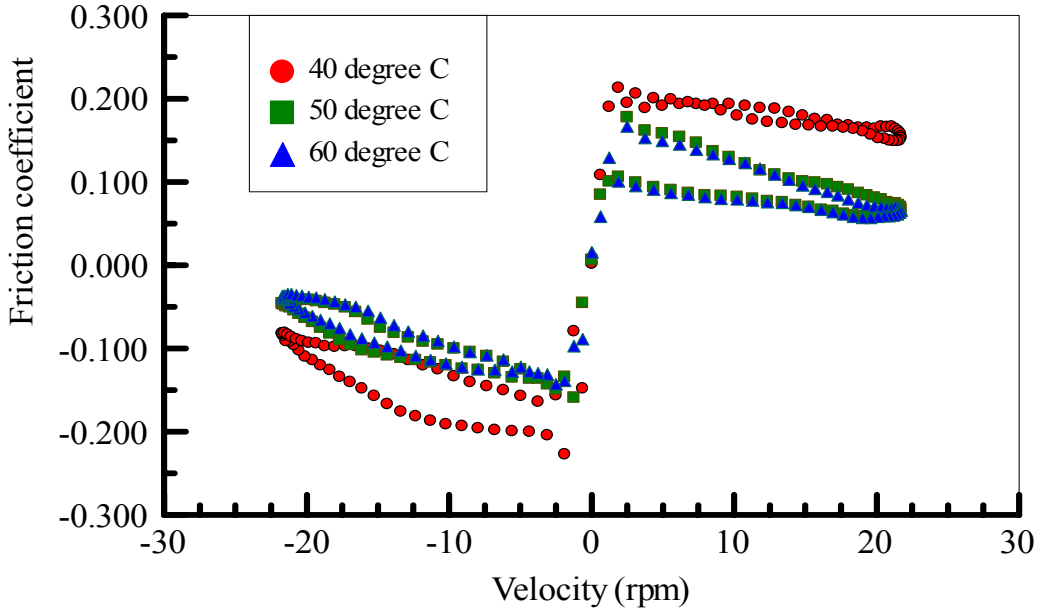

Figure 5.10 - Friction coefficient versus velocity (bronze bushing, 0.5 Hz oscillating frequency, SAE40 oil)

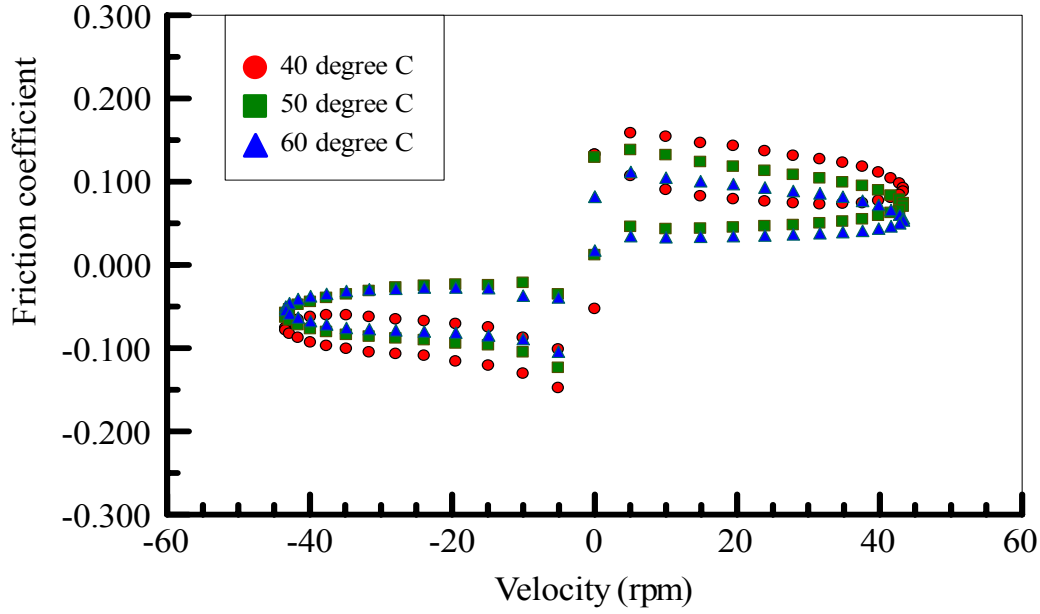

Figure 5.11 - Friction coefficient versus velocity (bronze bushing, 1.0 Hz oscillating frequency, SAE30 oil)

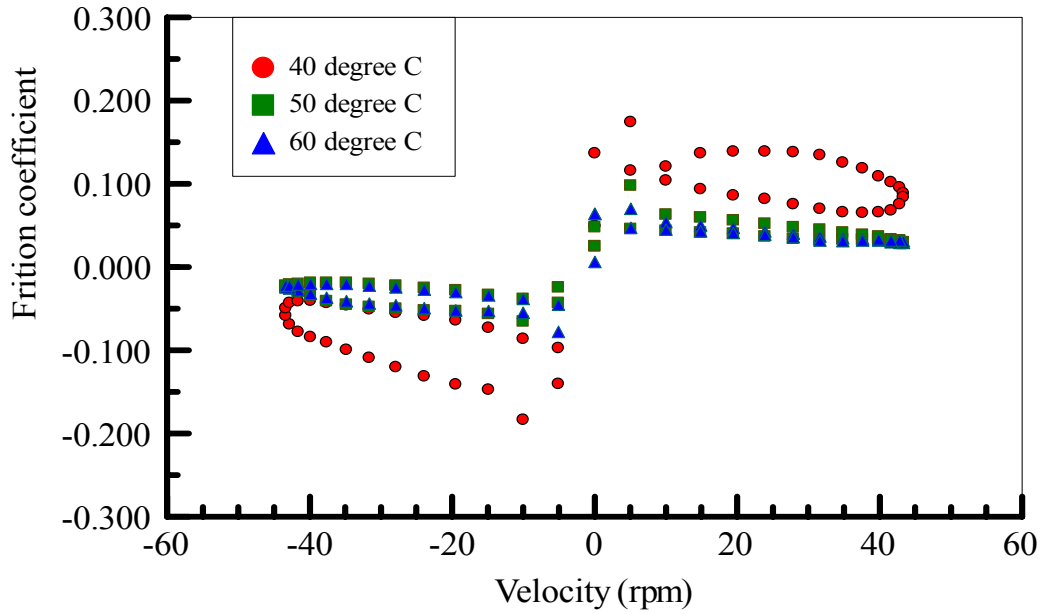

Figure 5.12 - Friction coefficient versus velocity (bronze bushing, 1.0 Hz oscillating frequency, SAE40 oil)

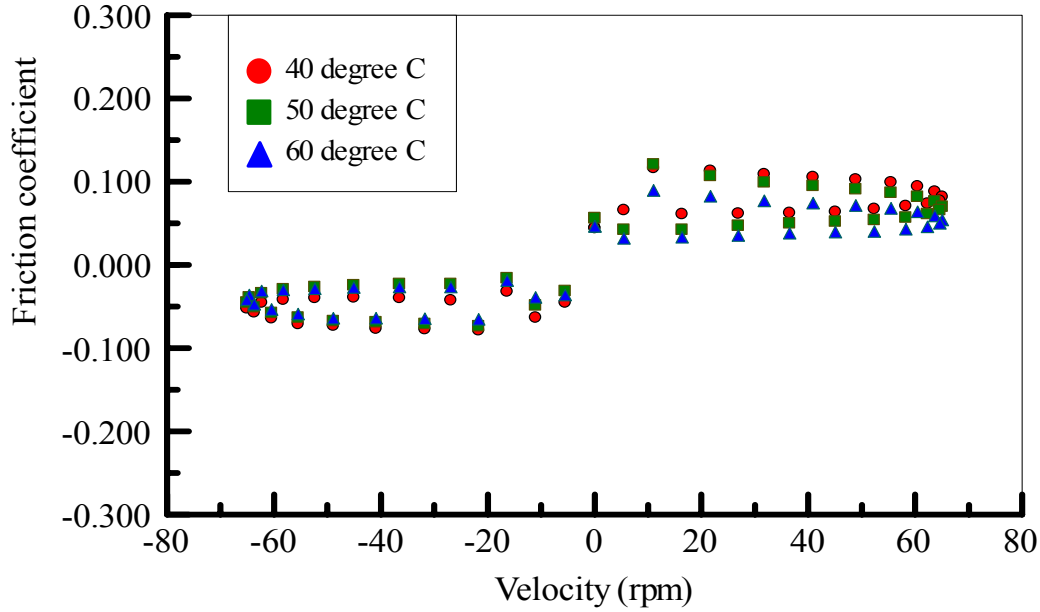

Figure 5.13 - Friction coefficient versus velocity (bronze bushing, 1.5 Hz oscillating frequency, SAE30 oil)

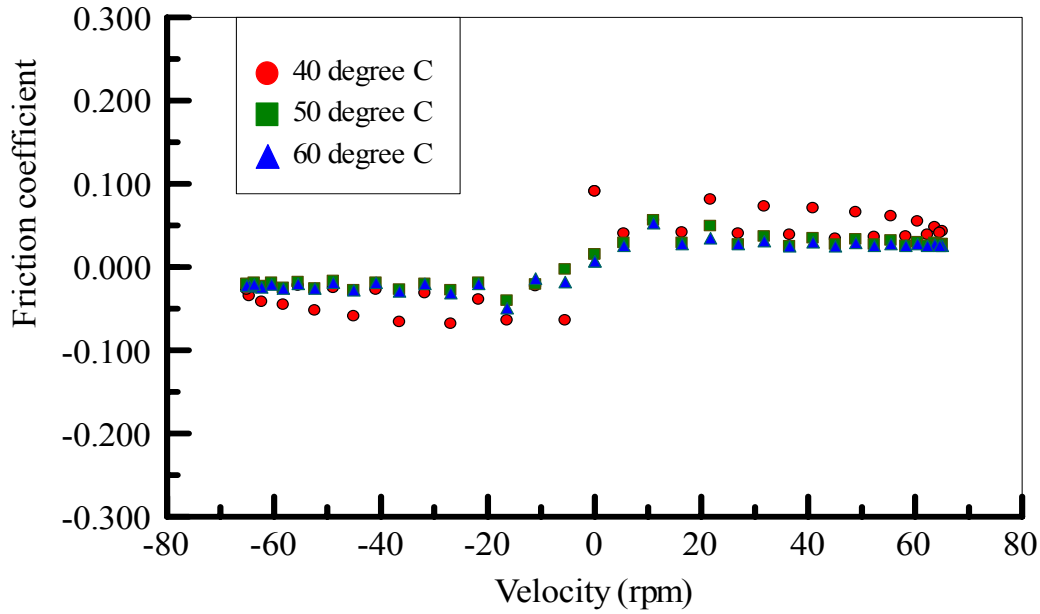

Figure 5.14 - Friction coefficient versus velocity (bronze bushing, 1.5 Hz oscillating frequency, SAE40 oil)

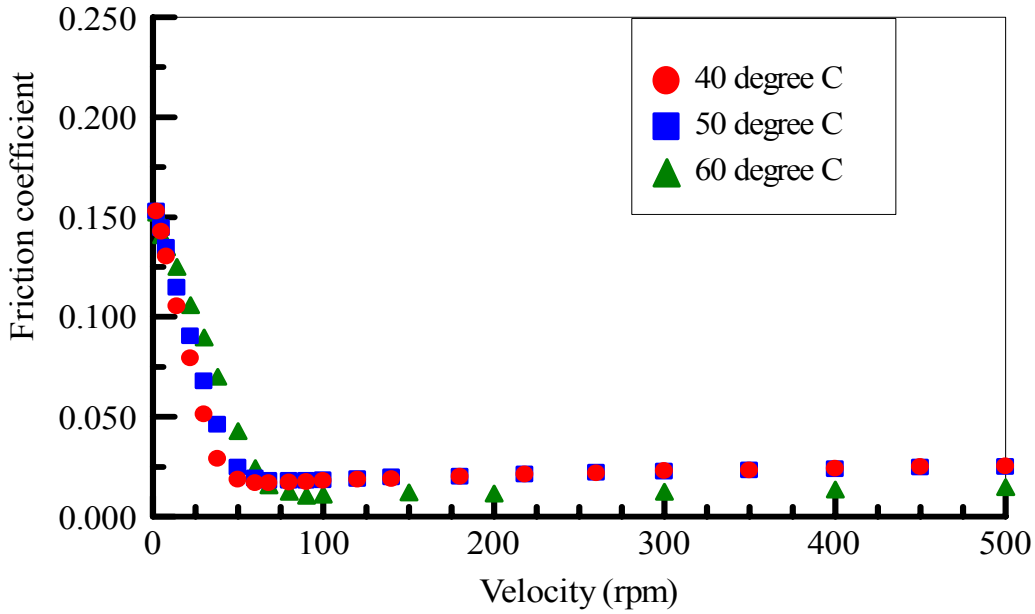

Figure 5.15 - The Stribeck curve (SAE30 oil, 445N load, bronze bushing, unidirectional rotation)

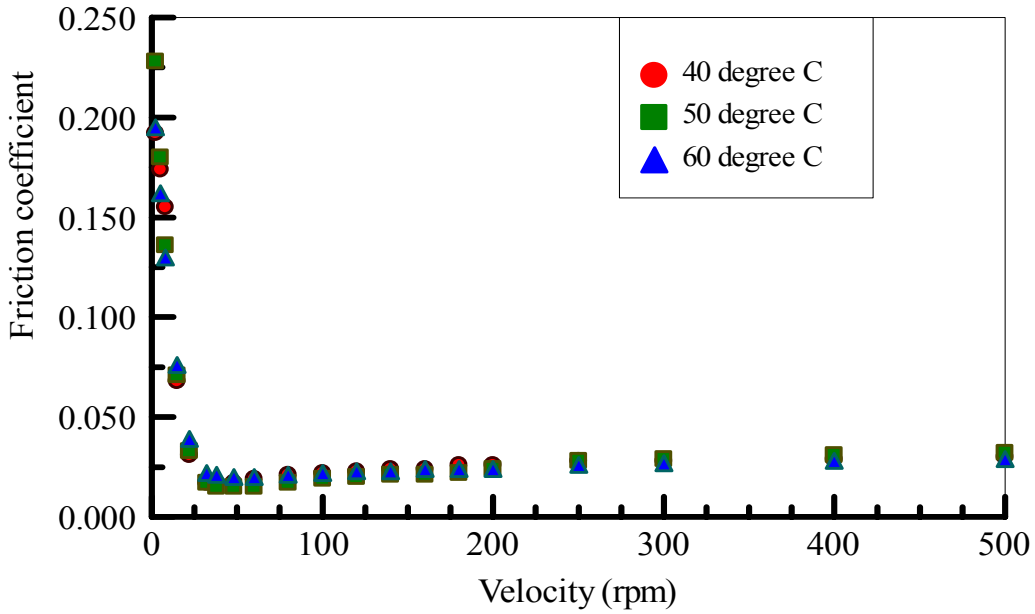

Figure 5.16 - The Stribeck curve (SAE40 oil, 445N load, bronze bushing, unidirectional rotation)

Some curves are overlapped due to the small difference of the friction coefficient, especially for SAE40 oil. On the Stribeck curve, the speed point which corresponds to the lowest friction coefficient is called the lift-off speed [57]. It is the watershed between mixed and hydrodynamic lubrication. The lift-off speeds with different oil inlet temperatures are tabulated in Table 5.3.

Table 5.3- The lift-off speed (rpm)

SAE30 oil			SAE40 oil		
40^0C	50^0C	60^0C	40^0C	50^0C	60^0C
55	68	90	38	44	58

In the case of oscillatory motion, the maximum sliding speeds in oscillation are 23 rpm, 46 rpm, and 68 rpm for 0.5 Hz, 1.0 Hz, and 1.5 Hz oscillating frequencies, respectively. Comparing them with the lift-off speeds in Table 5.3, it is known that the tested oscillating journal bearing mainly operates in boundary and mixed lubrication regimes.

When the oil temperature is higher, the viscosity decreases. Under uni-directional rotation condition, less viscosity translates to more metal-to-metal contact to support the same load, which results in a higher coefficient of friction. By definition, viscosity represents the resistance to flow. A lower viscosity means greater flowability. Under oscillatory condition, the acceleration of the shaft brings more oil into the contact track, which separates shaft and bushing asperity surfaces better. The coefficient of friction becomes lower.

5.2.4.3 Oscillating Frequency Effect

Figs. 5.17-5.24 present the oscillating frequency effect on the local history of the friction coefficient for 222 N, 445 N, 667 N, and 890 N loads, respectively. The oil inlet temperature is 40^0C, and bronze bushing is used.

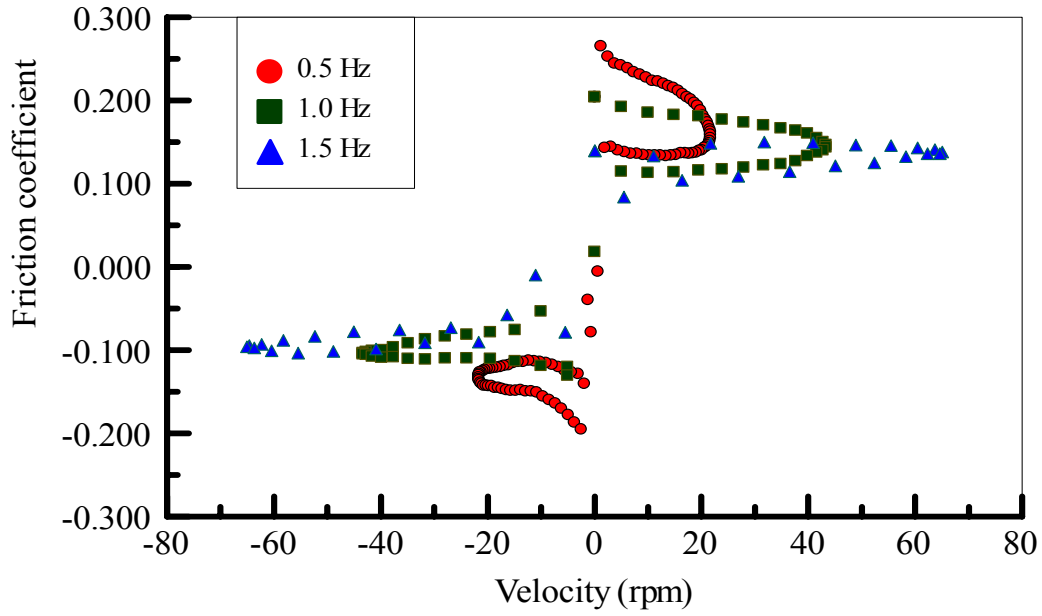

Figure 5.17 - Friction coefficient versus velocity (bronze bushing, 222 N load, SAE30 oil)

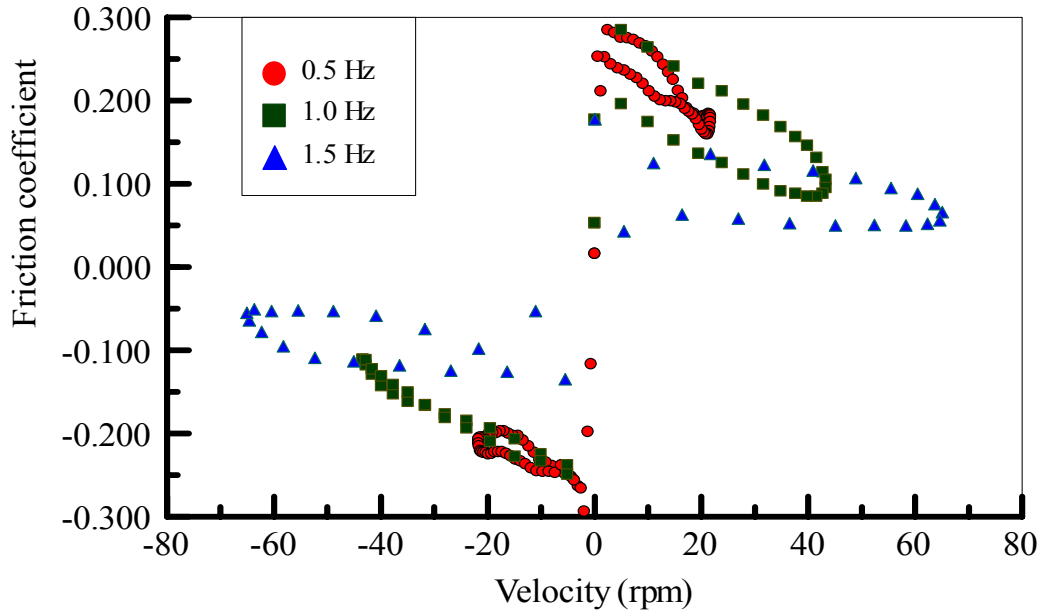

Figure 5.18 - Friction coefficient versus velocity (bronze bushing, 222 N load, SAE40 oil)

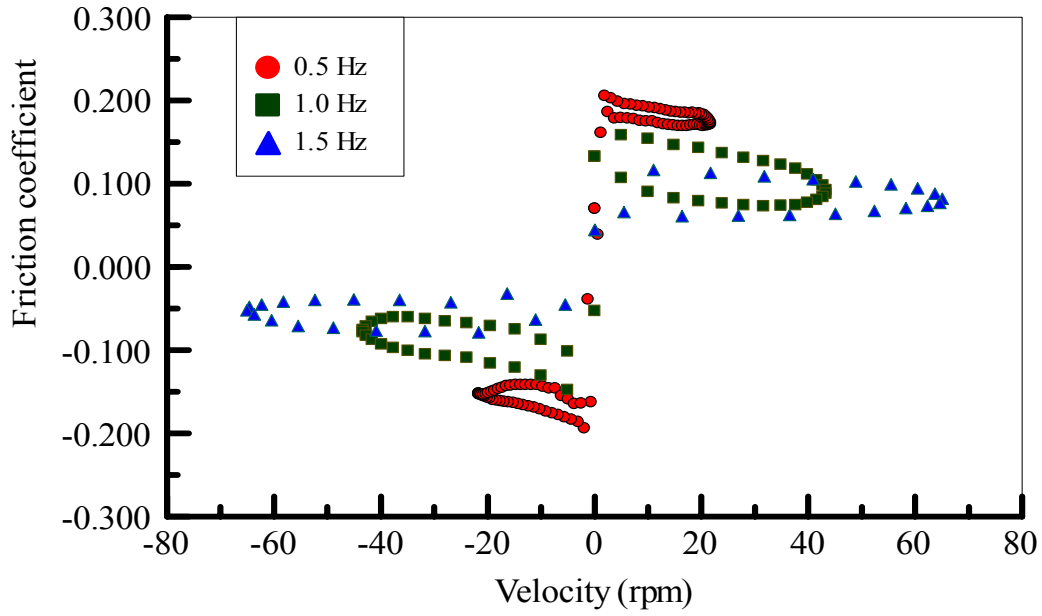

Figure 5.19 - Friction coefficient versus velocity (bronze bushing, 445 N load, SAE30 oil)

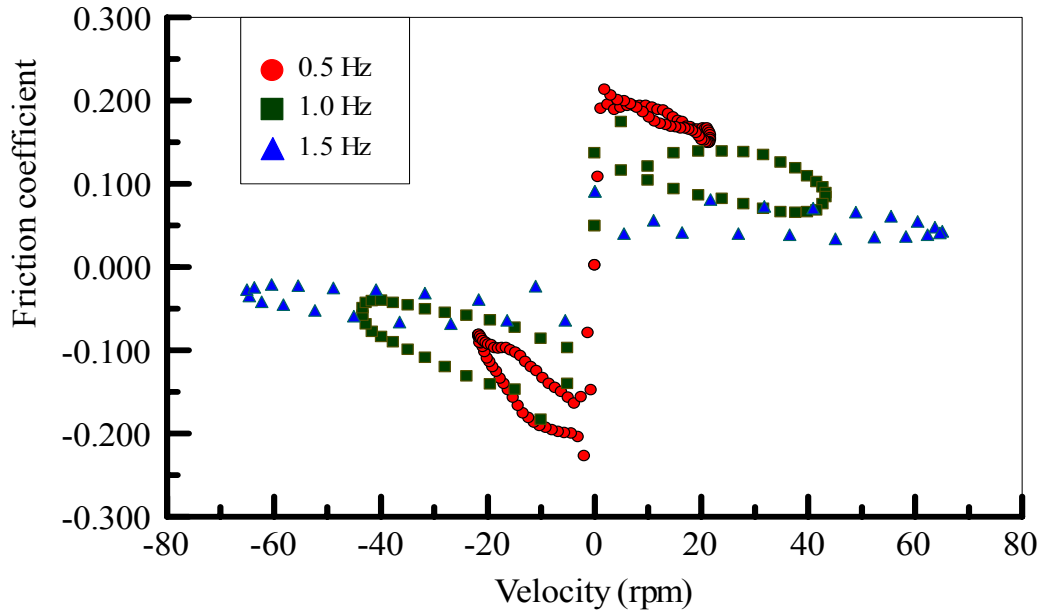

Figure 5.20 - Friction coefficient versus velocity (bronze bushing, 445 N load, SAE40 oil)

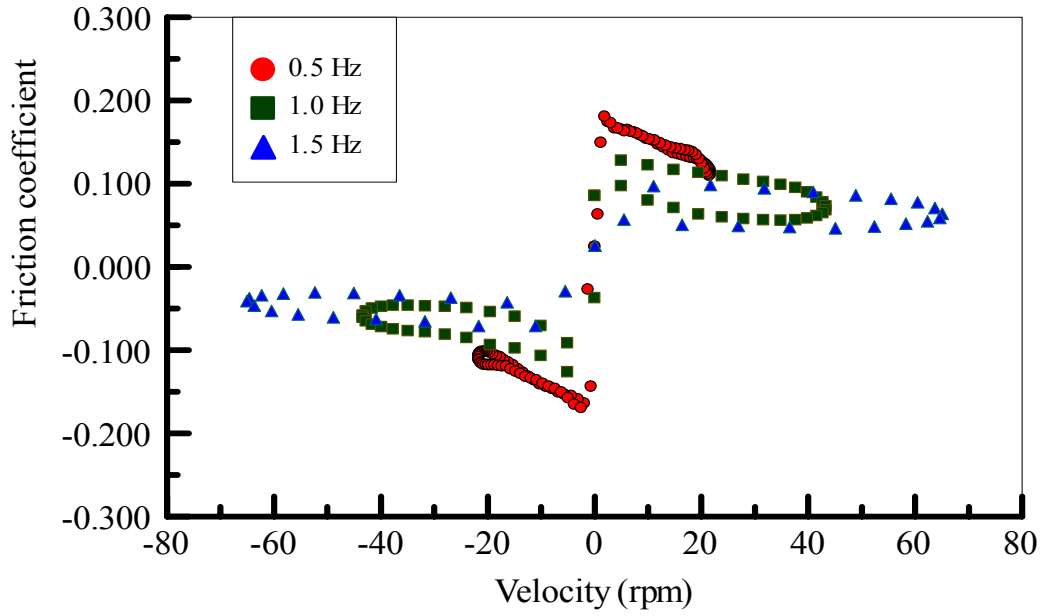

Figure 5.21 - Friction coefficient versus velocity (bronze bushing, 667 N load, SAE30 oil)

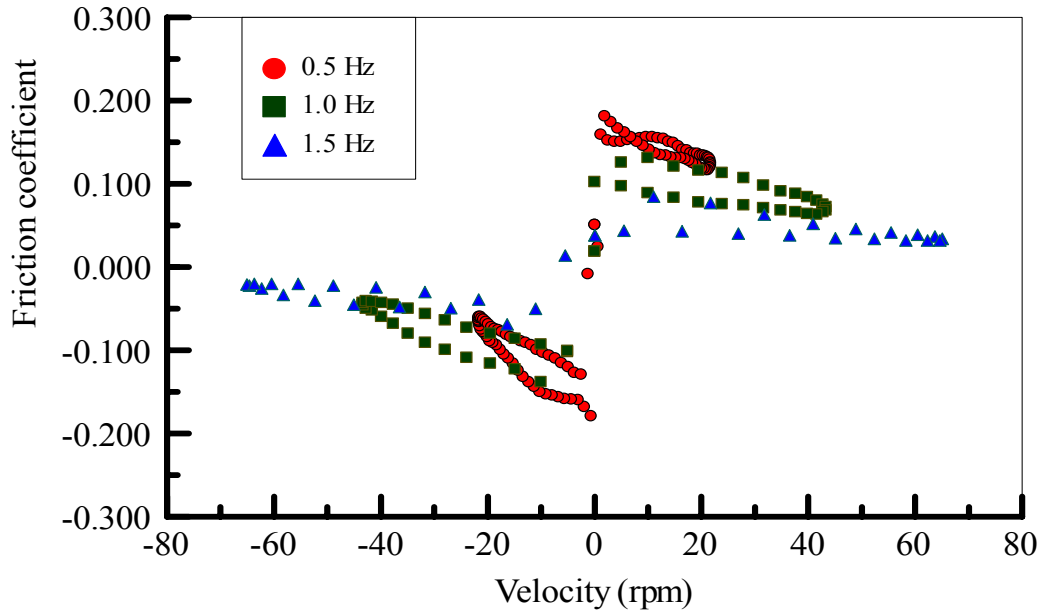

Figure 5.22 - Friction coefficient versus velocity (bronze bushing, 667 N load, SAE40 oil)

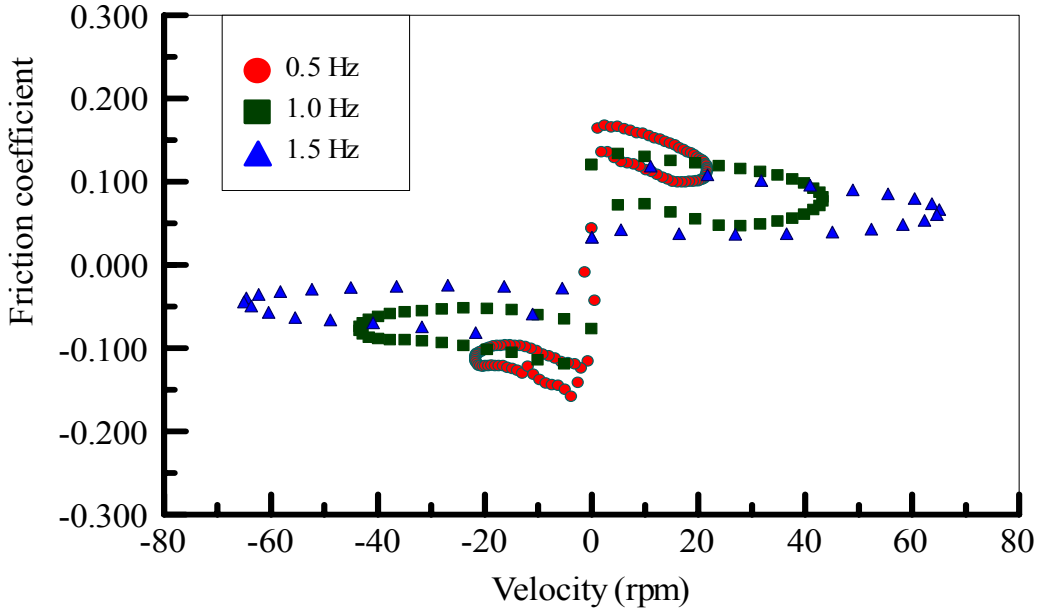

Figure 5.23 - Friction coefficient versus velocity (bronze bushing, 890 N load, SAE30 oil)

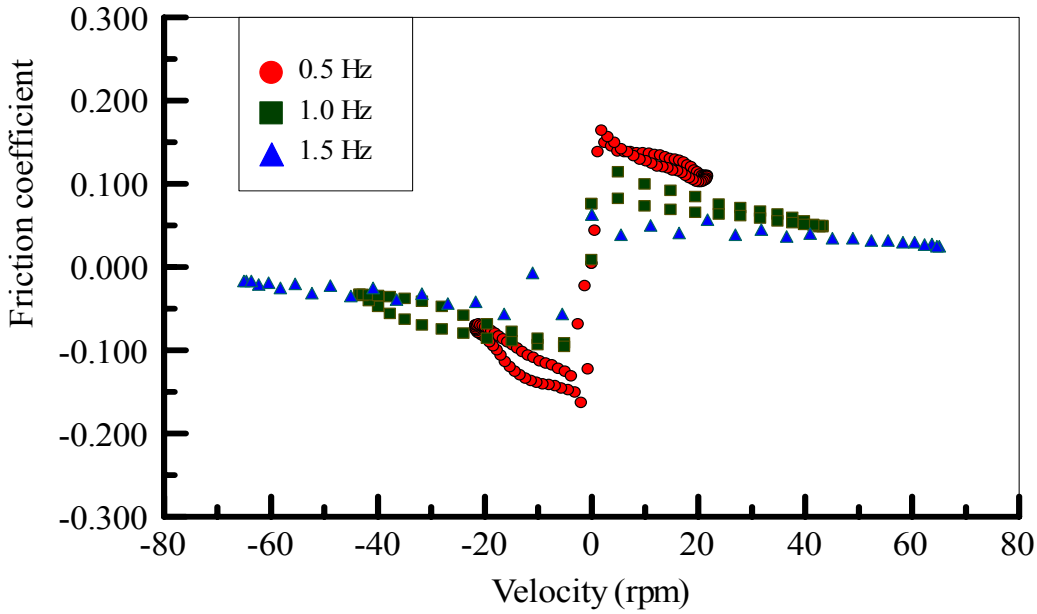

Figure 5.24 - Friction coefficient versus velocity (bronze bushing, 890 N load, SAE40 oil)

Under each load, the friction hysteresis loop is flattened by a higher oscillating frequency. The higher the velocity of the shaft, the greater is the amount of oil drawn into the shaft and bushing contact track, which results in a thicker film thickness and a lower friction coefficient.

A flatter friction coefficient curve implies that there is less variability for the coefficient of friction as the velocity changes, which translates to more stable friction performance. This is preferred for friction control of precision machinery in which the bearings operate in oscillatory fashion.

The analysis on the load effect, the oil inlet temperature effect and the oscillating frequency effect reveals that when more oil is drawn into asperity contact region, the friction level is lower and the friction hysteresis loop is narrower and flatter.

The area under the friction-velocity curve represents the total frictional heat flux $\sum q$ in that period. According to its variation, the velocity can be divided into four stages: positive acceleration, positive deceleration, negative acceleration and negative deceleration (referring to Fig. 5.1). In one stage, the total frictional heat flux can be expressed as

$$\sum q = \int_v f(v) p dv \tag{5.1}$$

Assuming that the pressure p is constant, Eq. (1) simplifies into

$$\sum q = p \int_v f(v) dv \tag{5.2}$$

Let $\sum q_1$ represent the area under the friction curve with an increasing velocity and $\sum q_2$ denote the area under the friction curve with a decreasing velocity. Then, the area within the hysteresis loop can be formulated as

$$\Delta\left(\sum q\right) = \sum q_1 - \sum q_2 = p\int_v f_1(v)dv - p\int_v f_2(v)dv = p\int_v \left(f_1(v) - f_2(v)\right)dv \qquad (5.3)$$

The term $\Delta\left(\sum q\right)$ can be used to characterize the bandwidth of the hysteresis loop. When $\Delta\left(\sum q\right)$ is bigger, the bandwidth is bigger; when $\Delta\left(\sum q\right)$ is smaller, the bandwidth is smaller.

5.2.4.4 Bushing Type Effect

The performance of both bronze and steel bushings is studied by examining the local history of the friction coefficient. The results of imposing 445 N load with SAE30 and SAE40 oil at 40^0 C inlet temperature are illustrated in Figs. 5.25-5.30.

The results indicate that the steel bushing has a narrower and flatter hysteresis loop than does the bronze bushing. The radial clearance is 0.089 mm for bronze bushing and0.43 mm for steel bushing. When the clearance is bigger, the effect of retardation on the lubricant flow by the bearing surface asperities is smaller. Hence, the hysteresis loop is narrower.

5.2.4.5 Comparison of Oscillatory and Uni-directional Rotation

Figs. 5.32-5.39 compare the friction performance of bearings under oscillatory and uni-directional rotation. The oil inlet temperature is 40 ^{0}C, and bronze bushing is used.

When the load is bigger and the oscillating speed is higher, the friction coefficient under oscillatory motion becomes smaller than that under uni-directional motion at the same speed point. From discussion in §5.2.4.1 and §5.2.4.3, it is known that increasing load and oscillating speed involves more oil into the contact track, which separates the friction surfaces better and results in a smaller friction coefficient.

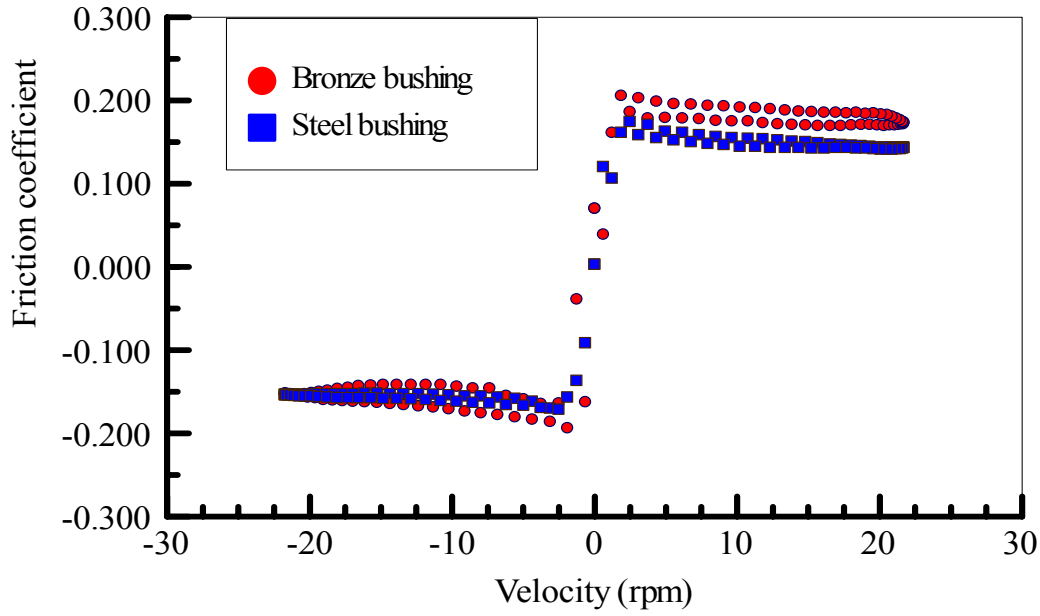

Figure 5.25 - Friction coefficient versus velocity (0.5 Hz oscillating frequency, SAE30 oil)

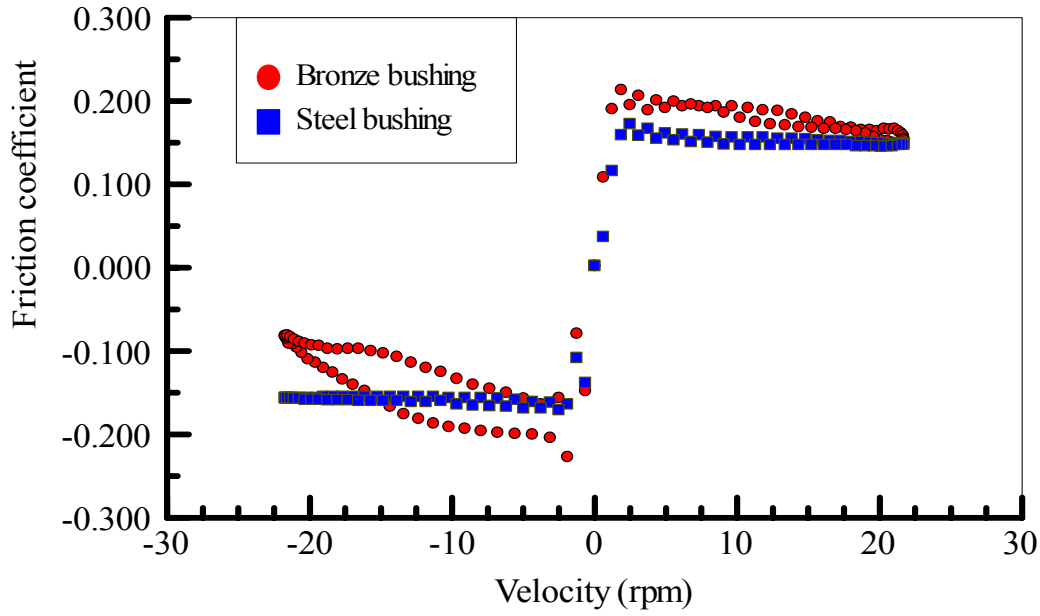

Figure 5.26 - Friction coefficient versus velocity (0.5 Hz oscillating frequency, SAE40 oil)

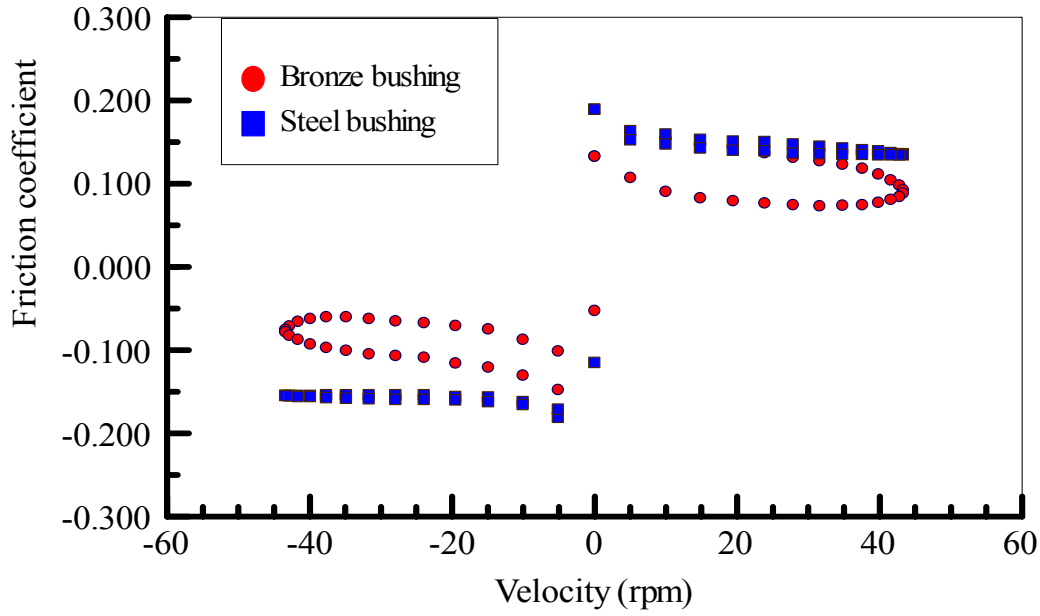

Figure 5.27 - Friction coefficient versus velocity (1.0 Hz oscillating frequency, SAE30 oil)

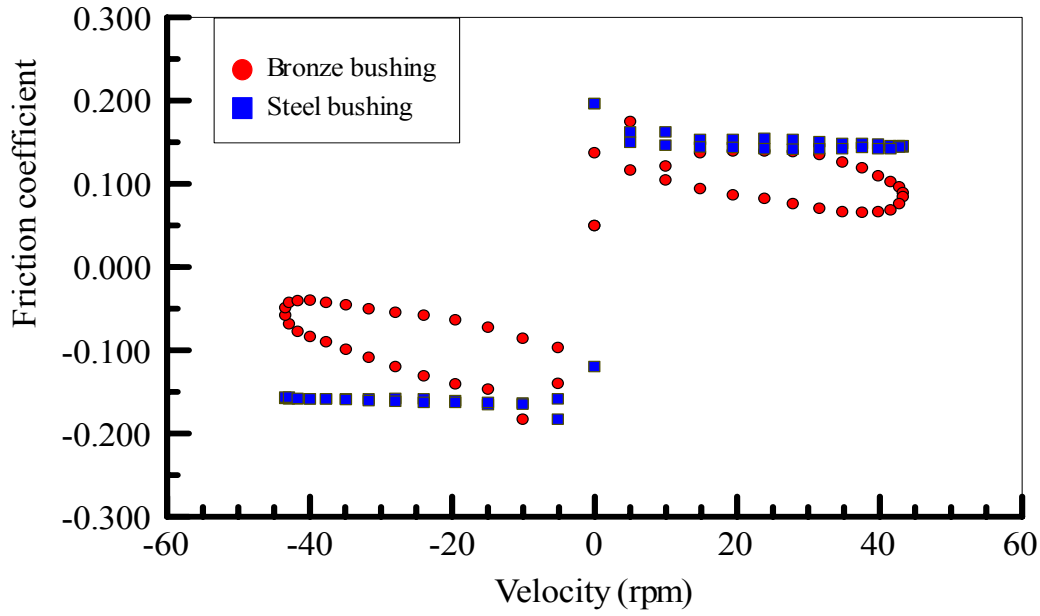

Figure 5.28 - Friction coefficient versus velocity (1.0 Hz oscillating frequency, SAE40 oil)

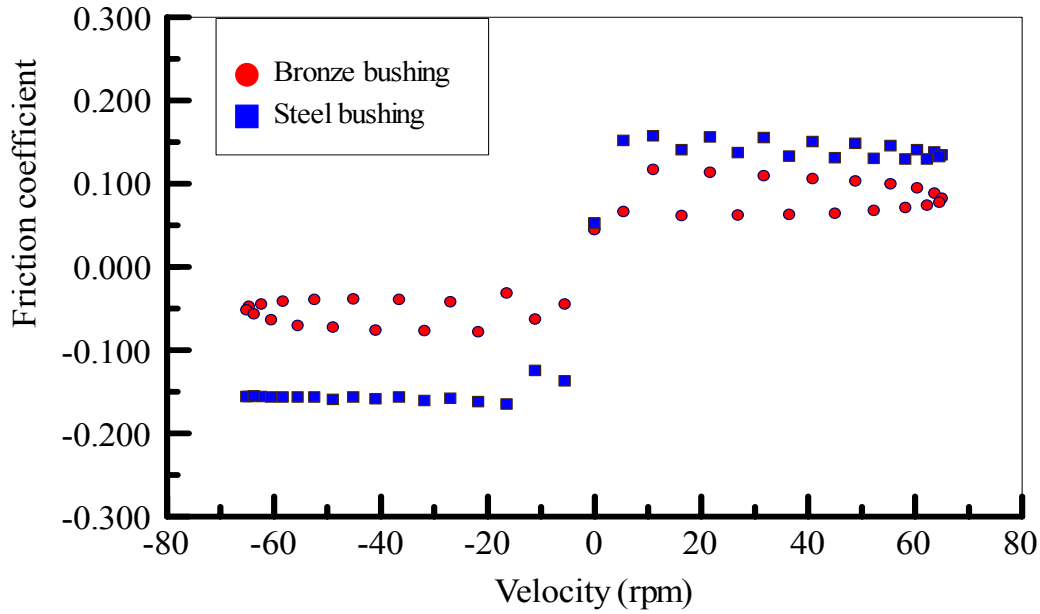

Figure 5.29 - Friction coefficient versus velocity (1.5 Hz oscillating frequency, SAE30 oil)

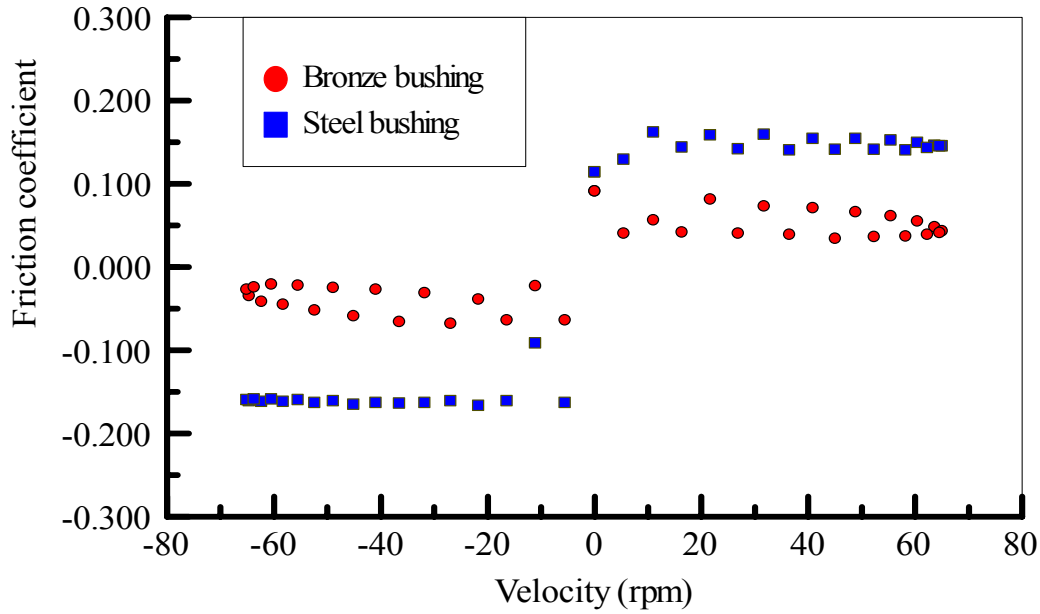

Figure 5.30 - Friction coefficient versus velocity (1.5 Hz oscillating frequency, SAE40 oil)

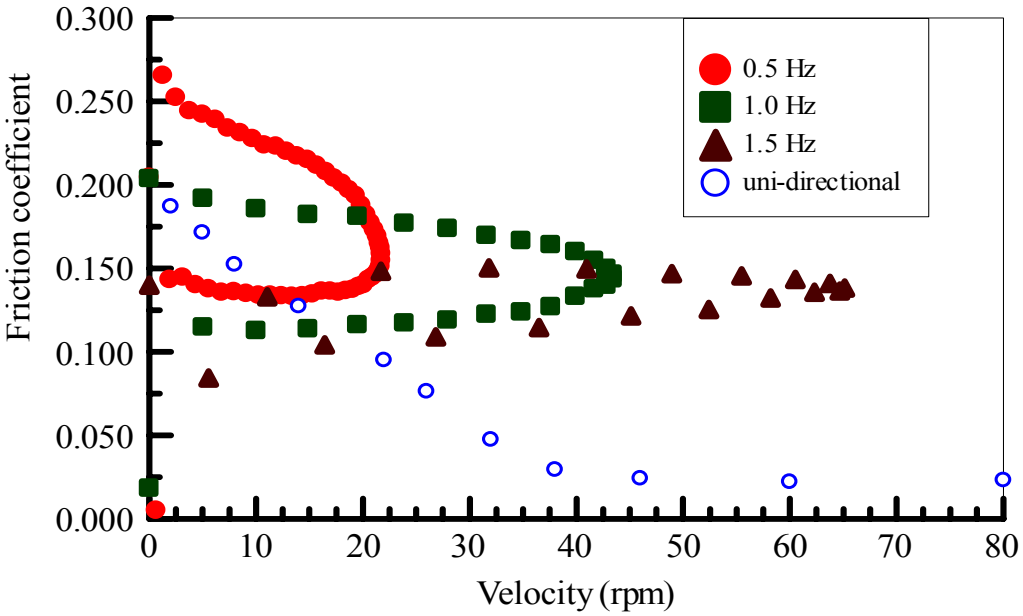

Figure 5.32 - Comparison of the friction of oscillatory and uni-directional rotation (bronze bushing, SAE30 oil, 222 N load)

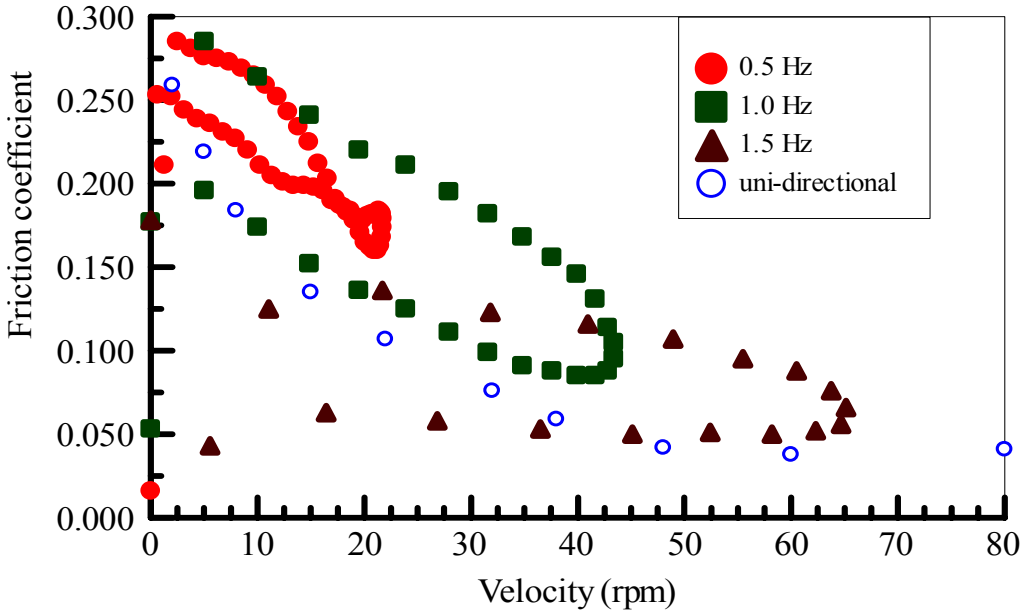

Figure 5.33 - Comparison of the friction of oscillatory and uni-directional rotation (bronze bushing, SAE40 oil, 222 N load)

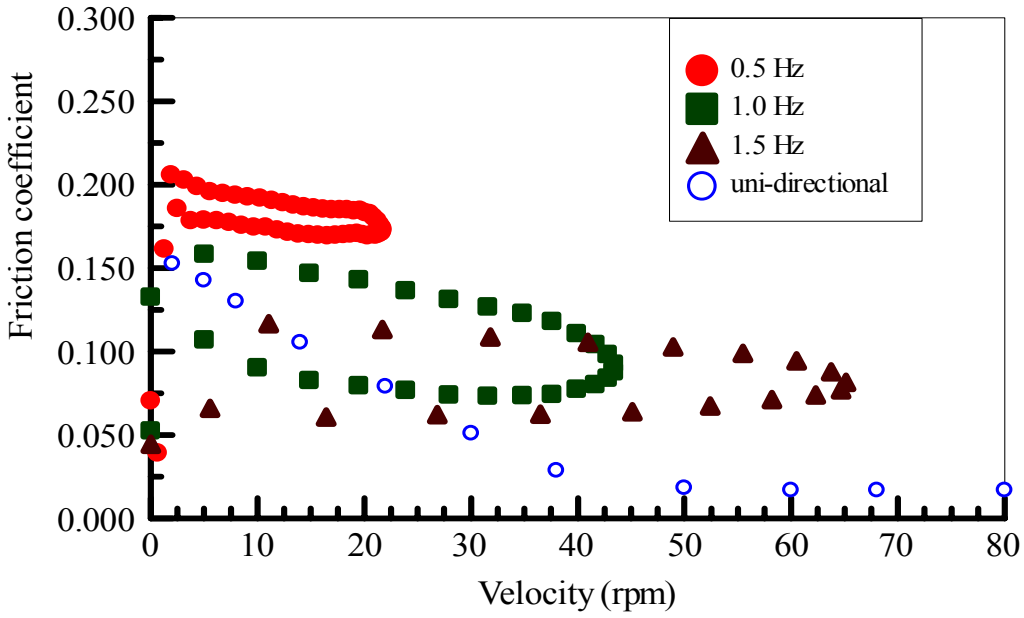

Figure 5.34 - Comparison of the friction of oscillatory and uni-directional rotation (bronze bushing, SAE30 oil, 445 N load)

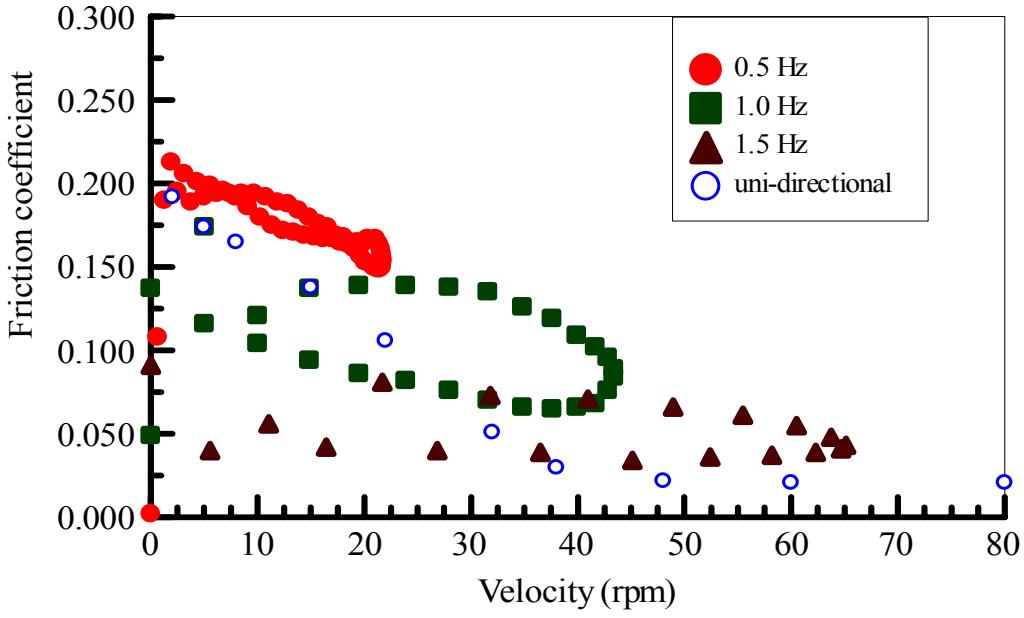

Figure 5.35 - Comparison of the friction of oscillatory and uni-directional rotation (bronze bushing, SAE40 oil, 445 N load)

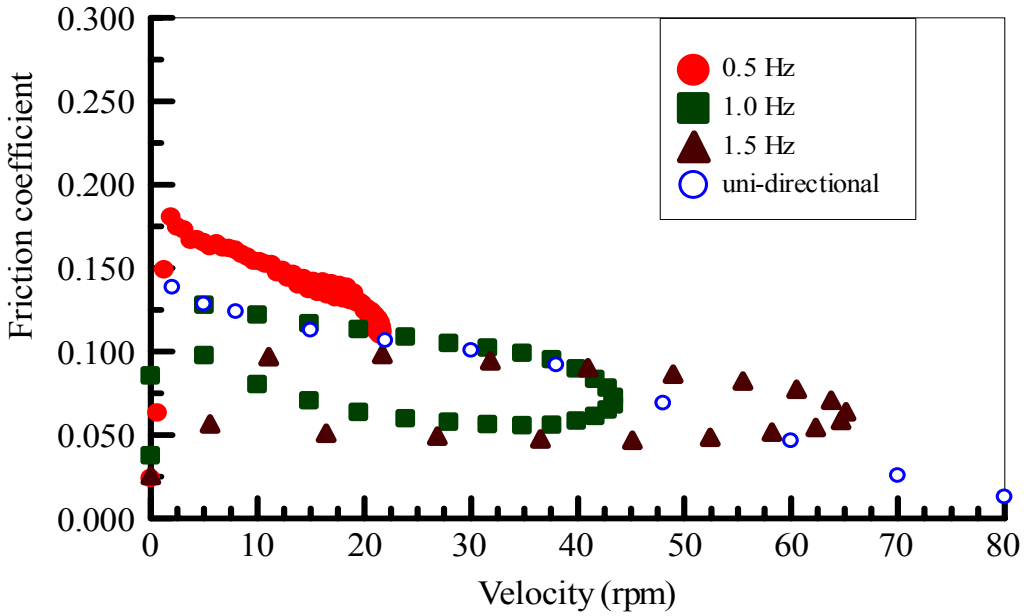

Figure 5.36 - Comparison of the friction of oscillatory and uni-directional rotation (bronze bushing, SAE30 oil, 667 N load)

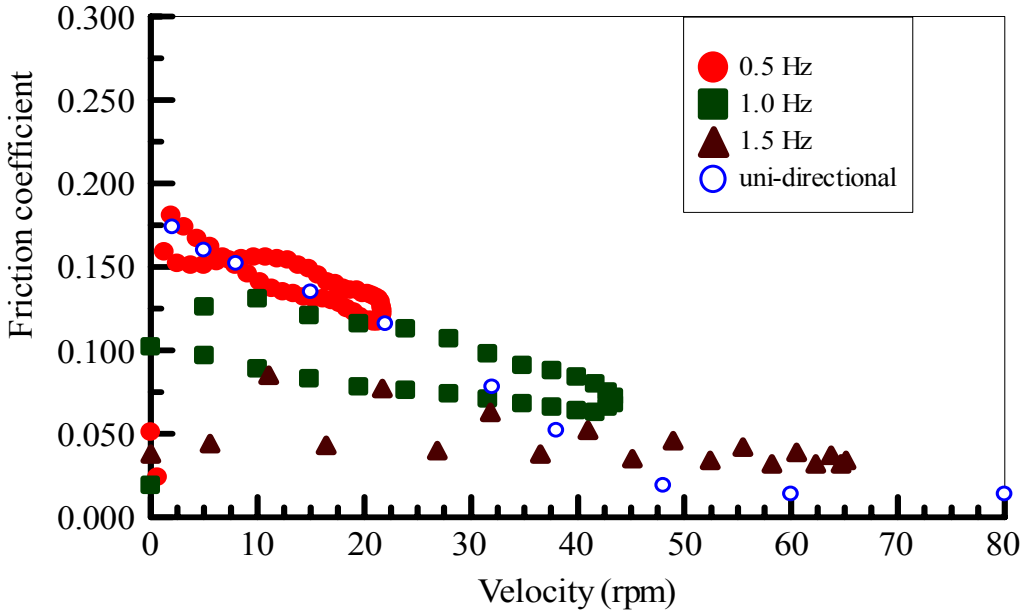

Figure 5.37 - Comparison of the friction of oscillatory and uni-directional rotation (bronze bushing, SAE40 oil, 667 N load)

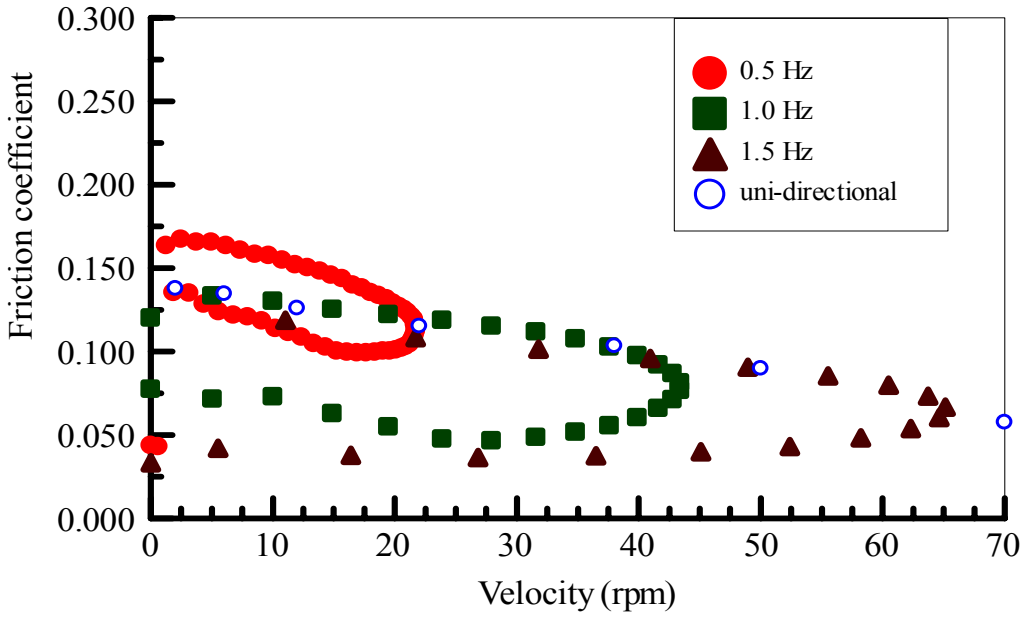

Figure 5.38 - Comparison of the friction of oscillatory and uni-directional rotation (bronze bushing, SAE30 oil, 890 N load)

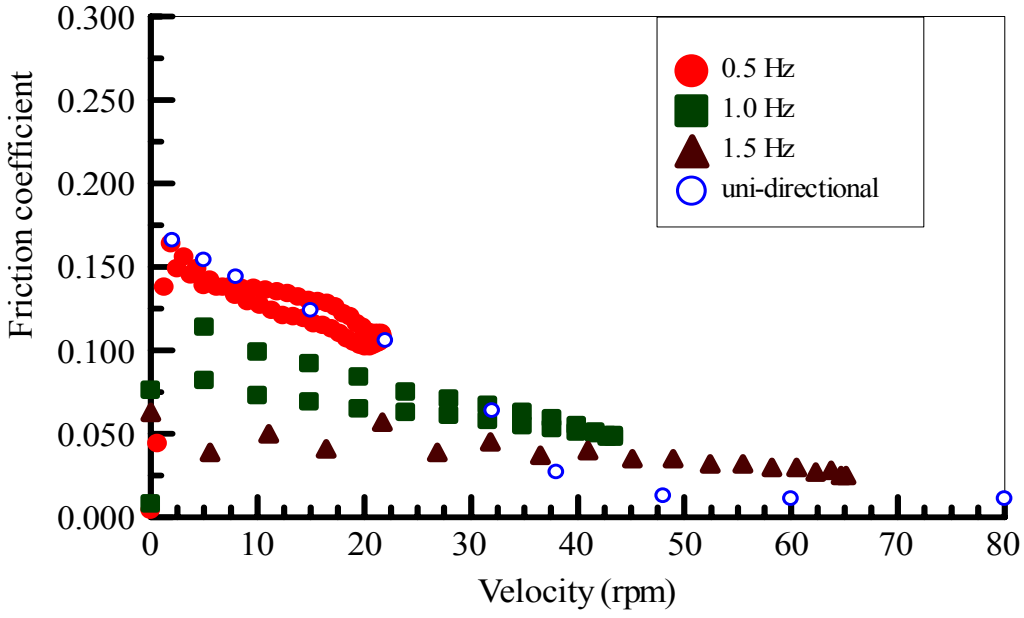

Figure 5.39 - Comparison of the friction of oscillatory and uni-directional rotation (bronze bushing, SAE40 oil, 890 N load)

5.2.4.6 Further Exploration of the Friction Hysteresis Phenomenon

5.2.4.6.1 Comparison of Dry and Lubricated Tests

As stated earlier, the tested bearing primarily operates in boundary and mixed lubrication regime. In mixed lubrication regime, both asperity interaction and hydrodynamic pressure exist to support the applied load. To examine the role of asperity interaction in the friction hysteresis, the bearing is tested without lubricant. The steel bushing is chosen to minimize the effect of wear, with 445 N applied load. Examination of surfaces after the experiments shows no visible wear scar.

In dry tests (Fig. 5.40), the friction hysteresis phenomenon still exists. Plastic deformation at asperity level [169], material damping, and viscous dissipation, etc [170], all contribute to the phenomenon. However, without lubricant the friction level rises with increasing oscillating frequency. With lubricant, the friction level drops with increasing oscillating frequency and the friction hysteresis loop is more smooth and narrow.

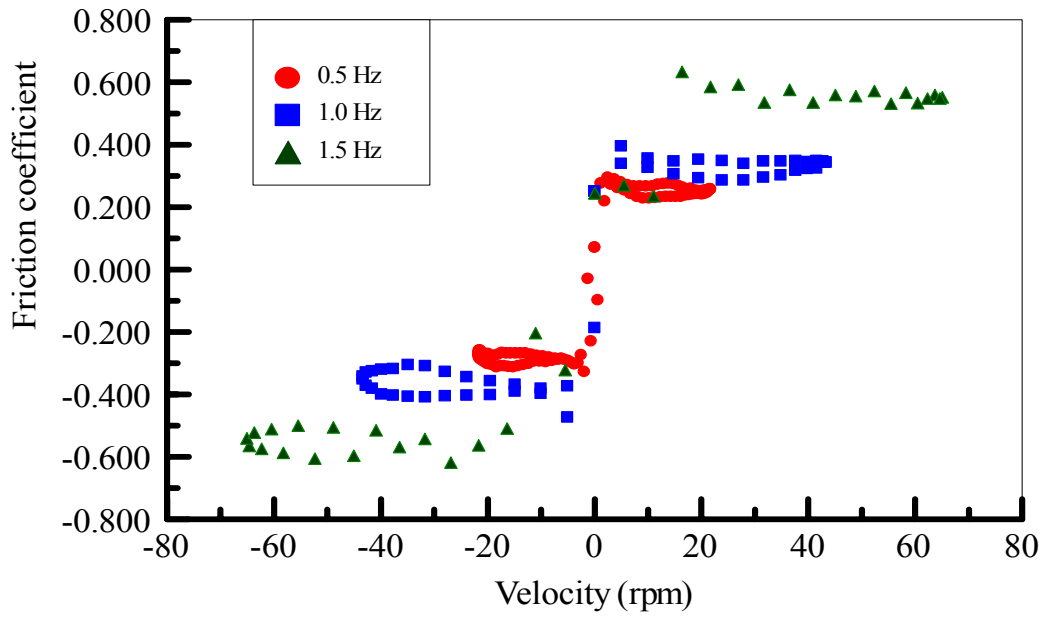

Figure 5.40 - Friction coefficient versus velocity (dry)

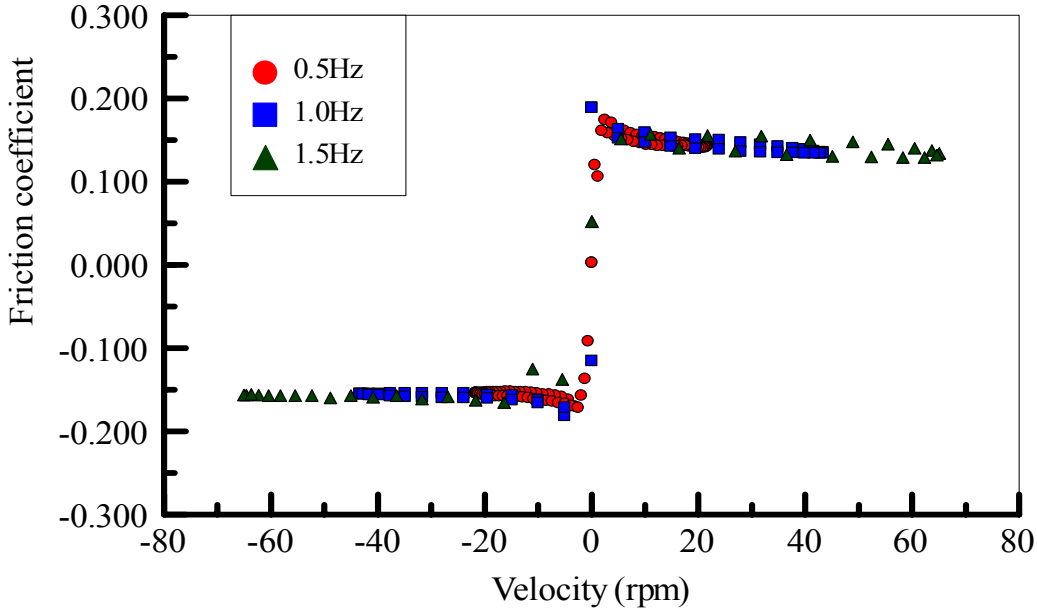

Figure 5.41 - Friction coefficient versus velocity (SAE30 oil)

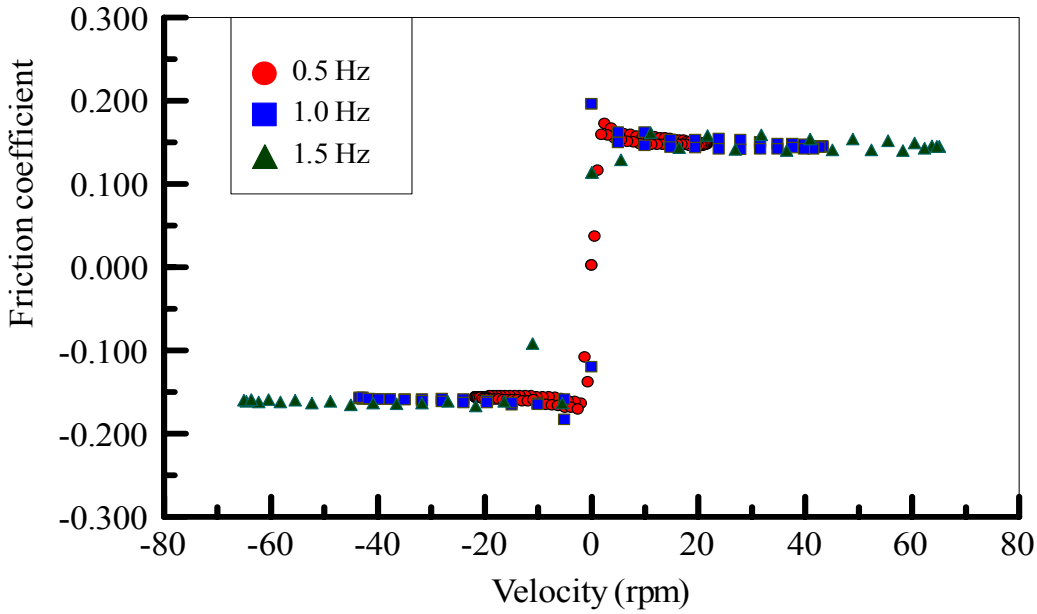

Figure 5.42 - Friction coefficient versus velocity (SAE40 oil)

5.2.4.6.2 Function of oil

To explore the hysteresis characteristic associated with oil, the variation of the lubricant flow with the accelerating/decelerating shaft is analyzed preliminarily. The four stages of the velocity history are shown in Fig. 43. Despite of boundary or mixed lubrication status, the shaft is completely separated from the bushing for clear demonstration.

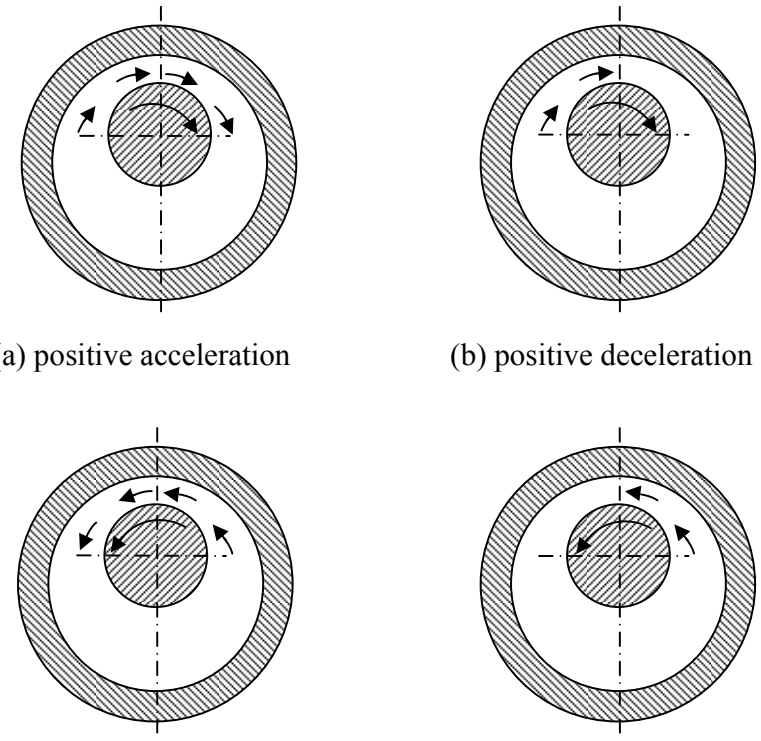

(a) positive acceleration (b) positive deceleration

(c) negative acceleration (d) negative deceleration

Figure 5.43 - Oscillating process

The effect of oil on the friction hysteresis is represented by the variation of the lubricant flow. Referring to Fig. 5.43, in stage (a), the shaft accelerates to the highest speed. It brings the volumetric flow forward (Fig. 5.44a). In stage (b), the shaft decelerates to zero speed. Once the slowdown process is triggered, the surface asperities

of shaft and bushing will act as barriers for the flow and tend to lower the flow rate and in some regions create backflow (Fig. 5.44b). Due to inertia, the flow will not be the same as that in stage (a) at the same shaft speed. Hence, the hysteresis feature occurs. As for the other half oscillating cycle - stage (c) and (d), a similar process is followed.

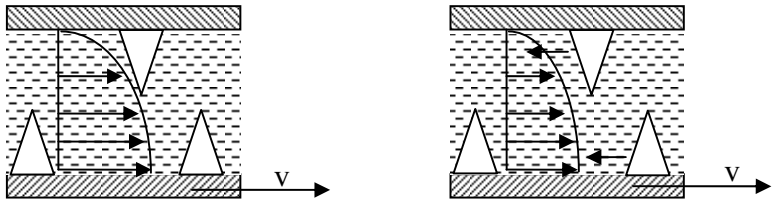

(a) (b)

Figure 5.44 - Idealized illustration of oscillating flow between asperities

5.2.4.6.3 Discussion

In the discussion above, the friction coefficient is plotted versus the shaft velocity. The four stages of the velocity variation have not been designated on those curves. However, this variation is an important feature of the friction hysteresis.

Corresponding to the four stages of the velocity history, the variation of the friction coefficient is narrated by Tables 5.4-5.8. If the absolute value of the friction coefficient in one stage is greater than the other in the same half oscillating cycle, it is remarked as "High", otherwise, "Low". In the case of the friction hysteresis disappears, it is remarked as "Identical".

Examination of the data reveals that there are three types of friction variation with the velocity history: High-Low-Low-High, High-Low-High-Low, and Low-High-High-Low. Most of the experiments with SAE30 oil present the first type variation. Most of the experiments with SAE40 oil show the second type variation. The experiments without

lubricant display all three types. They are exemplified in Figs. 5.45-5.47. The friction coefficient is taken as its absolute value. The velocity history is indicated by arrows.

With this plotting method, the hysteresis loop displays a lobed shape. Examination of the velocity input (Fig. 1) indicates that the positive velocity part is not symmetric to the negative one. It is determined by the characteristics of four bar linkage on the test rig. Therefore, the left half and the right half of the whole hysteresis loop are not symmetric.

Table 5.4- the friction coefficient variation with the velocity history (SAE30 oil, 40^0C oil inlet temperature)

Bushing Type	Load (N)	Oscillation Frequency (Hz)	Friction variation with velocity history			
			Positive increment	Positive decrement	Negative increment	Negative decrement
Bronze	222	0.5	High	Low	Low	High
		1.0	High	Low	Low	High
		1.5	High	Low	Low	High
	445	0.5	Low	High	High	Low
		1.0	High	Low	Low	High
		1.5	High	Low	Low	High
	667	0.5	Identical			
		1.0	High	Low	Low	High
		1.5	High	Low	Low	High
	890	0.5	High	Low	Low	High
		1.0	High	Low	Low	High
		1.5	High	Low	Low	High
Steel	445	0.5	High	Low	Low	High
		1.0	High	Low	Low	High
		1.5	High	Low	Low	High

Table 5.5- the friction coefficient variation with the velocity history (SAE30 oil, bronze bushing, 445 N load, 50^0C, 60^0C oil inlet temperature)

Temperature (^{0}C)	Oscillation Frequency (Hz)	Friction variation with velocity history			
		Positive increment	Positive decrement	Negative increment	Negative decrement
50	0.5	High	Low	Low	High
	1.0	High	Low	Low	High
	1.5	High	Low	Low	High
60	0.5	High	Low	Low	High
	1.0	High	Low	Low	High
	1.5	High	Low	Low	High

Table 5.6- the friction coefficient variation with the velocity history (SAE40 oil, 40^0C oil inlet temperature)

Bushing Type	Load (N)	Oscillation Frequency (Hz)	Friction variation with velocity history			
			Positive increment	Positive decrement	Negative increment	Negative decrement
Bronze	222	0.5	High	Low	Low	High
		1.0	High	Low	Identical	
		1.5	High	Low	High	Low
	445	0.5	High	Low	High	Low
		1.0	High	Low	High	Low
		1.5	High	Low	High	Low
	667	0.5	High	Low	High	Low
		1.0	High	Low	High	Low
		1.5	High	Low	High	Low
	890	0.5	High	Low	High	Low
		1.0	High	Low	High	Low
		1.5	High	Low	High	Low
Steel	445	0.5	High	Low	High	Low
		1.0	High	Low	High	Low
		1.5	High	Low	Identical	

Table 5.7- the friction coefficient variation with the velocity history (SAE40 oil, bronze bushing, 445 N load, 50^0C, 60^0C oil inlet temperature)

Temperature (^{0}C)	Oscillation Frequency (Hz)	Friction variation with velocity history			
		Positive increment	Positive decrement	Negative increment	Negative decrement
50	0.5	High	Low	High	Low
	1.0	High	Low	High	Low
	1.5	High	Low	High	Low
60	0.5	High	Low	High	Low
	1.0	High	Low	High	Low
	1.5	High	Low	High	Low

Table 5.8- the friction coefficient variation with the velocity history (dry, steel bushing, 445 N load)

Oscillation Frequency (Hz)	Friction variation with velocity history			
	Positive increment	Positive decrement	Negative increment	Negative decrement
0.5	High	Low	Low	High
1.0	High	Low	High	Low
1.5	Low	High	High	Low

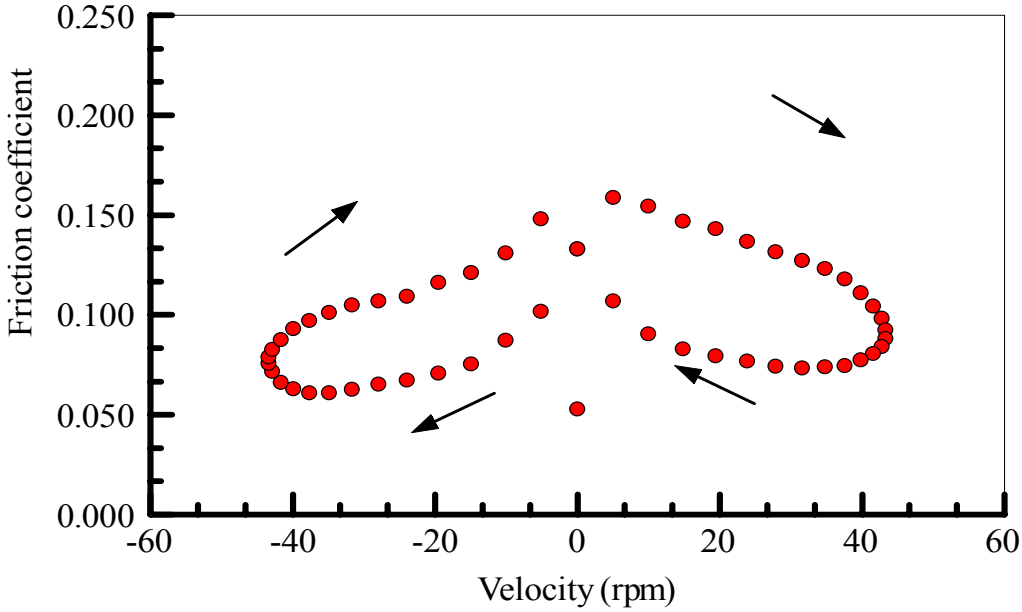

Figure 5.45 - the friction coefficient variation with the velocity history (445 N load, bronze bushing, 1.0 Hz oscillating frequency, SAE30 oil, 40^0C oil inlet temperature)

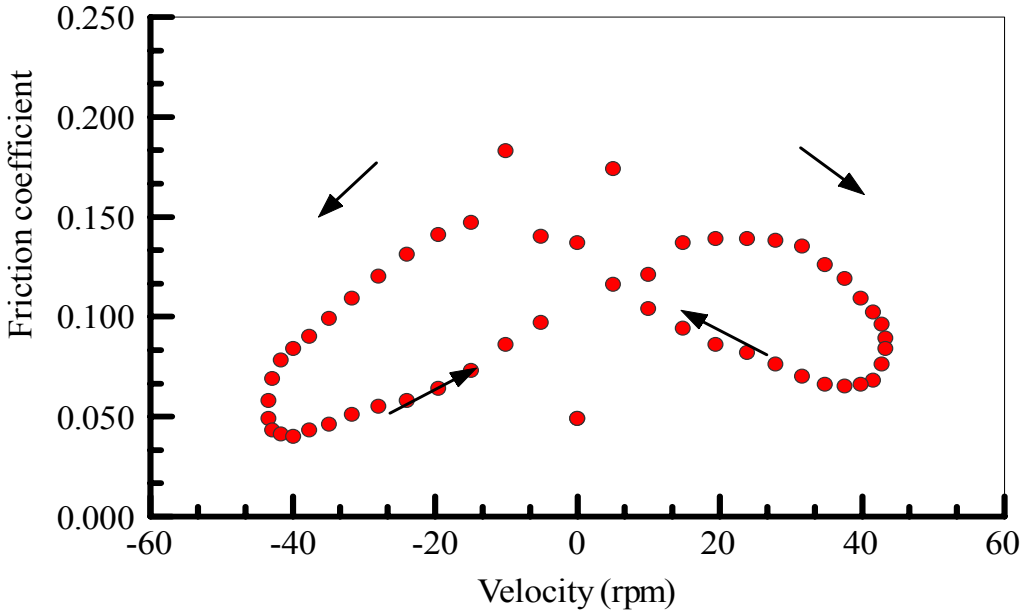

Figure 5.46 - the friction coefficient variation with the velocity history (445 N load, bronze bushing, 1.0 Hz oscillating frequency, SAE40 oil, 40^0C oil inlet temperature)

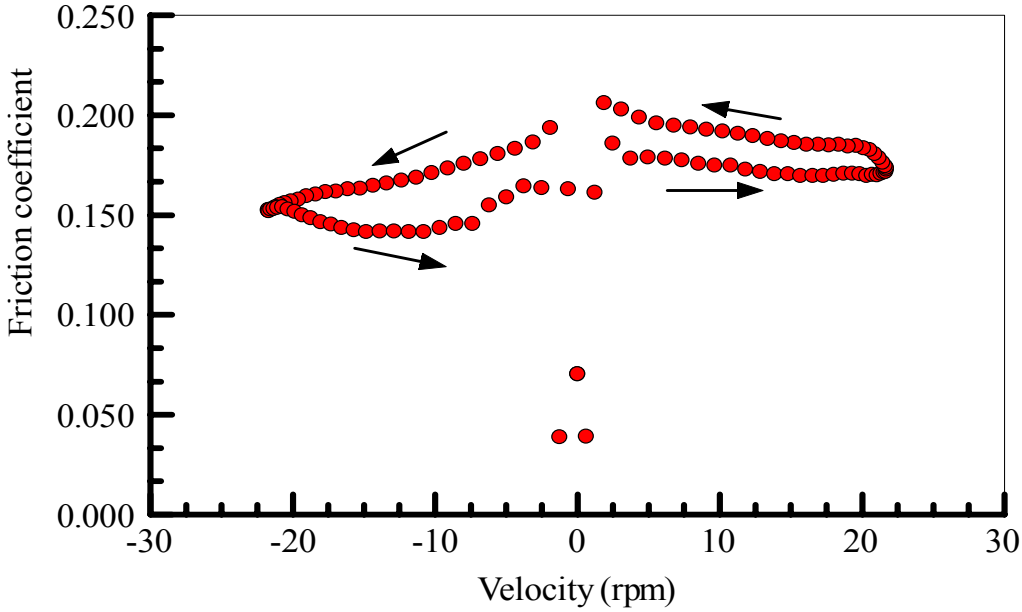

Figure 5.47 - the friction coefficient variation with the velocity history (445 N load, bronze bushing, 0.5 Hz oscillating frequency, SAE30 oil, 40^0C oil inlet temperature)

5.3. Conclusions

The friction hysteresis phenomenon of an oil lubricated oscillatory journal bearing is investigated by varying load, oil type, inlet oil temperature, oscillating frequency, and bushing type. The following conclusions can be drawn on the basis of the experimental results.

- Heavier load, faster oscillating speed, and higher oil inlet temperature lower the magnitude of the friction hysteresis loop. Heavier load narrows the bandwidth of the loop.

- In the cases of 667 N load, 0.5 Hz oscillating frequency, bronze bushing, SAE30 oil, the bandwidth of the hysteresis loop tends to zero. A flatter or narrower friction hysteresis loop requires less friction compensation in precision machine control.

- The friction hysteresis loop is narrower when the bearing clearance is bigger.

- With oil, the friction level is lower when the oscillating frequency increases. Without lubricant, the friction hysteresis still exists, while the friction level increases with increasing oscillating frequency.

- The inertia of the lubricant flow contributes to the friction hysteresis. The friction variation with the velocity history displays three types of lobed shapes of hysteresis.

5.4. Nomenclature

f	coefficient of friction
p	pressure, Pa
q	heat flux, W/m^2
r	bar length, m
v	linear velocity, rpm
θ	angle, radian
ω	angular velocity, rad/s

Subscripts

1, 2, 3, 4	bar number, oscillating stage

CHAPTER 6 AN EXPERIMENTAL STUDY OF GREASE-LUBRICATED JOURNAL BEARINGS UNDERGOING OSCILLATORY MOTION

6.1. Introduction

Journal bearings have broad range of applications in industry. Most of them are designed to rotate uni-directionally and operate with a relatively thick film of fluid that separates the journal and the bushing so that the hydrodynamic lubrication regime prevails. Nevertheless, in some applications such as robotic arms and construction machinery, the bearings oscillate periodically at a specified frequency and amplitude. Correspondingly, their lubrication state often traverses from boundary, to mixed, and to hydrodynamic regime.

Grease is widely used in journal bearings that are intended to function under relatively low speed and heavily loaded operating conditions. Grease offers some advantages over conventional oil in terms of leakage, maintenance, and stability. The dimensions of a grease bearing are smaller than that of an oil-lubricated bearing with the identical load capacity [76], and there is no need for an elaborate oil supply system. Moreover, experiments have shown that in boundary or mixed lubrication regime, the coefficient of friction with certain grease can be even lower than that of oil due to a deposited thickener layer [98].

Compared with oil lubrication, the mechanism of grease lubrication is much less understood [77, 78]. Furthermore, an extensive literature survey [171] reveals that experimental grease studies [73-75, 79-84] have primarily concentrated on constant rotational motion, and that there exists very limited data for bearings that undergo oscillation.

This paper is devoted to the examination of the friction performance of a grease-lubricated journal bearing under oscillatory motion. The effects of load, oscillating frequency, and grease type are examined. The variation of hysteresis loop is analyzed qualitatively.

6.2. Experimental

Lewis LRI-8H tribometer is used for measuring the coefficient of friction of journal bearings. Its detailed description is available in [57]. Briefly, the machine is capable of measuring the friction coefficient under varying operating conditions such as load and speed. Load is applied through a level mechanism. The friction force is registered by a measuring cell and data are continuously recorded into a computer via an automated data acquisition system. The coefficient of friction, the oscillating frequency, and the load are processed by software, displayed on computer screen, and recorded for future analysis.

The time interval of data reading is adjustable and is independent of the duration of the test. Two types of sampling frequencies are adopted. One is for recording the global history of the coefficient of friction. The other is for recording the local history of the coefficient of friction in one oscillation cycle. In the current study, a minimum of 20 seconds for the global history and a 0.0185 second for the local history are taken.

6.2.1 Bearing Parameters

The shaft is made up of hardened AISI 1020 steel. Its diameter is 24.54 mm. Steel bushing is used in tests. The inner diameter and the length are 25.4 mm.

Two different greases are chosen as the lubricant. One is Moly#5. The other is ALG#1.

The following table shows the combination of load and grease tested.

Table 6.1- Grease properties

	NLGI Grade	Thickener type	Dropping point (^{0}C)	Viscosity (cSt) @ 40 ^{0}C
Moly #5	1	Lithium complex	260	357
ALG #1	1	Calcium sulfonate	260	150

Table 6.2- Experiment cases

Bushing	Grease	Load (N)
Steel	Moly#5	445
		667
		890
	ALG#1	445
		667
		890

The error of the friction coefficient is based on the accuracy of the load cell. A 44 N load cell is used in experiments reported in this paper. For a given load cell, the amount of the friction force error is fixed. With increasing loads, the error of the friction coefficient becomes smaller. It is tabulated in Table 6.3.

Table 6.3- Error of the friction coefficient associated with load

Load (N)	445	667	890
Error (±)	0.0034	0.0023	0.0017

6.2.2 Experiment Procedure

Before any measurement is taken, the system is balanced so that the coefficient of friction is nil when the shaft is in its static position. The system is run-in for one hour with 1.0 Hz oscillating frequency and 450 N load. Upon completion of each test, the system is given enough time—typically 2 hours— to cool down. For each test, the global history of the coefficient of friction is monitored. The friction coefficient tends to oscillate periodically around a relatively constant value. By observation, this state is normally reached in 4 minutes. The total measuring time for each test is 8 minutes.

Starting from the moment of 4 minutes, the local history loop of the coefficient of friction in one oscillation cycle is extracted for comparison.

6.2.3 Development of Oscillatory Motion

The oscillatory motion of the shaft is generated by a four-bar linkage device. Its schematic is like Fig. 6.1.

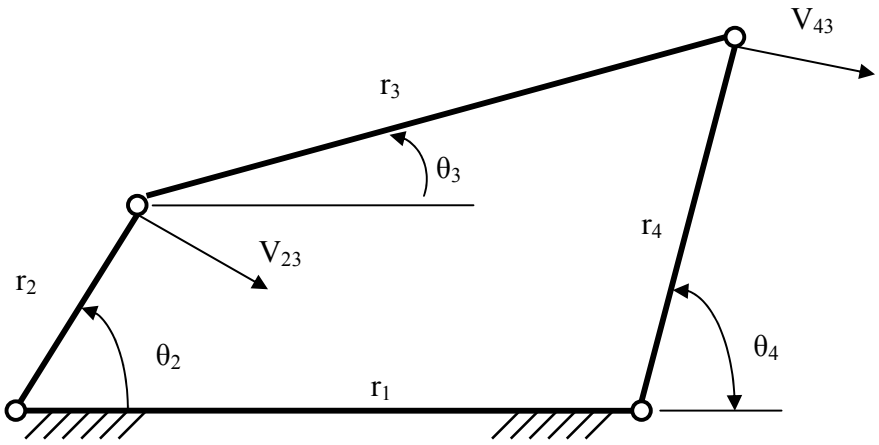

Figure 6.1 - A four-bar linkage device

The active bar (rotational) is bar 2 (r_2) and the passive one (oscillatory) is bar 4 (r_4). The angular velocity of the shaft is the same as that of bar 4. The objective is to establish an appropriate expression for the angular velocity of bar 4 as a function of time $\omega_4(t)$ for a specified oscillating frequency.

By the geometric dimension, the following equations can be established.

$$r_1 + r_4\cos\theta_4(t) - r_2\cos\theta_2(t) - r_3\cos\theta_3(t) = 0 \qquad (6.1)$$

$$r_4\sin\theta_4(t) - r_2\sin\theta_2(t) - r_3\sin\theta_3(t) = 0 \qquad (6.2)$$

where $\theta_2(t)$ is the corresponding oscillating angle. Combining Eqs. (6.1) and (6.2), $\theta_3(t)$ and $\theta_4(t)$ can be solved numerically.

The projections of linear velocity v_{23} and v_{43} on the horizontal line are the same. It reads

$$r_2\omega_2(t)\cos\left(\frac{\pi}{2}-\theta_2(t)+\theta_3(t)\right)=r_4\omega_4(t)\cos\left(\frac{\pi}{2}-\theta_4(t)+\theta_3(t)\right) \qquad (6.3)$$

Therefore,

$$\omega_4(t)=\frac{r_2\omega_2(t)\cos\left(\frac{\pi}{2}-\theta_2(t)+\theta_3(t)\right)}{r_4\cos\left(\frac{\pi}{2}-\theta_4(t)+\theta_3(t)\right)} \qquad (6.4)$$

The corresponding linear velocity (rpm) is

$$v_4(t)=\omega_4(t)\times\frac{60}{2\pi} \qquad (6.5)$$

In the current study, an oscillation angle of $\pm 45^0$ is set up with parameters in Table 6.4.

Table 6.4- Bar parameters

r_1 (mm)	r_2 (mm)	r_3 (mm)	r_4 (mm)
637	55.22	633	77.8

Oscillating frequencies of 0.5, 1.0, and 1.5 Hz are put into tests respectively. The resulting $\omega_4(t)$ is showed by Fig. 6.2.

6.2.4 Results and Discussion

The repeatability of the coefficient of friction in several oscillation cycles is demonstrated in Fig. 6.3. The discrepancy between cycles is small. Hence, it is reasonable to sample one cycle for comparison.

In what follows, the coefficient of friction is plotted against the shaft velocity (rpm). The result reveals the existence of a friction hysteresis loop, where it becomes negative

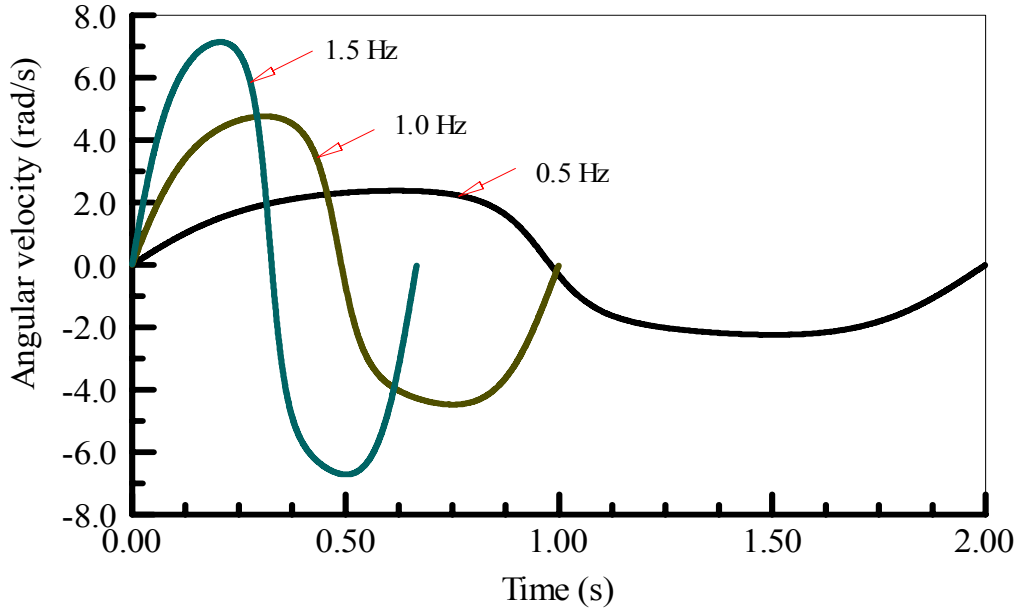

Figure 6.2 - the angular velocity of the shaft with different oscillating frequencies

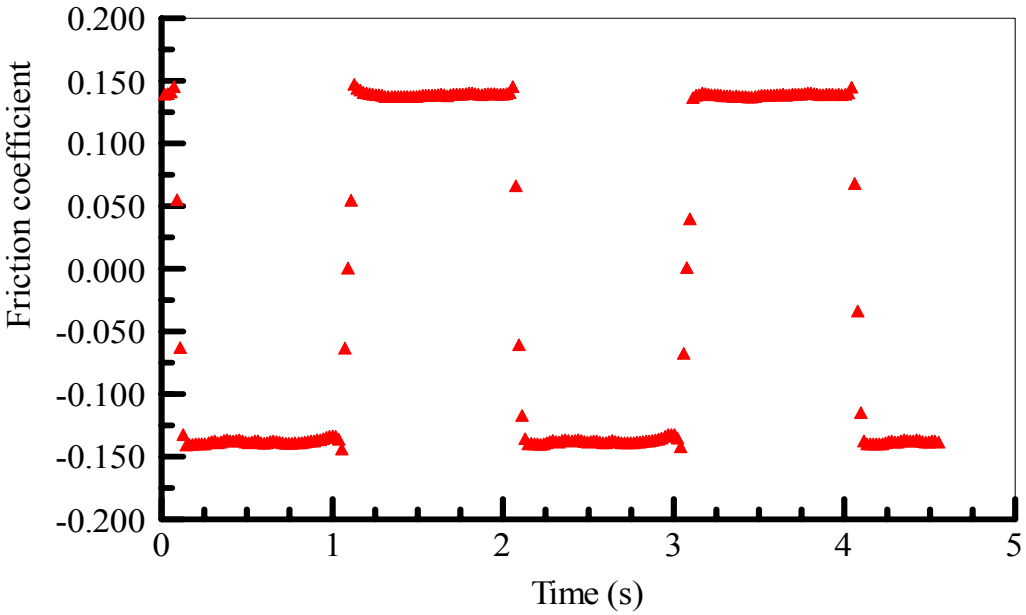

Figure 6.3 - local history of the coefficient of friction, 667 N load, 1.0 Hz oscillating frequency, Moly#5 grease

when the velocity is reversed. During the velocity reversal as the shaft traverses in the vicinity of zero velocity, the coefficient of friction experiences a steep change. It is

instantaneous friction value for the boundary lubrication regime when the speed is close to nil.

6.2.4.1 Load Effect

Figs. 6.4-6.9 show the variation of the local history of the friction coefficient with different loads for 0.5 Hz, 1.0 Hz, and 1.5 Hz frequencies, respectively.

Examination of the velocity input (Fig. 6.2) indicates that the velocity profile is not perfectly symmetric, a characteristic of the four bar linkage that produces the necessary oscillation in the test rig. Consequently, the hysteresis loop exhibits a slight asymmetric behavior.

An important concept in grease lubrication is the replenishment mechanism [172]. The lubricant film is maintained by the replenishment mechanism which establishes a balance between the lubricant loss from and supplied to the contact track under the

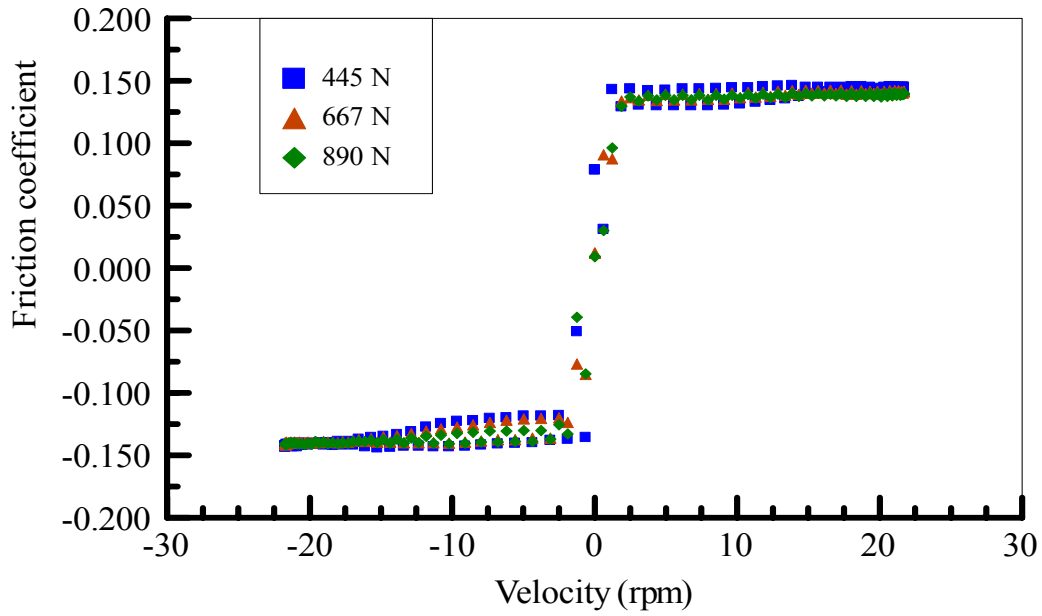

Figure 6.4 - Friction coefficient versus velocity (0.5 Hz oscillating frequency, ALG#1 grease)

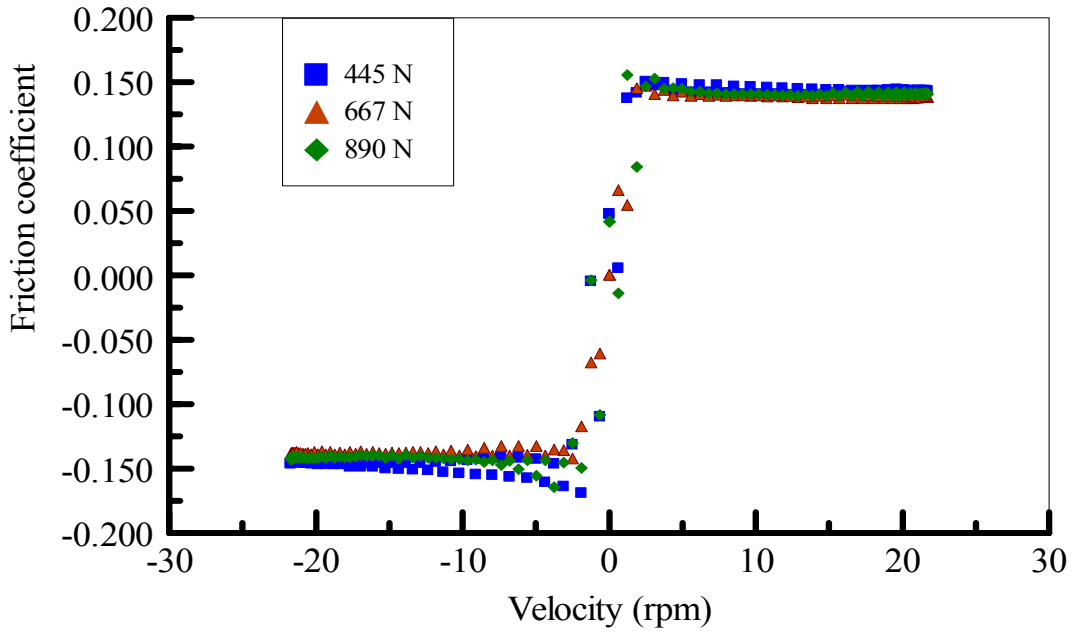

Figure 6.5 - Friction coefficient versus velocity (0.5 Hz oscillating frequency, Moly#5 grease)

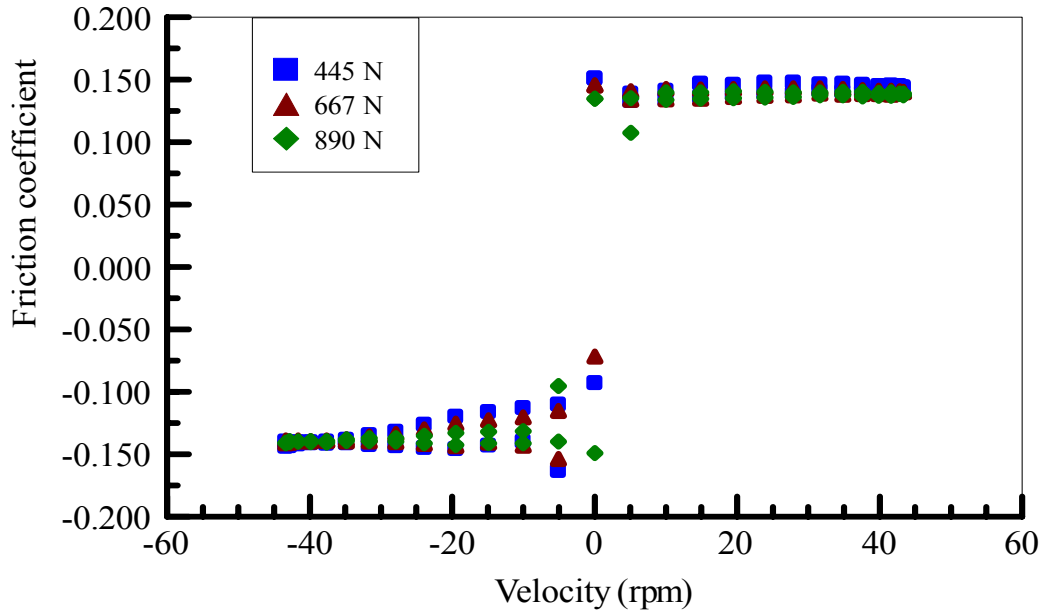

Figure 6.6 - Friction coefficient versus velocity (1.0 Hz oscillating frequency, ALG#1 grease)

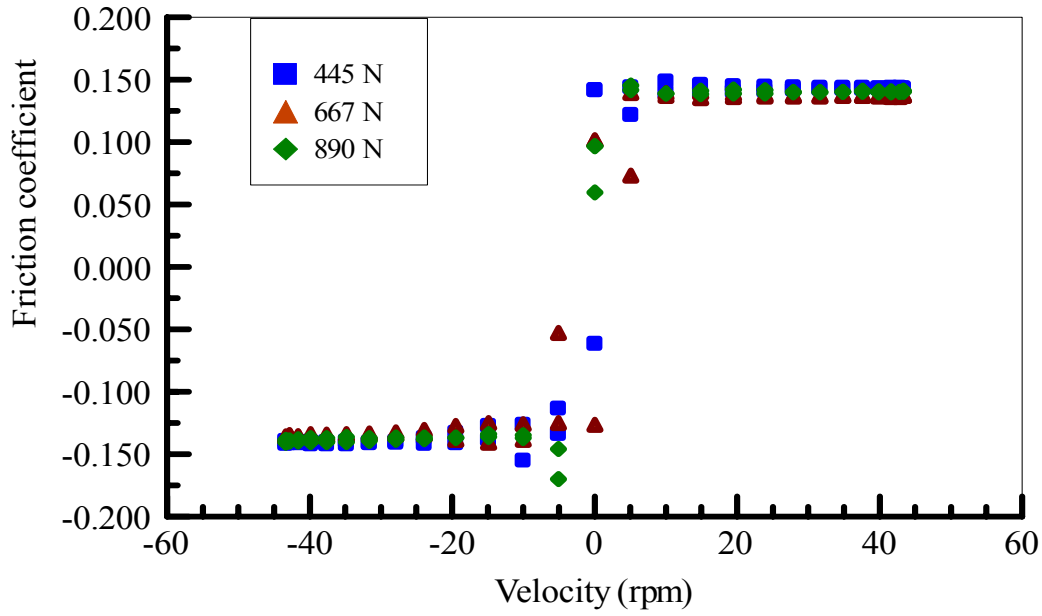

Figure 6.7 - Friction coefficient versus velocity (1.0 Hz oscillating frequency, Moly#5 grease)

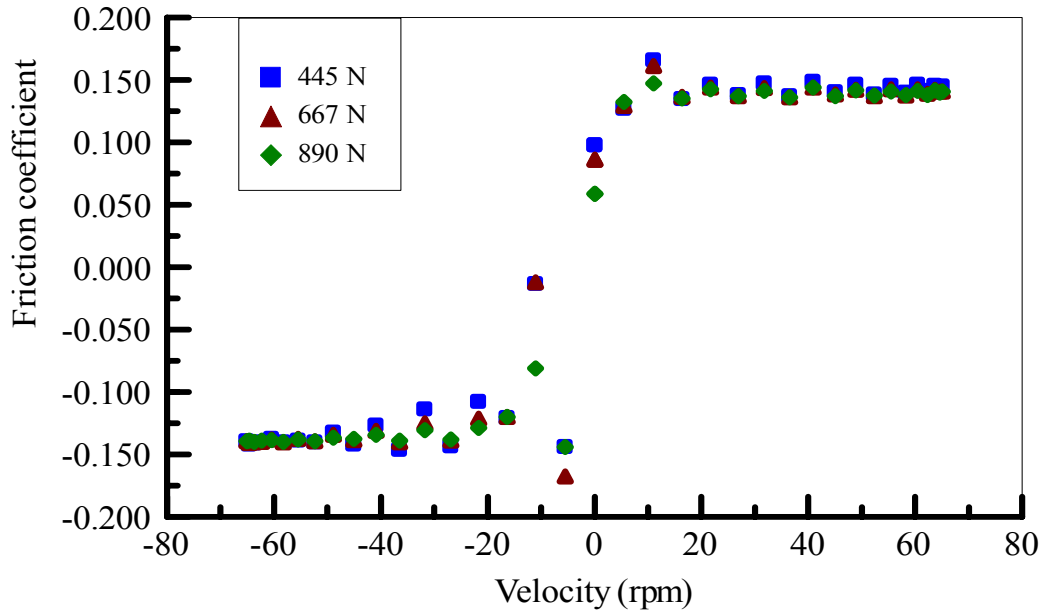

Figure 6.8 - Friction coefficient versus velocity (1.5 Hz oscillating frequency, ALG#1 grease)

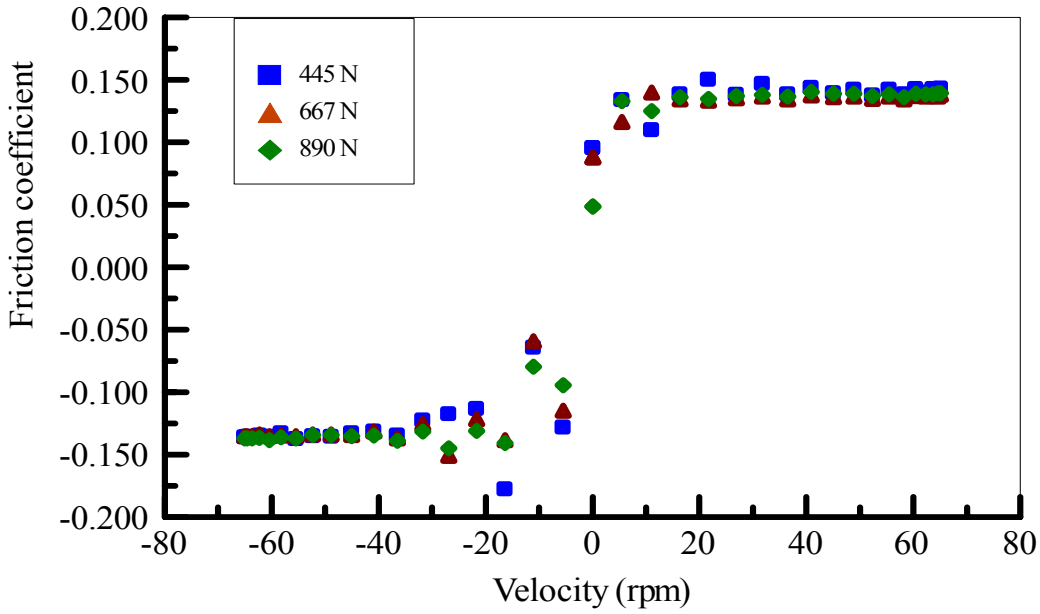

Figure 6.9 - Friction coefficient versus velocity (1.5 Hz oscillating frequency, Moly#5 grease)

driving force of gravitation, mechanically induced flow, and surface tension [21, 66, 67, 69, 71, 173, 174]. In typical journal bearings that operate under a constant, uni-directional motion, once the bulk grease is "overrolled," there is no replenishment of bulk grease into the contact track [71]. When dealing with the oscillatory motion, the grease reservoir outside the contact region replenishes grease to the contact region when the shaft changes rotational direction. As a result, the lubricant film remains fairly uniform during the oscillation. Hence, as the experimental results indicate (See §6.2.4.2), even though the bearing undergoes a transition from boundary to mixed lubrication regimes, the friction curve remains very smooth over a wide range of speeds.

The load and the oscillating frequency are two critical factors in determining the hysteresis loop "bandwidth," which represents the extent of the friction hysteresis. The results shown in Figs. 6.4-6.9 reveal that the bandwidth of the hysteresis loop is

"squeezed" when the load is greater. In general, occurrence of hysteresis is representative of a retardation of the friction coefficient. When the load on the shaft is greater, the interaction of shaft and grease becomes stronger, and the retardation effect of the friction coefficient with the shaft velocity variation becomes less pronounced. As a result, the friction hysteresis loop becomes narrower.

A flatter or narrower bandwidth implies that the friction difference between increasing velocity and decreasing velocity is smaller. In precision control industry, such as in robotic applications, the control engineer requires a suitable friction model to compensate the effects of friction [162-168, 175-177]. A flatter friction curve offers a more stable performance, and less complication in terms of modeling for control purposes.

The area under the friction-velocity curve represents the total frictional heat flux, $\sum q$, in that period. The velocity in one oscillation cycle can be divided into four stages: positive acceleration, positive deceleration, negative acceleration and negative deceleration (referring to Fig. 6.2). In one stage, the total frictional heat flux can be expressed as

$$\sum q = \int_v f(v) p dv \tag{6.6}$$

Assuming that the pressure p is constant, Eq. (6.6) simplifies into

$$\sum q = p \int_v f(v) dv \tag{6.7}$$

Let $\sum q_1$ represent the area under the friction curve with an increasing velocity and $\sum q_2$ denote the area under the friction curve with a decreasing velocity. Then, the area within the hysteresis loop can be formulated as

$$\Delta\left(\sum q\right) = \sum q_1 - \sum q_2 = p\int_v f_1(v)dv - p\int_v f_2(v)dv = p\int_v \left(f_1(v) - f_2(v)\right)dv \qquad (6.8)$$

The term $\Delta\left(\sum q\right)$ can be used to characterize the bandwidth of the hysteresis loop. When $\Delta\left(\sum q\right)$ is bigger, the bandwidth is bigger; when $\Delta\left(\sum q\right)$ is smaller, the bandwidth is smaller.

6.2.4.2 Oscillating Frequency Effect

The local history of the coefficient of friction varying with oscillating frequency is shown in Figs. 6.10-6.15. The results show that the hysteresis loop is "stretched" when the oscillating frequency is increased. When the oscillating frequency is large, the maximum velocity becomes higher. At 1.5 Hz oscillating frequency, a maximum speed of 68 rpm (7.1 rad/s) is reached. The speed at which lift-off occurs corresponds to the lowest friction coefficient when plotted against the unidirectional speed, i.e. the so-called Stribeck curve [57]. This point is the watershed between mixed and hydrodynamic lubrication. From the experiment results under constant rotation (Figs. 6.16 and 6.17), the smallest lift-off speed is about 85 rpm (8.9 rad/s). Hence, it may be concluded that under these operating conditions, the oscillatory bearing operates in boundary and mixed lubrication regimes. With increasing speed, the friction becomes lower.

The experimental results also indicate that for a given load, the hysteresis loops have a similar shape for three different oscillating frequencies. Therefore, the load has a greater effect on the shape of the hysteresis loop compared to that of the oscillating frequency.

Figs. 6.18-6.20 compare the hysteresis loop of ALG#1 and Moly#5 greases under an imposed load of 445 N. The results reveal that the retardation effect of the friction coefficient is less distinct with Moly#5 grease. This can be attributed to the reduction of

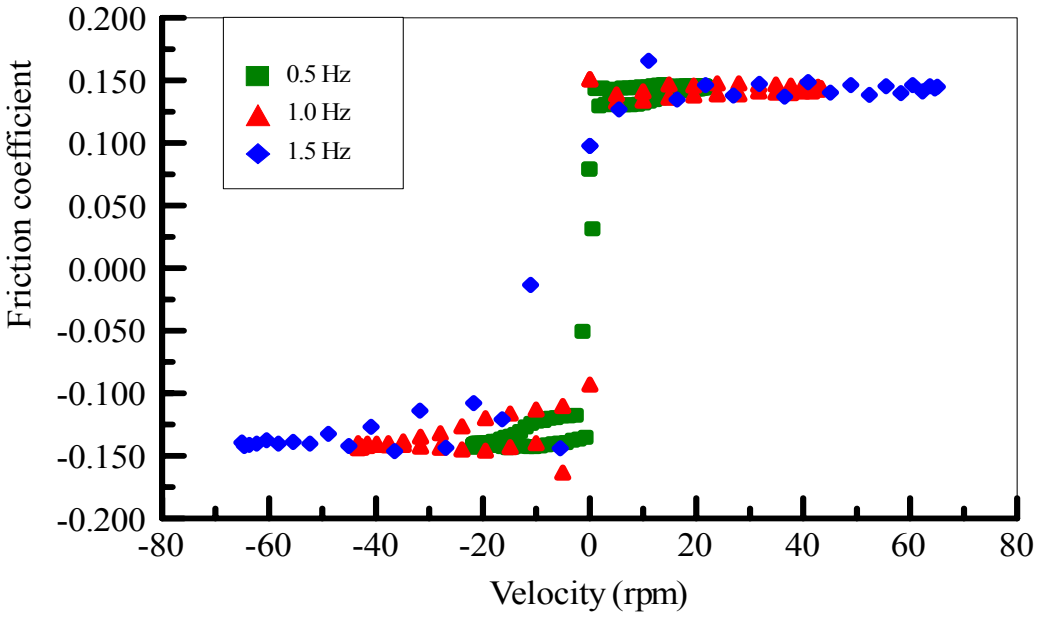

Figure 6.10 - Friction coefficient versus velocity (445 N load, ALG#1 grease)

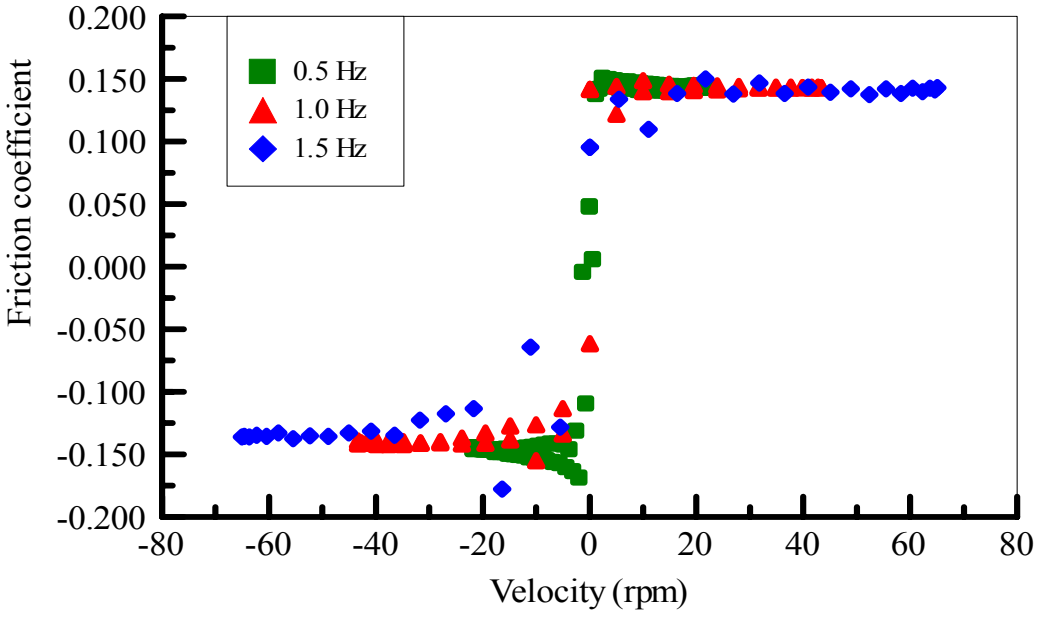

Figure 6.11 - Friction coefficient versus velocity (445 N load, Moly#5 grease)

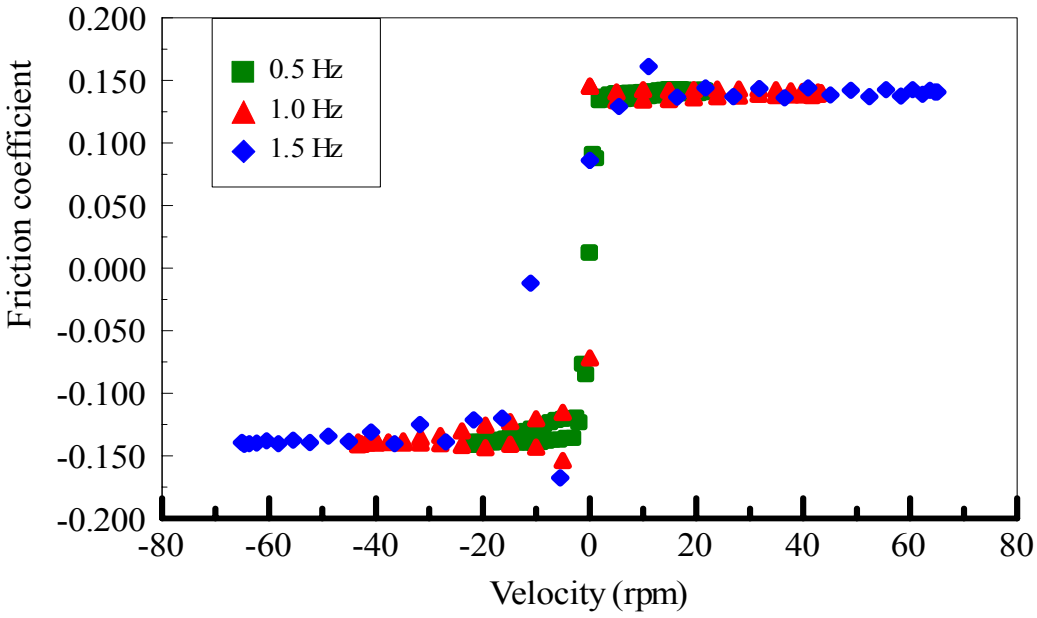

Figure 6.12 - Friction coefficient versus velocity (667 N load, ALG#1 grease)

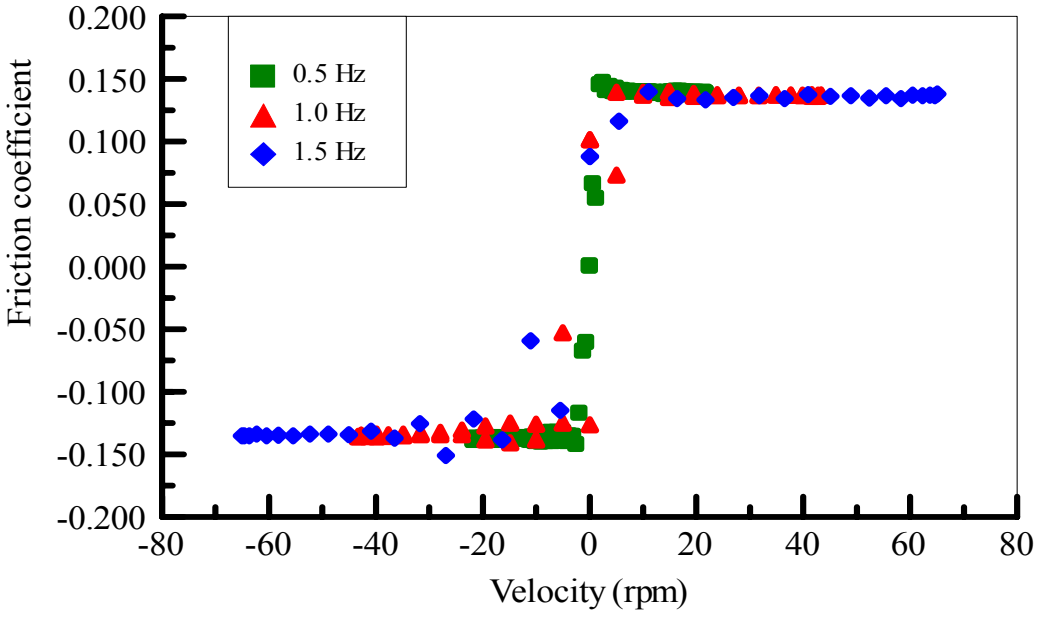

Figure 6.13 - Friction coefficient versus velocity (667 N load, Moly#5 grease)

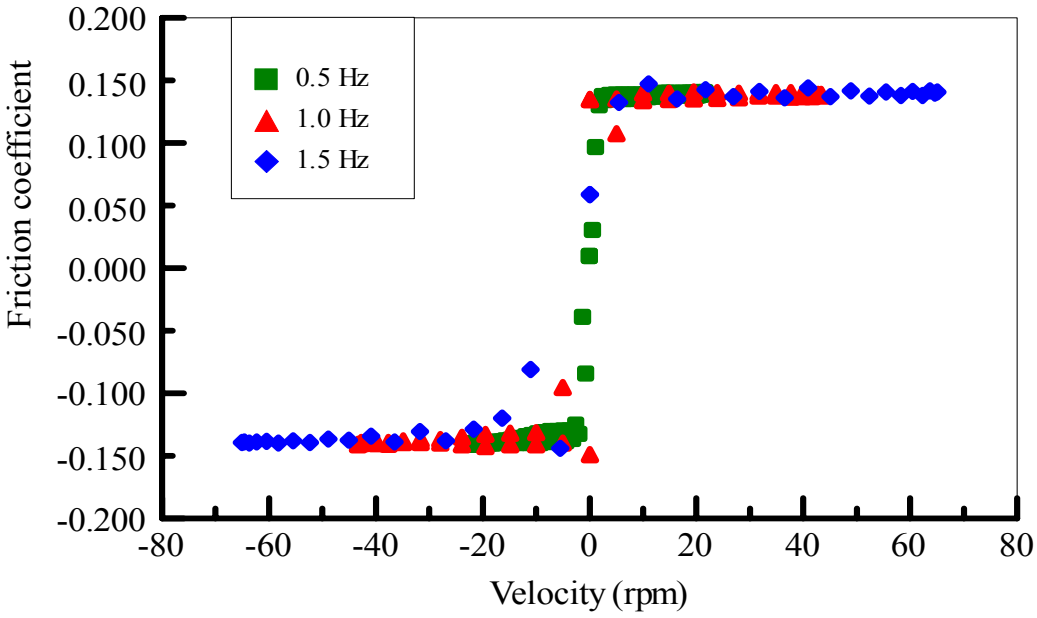

Figure 6.14 - Friction coefficient versus velocity (890 N load, ALG#1 grease)

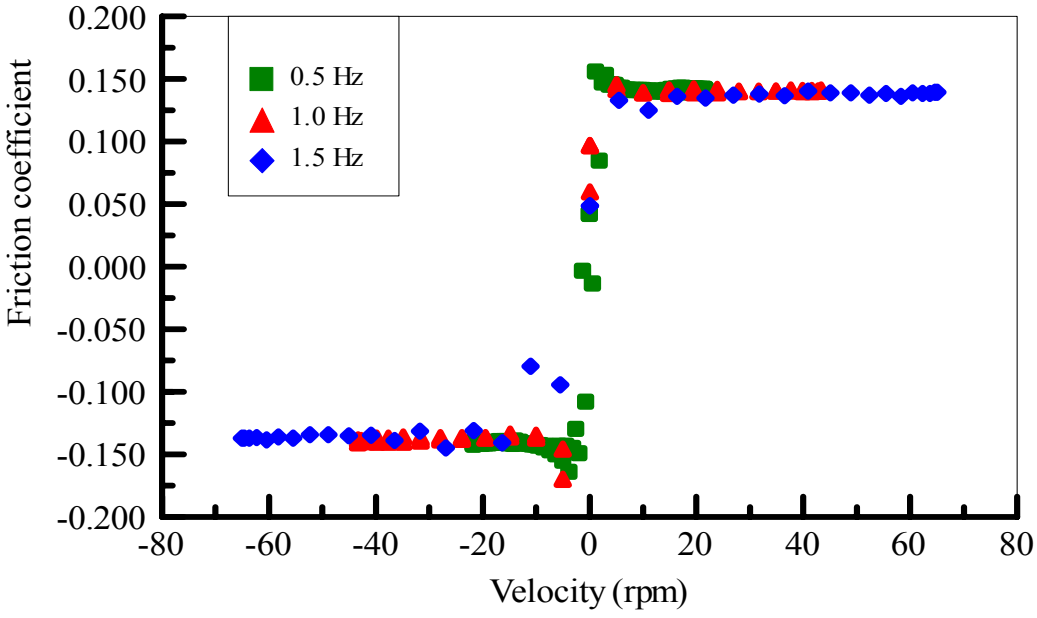

Figure 6.15 - Friction coefficient versus velocity (890 N load, Moly#5 grease)

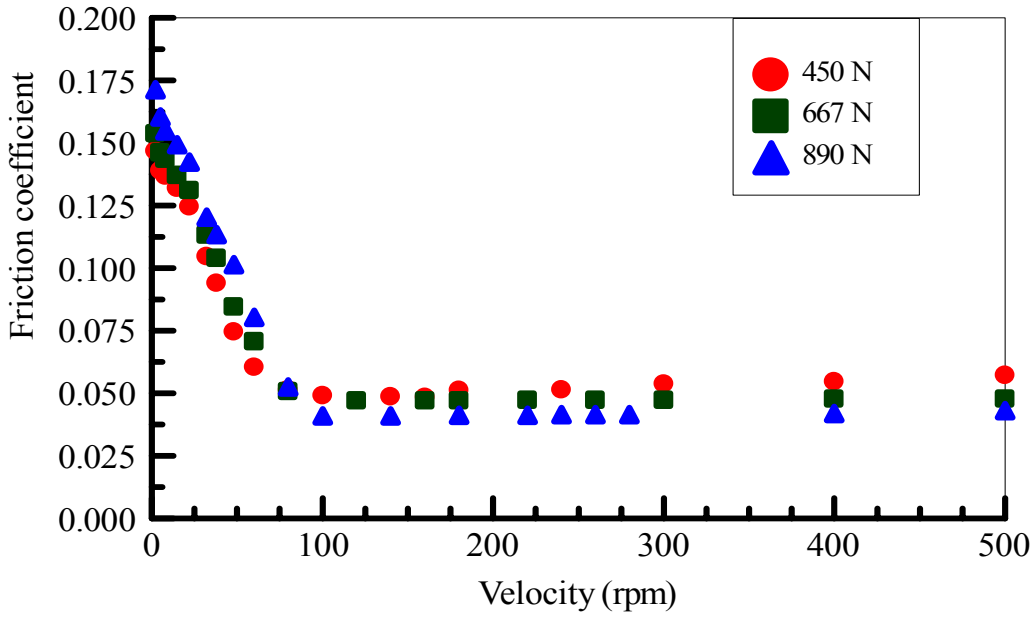

Figure 6.16 - The friction coefficient as a function of velocity (ALG#1 grease, constant rotation)

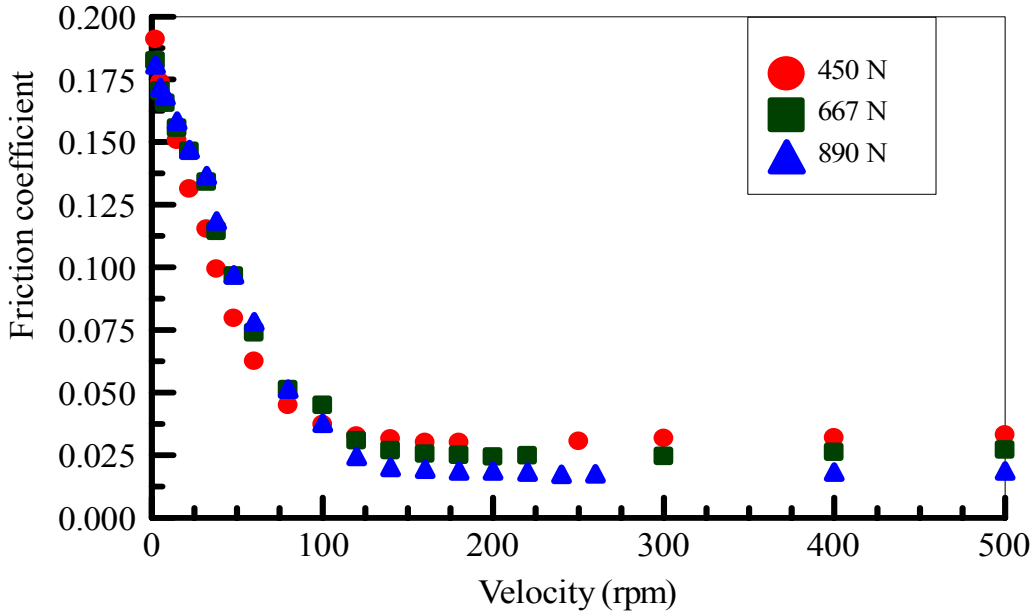

Figure 6.17 - The friction coefficient as a function of velocity (Moly #5 grease, constant rotation)

6.2.4.3 Lubricant Effect

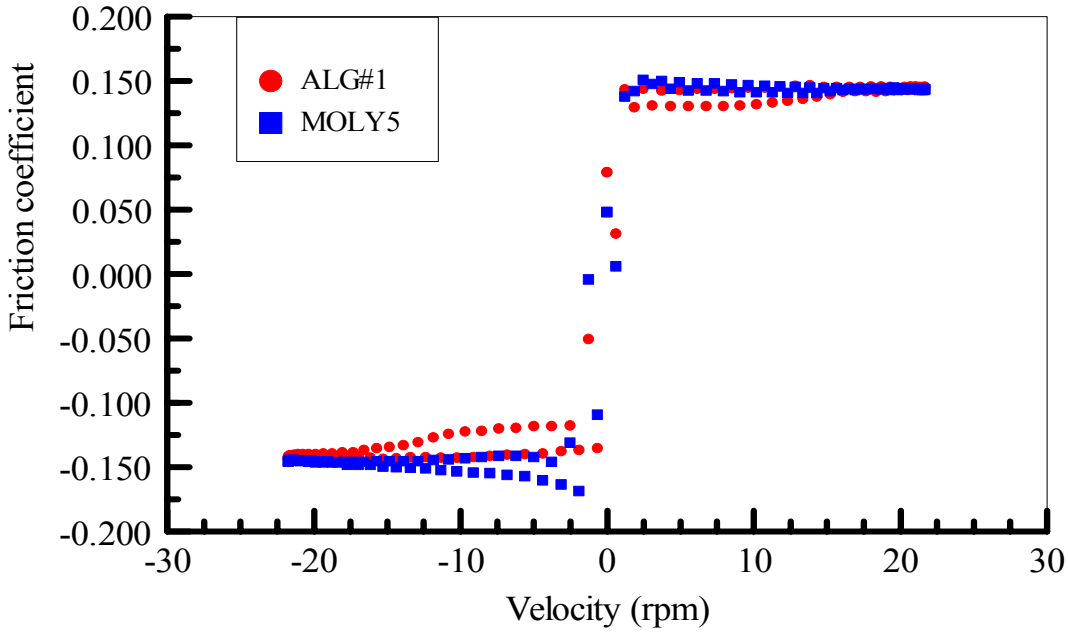

Figure 6.18 - Friction coefficient versus velocity (445 N load, 0.5 Hz oscillating frequency)

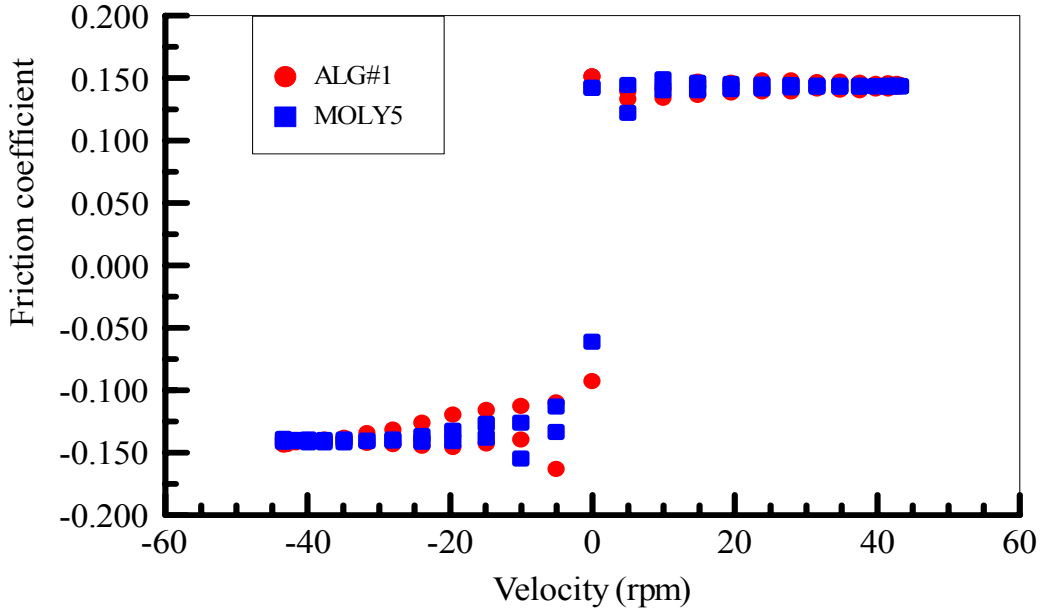

Figure 6.19 - Friction coefficient versus velocity (445 N load, 1.0 Hz oscillating frequency)

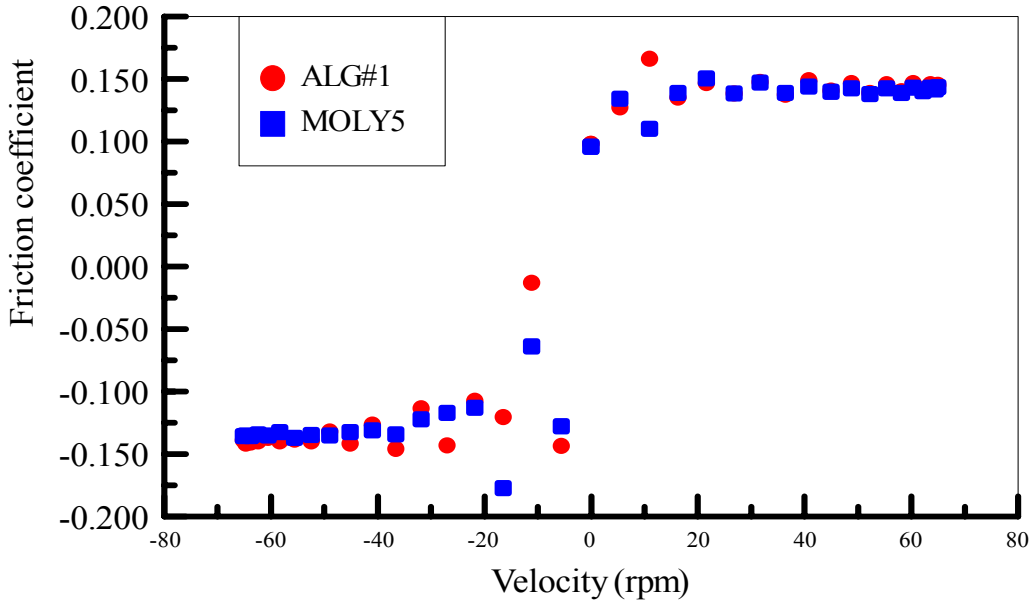

Figure 6.20 - Friction coefficient versus velocity (445 N load, 1.5 Hz oscillating frequency)

the bandwidth of the hysteresis loop with heavier lubricant. From Table 6.3, the base oil viscosity of Moly#5 grease (357 cSt) is much greater than that of ALG#1 grease (150 cSt). A greater viscosity means less "flowability." Therefore, the velocity of Moly#5 grease is more easily changed when the shaft speed varies.

6.2.4.4 Comparison with Oil Lubrication

Figs. 6.21-6.23 compare the friction performance of grease and oil lubricated journal bearings. SAE 40 oil is chosen for comparison, for it has the same viscosity (150 cSt) as the base oil of ALG#1 grease at 40^0 C inlet temperature. The applied load is 445 N. As stated earlier, the bearing operates in boundary and mixed lubrication regimes. At low speeds the thickener of grease enters the contact and deposits a film which reduces asperity interaction [98], a characteristic that oil lacks. The friction with grease is lower than that with oil. In boundary and mixed lubrication regimes, ALG#1 grease produces better friction performance than SAE40 oil.

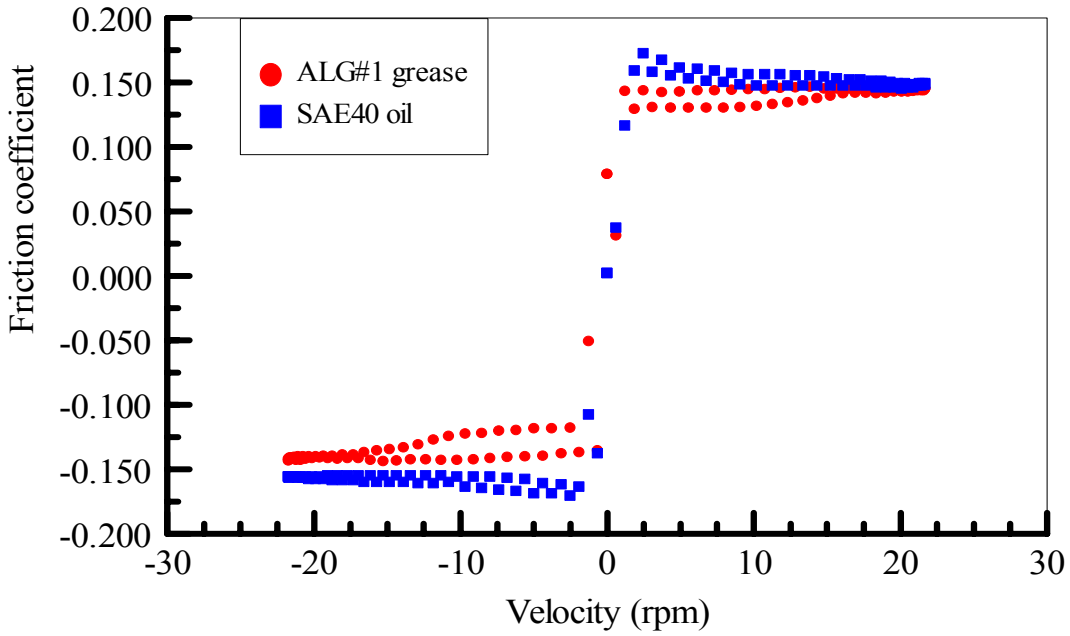

Figure 6.21 - Comparison of the friction of ALG#1 grease and SAE40 oil (445 N load, 0.5 Hz oscillating frequency)

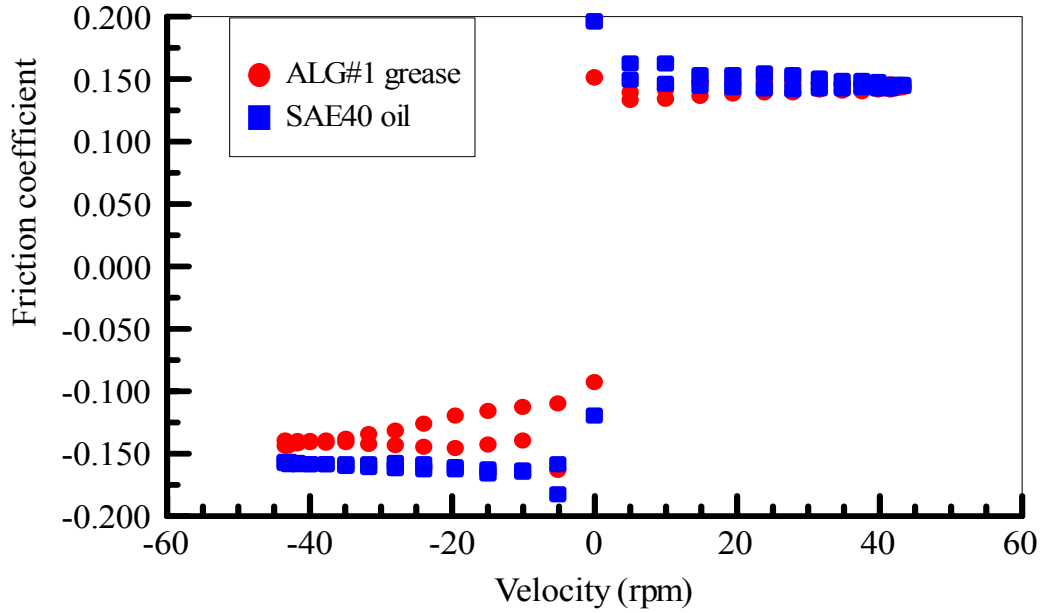

Figure 6.22 - Comparison of the friction of ALG#1 grease and SAE40 oil (445 N load, 1.0 Hz oscillating frequency)

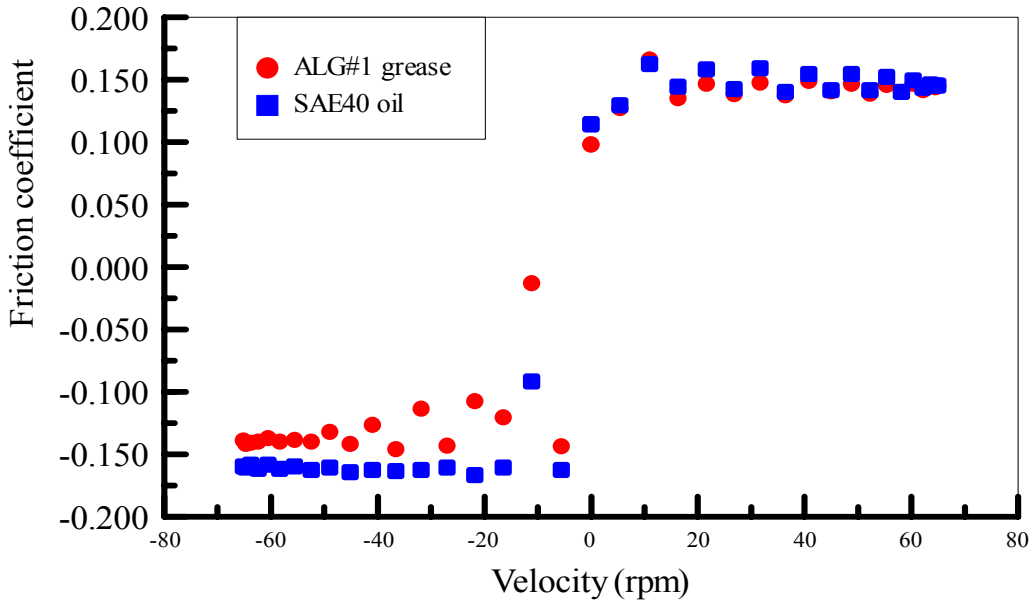

Figure 6.23 - Comparison of the friction of ALG#1 grease and SAE40 oil (445 N load, 1.5 Hz oscillating frequency)

6.2.4.5 Comparison of Oscillatory and Uni-directional Rotation

Figs. 6.24-6.29 compare the friction performance of grease-lubricated journal bearings under oscillatory motion and uni-directional rotational motion. Akin to oil-lubricated bearings, the grease-lubricated rotational bearing exhibits the Stribeck-type phenomenon in boundary and mixed lubrication regimes, which means the friction coefficient drops with increasing velocity. However, the grease-lubricated oscillatory bearing presents relatively stable friction output in the same regimes. For boundary and mixed lubrication regimes, the friction drop implies a bigger separation of friction surfaces. For uni-directional rotation, increasing velocity results in a greater film thickness, and improves the surfaces separation. In bearing that undergoes oscillatory motion, as discussed in §6.2.4.1, the lubricant film remains fairly uniform during the oscillation due to the replenishment of bulk grease, resulting in a more stable friction output. Therefore, when the oscillating frequency is low (0.5 Hz), the friction coefficient

under oscillatory motion is smaller than that under uni-directional motion at the same speed point (See Figs. 6.28-6.29).

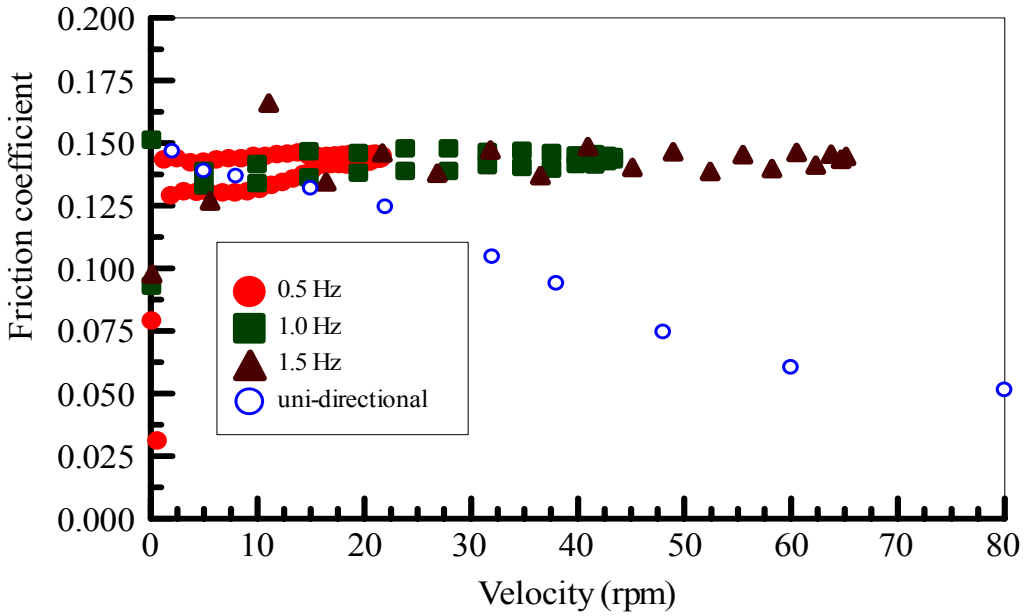

Figure 6.24 - Comparison of the friction of oscillatory and uni-directional rotation (ALG#1 grease, 445 N load)

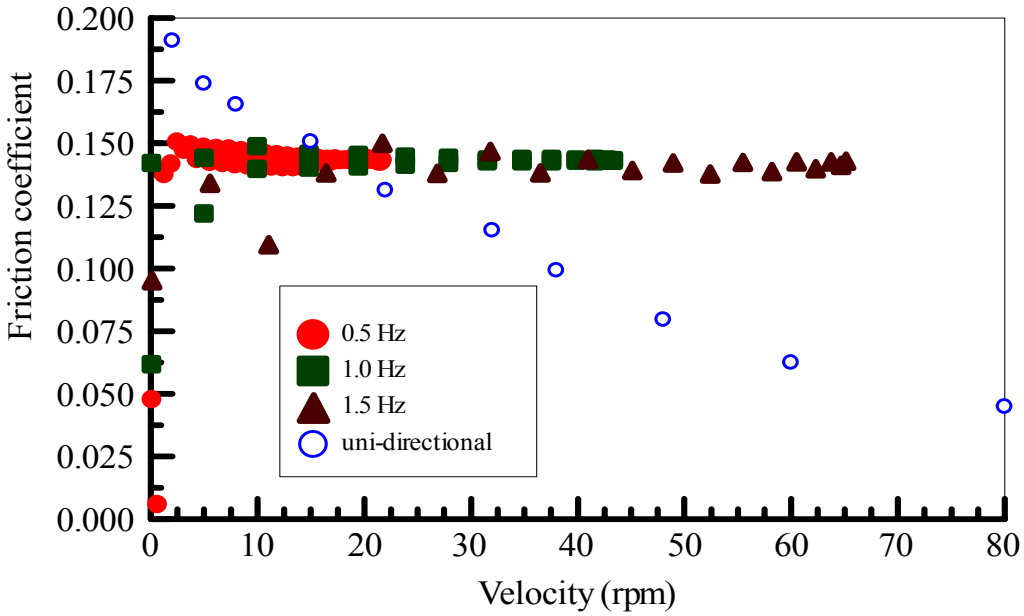

Figure 6.25 - Comparison of the friction of oscillatory and uni-directional rotation (Moly#5 grease, 445 N load)

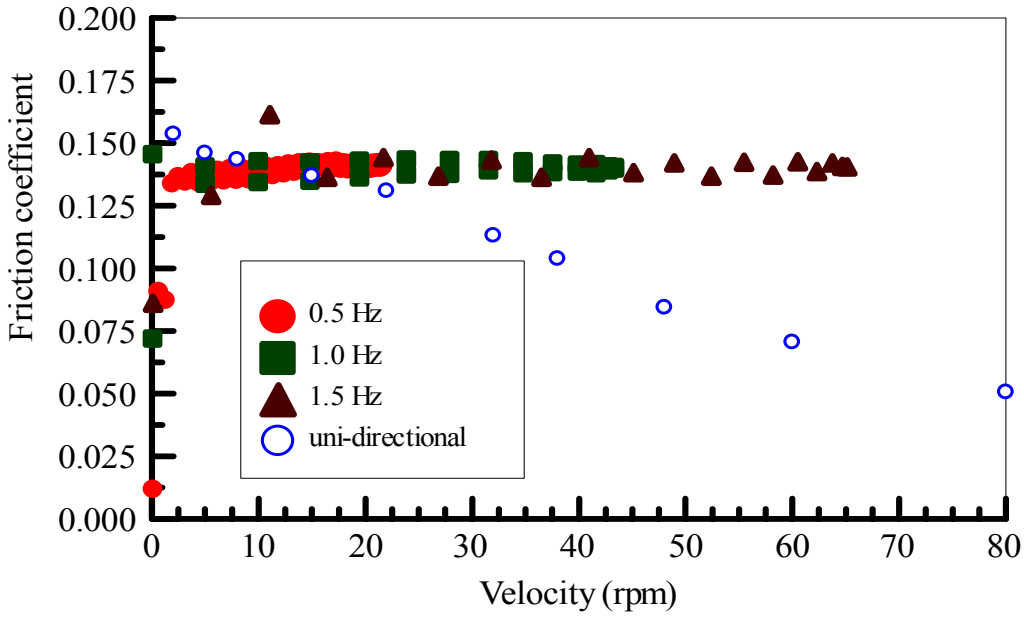

Figure 6.26 - Comparison of the friction of oscillatory and uni-directional rotation (ALG#1 grease, 667 N load)

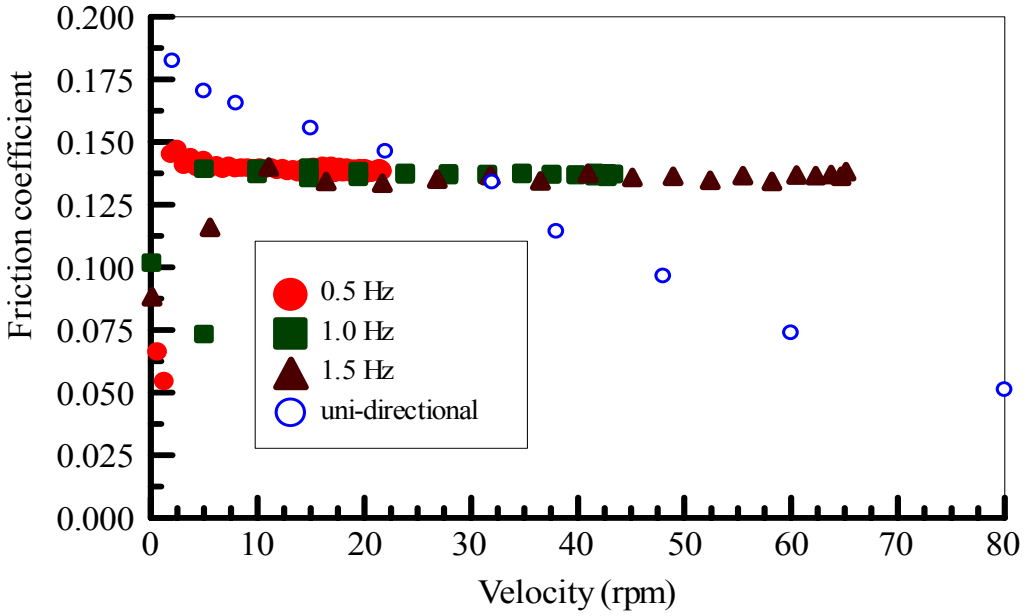

Figure 6.27 - Comparison of the friction of oscillatory and uni-directional rotation (Moly#5 grease, 667 N load)

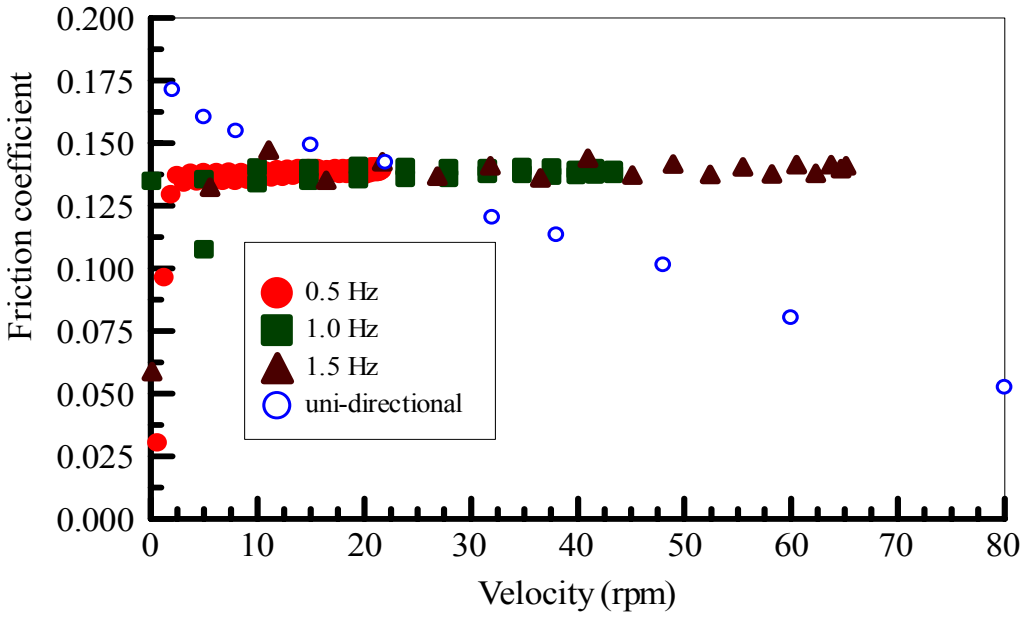

Figure 6.28 - Comparison of the friction of oscillatory and uni-directional rotation (ALG#1 grease, 890 N load)

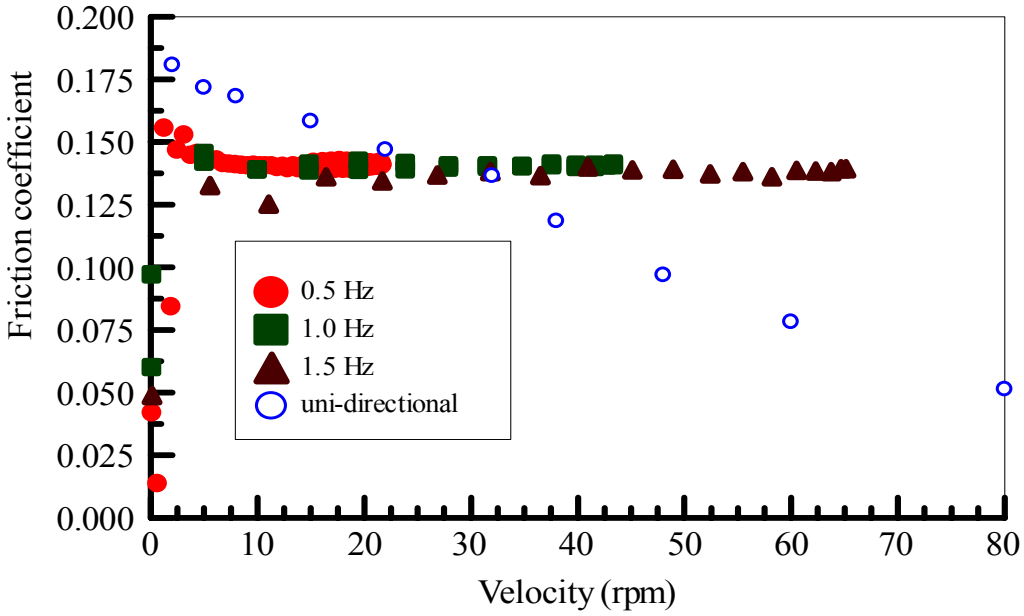

Figure 6.29 - Comparison of the friction of oscillatory and uni-directional rotation (Moly#5 grease, 890 N load)

6.2.4.6 Exploration of the Friction Hysteresis Phenomenon

6.2.4.6.1 Comparison of Dry and Lubricated Tests

In mixed lubrication regime, both asperity interaction and hydrodynamic pressure support the applied load. To examine the role of asperity interaction in the friction hysteresis, the bearing was tested without lubricant. A steel bushing was used in these experiments and the applied load was 445 N. There was no visible debris after each test.

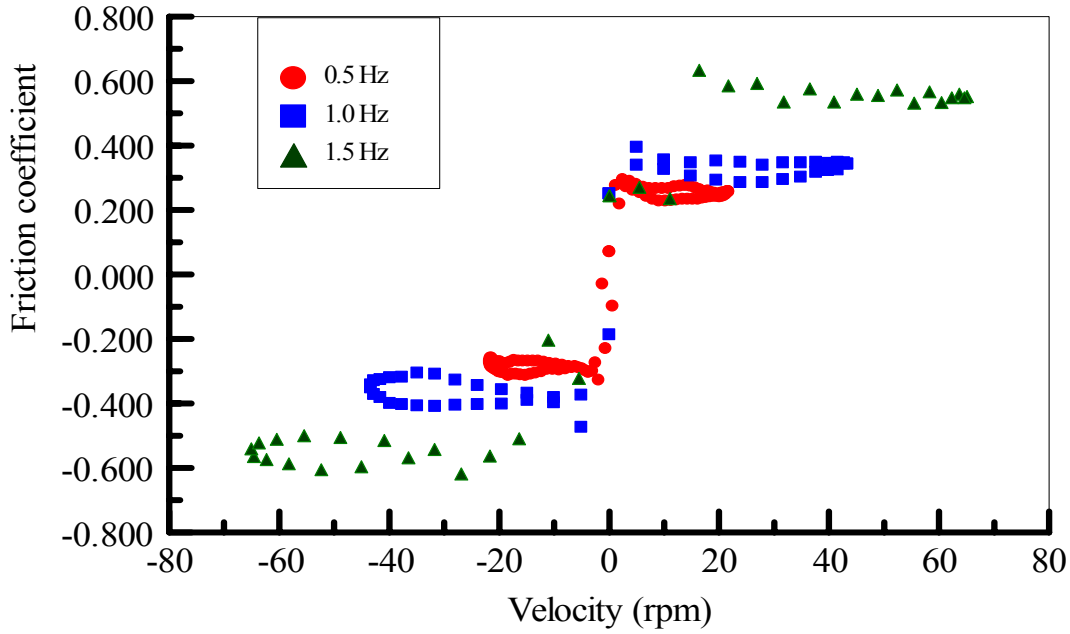

Figure 6.30 - Friction coefficient versus velocity (445 N load, dry)

In dry tests, the friction hysteresis phenomenon still exists. Plastic deformation, material damping, and viscous dissipation, etc. [170], all contribute to the friction hysteresis. However, the use of lubricant has a pronounced influence on both the friction level and the friction hysteresis loop. Without lubricant (Fig. 6.30), the friction level rises with increasing oscillating frequency; with lubricant (Figs. 6.10-6.11), the friction level drops with increasing oscillating frequency.

6.2.4.6.2 Function of grease

To explore the hysteresis characteristic associated with grease, the lubricant flow at the scale of asperities is analyzed. The velocity history in one oscillation cycle is divided into four stages: positive acceleration, positive deceleration, negative acceleration and negative deceleration. This is illustrated in Fig. 6.31, where for clarity the shaft is shown completely separated from the bushing. Despite of boundary or mixed lubrication status, the shaft is completely separated from the bushing for clear demonstration.

The effect of grease on the friction hysteresis is represented by the variation of the lubricant flow. Referring to Fig. 6.31, in stage (a), the shaft accelerates to the highest speed. It brings the volumetric flow forward (Fig. 6.32a). In stage (b), the shaft decelerates to zero speed. Once the slowdown process is triggered, the surface asperities of shaft and bushing will act as barriers for the flow and tend to lower the flow rate and in some regions create backflow (Fig. 6.32b). Due to inertia, the flow will not be the same as that in stage (a) at the same shaft speed. Hence, the hysteresis feature occurs. As for the other half oscillating cycle - stage (c) and (d), a similar process is followed.

6.3. Conclusions

The friction performance of grease-lubricated oscillatory journal bearing is examined by varying load, oscillating frequency and grease type. The following conclusions can be drawn based on results of the experiments.

- The area within the friction hysteresis loop tends to be squeezed by higher load.
- A flatter or narrower friction hysteresis loop requires less friction compensation in precision machine control.
- The friction hysteresis is stretched by higher oscillating frequency.

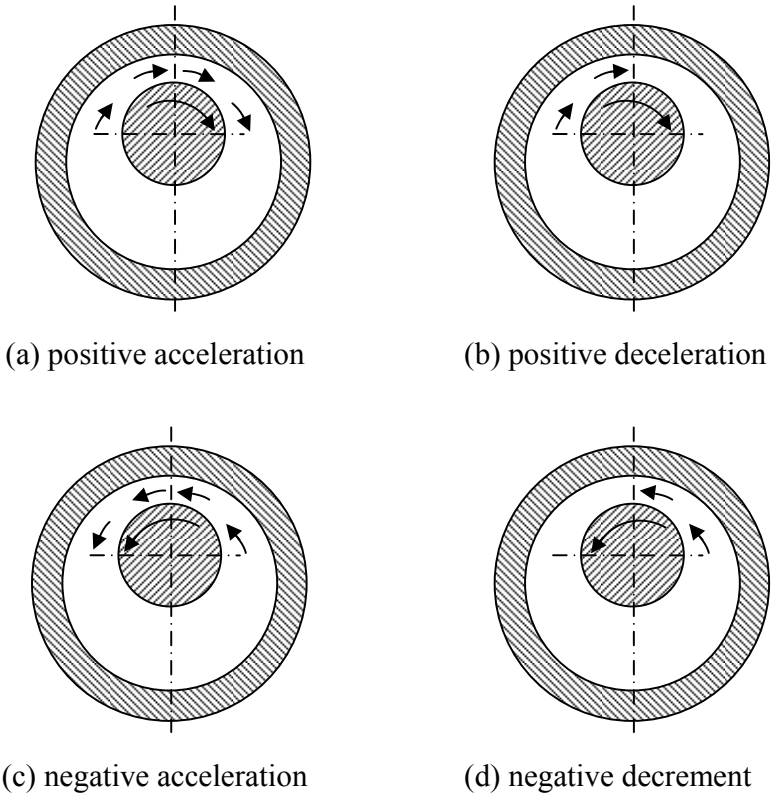

Figure 6.31 - Oscillating process

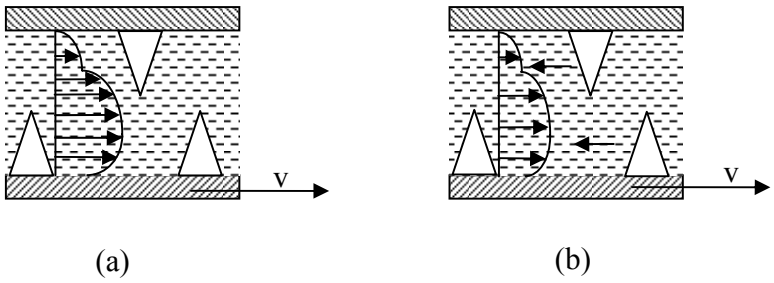

Figure 6.32 - Idealized illustration of oscillating flow between asperities

- Under the identical load, the hysteresis loops have a similar shape for different frequencies.
- Higher viscosity tends to reduce the bandwidth of the hysteresis loop.

- For bearings operating in boundary or mixed lubrication regimes, the use of appropriate grease is preferred to oil.
- At low oscillating frequencies (0.5 Hz), the friction coefficient under oscillatory motion is smaller than that under uni-directional motion at the same speed point.
- The inertia of the lubricant flow contributes to the friction hysteresis.

6.4. Nomenclature

f	coefficient of friction
p	pressure, Pa
q	heat flux, W/m^2
r	bar length, m
v	linear velocity, rpm
θ	angle, radian
ω	angular velocity, rad/s

Subscripts

1, 2, 3, 4	bar number

CHAPTER 7 DYNAMIC FRICTION MODELING OF OIL-LUBRICATED LONG JOURNAL BEARINGS

7.1 Introduction

The application of oscillatory bearings in automation industry and necessity of friction compensation has been instrumental in encouraging researchers in control area to devote much effort to the modeling of dynamic friction. Frictional characteristics of oil-lubricated journal bearings undergoing uni-directional sliding motion can be described by the classic Stribeck curve. However, for journal bearings undergoing oscillatory sliding motion, this curve is not able to represent the friction properties completely. The friction hysteresis occurs. It is a friction retardation phenomenon when the sliding velocity increases or decrease to the same value.

Significant progress has been made ever since Bell [139-141] disclosed the existence of friction hysteresis in lubricated sliding surfaces. The proposed models include: classic model [162] which approximates the discontinuity at the origin by linear function; Dahl model [142, 143] which describes the time derivative of the friction as a function of displacement; Karnopp model [175] which reduces the order of the system at the instant of zero velocity; the reset-integrator model [162] which attempts to overcome the complexity of Karnopp model; the bristle-model [162] which represents the friction force by the number of bristles; Armstrong model [147, 163, 164, 176, 177] which describes tribological behavior by seven parameters; and LuGre model [165-167] which expresses friction by the average deflection force of elastic springs. While these models simple or complicated capture the friction hysteresis, they are not intended to describe it from the view of the underlying lubrication mechanism which is the ultimate cause of the friction hysteresis.

Three models made the attempt. The first was introduced by Hess et al. [154, 155] who simulated hysteresis by superimposing a time lag into an empirical model under steady operation conditions. The time lag was defined as the time difference between the lowest velocity and the biggest friction force. The results were limited to particular conditions, such as the amplitude of oscillation, under which the time delay was determined. Instead of time lag, Polycarpou [151-153] proposed two models by incorporating sliding velocity and instantaneous separation of sliding surfaces. They showed that fluctuation in normal separation was the principal cause of hysteresis. To apply these models, instantaneous film thickness must be measured. Harnoy [156-160] modeled the mixed lubrication regime simply as a "spring" and applied the short bearing theory to predict bearing friction in the hydrodynamic regime. He successfully predicted the general characteristics of friction hysteresis loop.

In the current chapter, a dynamic friction model of oil-lubricated long journal bearings is developed. Simulation results capture the general trend of friction hysteresis loop. The assumption of long bearing is more pertinent for the bearings tested in the experimental studies conducted in this dissertation.

7.2 Theoretical Development

7.2.1 Mixed Lubrication Modeling

Mixed lubrication is a lubrication state in which both fluid film and asperity contact exist to support the applied load. A thorough understanding of this lubrication state still remains rudimentary. When the minimum film thickness h_m is below a certain transition value h_{tr}, asperity contact occurs. It is assumed that the reaction force is an increasing function of elastic deformation δ of asperities. The parameter δ is simply expressed as

$$\delta = h_{tr} - h_m \tag{7.1}$$

The elastic reaction force W_e is represented by:

$$W_e = K(\delta)\delta \tag{7.2}$$

where $K(\delta)$ is an equivalent stiffness of the surface asperities.

The eccentricity ratio ε_{tr} corresponds to the transition speed U_{tr} and the transition minimum film thickness h_{tr}. It is known that:

$$h_m = C(1-\varepsilon) \tag{7.3}$$

$$h_{tr} = C(1-\varepsilon_{tr}) \tag{7.4}$$

where C is the radial clearance.

Combining these equations, the elastic reaction force W_e reads:

$$W_e = \kappa(\varepsilon)C(\varepsilon - \varepsilon_{tr})\Delta_1 \tag{7.5}$$

where $\kappa(\varepsilon) = K(\varepsilon)$ and Δ_1 is defined as:

$$\Delta_1 = \begin{cases} 0 & \text{at } \varepsilon < \varepsilon_{tr} \\ 1 & \text{at } \varepsilon > \varepsilon_{tr} \end{cases}$$

In the mixed lubrication condition, the total bearing load capacity $\vec{W}$ is a summation of the elastic reaction $\vec{W_e}$ and the hydrodynamic force $\vec{W_h}$:

$$\vec{W} = \vec{W_e} + \vec{W_h} \tag{7.6}$$

7.2.2 The Friction Coefficient

The friction force F_{fh} for a long journal bearing in hydrodynamic lubrication regime is [25]:

$$F_{fh} = \frac{\mu L U}{\pi}\left(\frac{R}{C}\right)\left(\frac{\varepsilon \sin\varphi}{2} + \frac{2\pi^2 S}{\left(1-\varepsilon^2\right)^{0.5}}\right)\frac{1}{S}$$

where

$$S = \frac{\left(2+\varepsilon^2\right)\left(1-\varepsilon^2\right)}{6\pi\varepsilon}\left[\frac{1}{\pi^2\left(1-\varepsilon^2\right)+4\varepsilon^2}\right]^{0.5}$$

$$\varphi = \tan^{-1}\left[\frac{\pi}{2\varepsilon}\left(1-\varepsilon^2\right)^{0.5}\right]$$

The friction force F_f is the sum of mechanical and viscous forces. F_f is described as:

$$F_f = f_c \kappa(\varepsilon) C(\varepsilon - \varepsilon_{tr})\Delta_1 + \frac{\mu L U}{\pi}\left(\frac{R}{C}\right)\left(\frac{\varepsilon \sin\varphi}{2} + \frac{2\pi^2 S}{\left(1-\varepsilon^2\right)^{0.5}}\right)\frac{1}{S}\Delta_2 \qquad (7.7)$$

Where

$$\Delta_2 = \begin{cases} 0 & \text{at } \varepsilon > \varepsilon_{tr} \\ 1 & \text{at } \varepsilon < \varepsilon_{tr} \end{cases}$$

where f_c is the Coulomb's friction coefficient.

Introducing dimensionless parameters

$$\overline{F} = \frac{C^2}{\mu U_{tr} L R^2} F$$

$$\overline{\kappa}(\varepsilon) = \frac{C^3}{\mu U_{tr} L R^2}\kappa(\varepsilon)$$

$$\overline{U} = \frac{U}{U_{tr}}$$

Equation (7.7) becomes

$$\overline{F_f} = f_c \overline{\kappa}(\varepsilon)(\varepsilon - \varepsilon_{tr})\Delta_1 + \frac{C\overline{U}}{\pi R}\left(\frac{\varepsilon \sin\varphi}{2} + \frac{2\pi^2 S}{\left(1-\varepsilon^2\right)^{0.5}}\right)\frac{1}{S}\Delta_2 \qquad (7.8)$$

The friction coefficient is a ratio of the friction force and the external load F :

$$f = \frac{F_f}{F} \tag{7.9}$$

7.2.3 Load Capacity of Constant Velocity

For long journal bearings at steady speed, the load capacity considering the elastic reaction force of asperity contact is [25]:

$$\begin{aligned} F\cos\varphi &= \kappa(\varepsilon)C(\varepsilon-\varepsilon_{tr})\Delta_1 + \frac{12\varepsilon^2}{(1-\varepsilon^2)(2+\varepsilon^2)}\frac{\mu LR^2}{C^2}U\Delta_2 \\ F\sin\varphi &= \frac{6\pi\varepsilon}{(1-\varepsilon^2)^{0.5}(2+\varepsilon^2)}\frac{\mu LR^2}{C^2}U\Delta_2 \end{aligned} \tag{7.10}$$

Its dimensionless form is

$$\begin{aligned} \overline{F}\cos\varphi &= \overline{\kappa}(\varepsilon)(\varepsilon-\varepsilon_{tr})\Delta_1 + \frac{12\varepsilon^2}{(1-\varepsilon^2)(2+\varepsilon^2)}\overline{U}\Delta_2 \\ \overline{F}\sin\varphi &= \frac{6\pi\varepsilon}{(1-\varepsilon^2)^{0.5}(2+\varepsilon^2)}\overline{U}\Delta_2 \end{aligned} \tag{7.11}$$

The friction coefficient can be obtained from

$$f = \frac{\overline{F_f}}{\overline{F}} \tag{7.12}$$

7.2.4 Dynamic Modeling of Long Journal Bearings

A long journal bearing configuration is shown in Figure 7.1. The bearing sleeve center is O_1. O_2 is the journal center. X coordinate is along these two centers and Y is perpendicular to it. x is the tangential direction. φ is the attitude angle. e is the eccentricity.

The general Reynolds' equation for a dynamic loaded long journal bearing is [178]:

$$\frac{d}{dx}\left(\frac{h^3}{\mu}\frac{dP}{dx}\right) = 6U\frac{dh}{dx} + 6h\frac{dU}{dx} + 12V_0 \tag{7.13}$$

Where

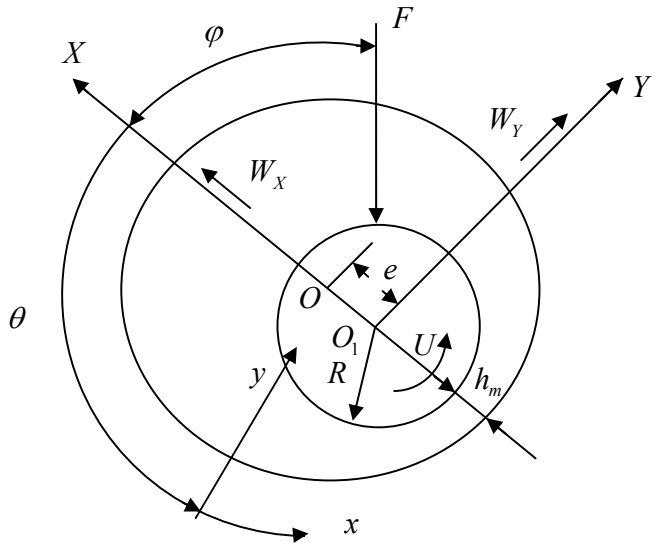

Figure 7.1 - Bearing configuration

$$dx = Rd\theta \tag{7.14}$$

$$h = C + C\varepsilon\cos\theta \tag{7.15}$$

$$U = R\omega + C\frac{d\varepsilon}{dt}\sin\theta - C\varepsilon\frac{d\phi}{dt}\cos\theta \tag{7.16}$$

$$V_0 = C\frac{d\varepsilon}{dt}\cos\theta + C\varepsilon\frac{d\phi}{dt}\sin\theta \tag{7.17}$$

Substituting equations (7.14), (7.15), (7.16), and (7.17) into (7.13), simplifying it, we have

$$\frac{d}{d\theta}\left(h^3\frac{dP}{d\theta}\right) = 6\mu R^2\left[\left(\omega - 2\frac{d\phi}{dt}\right)\frac{dh}{d\theta} + 2C\frac{d\varepsilon}{dt}\cos\theta\right] \tag{7.18}$$

The boundary conditions are

$P = 0$ at $\theta = 0$

$P = 0$ at $\theta = \pi$

Integrating equation (7.18) twice with two boundary conditions, the pressure expression is

$$P = \frac{6\mu R^2}{C^2}\left\{\left(\omega\varepsilon - 2\varepsilon\frac{d\phi}{dt}\right)\left(I_3^{01} + \frac{3\varepsilon}{\left(2+\varepsilon^2\right)}I_3^{00}\right) + \left[2I_3^{10} - \frac{8\left(1-\varepsilon^2\right)^{\frac{1}{2}}}{\pi\left(2+\varepsilon^2\right)}I_3^{00} - \frac{1}{\varepsilon\left(1+\varepsilon\right)^2}\right]\frac{d\varepsilon}{dt}\right\} \tag{7.19}$$

Using the table in [179]

$$I_1^{00} = \frac{1}{\left(1-\varepsilon^2\right)^{\frac{1}{2}}}\cos^{-1}\left(\frac{\varepsilon+\cos\theta}{\left(1+\varepsilon\cos\theta\right)}\right)$$

$$I_2^{00} = \frac{1}{\left(1-\varepsilon^2\right)}\left[\frac{-\varepsilon\sin\theta}{\left(1+\varepsilon\cos\theta\right)} + I_1^{00}\right]$$

$$I_3^{00} = \frac{1}{2\left(1-\varepsilon^2\right)}\left[\frac{-\varepsilon\sin\theta}{\left(1+\varepsilon\cos\theta\right)^2} + 3I_2^{00} - I_1^{00}\right]$$

$$I_3^{01} = \frac{1}{\varepsilon}\left(-I_3^{00} + I_2^{00}\right)$$

$$I_3^{10} = \frac{1}{2\varepsilon\left(1+\varepsilon\cos\theta\right)^2}$$

Introducing dimensionless parameters,

$$\overline{P} = \frac{C^2}{\mu R^2\omega_{tr}}P$$

$$\overline{U} = \frac{U}{U_{tr}} = \frac{\omega R}{\omega_{tr}R} = \frac{\omega}{\omega_{tr}}$$

$$\bar{t} = \omega_{tr}t$$

the pressure expression becomes

$$\overline{P} = 6\left\{\left(\overline{U}\varepsilon - 2\varepsilon\frac{d\phi}{d\bar{t}}\right)\left(I_3^{01} + \frac{3\varepsilon}{\left(2+\varepsilon^2\right)}I_3^{00}\right) + \left[2I_3^{10} - \frac{8\left(1-\varepsilon^2\right)^{\frac{1}{2}}}{\pi\left(2+\varepsilon^2\right)}I_3^{00} - \frac{1}{\varepsilon\left(1+\varepsilon\right)^2}\right]\frac{d\varepsilon}{d\bar{t}}\right\} \tag{7.20}$$

The loading capacity is obtained by integrating the pressure in the region of $0 < \theta < \pi$:

$$W_X = -RL\int_0^{\pi} P\cos\theta\, d\theta$$
$$W_Y = RL\int_0^{\pi} P\sin\theta\, d\theta \tag{7.21}$$

Introducing the dimensionless parameter

$$\overline{W} = \frac{C^2}{\mu\omega_{tr}LR^3}W$$

equation (7.21) reads:

$$\overline{W_X} = -\int_0^{\pi} \overline{P}\cos\theta\, d\theta = \overline{W_X}\left(\varepsilon, \dot{\varepsilon}, \dot{\varphi}, \overline{U}\right)$$
$$\overline{W_Y} = \int_0^{\pi} \overline{P}\sin\theta\, d\theta = \overline{W_Y}\left(\varepsilon, \dot{\varepsilon}, \dot{\varphi}, \overline{U}\right) \tag{7.22}$$

Applying Newton's second law to X and Y directions, the dynamic equations are:

$$F\cos\varphi - W_X - \kappa(\varepsilon)C(\varepsilon - \varepsilon_{tr})\Delta_1 = m\left(\ddot{e} - e\dot{\varphi}^2\right) \tag{7.23}$$

$$F\sin\varphi - W_Y + f_c\kappa(\varepsilon)C(\varepsilon - \varepsilon_{tr})\Delta_1 = -m\left(e\ddot{\varphi} + 2\dot{e}\dot{\varphi}\right) \tag{7.24}$$

Introducing the dimensionless parameter

$$\overline{m} = \frac{C^3\omega_{tr}}{\mu LR^3}m$$

equations (7.23) and (7.24) becomes:

$$\overline{F}\cos\varphi - \overline{W_X} - \overline{\kappa}(\varepsilon)(\varepsilon - \varepsilon_{tr})\Delta_1 = \overline{m}\ddot{\varepsilon} - \overline{m}\varepsilon\dot{\varphi}^2 \tag{7.25}$$

$$\overline{F}\sin\varphi - \overline{W_Y} + f_c\overline{\kappa}(\varepsilon)(\varepsilon - \varepsilon_{tr})\Delta_1 = -\left(\overline{m}\varepsilon\ddot{\varphi} + 2\overline{m}\dot{\varepsilon}\dot{\varphi}\right) \tag{7.26}$$

7.3 Numerical Solutions

In this chapter, it is assumed that $\overline{\kappa}(\varepsilon)$ is linear function of ε [157].

$$\overline{\kappa}(\varepsilon) = \overline{\kappa_0}\frac{(\varepsilon - \varepsilon_{tr})}{(\varepsilon_b - \varepsilon_{tr})}$$
$$\overline{\kappa_0} = \frac{\overline{F}}{(\varepsilon_b - \varepsilon_{tr})} \tag{7.27}$$

where ε_b is the eccentricity ratio corresponding to the mark between mixed lubrication boundary lubrication.

The oscillating velocity takes the form of

$$\overline{U} = 1.1 + \sin(\alpha \bar{t}) \tag{7.28}$$

Equation (7.25) and (7.26) are solved for ε and φ using a forth-order Runge-Kutta method. The solution is Combined with equation (7.8) and (7.12) to evaluate the friction coefficient can be calculated.

7.4 Results and Discussion

The input parameters [157] are listed in Table 7.1.

Table 7.1 - input parameters

ε_b	ε_{tr}	f_c	$\frac{RC}{L^2}$	$\overline{m}$
0.99	0.96	0.2	0.0001	100

$\overline{F}$ can be calculated with $\overline{U} = 1$ and $\varepsilon = \varepsilon_{tr}$. From those input parameters, $\overline{F}$ reads 53. The oscillating frequency effect on the hysteresis is shown in Figure 7.2. α is varied from 0.4 to 0.5 to 0.6. The mass effect on the hysteresis is examined in Figure 7.3. $\overline{m}$ is changed from 10 to 50 to 100.

As it is shown in Figure 7.2, the friction hysteresis is captured by the dynamic friction modeling. The general trend of friction hysteresis of long journal bearings agrees with Harnoy's theory for short journal bearings. With higher oscillating frequency,

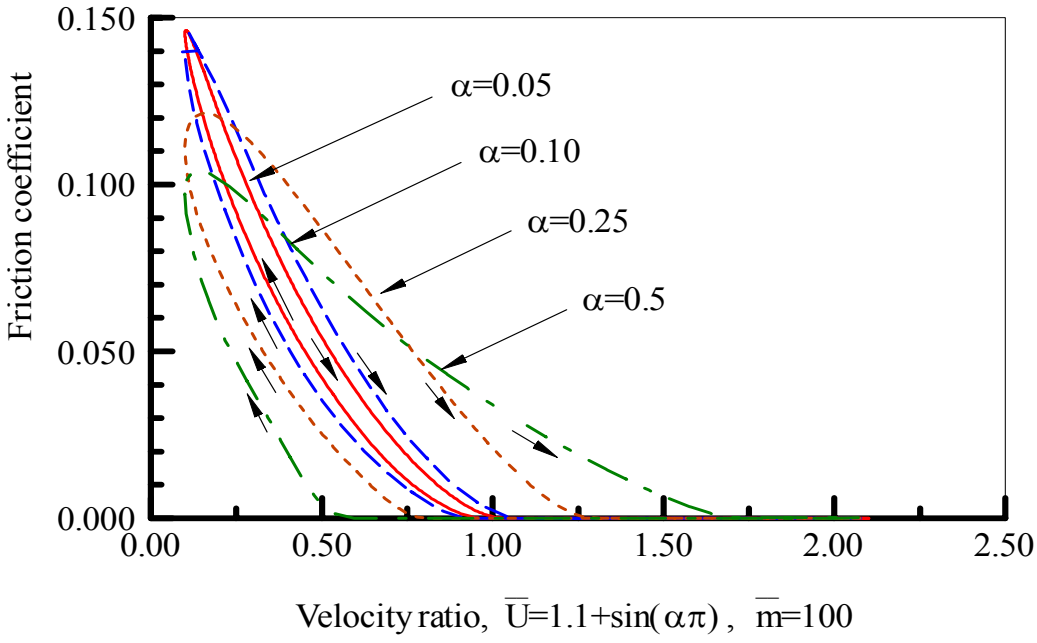

Figure 7.2 - Friction coefficient versus velocity, the oscillating frequency effect

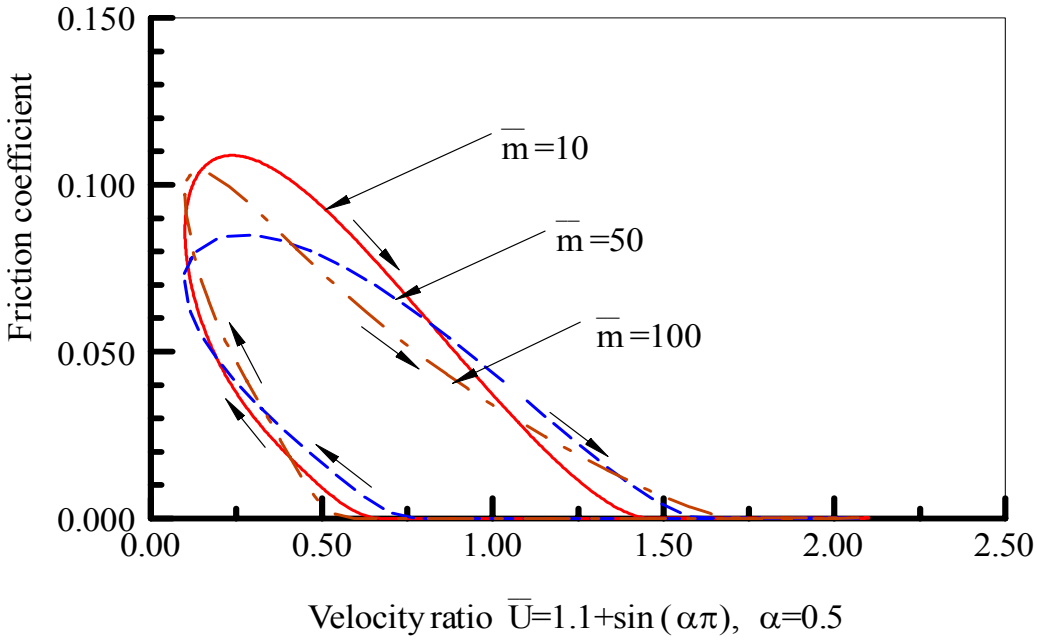

Figure 7.3 - Friction coefficient versus velocity, the mass effect

the hysteresis loop becomes flatter; with bigger mass, the bandwidth of the loop is squeezed.

However, the difference between simulation and experiment (See Chapters 5 and 6) is big. In Chapter 2, a mixed EHL model is used to describe the load carrying mechanism in mixed lubrication regime. Instead of using the simple spring concept as described in this chapter, it is worthwhile to combine the mixed EHL model into equations of motion to improve the prediction of the friction hysteresis.

7.5 Conclusion

A dynamic friction model of oil-lubricated long journal bearings is developed. In mixed lubrication regime, the load carrying mechanism is simply treated as a spring. Combining with hydrodynamic load carrying capacity developed in long journal bearing theory, the dynamic equations of journal bearings are established. The model predicts the general characteristics of the friction hysteresis phenomenon. Parametric study is carried out to examine the variation of the hysteresis loop. With higher oscillating frequency, the hysteresis loop becomes flatter; with bigger mass, the bandwidth of the loop is squeezed. A more accurate model of the load carrying mechanism in the mixed lubrication regime is required to improve the prediction.

7.6 Nomenclature

C	radial clearance, m
F	external load, N
F_f	friction force, N
F_{fh}	viscous force, N
f	friction coefficient

f_c Coulomb's friction coefficient

h film thickness, m

K equivalent stiffness of asperities, N/m

L bearing length, m

m shaft mass, kg

P oil pressure, Pa

R shaft radius, m

U shaft velocity, m/s

W load capacity, N

δ elastic deformation of asperities, m

μ dynamic viscosity, Pa.s

ε eccentricity ratio

φ attitude angle, rad

ω shaft angular velocity, rad/s

Subscripts

b boundary lubrication

e elastic

h hydrodynamic

m minimum

tr transition from mixed lubrication to hydrodynamic lubrication

X X direction

Y Y direction

CHAPTER 8 FINITE ELEMENT ANALYSIS OF THERMAL FIELD IN OSCILLATORY JOURNAL BEARINGS

8.1 Introduction

Friction and heat occur simultaneously. They are internally connected by energy transmission. When friction is not severe, like in oil-lubricated cases, heat generated by friction is minute and it might not cause serious problems. However, wherever the friction coefficient, the load, or the sliding velocity is severe, the frictional heat flux (fPV) might become excessive to the extent that it may result in failure.

Pin and bushing (journal bearing) assemblies undergoing oscillatory motion are considered to be vital components of large earth moving machinery. These machines are heavily-loaded, often to thousands of lbs. Typically the lubricant is grease and the friction coefficient is around 0.1. The sliding velocity is in the order of 0.01 m/s. Therefore, the friction heat is very high. It is necessary to understand the thermal field of oscillatory pin and bushing system.

The methodology of analyzing the thermal behavior of oscillatory pin and bushing has been addressed by Hazlett [180-182] and Krithivasan [183, 184]. However, their analysis has not been verified by experimental data. In this chapter, both simulation and experiment are carried out. Their comparison show good agreement.

8.2 Model Development

A schematic of pin and bushing assembly is illustrated by Figure 8.1. The contact angle is 2α. An oscillation cycle is exhibited in Figure 8.2. For the convenience of demonstration, it is assumed that the contact region is divided into two sections. The oscillation angle is represented by one section.

One important feature of thermal analysis of oscillatory journal bearings is the moving boundary conditions. It is demonstrated in Figure 8.2 demonstrates. Heat flux of the bushing is fixed, while heat flux of the pin oscillates on those sections involved into oscillation. Heat flux boundary is designated by dark block. Convection boundary of those sections involved into oscillation is designated by white block. At each time step, heat flux and convection are applied on corresponding sections.

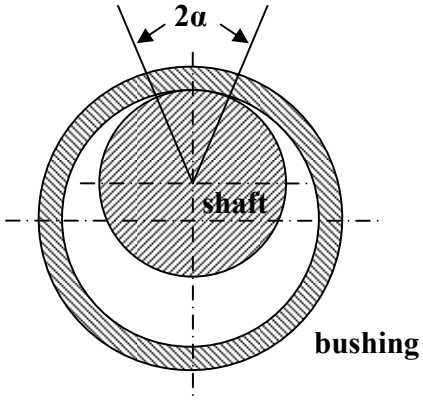

Figure 8.1 - pin bushing assembly

According to Hertzian contact theory [185], the half contact width b is

$$b = \sqrt{\frac{4WR'}{\pi E' L}} \tag{8.1}$$

where

$$R' = \frac{R_b R_p}{R_b - R_p}$$

$$E' = \frac{E_b E_p}{E_b\left(1 - v_p{}^2\right) + E_p\left(1 - v_b{}^2\right)}$$

W is the load. L is the length of the bearing. The mean pressure p_m is provided by

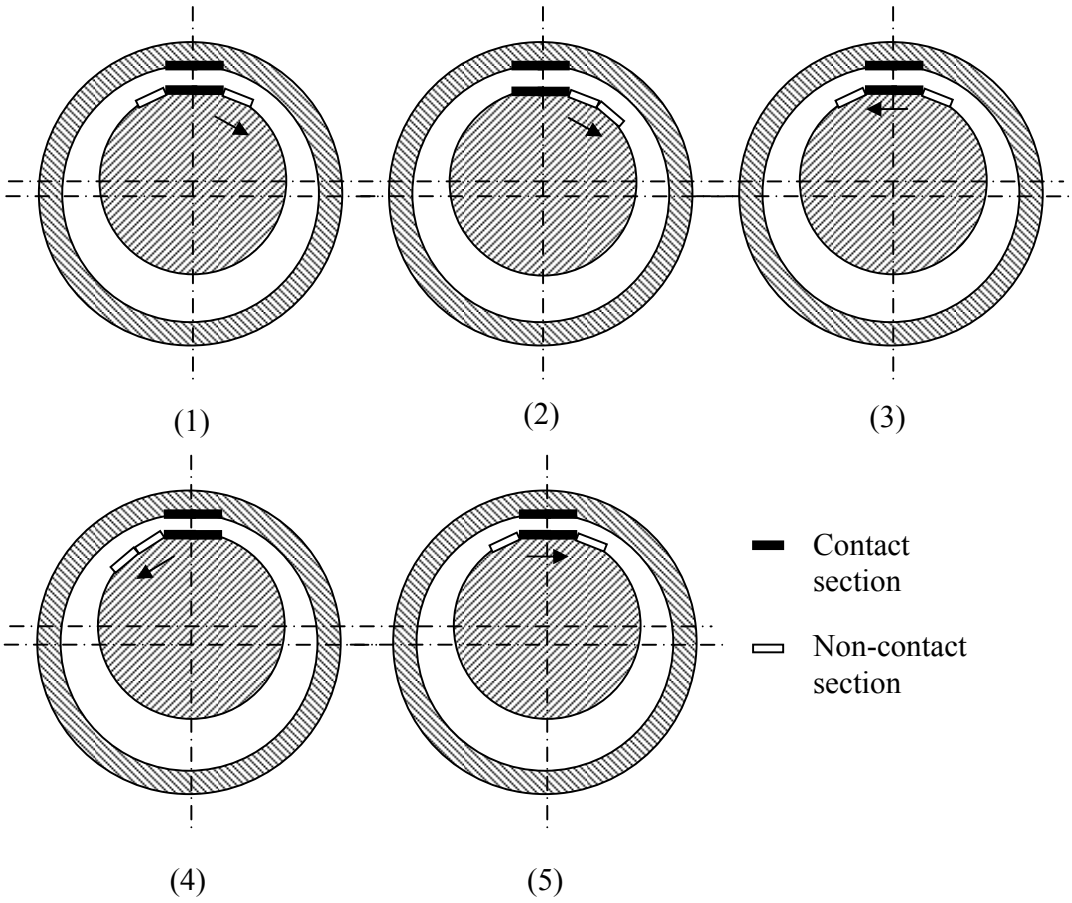

Figure 8.2 - one oscillation cycle

$$p_m = \frac{W}{2bL} \tag{8.2}$$

The heat flux q_m is calculated from

$$q_m = fp_m v \tag{8.3}$$

f is the friction coefficient. v is the sliding velocity of pin.

Assuming the sliding velocity is constant, the oscillation period T can be obtained from

$$T = \frac{4\beta R_p}{v} \tag{8.4}$$

β is the oscillating angle.

ANSYS software is employed to apply this methodology for thermal analysis of pin and bushing.

8.3 Simulation of Pin and Bushing Assemblies

Two pin and bushing assemblies are simulated. Their parameters are listed in Table 8.1.

Table 8.1 - Bearing parameters

Bearing	Pin A	Pin B
Shaft diameter (mm)	179.83	119.85
Radial clearance (mm)	0.358	0.36
Inside diameter of bushing (mm)	180.546	120.57
Outside diameter of bushing (mm)	230.05	168.07
Bearing length (mm)	130	149
L/D Ratio	0.72	1.24
Load (KN)	3673	1541.5
Oscillation angle (^{0})	$\pm$ 45	$\pm$ 42
Oscillation velocity (rpm)	1.46	1.71

Applying equations (8.1)-(8.4), the calculated contact and oscillation parameters are:

Table 8.2 - Contact and oscillation parameters

Bearing	Pin A	Pin B
Contact angle (^{0})	109.52	66
Contact pressure (MPa)	164.38	149.52
Heat flux (kW/m^2)	226.433	160.929
Oscillating period (s)	20.55	16.37

Material properties of pin and bushing are tabulated in Table 8.3 [186].

Table 8.3 - Material properties

Density (kg/m^3)	7680
Thermal capacity (J/kg·K)	460
Thermal conductivity (W/m·K)	52

8.3.1 Results of PinA and PinB

The meshing of the finite element model is exemplified in Figure 8.3. Mesh is refined for those layers close to contact surface. There are 800 PLANE55 (2D thermal solid element) elements totally. The friction coefficient is taken constant as 0.1. The convection coefficient is 16 $W/m^2 \cdot K$ between pin and bushing clearance and 80 $W/m^2 \cdot K$ between bushing outside surface and air. It takes twenty four hours for a Pentium III 547 MHz PC to run the program of Pin A.

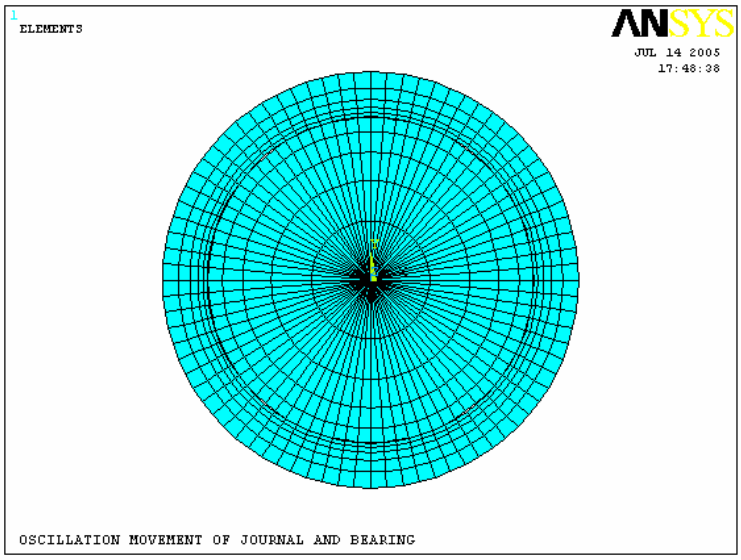

Figure 8.3 - Meshing

The thermal field of Pin A (240 minutes) is shown by Figure 8.4.

The thermal field of Pin B (136 minutes) is shown by Figure 8.6.

The maximum temperature happens in the center of contact region on the bushing side. Its history is displayed by Figure 8.5.

The history of the maximum temperature is displayed by Figure 8.7.

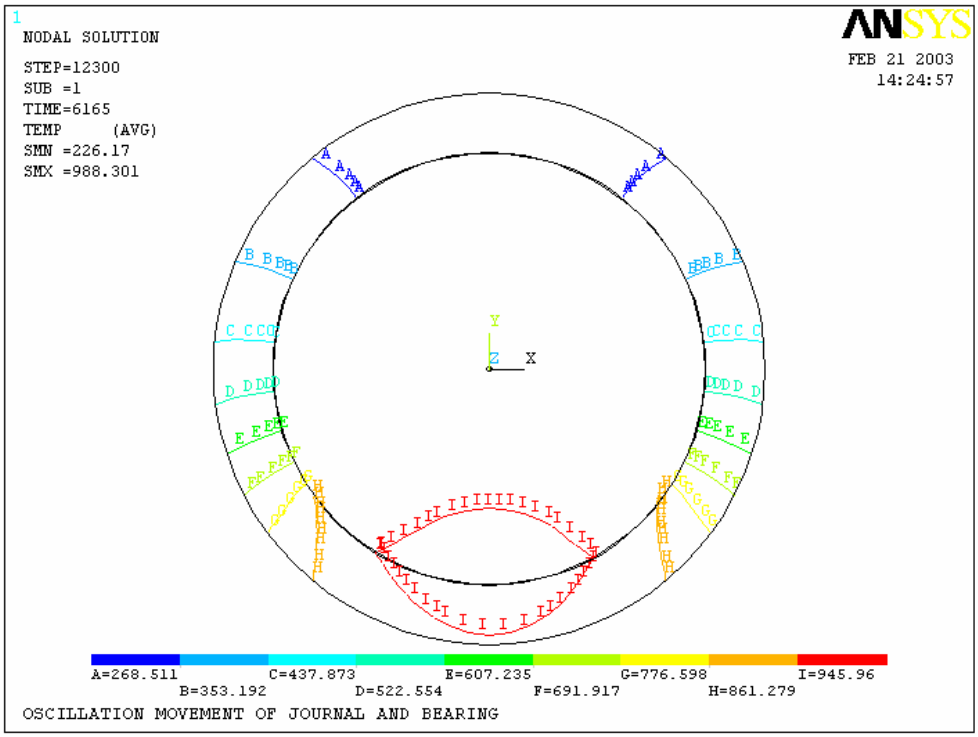

Figure 8.4 – Thermal field of Pin A, 240 minutes

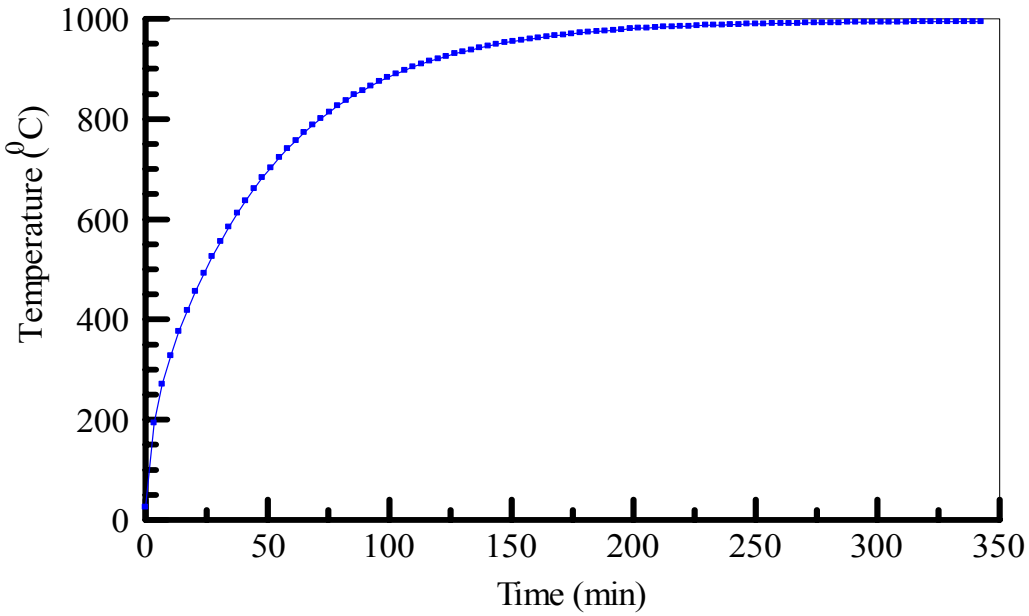

Figure 8.5 – History of the maximum temperature, Pin A

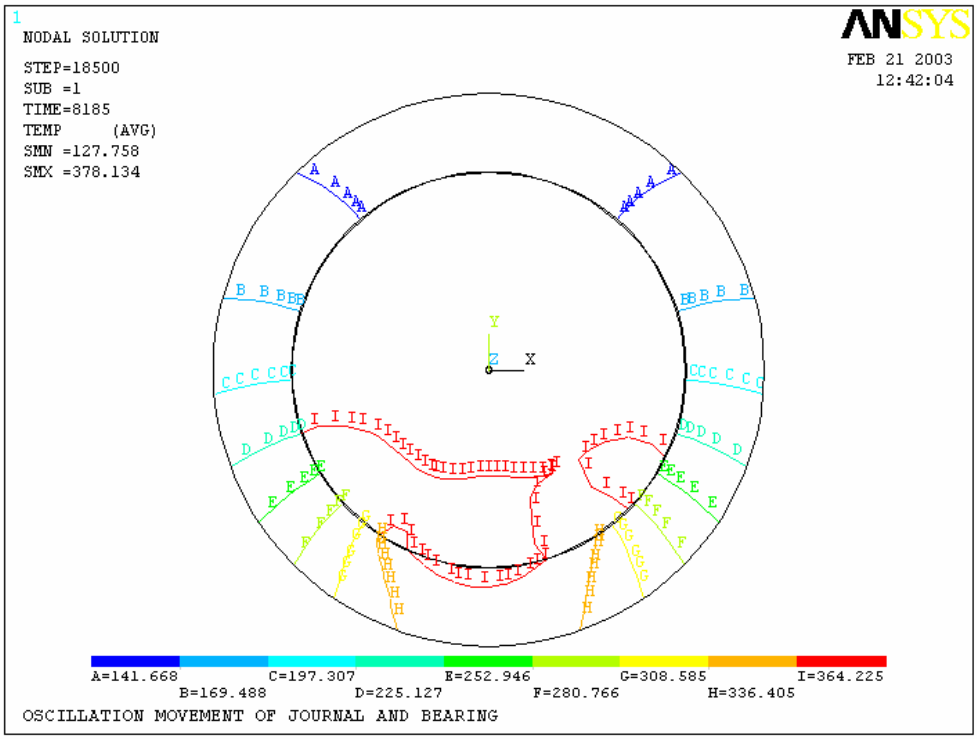

Figure 8.6 – Thermal field of Pin B, 136 minutes

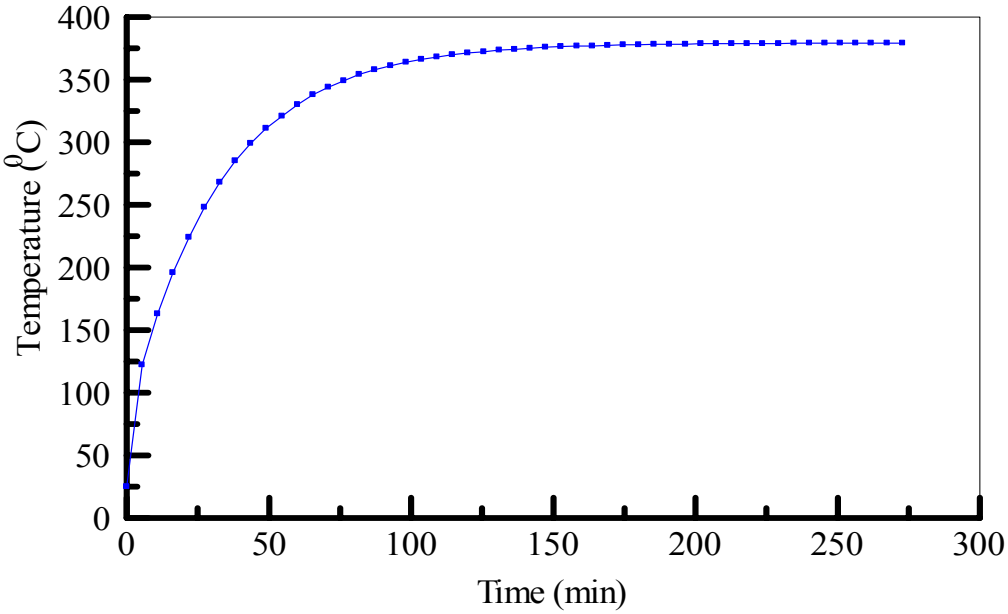

Figure 8.7 – History of the maximum temperature, Pin B

The maximum temperature reaches a very high value, as it is indicated in Figure 8.5 and 8.7.

8.3.2 Harmonic Oscillating Speed

In the calculation above, the oscillating velocity is assumed to be constant. While in the actual operating conditions, this is not true. A harmonically varying sliding velocity is considered to be more realistic. It takes the form of cosinusoidal function sweeping through the same angle as the constant velocity does in the same period.

For Pin A, the angular velocity is

$$\omega = A\cos\left(\frac{2\pi}{T}t\right) \tag{8.5}$$

Where $T = 20.55\,\text{s}$.

The oscillating angle is $\pm\frac{\pi}{4}$. it reads

$$\int_0^{\frac{T}{4}} A\cos\left(\frac{2\pi}{T}t\right)dt = \frac{\pi}{4} \tag{8.6}$$

It is solved for $A = 0.2401\,\text{rad/s}$. The angular velocity is expressed by

$$\omega = 0.2401\cos(0.3058t) \tag{8.7}$$

Other input parameters are the same. The history of maximum temperature is shown in Figure 8.8.

8.3.3 Intervals between Oscillating Cycles

Another factor in actual operating conditions to be considered is the interval between oscillating cycles. Excavator loading is intermittent. When the load is dumped and before pin and bushing is loaded again, there will be short period the load is approximate zero. In the simulation, this period is regards as 30-second. During this

interval, a zero heat flux is applied on pin and bushing while convection boundary keeps the same. The history of the maximum temperature is shown in Figure 8.8.

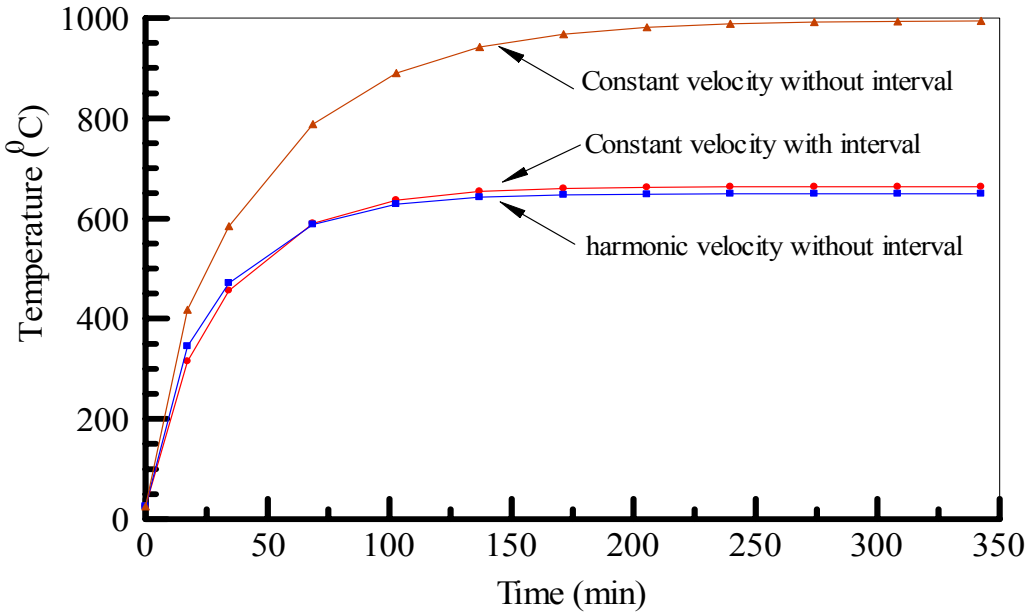

Figure 8.8 - Comparison of the maximum temperature, PinA

The harmonic sliding velocity and the interval reduces the temperature level tremendously.

8.4 Simulation of LaboratoryTests

Laboratory tests of pin and bushing assembly are carried out on Lewis LRI-8H tribometer. Its schematic is shown in Figure 1.1, Chapter 1. The main difference is the lubrication circuit is got rid of, for grease is used as the lubricant. The test rig is set up for oscillatory motion.

Due to the heavy loading (over 4.4 KN), the main concern here is not only the friction coefficient, but the temperature. Four K-type thermocouples are mounted on the outside surface of the bushing. They are located 45^0 evenly around the circumference. A

computerized data acquisition system allows monitoring the history of the coefficient of friction and the temperature. Its sampling frequency is 20 seconds.

The pin and bushing assembly on Lewis LRI-8H tribometer is drafted in Figure 8.9.

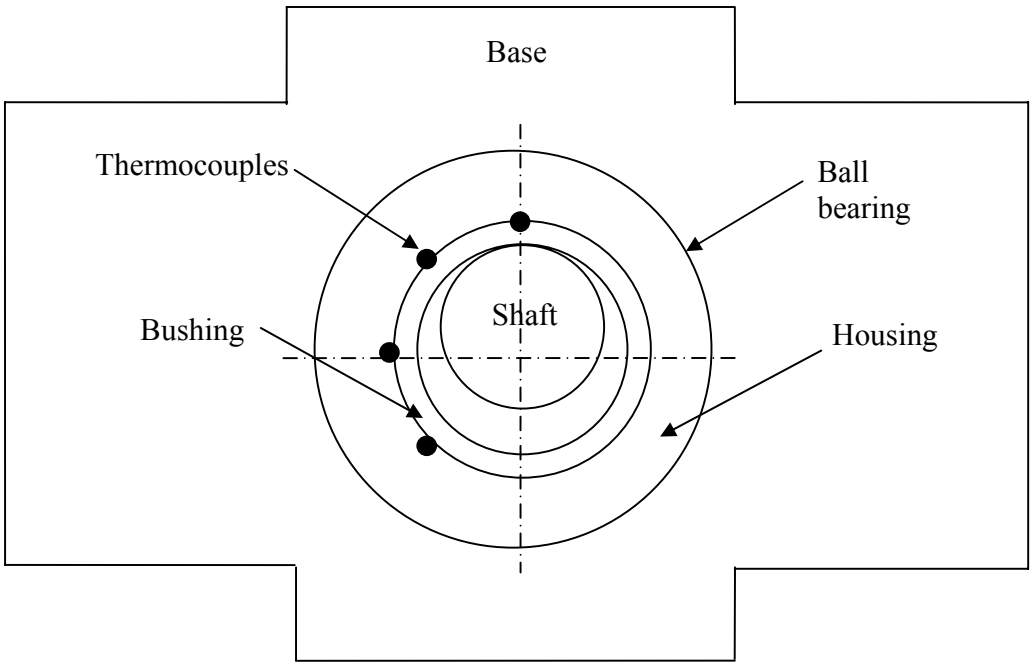

Figure 8.9 – Pin and bushing assembly on LRI-8H tribometer

8.4.1 Pin and Bushing Properties

The properties of pin and bushing are given in Table 8.4.

Table 8.4 - Bearing properties

Pin diameter (mm)	24.54
Inside diameter of bushing (mm)	25.40
Outside diameter of bushing (mm)	34.04
Bearing length (mm)	25.40
Poisson's ratio	0.29
Young's Modulus (Gpa)	200
Load (N)	4448
Lubricant	ALG#1 grease

The contact parameters are calculated and listed in Table 8.5.

Table 8.5 – Contact parameters

Contact angle (^{0})	8
Contact pressure (MPa)	103

Material properties are the same as those in Table 8.3.

The oscillating frequency is 1.34 Hz. The oscillation angle is $\pm 45^0$.

8.4.2 Experimental Results

Numerous experiments have been done. They are exemplified by Figures 8.10-8.15

The friction coefficient reaches steady state after 60 minutes. It oscillates around 0.123. The reading of thermocouple 1 has the highest value because its position is the closet to the contact center. The further the position away from the contact center, the lower the temperature is. Those experiments show good repeatability. Success in simulating one of them would verify the validity of simulation methodology.

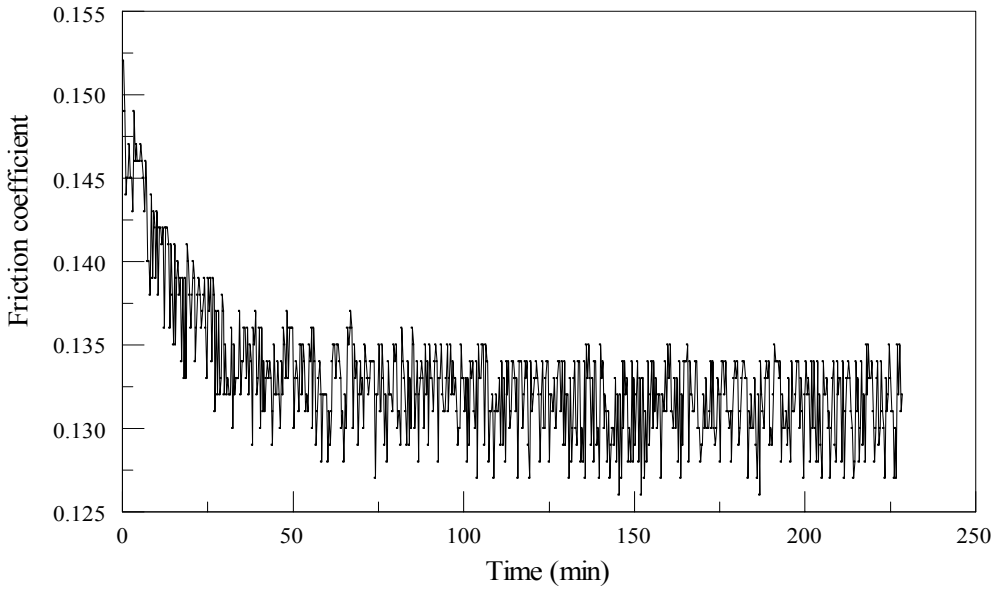

Figure 8.10 - History of the friction coefficient

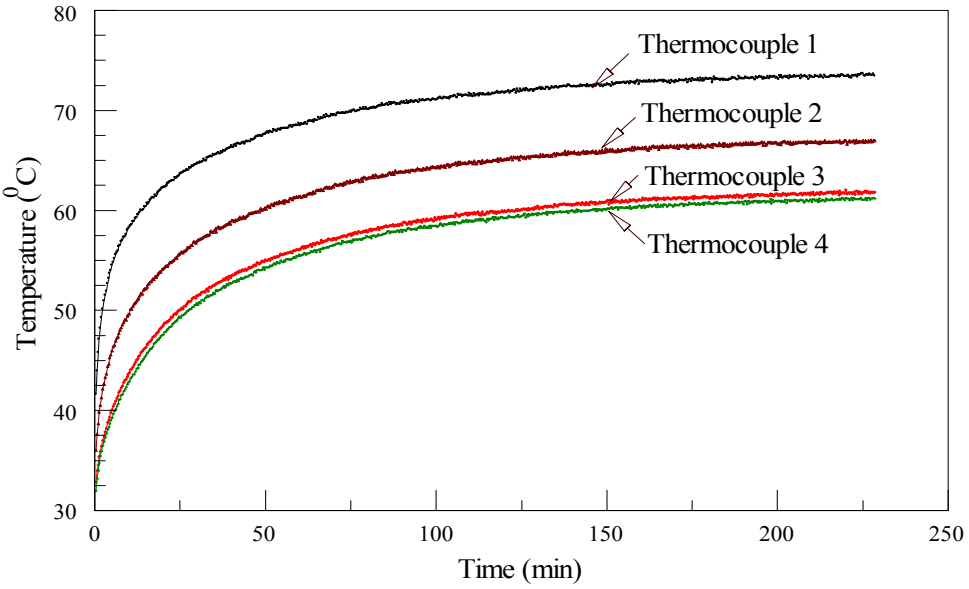

Figure 8.11 - History of temperature

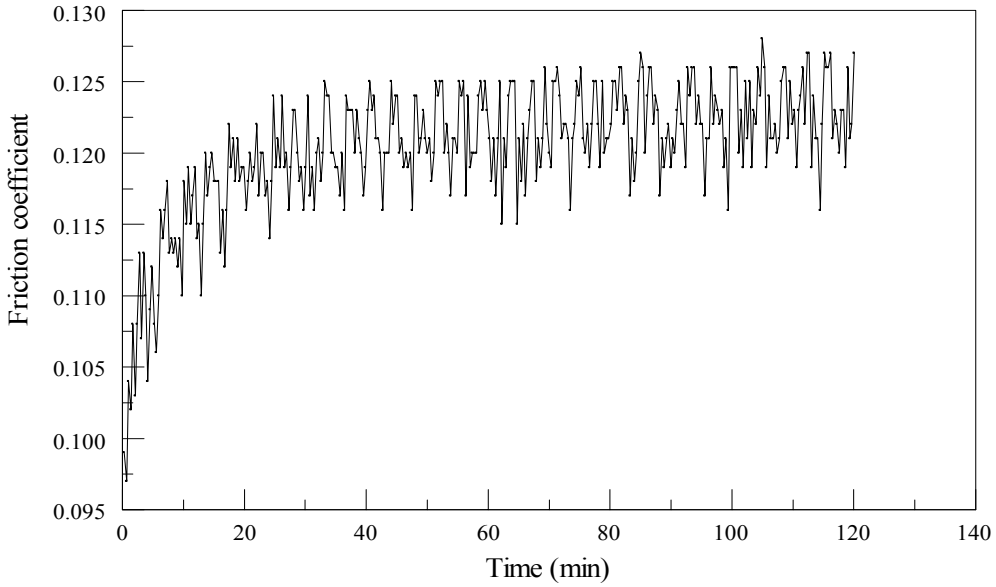

Figure 8.12 - History of the friction coefficient

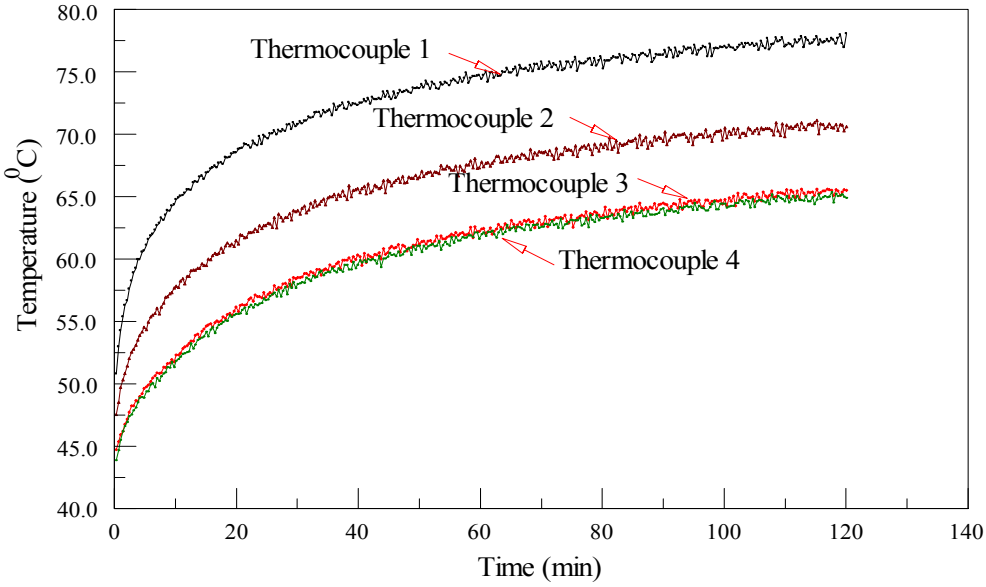

Figure 8.13 - History of temperature

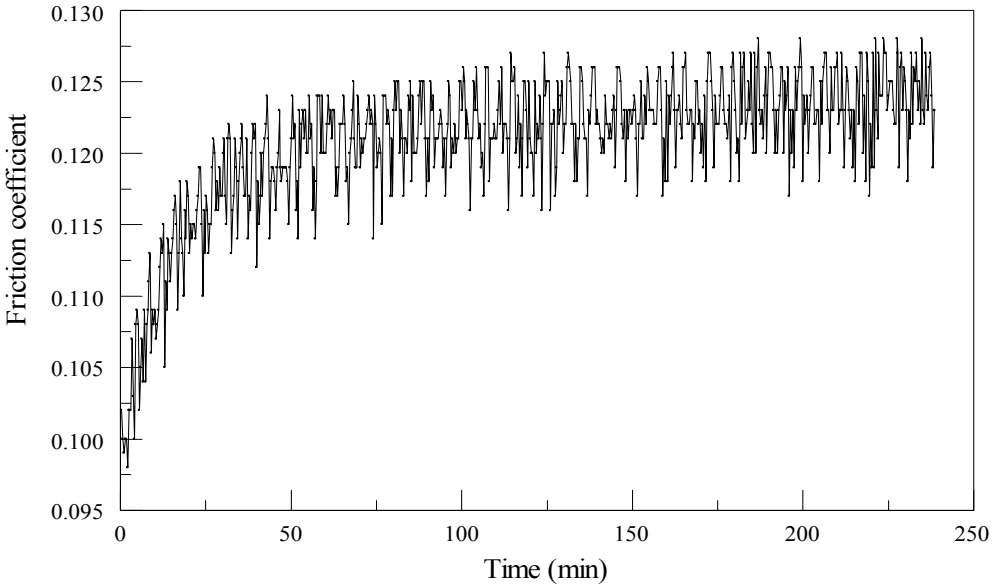

Figure 8.14 - History of the friction coefficient

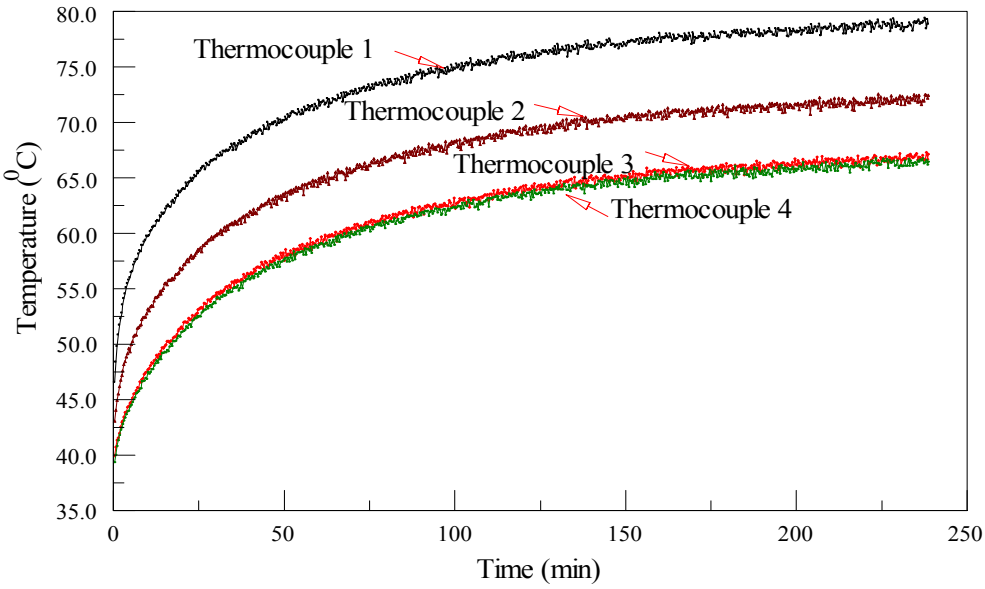

Figure 8.15 - History of temperature

8.4.3 Simulation

Besides applying the strategy of moving boundary conditions into ANSYS code, several other factors are considered into simulation of dummy tests.

8.4.3.1 Curve Fitting of the Friction Coefficient

The friction coefficient of experiments is curve fitted by a power function

$$f = c_1 t^{c_2} \qquad (8.8)$$

Where t is in minute.

The curve fitting of experimental result in Figure 8.14 is

$$f = 0.1024 t^{0.0366} \qquad (8.9)$$

The graph is shown in Figure 8.16.

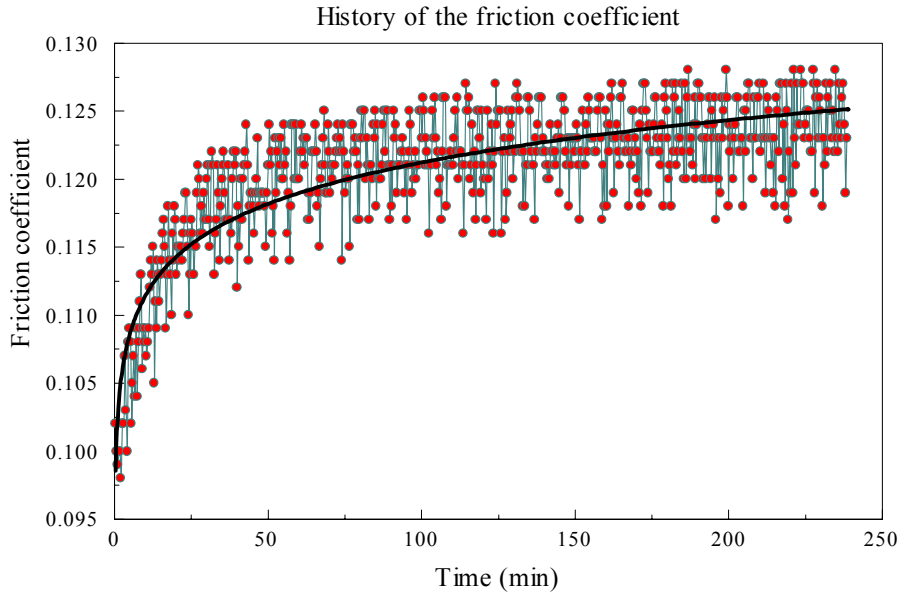

Figure 8.16 - Curve fitting of history of the friction coefficient

8.4.3.2 Velocity Input

As it is addressed in chapter 4, the velocity profile of the pin is not strictly harmonic. For its detailed development, see §6.2.3, Chapter 6. In current experiment, the oscillating frequency is changed to 1.34 Hz. The corresponding velocity profile is illustrated by Figure 8.17.

8.4.3.3 Quasi-3D Simplification

Two dimensional model is used in simulations. To compensate the heat conduction in the axial direction, a heat sink item is added to the modeling. Its development is as the following.

The pin length is L. Convection happens between one end of the pin and the ambient air. The convection coefficient is h_s. The other pin end is insulated. The heat diffusion equation of the pin is:

$$\frac{\partial^2 T'}{\partial r^2}+\frac{1}{r}\frac{\partial T'}{\partial r}+\frac{1}{r^2}\frac{\partial^2 T'}{\partial \theta^2}+\frac{\partial^2 T'}{\partial z^2}=0 \qquad (8.10)$$

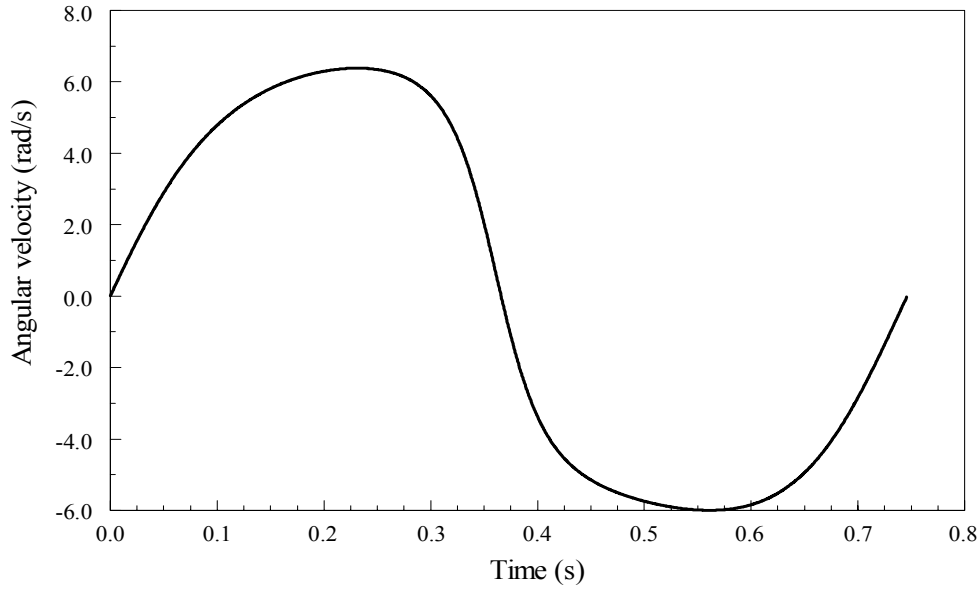

Figure 8.17 - the angular velocity of the shaft

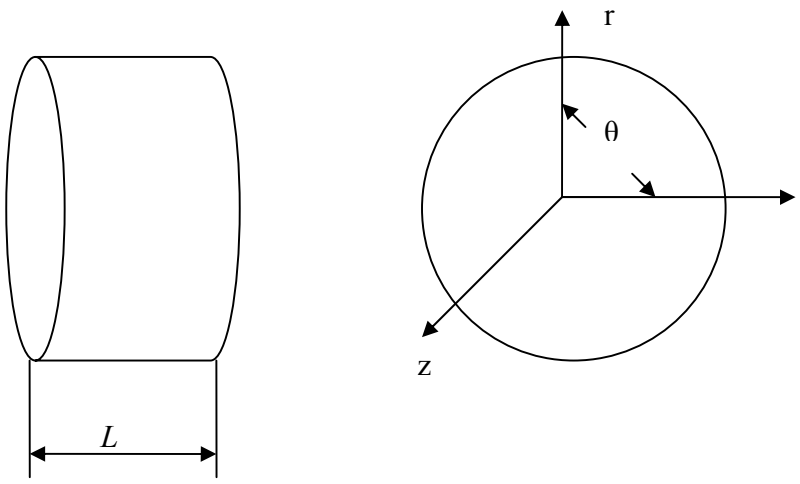

Figure 8.18 - Pin in polar coorinate

Where

$T' = T - T_\infty$

Integrating equation (8.10) in z direction, it reads

$$\int_0^L \left(\frac{\partial^2 T'}{\partial r^2} + \frac{1}{r}\frac{\partial T'}{\partial r} + \frac{1}{r^2}\frac{\partial^2 T'}{\partial \theta^2} \right) dz + \int_0^L \frac{\partial T'}{\partial z} dz = 0$$

$$\left(\frac{\partial^2 T'}{\partial r^2} + \frac{1}{r}\frac{\partial T'}{\partial r} + \frac{1}{r^2}\frac{\partial^2 T'}{\partial \theta^2} \right) z \Big|_0^L + \frac{\partial T'}{\partial z}\Big|_0^L = 0$$

$$\left(\frac{\partial^2 T'}{\partial r^2} + \frac{1}{r}\frac{\partial T'}{\partial r} + \frac{1}{r^2}\frac{\partial^2 T'}{\partial \theta^2} \right)(L-0) + \left(\frac{\partial T'}{\partial z}\Big|_L - \frac{\partial T'}{\partial z}\Big|_0 \right) = 0 \qquad (8.11)$$

The boundary condition at $z = 0$ is

$$-k\frac{dT'}{dz}\Big|_0 = h_s\left(T_\infty - T\right)$$

Which is equivalent to

$$\frac{dT'}{dz}\Big|_0 = \frac{h_s T'}{k} \qquad (8.12)$$

The boundary condition at $z = L$ is

$$-k\frac{dT'}{dz}\Big|_L = 0$$

Which is equivalent to

$$\frac{dT'}{dz}\Big|_L = 0 \qquad (8.13)$$

Substituting equations (8.12) and (8.13) into (8.11), it obtains

$$\frac{\partial^2 T'}{\partial r^2} + \frac{1}{r}\frac{\partial T'}{\partial r} + \frac{1}{r^2}\frac{\partial^2 T'}{\partial \theta^2} = \frac{h_s T'}{kL} \qquad (8.14)$$

The right hand side of equation (8.14) acts like a heat sink item. In ANSYS modeling, a heat generation item (negative to represent heat sink, $= -\frac{h_s T'}{L}$) is applied to shaft and bushing element by the command of "BF".

8.4.3.4 Simulation Results

Simulation of the thermal field in Figure 8.15 is carried out. The comparison of simulation and experiment is demonstrated by Figure 8.19.

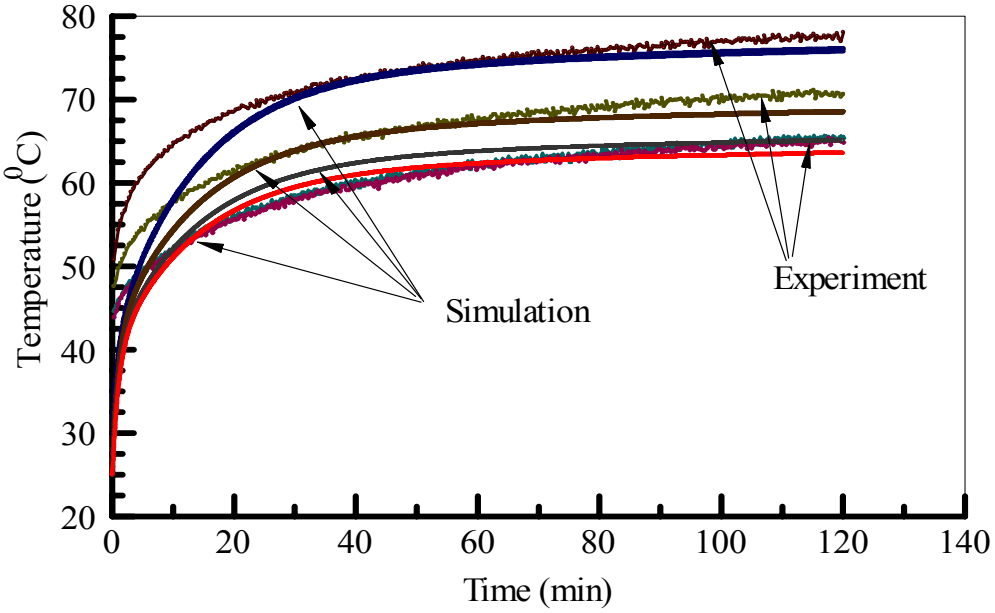

Figure 8.19 – Comparison of simulation and experiment

The simulation captures the right trend of experiment results. The temperature shows rapid increment during the initial stage. It is in this part that the discrepancy between simulation and experiment is big. Quasi-3D simplification introduces error, for the pin has a tapered end mounted in a bracket whose boundary is not insulated. Due to the way of applying load, the pin behaves like a cantilevered beam which causes the non-uniform heat flux along the axial direction. The housing and the ball bearing between housing and the supporting base causes some error also. More importantly, this modeling does not include thermo-mechanical coupling. The deformation of pin and bushing varies with temperature. So is the contact region. A model considering thermo-mechanical coupling will improve the results effectively.

8.5 Conclusion

The thermal field of oscillatory pin and bushing is examined. It is proved that moving boundary can represent the oscillatory motion effectively. Simulation of a pin and bushing system shows good results. A proper interval between oscillation cycles drops the temperature tremendously. Experiment results of laboratory tests are presented, and their simulation captures the right trend of temperature measurements on four positions. The friction coefficient reaches steady state after certain time. So does the thermal field. The further the position away from the contact center (heat source), the lower the temperature is.

8.6 Nomenclature

b	half contact width, m
E'	equivalent modulus, Pa
f	friction coefficient
L	length, m
p_m	mean pressure, Pa
q_m	heat flux, W/m^2
R'	equivalent radius, m
t	time,
T	oscillation period, s
v	linear velocity, m/s
W	load, N
ω	angular velocity, rad/s
α	half contact angle, rad

β	oscillation angle, rad
ν	possion's ratio

Subscripts

b	bushing
p	pin

REFERENCES

[1] Stribeck, R., 1902, "Kugellager für beliebige Belastungen," Zeitschrift des Vereines deutscher Ingenieure, **46** (37), pp. 1341-1348 (part I), **46** (38), pp. 1432-1438 (part II), **46** (39), pp. 1463-1470.

[2] Hirn, G., 1854, "Sur les principaux phénomènes qui presentment les frottements médiats," Bulletin of the Industrial Society of Mulhouse, **26**, pp. 188-277.

[3] Thurston, R. H., 1885, *A Treatise on Friction and Lost Work on Machinery and Millwork*, Wiley, New York.

[4] Dowson, Duncan, 1998, *History of Tribology*, 2nd Edition, Professional Engineering Publishing, London and Bury St Edmunds, UK.

[5] Hersey, M. D., 1938, Theory *of Lubrication*, 2nd Edition, John Wiley & Sons, Inc, New York, NY.

[6] Hersey, M. D., 1966, Theory *and Research In Lubrication*, John Wiley & Sons, Inc, New York, NY.

[7] Tzeng, Huey-M., 1995, "Dynamic Torque Characteristics of Disc-Drive Spindle Bearings," Advances in Information Storage and Processing Systems, 1995; Presented at the 1995 ASME International Mechanical Engineering Congress and Exposition, **1**, pp. 57-63.

[8] Shimomura, Takao, Hirabayashi, Hiroshi, and Nakajima, Toshikatsu, 1991, "A Study of the Relationship Between Frictional Characteristics and Surface Condition of Mechanical Face seals," Tribology Transactions, **34** (4), pp. 513-520.

[9] Kaneta, M., Todoroki, H., Nishikawa, H., Kanzaki, Y., and Kawahara, Y., Oct 2000, "Tribology of Flexible Seals for Reciprocating Motion," Journal of Tribology, **122**, pp. 787-795.

[10] Eguchi, Masao, Takesue, Masahiko, and Yamamoto, Takashi, 1991, "Friction Characteristic of A Paper-based Facing for A Wet Clutch, Experimental Results and Consideration by Stribeck Curve," Journal of Japanese Society of Tribologists, **36** (7), pp. 535-542.

[11] Tanaka, Kazuhiko, Kyogoku, Keiji, and Nakahara, Tsunamitsu, 1999, "Lubrication Characteristics on Sliding Surfaces in A Piston Pump and Motor During Running-in Tests," Fatigue and Fracture Mechanics, National Symposium on Fracture Mechanics, ASTM Special Technical Publication, N01339, West Conshohocken, PA, pp. 47-59.

[12] Smith, S. L., Dowson, D. and Goldsmith, A. A. J., 2001, "The Lubrication of Metal-on-metal Total Hip Joints: A Slide Down the Stribeck Curve," *Proc. of the Institution of Mechanical Engineers, Part J, Journal of Engineering Tribology*, **21**5 (5), pp. 483-493.

[13] Tu, Ching-Fang, and Fort, Tomlinson, Sept 2004, "A Study of Fiber-capstan Friction. 1. Stribeck Curves," Tribology International, **37** (9), pp. 701-710.

[14] Wilson, Robert E. and Barnard, Daniel P., 1922, "The Mechanism of Lubrication," Transactions of the Society of Automotive Engineers, **51**, pp. 203-238.

[15] McKee, S. A. and McKee, T. R., 1932, "Journal Bearing Friction in the Region of Thin-Film Lubrication," SAE journal, **31** (3), pp. 371-377.

[16] Bridgeman, O. C., McKee, S. A., and Bitner, F. G., 1932, "The Effect of Viscosity on Friction in the Region of Thin-Film Lubrication," *Proc. of Annual meeting of American Petroleum Institute*, **13** (3), pp. 154-158.

[17] Burwell, J. T., Kaye, J., Nymegen, D. W. V., and Morgan, D. A., June 1941, "Effects of Surface Finish," Journal of Applied Mechanics, 8 (T63, A), pp. 49-58.

[18] Ocvirk, F. W. and DuBois, G. B., June 1959, "Surface Finish and Clearance Effects on Journal-Bearing Load Capacity and Friction," Journal of Basic Engineering, Transactions of A.S.M.E, **81**, pp. 245-253.

[19] Vogelpohl, Georg, 1965, "Thermal Effects and Elasto-Kinetics in Self-acting Bearing Lubrication," *Proc. of International Symposium on Lubrication and Wear, Houston*, pp. 766-815.

[20] Forrester, P. G., 1946, "Kinetic Friction in or near the Boundary Region, II-The influence of Sliding Velocity and other Variables on Kinetic Friction in or near the Boundary Region," *Proc. of the Royal Society of London, Series A,* **187** (A1011), pp. 439-463.

[21] Lovell, M. R., Khonsari, M. M. and Marangoni, R. D., Apr 1993, "The response of Balls Undergoing Oscillatory Motion-Crossing from Boundary to Mixed Lubrication Regimes," Journal of Tribology, **115** (2), pp. 787-795.

[22] Spikes, H. A., 1997, "Mixed Lubrication - an Overview," Lubrication Science, **9** (3), pp. 2-33.

[23] Spikes, H. A. and Olver, A. V., 2003, "Basics of Mixed Lubrication," Lubrication Science, **16** (1), pp. 3-28.

[24] Jacobson, Bo, 2003, "The Stribeck Memorial Lecture," Tribology International, **36**, pp. 781-789.

[25] Khonsari, M. M. and Booser, E. R., 2001, *Applied Tribology Bearing– Design and Lubrication*, John Wiley & Sons, Inc, New York, NY.

[26] Raimoindi, A. A. and Szeri, A. Z., 1984, "Journal and Thrust Bearings," *Handbook of Lubrication, Vol. 2*, CRC Press, Boca Raton, FL, pp. 413-462.

[27] Tarasov, L. P., April 1945, "Relation of Surface Roughness Readings to Actual Surface Profile," Transactions of The ASME, **67**, pp. 189-196.

[28] Martin, F. A., 1963-1964, "Minimum Allowable Oil Film Thickness in Steadily Loaded Journal Bearings," *Proc. of Institution of Mechanical Engineers*, **178**, part 3N, pp. 161-167.

[29] Rubert, M. P., 1959, "Confusion in Measuring Surface Roughness," Engineering, London, **23**, pp. 393.

[30] Ocvirk, F. W., 1952, "Short Bearing Approximation for Full Journal Bearings," Technical Notes, TN2808, NACA, Washington.

[31] Davis, A. J., 1957, "Sleeve-bearings-Part II, running in characteristics," *Pro. of Institution of* Mechanical *Engineers*, London, **171** (35), pp. 951.

[32] Hamrock, Bernard J., Aug 1991, *Fundamentals of Fluid Film Lubrication*, NASA Reference Publication 1255.

[33] Cann, P., Ioannides, E., Jacobson, B., and Lubrecht, A. A., June 1994, "The lambda ratio- a re-examination," Wear, **175**, pp. 177-188.

[34] Masen, MA, C. H. Venner, P. M. Lugt and J. H. Tripp, 2002, "Effects of Surface Micro-Geometry On the Lift-off Speed Of an EHL Contact," Tribology Transactions, 45 (1), pp. 21-30.

[35] Blok, H., 1950, "Fundamental Mechanical Aspects of Thin-Film Lubrication," Annals of the New York Academy of Sciences, 53, pp. 779-795.

[36] Givens, J. W. and Talley S. K., Oct 1962, "Friction Measurement with the Tapered Spindle Top," Lubrication Engineering, 18, pp. 443-449.

[37] Dowson, Duncan, and Higginson, G. R., 1977, *Elasto-Hydrodynamic Lubrication*, Pergamon Press, Oxford, England.

[40] Gümbel, L., 1916, "Das Problem Der Lagerreibung," Mbl. berl. BezVer. dt. Ing. (VDI), pp. 87-104 and pp. 109-120.

[41] Falz, E., 1937, "Principles of the Design of Journal Bearings, General Discussion of Lubrication and Lubricants," the Institution of Mechanical Engineers, London, **1**, pp. 93-103.

[42] Cameron, A., 1966, *Principles of Lubrication*, Longmans Greens & Co Ltd, U.S.A.

[43] Greenwood, J. A., and Williamson, J. B. P., 1966, "Contact of Nominally Flat Surfaces," *Proceedings of the Royal Society of London*, Series A, **295**, pp. 300-319.

[44] Patir, N., and Cheng, H. S., 1978, "An Average Flow Model for Determining Effects of Three-dimensional Roughness On Partial Hydrodynamic Lubrication," Transactions of ASME, Journal of Lubrication Technology, **100**, pp. 8-14.

[45] Chang, L., 1995, "A Deterministic Model for Line Contact Partial Elastohydrodynamic Lubrication," Tribology International, **28**, pp. 75-84.

[46] Johnson, K. L., Greenwood, J. A., and Poon, S. Y., 1972, "A Simple Theory of Asperity Contact In Elastohydrodynamic Lubrication," Wear, **19**, pp. 91-108.

[47] Tallian, T.E., 1972, "The Theory of Partial Elastohydrodynamic Contacts," Wear, **21** (1), pp. 49-101.

[48] Karelitz, G. B., 1926, "The Lubrication of Waste-Packed Bearings," Transactions of ASME, **48**, pp. 1165-1199.

[49] Fuller, D. D., 1954, "Mixed Friction Conditions in Lubrication," Lubrication Engineering, September-October, pp. 256-261.

[50] Lenning, R. L., 1960, "The Transition from Boundary to Mixed Friction," Lubrication Engineering, December, pp. 575-582.

[51] Tsao, Yuh-Hwang, 1975, "A Model for Mixed Lubrication," Transactions of American Society of Lubrication Engineers, **18** (2), pp. 90-96.

[52] Soda, N., 1978, "Effect of Bearing Area and Surface Roughness in Fluid and Mixed Lubrication," Journal of Japanese Society of Lubrication Engineers, **23** (9), pp. 22-30.

[53] Soda, N., 1985, "Effect of Abbott Bearing Area on Characteristics of Stribeck Curve," Journal of Japanese Society of Tribologists, **31** (9), pp. 637-642.

[54] Yamaguchi, A. and Matsuoka, H., 1992, "A Mixed Lubrication Model Applicable to Bearing/Seal Parts of Hydraulic Equipment," Journal of Tribology, **114**, pp. 116-121.

[55] Gelinck, E. R. M. and Schipper, D. J., 1999, "Deformation of Rough Line Contacts," Journal of Tribology, **121** (3), pp. 449-454.

[56] Gelinck, E. R. M. and Schipper, D. J., 2000, "Calculation of Stribeck Curves for Line Contacts," Tribology International, **33**, pp. 175-181.

[57] Olsson, H., Åström, K. J., de Wit, Canudas C., Gäfvert, M., and Lischinsky, P., 1998, "Friction Models and Friction Compensation," European Journal of Control, **4** (3), pp. 176-195.

[58] Wang, Q., Shi, F. H. and Lee, S. C., 1997, "A Mixed-Lubrication Study of Journal Bearing Conformal Contacts," Journal of Tribology, **119** (3), pp. 456-461.

[59] Wang, Q., Shi, F. H. and Lee, S. C., 1998, "A Mixed-TEHD Model for Journal-Bearing Conformal Contact-Part II: Contact, Film Thickness, and Performance Analysis," **120** (2), pp. 206-213.

[60] Liu, W. K., Xiong, S. W., Guo, Y., Wang, Q., Wang, Y. S., Yang, Q. M. and Vaidyanathan, K., 2004, "Finite Element Method for Mixed Elastohydrodynamic Lubrication of Journal-Bearing Systems," International Journal For Numerical Methods in Engineering, **60** (10), pp. 1759-1790.

[61] Bair, S. and Winer, W. O., 1979, "A Rheological Model for EHL Contacts Based on Primary Laboratory Data," ASME Journal of Lubrication Technology, **101** (3), pp. 258-265.

[62] Khonsari, M. M. and Hua, D. Y., 1994, "Thermal Elastohydrodynamic Analysis Using a Generalized Non-Newtonian Formulation With Application to Bair-Winer Constitutive Equation," Journal of Tribology, **116** (1), pp. 37-45.

[63] Fein, R. S., 1997, "High Pressure Viscosity and EHL Pressure-Viscosity Coefficients," *Tribology Data Handbook*, CRC Press, Boca Raton, FL, pp. 638-644.

[64] Moes, H., 1992, "Optimum Similarity Analysis with Application to Elastohydrodynamic Lubrication," Wear, **159**, pp. 57-66.

[65] Whitehouse, D. J. and Archard J. F., 1970, "The Properties of Random Surfaces of Significance in Their Contact," *Proceedings of the Royal Society of London*, Series A, **316**, pp. 97-121.

[66] Baker, A. E., 1958, "Grease Bleeding – A Factor in Ball bearing Performance," NLGI Spokesman, **22**, pp. 271-277.

[67] Bauer, W. H., Finkelstein, A. P. and Wiberley, S. E., 1960, "Flow Properties of Lithium Stearate-Oil Model Greases as Function of Soap Concentration and Temperature," ASLE Transactions, **3**, pp. 215-224.

[68] Kageyama, H., Machidori, W. and Moriuchi, T., 1984, "Grease Lubrication in Elastohydrodynamic Contacts," NLGI Spokesman, **48** (3), pp. 72-81.

[69] Pemberton, J. and Cameron, A., 1976, "A Mechanism of Fluid Replenishment in Elastohydrodynamic Contacts," Wear, **37** (1), pp. 185-190.

[70] Aström, H., Östensen, J. O. and Höglund, E., 1993, "Lubricating Grease Replenishment in an Elastohydrodynamic Point Contact," Journal of Tribology, **115** (3), pp. 501-506.

[71] Cann, P. M. and Spikes, H. A., 1995, "Visualization of Starved Grease and Fluid Lubricant Films," *Lubricants and Lubrication*, Elsevier Science, pp. 161-166.

[72] Lewis, Walter J, 1990, "The Design of High Speed Grease Lubricated Spindles for Machine Tool Production Equipment," SAE Transactions, **99**, sect 5, pp. 1061-1070.

[73] Bradford, L. J., Barber, E. M. and Muenger, J. R., 1961, "Grease Lubrication Studies with Plain Bearings, Transactions of Journal of Basic Engineering," **83**, pp. 153-161.

[74] Horth, A. C., 1968, "Friction Reduction with Greases," NLGI Spokesman, **32**, pp. 155-161.

[75] Godfrey, D., 1964, "Friction of Greases and Grease Components during Boundary Lubrication," ASLE Transactions, **7**, pp. 24-31.

[76] Reinhoudt, J. P., 1970, "A Grease-lubricated Hydrodynamic Bearing System for A Satellite Flywheel," Journal of the American Society of Lubrication Engineers, **26** (3), pp. 95-100.

[77] Wikström, V., 1996, "Rolling Bearing Lubrication at Low Temperature," Doctoral Thesis, Division of Machine Elements, Lulea University of Technology.

[78] Östensen, J. O., 1995, "Lubrication of Elastohydrodynamic Contacts mainly Concerning Low Temperature," Doctoral Thesis, Division of Machine Elements, Lulea University of Technology.

[79] Westcott, A. L., 1913, "The Lubricating Value of Cup Greases," Journal of the American Society of Mechanical Engineers, **35**, pp. 1143-1167.

[80] Cohn, G. and Oren, J. W., 1949, "Film pressure in Grease-lubricated Sleeve Bearings," Transactions of the American Society of Mechanical Engineers, **71**, pp. 555-560.

[81] Chakrabarti, R. K. and Harker, R. J., 1960, "Frictional Resistance of a Radially Loaded Journal Bearing with Grease Lubrication," Lubrication Engineering, **16**, pp. 274-280.

[82] Glaeser, W. A., 1977, "Operating Limitations of Heavily Loaded Grease-lubricated Cast Bronze Bearings," ASLE Transactions, **20** (4), pp. 309-314.

[83] Stolarski, T. and Olszewski O., 1976, "An Experimental Study of the Frictional Mechanism in a Journal Bearing Lubricated with Grease Containing Powered PTFE," Wear, **39**, pp. 377-387.

[84] Muijderman, E.A., Remmers, G. and Tielemans, L. P. M., 1980, "Grease-lubricated Spiral-groove Bearings," Phillips Technical Review, **39** (6/7), pp. 184-198.

[85] Lawrence, K. B., 1950, "A Mathematical Evaluation of Pressures in a grease-lubricated bearing," Transactions of the American Society of Mechanical Engineers, **72**, pp. 429-443.

[86] Milne, A. A., 1958, "A Theory of Grease Lubrication of A Slider Bearing," *Proc. International Congress on Rheology (2nd, Oxford)*, pp. 427-436.

[87] Wada, S. and Hayashi, H., 1971, "Hydrodynamic Lubrication of Journal Bearings by Pseudo-plastic Lubricants-Part 1, Theoretical Studies," Bulletin of the JSME, **14**, pp. 268-278.

[88] Wada, S. and Hayashi, H., 1971, "Hydrodynamic Lubrication of Journal Bearings by Pseudo-plastic Lubricants-Part 2, Experimental Studies," Bulletin of the JSME, **14**, pp. 279-286.

[89] Wada, S. and Hayashi, H., 1974, "Hydrodynamic Lubrication of Journal Bearings by Pseudo-plastic Lubricants-Part 3, Application to Journal Bearings," Bulletin of the JSME, **17**, pp. 1182-1191.

[90] Wada, S. and Kawakami, Y., 1986, "Hydrodynamic Lubrication of Porous Journal Bearings with grease," Bulletin of the JSME, **29** (249), pp. 943-949.

[91] Hayashi, H., Wada, S. and Nakarai N., 1977, "Hydrodynamic Lubrication of Journal Bearings by Non-Newtonian Lubricants," Bulletin of the JSME, **20**, pp. 224-231.

[92] Tichy, J.A., 1991, "Hydrodynamic Lubrication Theory for the Bingham Plastic Flow Model," Journal of Rheology, **35** (4), pp. 477-496.

[93] Wen, Shi Zhu and Ying, Tsi Neng, 1988, "A Theoretical and Experimental Study of EHL Lubricated With Grease," Journal of Tribology, **110** (1), pp. 38-43.

[94] Dong, Daming, 1988, "Theory of Elastohydrodynamic Grease-lubricated Line Contact Based on a Refined Rheological Model," Tribology International, **21** (5), pp. 261-267.

[95] Cheng, Jun, 1994, "Elastohydrodynamic Grease Lubrication Theory and Numerical Solution in Line Contacts," Tribology Transactions, **37** (4), pp. 711-718.

[96] Jang, J. Y. and Khonsari, M. M, 1997, "Performance Analysis of Grease-lubricated Journal Bearings Including Thermal Effects," Journal of Tribology, **119**, pp. 859-868.

[97] Lu, X. B. and Khonsari, M. M., 2005, "On the Lift-off Speed in Journal bearings," Tribology Letters, **20** (3-4), pp. 299-305.

[98] Cann, P. M., 2002, "Friction Properties of Grease in Elastohydrodynamic Lubrication," NLGI Spokesman, **66** (1), pp. 6-15.

[99] Harris, T., 2001, *Rolling Bearing Analysis,* John Wiley & Sons, New York, NY.

[100] Aihara, S. and Dowson, D., 1979, "A Study of Film Thickness in Grease-lubricated Elastohydrodynamic Contacts," *Proc. of the Society of Photo-optical Instrumentation Engineers*, pp. 104-115.

[101] Fogg, A., 1946, "Fluid Film Lubrication of Parallel Thrust Surfaces," Proc. of the Institution of Mechanical Engineers, 155, pp. 49-69.

[102] Shaw, M. C. and Mass, C., 1947, "An Analysis of the Parallel-surface Thrust Bearing," Transactions of ASME, **69**, pp. 381-387.

[103] Denny, D. F., 1961, "Some Measurements of Fluid Pressures between Plan Parallel Thrust Surfaces with Special Reference to Radial Face Seals," Wear, **4**, pp. 64-83.

[104] Zienkiewicz, O. C., 1957, "Temperature Distribution within Lubricating Films between Parallel Bearing Surfaces and Its Effect on the Pressures Developed," *Proc. of the Conference on Lubrication and Wear*, London, October 1-3, pp. 135-141.

[105] Davies, M. G., 1961, "The Generation of Lift by Surface Roughness in a Radial Face Seal," *Proc. of the 3rd International Conference on Fluid Sealing*, British Hydromechanics Research Association, Harlow, Essex, UK, pp. 1-15.

[106] Salama, M. E., 1950, "The Effect of Macro-roughness on the Performance of Parallel Thrust Bearings," *Proc. of the Institution of Mechanical Engineers*, **161**, pp. 149-161.

[107] Pape, J. G., 1968, "Fundamental Research on a Radial Face Seal," ASLE Transactions, **11** (4), pp. 302-309.

[108] Hamilton, D. B., Walowit, J. A., and Allen, C. M., 1966, "A Theory of Lubrication by Micro-irregularities," Journal of Basic Engineering, **88** (1), pp. 177-185.

[109] Anno, J. N., Walowit, J. A., and Allen, C. M., 1968, "Microasperity Lubrication," Journal of Lubrication Technology, Transactions of ASME, Series F, **9** (2), pp. 351-355.

[110] Anno, J. N., Walowit, J. A., and Allen, C. M., 1969, "Load Support and Leakage from Microasperity-lubricated Face Seals," Journal of Lubrication Technology, Transactions of ASME, Series F, **10**, pp. 726-731.

[111] Etsion, I., 1980, "The Effect of Combined Coning and Waviness on the Separating Force in Mechanical Face Seals," Journal of Mechanical Engineering Science, **22** (2), pp. 59-64.

[112] Tanner, R. I., 1960, "Non-Newtonian Flow and the Oil Seal Problem," Journal of Mechanical Engineering Sciences, **2** (1), pp. 25-28.

[113] Etsion, I., 1984, "A New Concept of Zero-leakage Noncontacting Mechanical Face Seal," Journal of Tribology, **106**, pp. 338-343.

[114] Lipschitz, A., 1985, "A Zero-leakage Film Riding Face Seal," Journal of Tribology, **107** (3), pp. 326-332.

[115] Lai, T., 1994, "Development of Non-contacting, Non-leaking Spiral Groove Liquid Face Seals," Lubrication Engineering, **50** (8), pp. 625-631.

[116] Etsion, I., Halperin, G. and Greenberg, Y., 1997, "Increasing Mechanical Seals Life with Laser-textured Seal Faces," Papers Presented at the 15th International Conference on Fluid Sealing, Maastricht, The Netherland, pp. 3-11.

[117] Etsion, I., 2000, "Improving Tribological Performance of Mechanical Seals by Laser Surface Texturing," *Proc. of the 17th International Pump Users Symposium*, Mainz, Germany, pp. 17-21.

[118] Kligerman, Y. and Etsion, I., 2001, "Analysis of the Hydrodynamic Effects in a Surface Textured Circumferential Gas Seal," Tribology Transactions, **44** (3), pp. 472-478.

[119] Etsion, I. and Halperin, G., 2002, "A Laser Surface Textured Hydrostatic Mechanical Seal," Tribology Transactions, **45** (3), pp. 430-434.

[120] Tanaka, H., Gomi, K., and Miyake, Y., 1993, "Micro-Tribology of Carbon-coated Thin Film Media with Well-defined Surface Texture," IEEE Transactions on Magnetics, **29** (1), pp. 270-275.

[121] Tagawa, N. and Bogy, D. B., 2002, "Air Film Dynamics for Micro-textured Flying Head Slider Bearings in Magnetic Hard Disk Drives," Journal of Tribology, **124** (3), pp. 568-574.

[122] Tagawa, N. and Mori, A., 2003, "Thin Film Gas Lubrication Characteristics of Flying Head Slider Bearings over Patterned Media in Hard Disk Drives," Microsystem Technologies, **9** (5), pp. 362-368.

[123] Wang, X. L., Kato, K., Adachi, K. and Aizawa, K., 2001, "The Effect of Laser Texturing of SiC Surface on the Critical Load for the Transition of Water Lubrication Mode from Hydrodynamic to Mixed," Tribology International, **34** (10), pp. 703-711.

[124] Wang, X. L., Kato, K., Adachi, K. and Aizawa, K., 2003, "Loads Carrying Capacity Map for the Surface Texture Design of SiC Thrust Bearing Sliding in Water," Tribology International, **36** (3), pp. 189-197.

[125] Wakuda, M., Yamauchi, Y., Kanzaki, S. and Yasuda, Y., 2003, "Effect of Surface Texturing on Friction Reduction between Ceramic and Steel Materials under Lubricated Sliding Contact," Wear, **254** (3-4), pp. 356-363.

[126] Brizmer, V., Etsion, I., 2003, "A Laser Surface Textured Parallel Thrust Bearing," Tribology Transactions, **46** (3), pp. 387-403.

[127] Ronen, A., Etsion, I. and Kligerman, Y., 2001, "Friction-Reducing Surface-Texturing in Reciprocating Automotive Components," Tribology Transactions, **44** (3), pp. 359-366.

[128] Ryk, G., Kligerman, Y. and Etsion, I., 2002, "Experimental Investigation of Laser Surface Texturing for Reciprocating Automotive Components," Tribology Transactions, **45** (4), pp. 444-449.

[129] Kligerman, Y., Etsion, I. and Shinkarenko, A., 2005, "Improving Tribological Performance of Piston Rings by Partial Surface Texturing," Journal of Tribology, **127** (3), pp. 632-638.

[130] Etsion, I. and Burstein, L., 1996, "A Model for Mechanical Seals with Regular Microsurface Structure," Tribology Transactions, **39** (3), pp. 677-683.

[131] Etsion, I., Kligerman, Y. and Halperin, G., 1999, "Analytical and Experimental Investigation of Laser-textured Mechanical Seal Faces," Tribology Transactions, **42** (3), pp. 511-516.

[132] Wang, Q. Jane and Zhu, D., 2005, "Virtual Texturing: Modeling the Performance of Lubricated Contacts of Engineered Surfaces," Journal of Tribology, **127** (4), pp. 722-728.

[133] Geiger, M., Roth, S., and Becker, W., 1998, "Influence of Laser-produced Microstructures on the Tribological Behavior of Ceramics," Surface & Coating Technology, **100-101**, pp. 17-22.

[134] Etsion, I., 2005, "State of the Art in Laser Surface Texturing," Journal of Tribology, **127** (1), pp. 248-253.

[135] Lo, Sy-Wei and Wilson, W. R. D., 1999, "A Theoretical Model of Micro-Pool Lubrication in Metal Forming," Journal of Tribology, **121** (4), pp. 731-738.

[136] Lo, Sy-Wei and Tzu-Chern Horng, 1999, "Lubricant Permeation from Micro Oil Pits Under Intimate Contact Condition," Journal of Tribology, **121** (4), pp. 633-638.

[137] Dowson, D. and Taylor, C. M., 1979, "Cavitation in Bearings", Annual Review of Fluid Mechanics, **11**, pp. 35-66.

[138] Sampson, J. B., Morgan, F., Reed, D. W. and Muskat, M., 1943, "Study in Lubrication, XII, Friction Behavior during the Slip Portion of the Stick-Slip Process," Journal of Applied Physics, **14** (12), pp. 689-700.

[139] Bell, R. and Burdekin, M., 1966-67, "Dynamic Behavior of Plain Slideways," *Proceedings of Institution of Mechanical Engineers*, **181** (1), pp. 169-181.

[140] Bell, R. and Burdekin, M., 1969-70, "A Study of the Stick-Slip Motion of Machine Tool Feed Drives," *Proceedings of Institution of Mechanical Engineers*, **184** (1), pp. 543-557.

[141] Bell, R. and Burdekin, M., 1969-70, "An Investigation into the Steady-State Characteristics of Plain Slideways," *Proceedings of Institution of Mechanical Engineers*, **184** (1), pp. 1075-1087.

[142] Dahl, P. R., May 1968, "A Solid Friction Model," TOR0158 (3107-18)-1, the Aerospace Corporation, El Segundo, California.

[143] Dahl, P. R., 1976, "Solid Friction Damping of Mechanical Vibrations," AIAA Journal, **14** (12), pp. 1675-1682.

[144] Dahl, P. R., May 24-27, 1977, "Measurement of Solid Friction Parameters of Ball Bearings," *Proceedings of 6th Symposium on Incremental Motion Control Systems and Devices,* pp. 1910-1914.

[145] Fleischer, G., Gröger, H., and Thum, H., 1980, *Verschleiss und Zuverlässigkeit*, VEB Verlag Technik, Berlin.

[146] Todd, M. J. and Johnson, K. L., 1987, "A Model for Coulomb Torque Hysteresis In Ball Bearings," International Journal of Mechanical Science, **29** (5), pp. 339-354.

[147] Armstrong-Helouvry, B., 1994, "Survey of Models, Analysis Tools and Compensation Methods for the Control of Machines with Friction," Automatica, the Journal of International Federation of Automatic Control, **30** (7), pp. 1083-1138.

[148] Dupont, P. E. and Dunlap, E. P., 1995, "Friction Modeling and PD Compensation at Very Low Velocities," Journal of Dynamic Systems, Measurements, and Control, **117** (1), pp. 8-14.

[149] Yang, Chii-Rong, Lee, Rong-Tsong, and Chiou, Yuang-Cheng, 1997, "Study on Dynamic Friction Characteristics in Reciprocating Friction Drive System," Tribology International, **30** (10), pp. 719-731.

[150] F. Van De Velde, P. De Baets, and J. Degreck, 1998, "The Friction Force During Stick-Slip with Velocity Reversal," Wear, **216** (2), pp. 138-149.

[151] Polycarpou, A. A. and Soom, A., 1995, 'Boundary and Mixed Friction in the Presence of Dynamic Normal loads: Part I – System Model," Journal of Tribology, **117** (2), pp. 255-260.

[152] Polycarpou, A. A. and Soom, A., 1995, "Boundary and Mixed Friction in the Presence of Dynamic Normal loads: Part II – Friction Transients," Journal of Tribology, **117** (2), pp. 261-266.

[153] Polycarpou, A. A. and Soom, A., 1995, "Two Dimensional Models of Boundary and Mixed Friction at a Line Contact," Journal of Tribology, **117** (1), pp. 178-184.

[154] Hess, D. P. and Soom, A., 1990, "Friction at A Lubricated Line Contact Operating at Oscillating Sliding Velocities," Journal of Tribology, **112** (1), pp. 147-152.

[155] Hess, D. P., 1997, "Apparent Multi-Valued Friction in Lubricated Contact Systems from Tangential Dynamics," Journal of Tribology, **119** (4), pp. 632-636.

[156] Harnoy, A. and Rachoor, H., 1993, "Angular-Compliant Hydrodynamic Bearing Performance under Dynamic Loads," Journal of Tribology, **115** (3), pp. 342-347.

[157] Harnoy, A. and Friedland, B., 1994, "Dynamic Friction Model of Lubricated Surfaces for Precise Motion Control," Tribology Transactions, **37** (3), pp. 608-614.

[158] Harnoy, A., Friedland, B., Semenock, R., Rachoor, H., and Aly, A., June 1994, "Apparatus for Empirical Determination of Dynamic Friction," *Proceedings of the American Control Conference*, Baltimore, Maryland, pp. 546-550.

[159] Harnoy, A., Friedland, B., Semenock, and R., Rachoor, H., 1994, "Modeling and Simulation of Elastic and Friction Forces in Lubricated Bearings for Precise Motion Control," Wear, 172, pp. 155-165.

[160] Rachoor, H., January 1996, Investigation of Dynamic Friction in Lubricated Surfaces, Ph. D thesis, New Jersey Institute of Technology.

[161] Lu, X. B. and Khonsari, M. M., "An Experimental Study of Grease-lubricated Journal Bearings undergoing Oscillatory Motion," in process.

[162] D. A. Haessig, Jr. and Friedland, B., 1991, "On the Modeling and Simulation of Friction," Journal of Dynamic Systems, Measurements, and Control, **113** (3), pp. 354-362.

[163] Armstrong-Helouvry, B., June 19-21, 1989, "Control of Machine with Non-linear Low-Velocity Friction: A Dimensional Analysis," Experimental Robotics I: the First International Symposium, Montreal, pp. 180-195.

[164] Armstrong-Helouvry, B., 1991, *Control of Machines with Friction*, Kluwer Academic Publishers, New York.

[165] de Wit, Canudas C., Olsson, H., Åström, K. J., and Lischinsky, P., June 1993, "Dynamic Friction Models and Control Design," *Proceedings of the American Control Conference*, San Francisco, California, pp. 1920-1926.

[166] de Wit, Canudas C., Olsson, H., Åström, K. J., and Lischinsky, P., March 1995, "A New Model for Control of Systems with Friction," IEEE Transactions on Automatic Control, **40** (3), pp. 419-425.

[167] Olsson, H., Åström, K. J., de Wit, Canudas C., Gäfvert, M., and Lischinsky, P., 1998, "Friction Models and Friction Compensation," European Journal of Control, **4** (3), pp. 176-195.

[168] Berger, E. J., 2002, "Friction Modeling for Dynamic System Simulation," Applied Mechanics Review, **55** (6), pp. 535-577.

[169] Tabor, D., 1964, "Friction and Wear," *Proceedings of International Symposium on Lubrication and Wear*, pp. 701-761.

[170] Salehi, M. and Heshmat, H., September 3-7, 2001, "Frictional Dampers Dynamic Characterization – Theory and Experiments," *Boundary and Mixed Lubrication: Science*

and Applications, the 28th Leed – Lyon Symposium on Boundary and Mixed Lubrication, Elsevier Science Publisher, pp. 515-526.

[171] Lu, X. B. and Khonsari, M. M., 2006, "An Experimental Investigation of Grease-lubricated Journal Bearings", to appear in ASME Journal of Tribology.

[172] Cann, P. M., 1999, "Thin-film Grease Lubrication," Proceedings of the Institution of Mechanical Engineers, Part J, Journal of Engineering Tribology, **213** (5), pp. 405-416.

[173] Cann, P. M., 1999, "Starved Grease Lubrication of Rolling Contacts," Tribology Transactions, **42** (4), pp. 867-873.

[174] Cann, P. M., Damiens, B., and Lubrecht, A. A., 2004, "The Transition between Fully Flooded and Starved Regimes in EHL," Tribology International, **37** (10), pp. 859-864.

[175] Karnopp, D., 1985, "Computer Simulation of Slip-Stick Friction in Mechanical Dynamic Systems," Journal of Dynamic Systems, Measurements, and Control, **107** (1), pp. 100-103.

[176] Armstrong-Helouvry, B., May 1992, "Frictional Lag and Stick-Slip," *Proceedings of the 1992 IEEE International Conference on Robotics and Automation*, Nice, France, 2, pp. 1448-1453.

[177] Armstrong-Helouvry, B., October, 1993, "Stick Slip and Control in Low-Speed Motion," IEEE Transactions on Automatic Control, **38** (10), pp. 1483-1496.

[178] Pinkus, O. and Sternlicht, B., 1961, *Theory of Hydrodynamic Lubrication*, McGraw-Hill Book Company, Inc.

[179] Booker, F., 1965, "A table of the journal-bearing integral," Journal of Basic Engineering, **87** (2), pp. 533-535.

[180] Hazlett, T. L., 1990, "Thermalelastic Behavior of Journal Bearings Undergoing Seizure - A Finite Element Study," M.S. Thesis, University of Pittsburgh, Pittsburgh, Pennsylvania.

[181] Hazlett, T.L. and Khonsari, M.M., 1992, "Finite element model of journal bearing undergoing rapid thermally induced seizure," Tribology International, **25** (3), pp. 177-182.

[182] Hazlett, T.L. and Khonsari, M.M., 1992, "Thermalelastic Behavior of Journal Bearings Undergoing Seizure," **25** (3), pp. 183-187.

[183] Krithivasan, R., 2002, "Transient Thermomechanical Interactions of Shaft-Bushing Pair in Bearings - A Finite Element Study," M.S. Thesis, Louisiana State University, Baton Rouge, Louisiana.

[184] Krithivasan, R. and Khonsari, M.M., 2003, "Thermally induced seizure in journal bearings during startup and transient flow disturbance," Journal of Tribology, **125** (4), pp. 833-841.

[185] Stachowiak, G. W. and Batchelor, A. W., 2001, *Engineering Tribology*, Butterworth-Heinemann, 2nd Edition, U.S.A.

[186] Incropera, F. P. and DeWitt, D. P., 1996, *Introduction to Heat Transfer, 3rd Edition*, John Wiley & Sons, Inc.

VITA

Xiaobin Lu was born in Shandong, China, on June 27, 1975. He finished his education through high school at Laizhou, Shandong. In 1993, he became an undergraduate student at Zhongyuan Institute of Technology, where he spent four years studying machine design and manufacturing. After that, he was enrolled in the graduate program at University of Petroleum, China. He was awarded a master degree in May 2000.

After graduation, he was hired by China Academy of Launch Vehicle as a mechanical engineer and developed seals used in cryogenic environment.

In January 2002, he joined in Center for Rotating Machinery (CeRoM) at Louisiana State University as a doctoral candidate under the supervision of Professor Michael M. Khonsari.